

DUDLEY KNOX LIBRARY
NAVAL POSTGRADUATE SCHOOL
MONTEREY, CALIF. 93940

AN INVESTIGATION INTO THE PHENOMENON OF
LOCALIZED CORROSION IN VARIOUS
AUSTENITIC, FERRITIC, DUPLEX AND CAST
STAINLESS STEELS

by

Rogest William Dively, II
(B.S. University of Miami, 1971)

and

John Robert McNamee, Jr.
(B.S. U.S. Naval Academy, 1970)

Submitted Jointly in Partial Fulfillment
of the Requirements of the Degrees of

OCEAN ENGINEER

and

MASTER OF SCIENCE IN
MATERIALS SCIENCE AND ENGINEERING

at the

MASSACHUSETTS INSTITUTE OF TECHNOLOGY

June 1982

© Massachusetts Institute of Technology

AN INVESTIGATION
INTO THE PHENOMENON OF LOCALIZED CORROSION
IN VARIOUS AUSTENITIC, FERRITIC, DUPLEX, AND CAST
STAINLESS STEELS

by

ROGEST WILLIAM DIVELY, II

and

JOHN ROBERT McNAMEE, JR.

Submitted jointly to the Department of Ocean Engineering
on May 7, 1982 in partial fulfillment
of the requirements for the Degrees of Ocean
Engineer and Master of Science in Materials Science
and Engineering

ABSTRACT

Thirty-six wrought and nine cast alloys were defined by the United States Navy as possible replacements of Type 316 stainless steel. Forty-three of these same alloys were included in an experimental program undertaken in an attempt to: (1) evaluate the relative resistance to localized corrosion in chloride-containing environments, and (2) develop an understanding of the mechanism involved in the breakdown of passive behavior. Techniques used in this study included cyclic anodic polarization, application of a constant potential in the presence of an intentionally applied crevice, and Auger Electron Spectroscopy.

Results from this investigation indicate that the use of the slow scan rate cyclic anodic polarization method developed in this study can be used confidently to predict the relative susceptibility to localized corrosion, especially when complemented by other techniques.

Of all the alloying elements considered, molybdenum was the most effective in increasing localized corrosion resistance. Austenitic alloys with greater than 5% Mo, and ferritic alloys with greater than 25% Cr and 3% Mo showed no tendency to corrode locally. Evidence suggests that a

minimum of 0.4% Nitrogen is also an important factor for increased localized corrosion resistance.

Compositional profile analysis at the active corrosion site shows an enrichment of chromium in the passive layer. The role of molybdenum in improved resistance to localized corrosion is in the form of the molybdate ion serving to protect the exposed metal surface and/or block the entrance of a mobile charge carrier (chloride ion). The presence of sulfur at the active site supports the theory of localized corrosion initiation at the site of sulfide inclusions.

Thesis Supervisor: R. M. Latanision
Title: Professor of Materials Science
and Engineering

ACKNOWLEDGEMENTS

We would like to thank the United States Navy for sponsoring our studies at M.I.T. We also would like to thank Mr. Harvey Hack and Mr. Terry Morton at the Naval Research and Development Center, Annapolis, Md. for their help in providing the alloying material, background information, and technical assistance necessary in order to have a meaningful thesis. We would like to thank Professor Ronald M. Latanision for his support as a thesis advisor and as a friend throughout our research effort.

Bryan Wilson has not only been a good friend, but also a fellow Naval Officer whose opinions and ideas have been a constant source of support. We add a special thanks to Megan and Jim for adding vitality to our work sessions.

To our wives Patricia and Cami, who beyond all others have understood, endured, and supported us during the past three years, we thank you!

TABLE OF CONTENTS

TITLE PAGE	1
ABSTRACT	2
ACKNOWLEDGEMENTS	4
TABLE OF CONTENTS	5
LIST OF FIGURES	8
LIST OF TABLES	12
DEDICATION	13
1. INTRODUCTION	14
2. BACKGROUND	17
2.1 MECHANISM OF CREVICE AND PITTING CORROSION IN AERATED CHLORIDE SOLUTIONS	17
2.2 PASSIVITY	24
2.3 BREAKDOWN OF PASSIVITY AND REPASSIVATION	30
2.4 CYCLIC ANODIC POLARIZATION	34
2.5 AUGER ELECTRON SPECTROSCOPY	37
3. MOTIVATION AND OBJECTIVES OF EXPERIMENTAL RESEARCH	42
4. PROCEDURES AND APPARATUS FOR EXPERIMENTAL RESEARCH	49

4.1	SAMPLE PREPARATION AND MOUNTING	49
4.2	ELECTROCHEMICAL POLARIZATION	57
4.2.1	ELECTROCHEMICAL CYCLIC POLARIZATION	57
4.2.2	ELECTROCHEMICAL POLARIZATION AT CONSTANT POTENTIAL	59
4.3	SURFACE ANALYSIS - AUGER ELECTRON SPECTROSCOPY	62
5.	RESULTS OF EXPERIMENTAL RESEARCH	65
5.0	OVERVIEW	65
5.1	FRAMEWORK FOR EVALUATION OF ALLOYS	65
5.2	ELECTROCHEMICAL RESULTS	71
5.2.1	AUSTENITIC 6% TO 16% NICKEL ALLOYS	71
5.2.2	AUSTENITIC 17% TO 40% NICKEL ALLOYS	72
5.2.3	AUSTENITIC > 40% NICKEL ALLOYS	73
5.2.4	DUPLEX AUSTENITIC- FERRITIC ALLOYS	73
5.2.5	FERRITIC ALLOYS	73
5.2.6	CAST ALLOYS	74
5.3	SURFACE ANALYSIS RESULTS	124
6.	DISCUSSION OF RESULTS	133

6.1 GENERAL TREND IN CYCLIC POLARIZATION TESTS	133
6.2 COMPARISON WITH PUBLISHED ELECTROCHEMICAL RESULTS	137
6.3 COMPARISON WITH IN OCEAN TEST RESULTS	140
6.4 ALLOYING EFFECTS	154
6.5 COMPOSITION PROFILE OF SURFACE AT ACTIVE CORROSION SITES	157
6.6 COMMENTS UPON PERTURBATIONS IN CYCLIC POLARIZATION CURVES	166
7. SUMMARY AND CONCLUSIONS	165
8. FUTURE WORK	168
9. REFERENCES	170
APPENDIX A	
CATALOG OF PARAMETERS USED IN ANALYSIS	180
APPENDIX B	
AUGER SPECTRA FOR ALLOYS T316, T439 , AND T444.	182

List of Figures

	Page
2.1.1 Parameter of Localized Corrosion.	23
2.2.1 Schematic Polarizarion Curve.	29
2.4.1 Identification of Key Parameters.	36
2.5.1 Auger Electron Generation	41
4.1.1.1 Sample Mounting Techniques	53
4.1.1.2 View of Mounted Sample	54
4.1.1.3 Comparison of Cyclic Polarization Diagrams - Inconel 625	55
4.1.1.4 Comparison of Cyclic Polarization Diagrams - Type 316	56
4.2.1 Experimental Set-up for Cyclic Anodic Polarization	61
5.1.1 Logic Circuit Diagram for the Ranking of Stainless Steels	69
5.2.1 Cyclic Polarization Diagram of Alloy T316	75
5.2.2 Cyclic Polarization Diagram of Alloy 3 ⁴ LN	76
5.2.3 Cyclic Polarization Diagram of Alloy T216	77
5.2.4 Cyclic Polarization Diagram of Alloy Rex 73 ⁴	78
5.2.5 Cyclic Polarization Diagram of Alloy 317L	79
5.2.6 Cyclic Polarization Diagram of Alloy 317 LM	80
5.2.7 Cyclic Polarization Diagram of Alloy 317 LT	81
5.2.8 Cyclic Polarization Diagram of Alloy 22-13-5	82

		Page
5.2.9	Cyclic Polarization Diagram of Alloy 904 L	83
5.2.10	Cyclic Polarization Diagram of Alloy 4X	84
5.2.11	Cyclic Polarization Diagram of Alloy 700	85
5.2.12	Cyclic Polarization Diagram of Alloy 254 SLX	86
5.2.13	Cyclic Polarization Diagram of Alloy 777	87
5.2.14	Cyclic Polarization Diagram of Alloy 254 SMO	88
5.2.15	Cyclic Polarization Diagram of Alloy 6X	89
5.2.16	Cyclic Polarization Diagram of Alloy 20Mod	90
5.2.17	Cyclic Polarization Diagram of Alloy 20Cb3	91
5.2.18	Cyclic Polarization Diagram of Alloy 20 Mo6	92
5.2.19	Cyclic Polarization Diagram of Alloy 254 SFeR	93
5.2.20	Cyclic Polarization Diagram of Alloy 825	94
5.2.21	Cyclic Polarization Diagram of Alloy G	95
5.2.22	Cyclic Polarization Diagram of Alloy G-3	96
5.2.23	Cyclic Polarization Diagram of Alloy 625	97
5.2.24	Cyclic Polarization Diagram of Alloy C-276	98

		Page
5.2.25	Cyclic Polarization Diagram of Alloy T329	99
5.2.26	Cyclic Polarization Diagram of Alloy 44LN	100
5.2.27	Cyclic Polarization Diagram of Alloy Ferralium	101
5.2.28	Cyclic Polarization Diagram of Alloy T439	102
5.2.29	Cyclic Polarization Diagram of Alloy T444	103
5.2.30	Cyclic Polarization Diagram of Alloy 26-1	104
5.2.31	Cyclic Polarization Diagram of Alloy 26-1S	105
5.2.32	Cyclic Polarization Diagram of Alloy 29-4	106
5.2.33	Cyclic Polarization Diagram of Alloy 29-4C	107
5.2.34	Cyclic Polarization Diagram of Alloy 29-4-2	108
5.2.35	Cyclic Polarization Diagram of Alloy SC-1	109
5.2.36	Cyclic Polarization Diagram of Alloy Monit	110
5.2.37	Cyclic Polarization Diagram of Alloy CA6N	111
5.2.38	Cyclic Polarization Diagram of Alloy CF8M	112
5.2.39	Cyclic Polarization Diagram of Alloy IN-862	113
5.2.40	Cyclic Polarization Diagram of Alloy CN7M	114
5.2.41	Cyclic Polarization Diagram of Alloy 625 cast	115

5.2.42	Cyclic Polarization Diagram of Alloy CW-12M-2	Page 116
5.2.43	Cyclic Polarization Diagram of Alloy Illium-PD	117
5.3.1	Composition/Depth Profile of T316 (300 mV - active site)	128
5.3.2	Composition/Depth Profile of T316 (300 mV - unaffected site)	129
5.3.3	Composition/Depth Profile of T316 (50 mV - active site)	130
5.3.4	Composition/Depth Profile of T439 (300 mV - active site)	131
5.3.5	Composition/Depth Profile of T444 (600 mV - active site)	132
6.1	Schmatic Polarization Diagrams for Groupings of Localized Corrosion Tendency	136
6.5.1	Mechanism for Mo Involvement in Resistance toward Localized Corrosion	162

List of Tables

	Page
3.1 Composition of Austenitic 6-16% Nickel Alloys	45
3.2 Composition of Austenitic 17-40% Nickel Alloys	46
3.3 Composition of Austenitic >40% Nickel Alloys	46
3.4 Composition of Duplex Austenitic-Ferritic Alloys	47
3.5 Composition of Ferritic Alloys	47
3.6 Composition of Cast Alloys	48
5.1.1 Groupings of Alloys toward Localized Corrosion Tendency via Cyclic Anodic Polarization Method	70
5.2.1 Tabulation of Parameters for Austenitic 6-16% Nickel Stainless Steels	118
5.2.2 Tabulation of Parameters for Austenitic 17-40% Nickel Stainless Steels	119
5.2.3 Tabulation of Parameters for Austenitic >40% Nickel Stainless Steels	120
5.2.4 Tabulation of Parameters for Duplex Austenitic- Ferritic Stainless Steels	121
5.2.5 Tabulation of Parameters for Ferritic Stainless Steels	122
5.2.6 Tabulation of Parameters for Cast Stainless Steels	123
6.3.1 Results from Crevice Testing at La Que Center for Corrosion Technology	150
6.3.2 Groupings of Alloys toward Crevice Attack via "In Ocean" Testing	151
6.3.3 Combined Groupings of Alloys - Polarization vs "In Ocean" Testing	152
6.3.4 New Groupings of Alloys - Polarization vs "In Ocean" Testing	153

DEDICATION

This work is dedicated to
Parker, Chester, and Cricket.

1.0 INTRODUCTION

Stainless steels are normally iron-based alloys containing 10.5% or more chromium. These metals have been used for many industrial, architectural, chemical, and consumer applications for almost a half century. They have been used in a variety of environments including marine environments. Once a specific task is defined, the alloy required to meet the demand is selected using four key factors:

1. Corrosion resistance

2. Mechanical properties

3. Fabrication operations

4. Total overall cost

For stainless steels factors 1 and 4 seem to predominate in decision making. Type 316 stainless steel represents a good example of this selection process. Over the years Type 316 stainless steel has performed most consistently in hostile environments. With slightly more nickel than Type 304 and 2-3% molybdenum, Type 316 has been considered a solid performer and its use is widespread throughout industry. Unfortunately, this stainless steel, while considered

one of the most corrosion resistant of the austenitic stainless steels, has not performed consistently in total immersion in seawater. Reasons for the susceptibility of Type 316 to corrosion, particularly to crevice corrosion, are numerous and have been investigated thoroughly during the past twenty years. Many hypotheses have been put forth at symposia around the world. Recently, the United States Navy at the Naval Research and Development Center (NSRDC, Annapolis , Maryland) undertook a project to evaluate a large number of stainless steels and nickel alloys to compare these alloys' corrosion performance in seawater to Type 316 stainless.

Thirty-six wrought and nine cast commercial molybdenum-containing stainless steel and nickel alloys were gathered by NSRDC. These samples have been tested in one of the most comprehensive evaluation programs undertaken for open publication. Initial testing was done at Laque Center for Corrosion Technology, Wrightsville Beach, North Carolina under the auspices of Robert M. Kain. 1) Thirty day seawater immersion tests were conducted on these samples using crevice washers to create a crevice condition. Analysis of the results of these tests has been by both Laque and NSRDC, under Harvey P. Hack. 2) Both Mr. Kain and Mr. Hack concentrated on the immersion tests conducted at Laque. Parallel research, under the guidance of Professor R. M. Latanision

at the Massachusetts Institute of Technology, has evaluated these same alloys in a variety of laboratory conditions in order to compare the laboratory results to the immersion tests, to actual performance tests of the alloys, and to current literature synopses reported in professional journals and conferences.

Research at the Institute has concentrated on development of a consistent methodology which would lend itself to strong correlation with the current immersion tests and performance tests of said metals in the field. This program has included cyclic anodic polarization tests, constant potential tests with induced crevices, and Auger Electron Spectroscopy (AES). The results of this laboratory work is the basis of this analysis which, hopefully, will provide a common ground for further work.

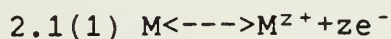
2.0 BACKGROUND

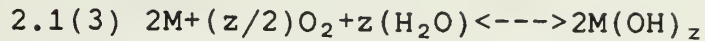
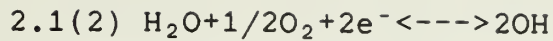
2.1 MECHANISM OF CREVICE AND PITTING CORROSION IN AERATED CHLORIDE SOLUTIONS

CREVICE CORROSION

Crevice corrosion is a form of localized attack that occurs within crevices or on shielded areas where a stagnant solution can occur. This is one form of what Pourbaix referred to as occluded cell corrosion (1). The model first postulated by France (2) and Fontana and Greene (3) and since modified by many investigators (4-8), is the most widely accepted and will be discussed in this section. Some of the parameters involved are shown in Figure 2.1.1 (9).

A stainless steel, when in an aerated neutral chloride solution, assumes a potential in the passive region where a small anodic current is balanced by a cathodic current resulting from the reduction of oxygen. Equations 2.1(1), 2.1(2), and 2.1(3) describe the general reactions. The product of these reactions can result in an increase in the thickness of the passive film (10).





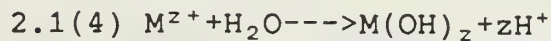
Tied to these equations, the model suggests a sequence of factors which leads to crevice corrosion initiation:

1. Depletion of oxygen in the crevice solution.
2. Increase in acidity and chloride content.
3. Breakdown of the passive film.

The reaction represented in equation 2.1(3) occurs over all of the surface of the metal. If a crevice is of such dimensions that the depletion of oxygen within the crevice is faster than the diffusion of oxygen from the bulk solution, then the crevice solution will eventually become totally deoxygenated. Once the crevice solution has been depleted of oxygen, the cathodic reaction necessarily takes place outside the crevice and a localized corrosion cell develops in which alloy dissolution proceeds within the crevice.

As the pH changes and the chloride content increases, the anodic reaction proceeds with the increase in concen-

tration of the metal ions, until the solubility product of the metal hydroxides is exceeded as described in equation 2.1(4). The deoxygenization also reduces the pH of the crevice solution.



The current required to maintain electric neutrality is primarily carried by the chloride ions (11), and this, coupled with the associated mass transport, leads to a build-up of the chloride concentration within the crevice.

When the crevice solution reaches a point where the passive film begins to breakdown, rapid localized corrosion results. The composition of the crevice solution at this point is termed the critical crevice solution (CCS), typically having a pH of between 1 and 2 and a chloride concentration in excess of 6N (12). It is important to realize that the CCS varies with the alloy and/or environmental conditions. Several investigations are presently being pursued to determine these values experimentally (13).

Thus far the electrochemical aspects have been discussed. Other factors which also seem to have an impact on crevice corrosion are the thermal and processing history of the material. The surface preparation also has an influ-

ence on the crevice, as acknowledged by both Rowlands and Oldfield, who incorporate factors for surface preparation in their crevice corrosion models (14&15).

Another factor in crevice corrosion initiation is the geometry of the crevice. Historically the consensus has suggested that a shallow and open crevice is desirable in order to minimize the occurrence of localized corrosion. A critical depth-gap dimension combination must exist for the crevice to become active. This geometry controls the localized environment; that is, the initiation site is subject to changes in environment such as deaeration, acidification, and Cl^- ion concentration. This concept is integral to any crevice analysis (16). In all situations, however, questions can be raised as to the role that factors such as geometry play. Suffice it to say that a case can be made for this factor qualitatively, but quantitative measurement has been inconsistent.

Once the onset of rapid corrosion is attained, the dissolution of the alloy inside the crevice is balanced by oxygen reduction outside the crevice and/or by hydrogen evolution within. Continued growth and activation is the case until some new factor is introduced or the local chemical environment is altered.

PITTING CORROSION

The mechanism of pitting follows the lines of crevice corrosion except for differences in initiation modes. Equations 2.1(1)-2.1(3) give the overall reaction picture. Pits may be initiated at inclusions, second phases, regions of compositional heterogeneity, and structural heterogeneities at the surface (17-19).

Pitting corrosion initiation is harder to define due to the difficulty in the identification of an initial site location. On the other hand, for many metals the critical pitting potential is known, making the occurrence of pitting fairly easy to define compared to crevice analysis.

Another factor that controls the initiation of pitting corrosion is the pH of the site. Below a certain pH localized corrosion is prevalent, while above a certain pH some form of passivation occurs. Inside a certain range pitting occurs. Mapping of this phenomenon is common using Pourbaix diagrams.

The concept of a critical pitting potential has been used in connection with the pitting process. This is the potential above which pitting initiates and propagates, but below which pitting does not occur. The pitting potential

was used to describe the initiation of pits in metals with perfect surfaces (free from inclusions, compositional heterogeneities, etc).

An understanding of the combined mechanism of pitting and crevice corrosion is one objective of this analysis. Both problems must be addressed. Stainless steels which are increasingly resistant to chloride-induced pitting and crevice corrosion, combined with the resistance to generalized corrosion and erosion in a marine environment, are appealing.

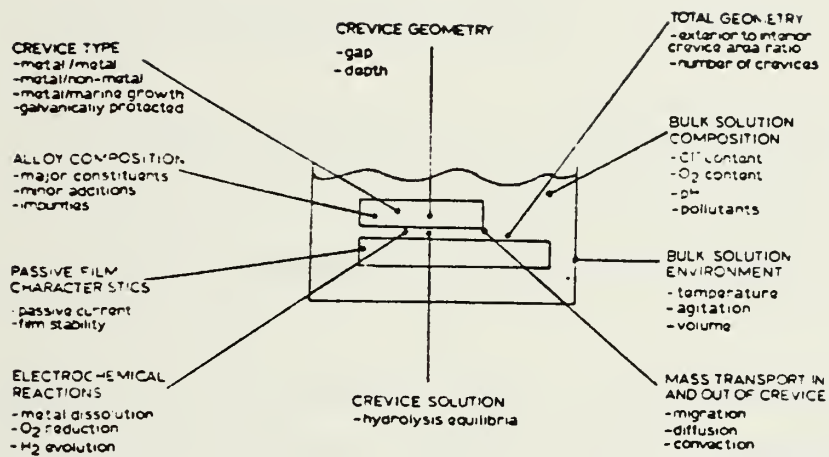


Figure 2.1.1 Parameters of Localized Corrosion

2.2 PASSIVITY

The passive behavior of metals has been studied for almost 200 years, and there still exist widely variant theories on the fundamentals of passivity. Uhlig (20) has proposed two definitions of passivity:

1. A metal is passive if it substantially resists corrosion in a given environment resulting from marked anodic polarization.
2. A metal is passive if it substantially resists corrosion in a given environment despite a marked thermodynamic tendency to react.

These two definitions may, in one instance or another, describe two possible general areas of passive behavior. Many different disciplines have been incorporated to elucidate the nature of the passive state, within the context of Uhlig's definitions.

As described in Section 2.1, stainless steels lose their passive properties in environments containing chloride ions and in conditions that allow the build-up of chloride and hydronium ion concentrations. In the process of attempting

to describe passivity, four theories have survived in one form or another:(21)

1. Metal modification
2. Reaction velocity
3. Oxide film (structured vs. amorphous)
4. Adsorption

These theories have been challenged and modified over the years and gradually they have become intermixed. For example, the first two theories have been incorporated to some extent into parts of the latter two theories.

In the case of stainless steels a variety of acceptable techniques has been used to study the nature of the passive film. It must be remembered that the nature of the experiment may not only depend on the particular environment (Cl^- concentration, potential), but the structure may also be affected by the technique used.

Chemical analysis and spectroscopic studies have revealed that the primary constituent of the passive film is some form of oxide of chromium, most probably an

oxy-hydroxide (22-25). Ellipsometric (26) and Auger electron spectrographic analysis shows a definite increase in film thickness with increasing applied anodic potentials, with a possible transition between an adsorbed layer and an oxide film (27). Recent ESCA, Auger, and low energy scattering techniques reveal that chromium is always enriched, and that the degree of enrichment varies directly with the amount of chromium in the base metal (28).

Alloying elements have been consistently linked to the variations of the passive film structure. Some elements seem to have a greater effect than others. Studies of the passive film structure of ferritic stainless steels formed in NaCl have revealed a stratified film structure with a total thickness of 10 atomic layers. The composition profile of iron in the film shows a deep minimum in the middle of the film and a marked increase near the oxide-solution interface. There is a narrow zone inside the film which is composed only of chromium oxide, behind which molybdenum rises to a level equal to its concentration in the alloy (29). Other alloying elements such as Ni have also been found to be components of the passive film, but their role in the passivation process is not exactly known (30), and there have been several conflicting reports in the literature in this regard.

An amorphous passive film structure exhibiting lower current densities, less susceptibility to breakdown and easy to repassive, has been described by Revesz and Kruger (31). Films formed in 1N H_2SO_4 on stainless steels of various Cr contents varied from well-oriented spinel structures (0-5% Cr) to amorphous (19% Cr). Amorphous character may be due to the formation of a mixed oxide of Fe and Cr, which generally have some amorphous character. Passivating films on stainless steels contain a substantial amount of water which exerts influences on the physical and chemical properties of the film (31). In halide environments, a competition for incorporation into the passive film between the halide and water may occur (32).

In recent years more sophisticated methods have been used to observe the passive film in a corrosive environment. "In situ" modulation spectrographic investigation of Fe-Cr alloys in 1M Na_2SO_4 has shown a change in composition of the passive film above approximately 20% Cr. The passive film of Fe-20Cr alloys was determined to be Cr (III) oxyhydroxide containing small amounts of ferric ions (33).

Passivity and the electrochemical process are tied together with the traditional schematic polarization curve. In the context of this study, a consideration of the potential-current density diagram shown in Figure 2.2.1, gives an

electrochemical appreciation of the concept of passivity. When the applied potential is increased from E_{corr} in the noble direction and the current density is recorded, a dramatic decrease in current density is observed after the primary passivation potential is reached (E_{pp}). A low current density, I_{pass} , is reached and remains low (although not necessarily constant) over a range of potentials, dependent upon the stainless steel/environment combination. This passive state is maintained until the onset of gaseous oxygen evolution or, in the case of chloride containing solutions, when the passive film breaks down, with the possible formation of pits (E_p). This behavior demonstrates Uhlig's first definition of passivity. Closer examination of the potential-current density diagram may reveal transient current excursions or a variability in the pitting potential, which tends to support Uhlig's second definition.

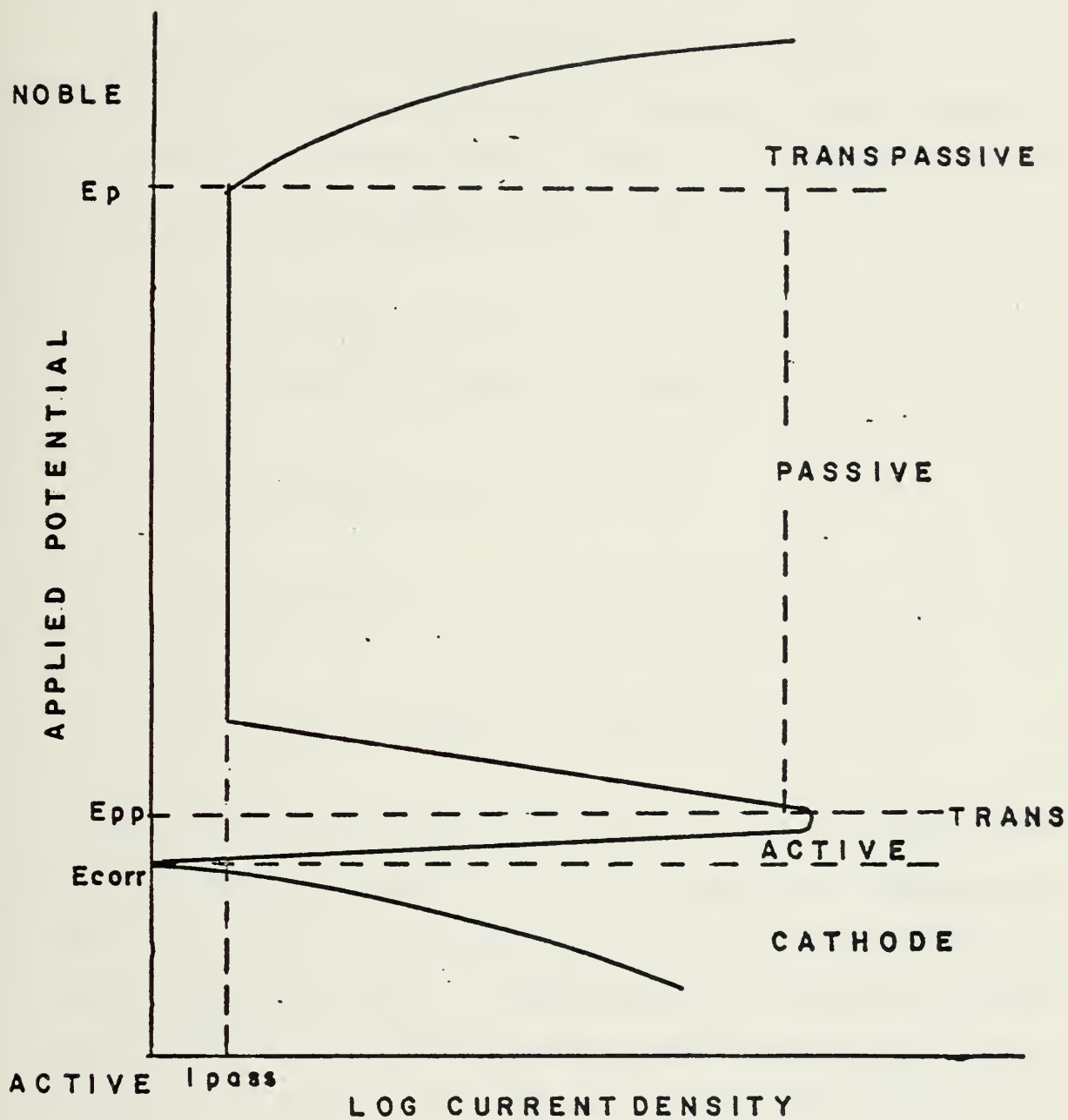


Figure 2.2.1 Schematic Polarization Curve

2.3 BREAKDOWN OF PASSIVITY AND REPASSIVATION

As mentioned in the previous section, a crucial step in the sequence of localized corrosion depends on the breakdown of passivity. Experimentally determined conditions for initiation of this breakdown are (33-34):

1. A critical solution composition around the site of localized corrosion.
2. A critical potential.
3. An induction time before breakdown.
4. Occurs at highly localized sites.

Any theory of localized corrosion postulated must be able to explain passivity or its breakdown encompassing these four points. The breakdown may proceed by mechanical and/or chemical means. Mechanically, a film on the base metal reaches a critical stress depending upon the innate properties of the film and solution and the variation of surface tension brought about by halide ions or potential gradients (35-38). A similar model considers the effect of mechanical properties of the film by ion interaction with

electron orbitals of the species in the film (modeling passive film as a p- or n- type semiconductor) (39-40).

In a chemically induced breakdown, the passive film is in equilibrium with an activated state and relative reaction rates must be considered. Reactions not only involving the passive film, but also with the base metal and with cations disassociated with the base metal, come into play. It is with this dynamic equilibrium of a passive/non-passive state, and these reactions that the greatest amount of effort is being expended to determine precise mechanisms, especially regarding alloying effects (41-53). Kolotyikin and Uhlig have suggested an adsorbed ion displacement model (54) where the adsorbed monolayer of oxygen is displaced by the damaging ion (Cl^-). This model explains the critical pitting potential as the potential above which Cl^- ions adsorb on the surface.

Richardson and Wood (55) have proposed an ion migration or penetration model requiring the penetration of damaging anions through the passive film, and have concluded that a breakdown does not occur at all because there will always exist microscopic pores and defects through which the anions can migrate. Anion lattice migration models, with migration via defects or by a process of ion exchange, have been proposed by Hoare (56).

Another distinguishing point with respect to theories is electrochemical, where the actively corroding pit or crevice operates in the diffusion vice kinetic regime. Most active sites spontaneously repassivate because of their operation in the diffusion regime where only a slight cathodic shift in potential is required for repassivation. They operate in the diffusion regime as the result of the relatively limited volume at the localized corrosion site. From these facts it has been proposed that, with regard to pitting, the repassivation potential cannot serve as a parameter characterizing the ability of the steel to corrode (57).

In the real life problem, a combination of mechanical and chemical mechanisms probably exists, as well as the introduction of other variables such as inclusions, surface finish, temperature, etc. (58).

A recent study by Smialowska, et al. suggests that the chloride ion is not incorporated into the passive film during the breakdown of passivity in chloride-containing environments (59).

Xps studies by Hashimoto, et al. on the breakdown of passivity of 19% Cr ferritic stainless steels in 1N HCl concluded that a passive film when formed is not uniform, but contains micropores, which are repeatedly formed and

repassivated. Repassivation was preceded by the formation of chromium oxy-hydroxide. The increase of the chromium content in the alloy interferes in the development of pits by increasing the rate of repassivation. Macro- and micro-heterogeneities based on crystalline defects in the alloy surface were judged responsible for active surface sites (60).

2.4 CYCLIC ANODIC POLARIZATION AS A MEANS FOR MEASURING THE TENDENCY FOR LOCALIZED CORROSION.

In the quest for an accelerated laboratory test for localized corrosion resistance, a wide range of methods have been considered as useful in alloy evaluation (61-79). While there probably does not exist a totally satisfactory method to rank steels in resistance to localized corrosion, arguments can be made for screening tests which give a relative performance indication. The difficulties in any technique are the many variables to consider, and so a variety of data must be gathered to develop a body of knowledge to help explain the mechanisms involved. As a first step in the studies conducted, cyclic anodic polarization data was generated for the alloys under investigation.

Figure 2.4.1 shows a generalized cyclic anodic plot (80). In the case of pitting, the more noble the value of E_p or the greater the value of $E_p - E_{corr}$ the greater the pitting resistance. Figure 2.4.1 shows three values of E_{corr} , corresponding to decreasing values of $E_p - E_{corr}$ as one proceeds from E_{corr_1} to E_{corr_3} .

For crevice corrosion Wilde (81) has shown that $E_p - E_x$ can be correlated with natural crevice corrosion weight loss after long-term exposures to seawater. The area of the

hysteresis loop can also be used in determining crevice corrosion resistance (82).

Over the past few years, particular attention has been given to polarization methods. Intensive efforts are now being extended to the rational interpretation of polarization diagrams. NACE Panel T-32-10 is responsible for the standardization of terminology and interpretation methods. Presently, this panel is involved in collecting information on rapid scan rate (60V/Hr) polarization of stainless steels in 1N H_2SO_4 so that a statistical analytical method may be applied and correlations can be made. Results of these studies will not be available for some years to come.

Recent studies by P. E. Morris at INCO Research Laboratories, New York have accumulated approximately 14,000 polarization diagrams of this type and has developed a rational procedure utilizing logic circuit diagrams to predict the behavior with a high degree of reliability of high nickel alloy steels (83).

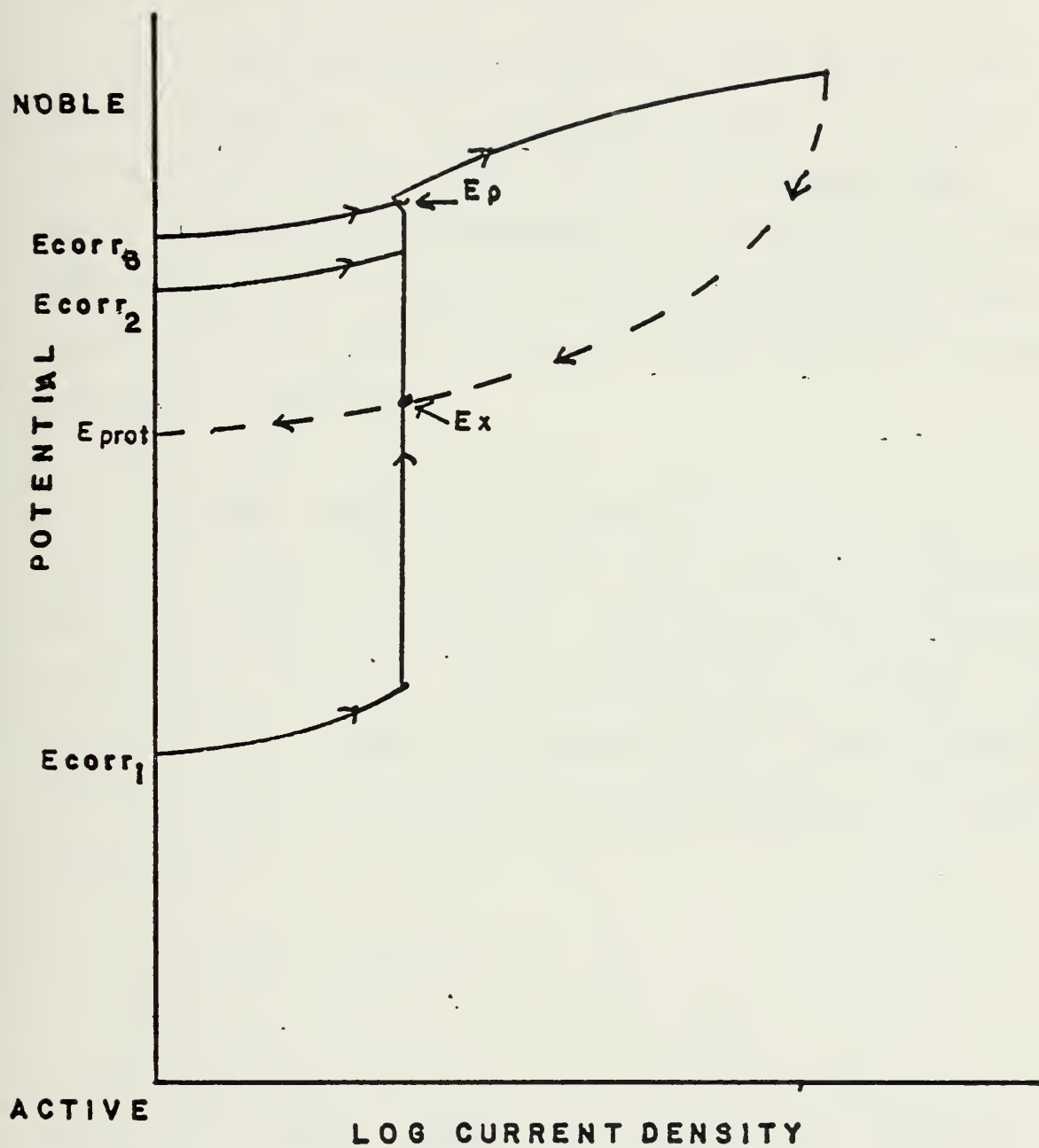


Figure 2.4.] Identification of Key Parameters

2.5 AUGER ELECTRON SPECTROSCOPY

Auger electron spectroscopy(84) has been of great use to vacuum physicists and surface scientists in studies of gas-solid reactions. More recently, AES has been used as a means of examining the chemistry of the passive film formed electrochemically, although certain reservations must be borne in mind, since AES cannot be used "in situ" in electrochemical experiments.

The Auger process is illustrated in Figure 2.5.1. An electron vacancy is created in the w-band by irradiation with low energy electrons. The electron from the x-band fills the vacancy and coulombically transfers the de-excitation energy to a y-band electron which is ejected from the sample and detected as an Auger electron of kinetic energy E_{wxy} .

$$E_{wxy} = E_w - E_x - E_y - \phi$$

Since kinetic energy is a function of the material's electronic energy levels, a qualitative analysis is possible. The core electron vacancy is produced by bombarding the sample with a 3-10 keV beam. The emitted electrons are analyzed using a retarding field energy analyzer or a cylindrical mirror analyzer. Because of the high background

signal from incident electrons, the background signal must be removed by electronic differentiation, and spectra are reported in $dN(E)/dE$ vs E coordinates.

The AES technique allows elemental profiling normal to the surface by noble gas ion sputtering. The depth of penetration by AES is approximately 10Å and resolution as the order of 50 nanometers (85-86).

AES studies of the composition of the passive film and of the localized active corrosion site have recently been reported (87-90). Because of the experimental difficulties in analyzing specimens that have been electrochemically treated in aqueous electrolytes, Olefjord and Elfstrom have reported the construction of an electrochemical cell that is directly attached to the AES sample chamber (91). This procedure allows the minimization of contamination of the sample and prevents oxide films from developing during transfer. The procedure described above has provoked new questions concerning sample preparation. Previously the controlling path to good Auger analysis was the factors time and cleanliness during the post-corrosion period just prior to sample introduction into the AES system. Now a poorly prepared sample is a much bigger problem.

In general every evaluation tool seems to have its good points and drawbacks. Using AES the drawbacks include:

1. Possibility of selective sputtering.
2. Relative sensitivity among elements to the incident electron beam leading to inaccurate quantitative analyses.
3. At relatively low chromium contents there is a general overlapping of the Cr 529 eV peak and the oxygen 510 eV peak blurring evaluation. The Mo and Sulfur and Argon peaks also have overlapping problems.

These drawbacks must be considered when interpreting the results from an AES experiment. For instance, a comprehensive study of selective sputtering and the relative sensitivities of Fe-Cr alloys by Frankenthal and Thompson came to the following conclusions(92):

1. Fe-Cr alloy surfaces do not undergo preferential sputtering when sputtered by Ar and Ne ions.
2. Adsorption of traces of carbon monoxide onto the surface leads to an apparent decrease of the

chromium content of the surface layer, the observed decrease in Cr/Fe composition ratio being directly proportional to the oxygen peak height.

3. Fe_2O_3 and Cr_2O_3 are both reduced by ion bombardment.

4. The relative sensitivity factor for iron, chromium, and their alloys is independent of alloy composition, when corrections are made for the molar volume.

Recent developments in digital processing and microcomputer technology have vastly increased the capabilities of AES, in that the spectra of many scans may be more accurately analyzed and compared quickly to previous results. Ease in processing created by these breakthroughs would seem to indicate a tremendous opportunity for more standardization in research.

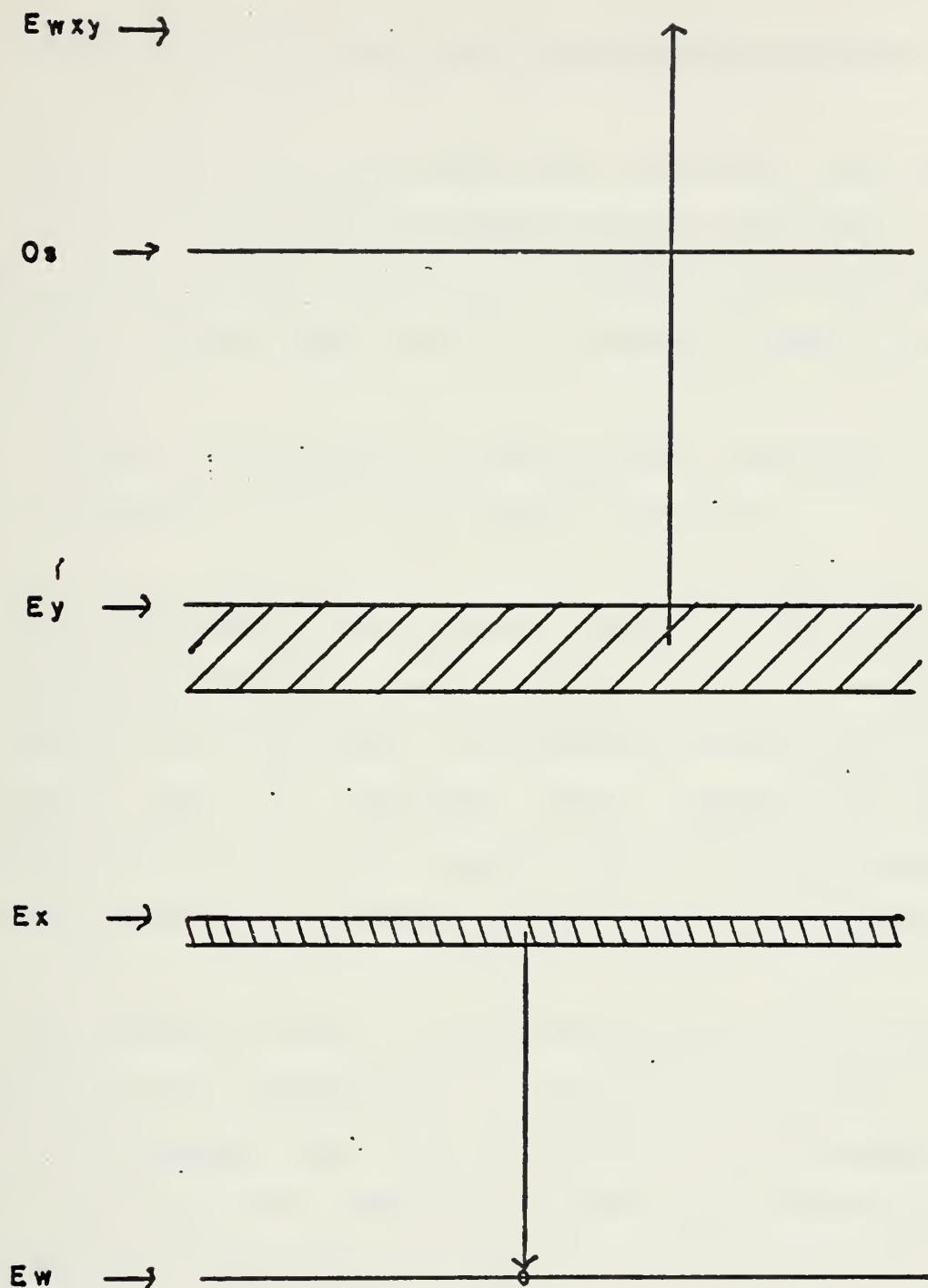


Figure 2.5.1 Auger Electron Generation

3.0 MOTIVATION AND OBJECTIVES OF EXPERIMENTAL RESEARCH

Uhlig, Sato, and many others have thoroughly researched the topic of localized corrosion during the past fifty years. Many theories have been proposed, some have been dismissed. Research has come to one definitive conclusion:

There is no one specific condition for localized corrosion. It is a very complex situation.

One would expect group consensus on the various theories and there has been some. Generalizations can be drawn about the subject and expanded to include theories relating to passivation and its breakdown. These subjects have been reviewed in the previous chapter and will be incorporated into the analysis of the experimental results in Section 5.

The approach used in this research has been linked to Type 316 since replacement of this stainless steel in a marine environment was the motivation for this analysis. From the forty-five commercial grade test samples, six groupings were made and are listed:

Group I : Austenitic stainless steels with
6 to 16% Nickel

Group II: Austenitic stainless steels with
17 to 40% Nickel

Group III: Alloys with >40% Nickel

Group IV: Duplex Austenitic - Ferritic alloys

Group V : Ferritic stainless steels

Group VI: Cast stainless steels

The results of the "in ocean" testing were cataloged by Harvey P. Hack using similar groupings in comparing alloy performance (112). Actual test results did not completely correlate along these lines, but as a starting point these groupings seemed reasonable. A complete list of alloys evaluated and their composition is shown in Tables 3.1 to 3.6.

Using these alloys, several key issues were considered:

1. Does the effect of alloying on the film breakdown manifest itself by altering the nature of the film, environment, or the base metal?
2. What is the role of passivation in breakdown?

3. Can the cyclic polarization data be generated in an efficient and reproducible manner?
4. Can definitive conclusions be drawn from polarization diagrams with respect to a metal's tendency towards localized corrosion. That is, can the values of E_{corr} , E_p , E_x , E_p-E_x , etc. be used to construct a relative listing of the tendency to corrode?

As mentioned before, different schools of thought exist relating to these issues. Scores of articles have been written on each subject over the years. It is time now to begin a detailed, comprehensive, all inclusive study using all the latest, standardized, up-to-date procedures. This study represents a modest contribution, but also a solid point of departure for continued research.

Table 3.] - AUSTENITIC 6% to 16% NICKEL ALLOYS

Alloy	Composition (wt %)							Other			UNS No.	Other Common Designations
	Cr	Ni	Mo	Mn	C	Si	S					
T316	17.5	10.7	2.4	1.60	0.04	0.52	0.004	0.03 P	-	0.28 Cu	S31600	-
34LN	16.8	13.76	4.21	1.57	0.03	0.52	0.004	-	0.14 N	-	-	-
T216*	20.	6.	2.5	8.	0.08	1.	-	-	0.35 N	-	S21600	XM-17
Rex 734	21.32	9.44	2.67	3.81	0.04	0.26	0.005	0.30 Nb	0.42 N	0.0025 B	-	-
T317L	18.92	12.25	3.58	1.71	0.025	0.20	0.009	0.035 P	0.056 N	-	S31703	832SNR
317 LH	19.52	14.52	4.08	1.32	0.016	0.40	0.025	0.28 Co	0.056 N	0.16 Cu	-	-
317H+	18.30	15.80	4.25	1.49	0.010	0.63	0.006	0.16 Co	-	0.16 Cu	-	-
22-13-5	21.08	13.70	2.28	4.81	0.045	0.47	0.025	-	-	-	S20910	XM-19, Nitronic 50
* Nominal												

Table 3.2 - AUSTENITIC 17% TO 40% NICKEL ALLOYS

Alloy	Composition (wt %)							Other	UNS No.	Other Common Designations
	Cr	Ni	Mo	Nb	C	Si	S			
904L	20.5	24.7	4.7	1.46	0.014	0.46	0.005	-	-	-
4X	20.15	24.38	4.44	1.45	0.014	0.57	0.001	0.19 P	-	AL-4X
700	20.70	25.20	4.45	1.65	0.013	0.42	0.008	0.28 Nb	N08700	Jessup 700
254 SIX	19.9	25.0	4.67	1.64	0.011	0.45	0.003	-	N08904	-
777	20.80	25.6	4.48	1.37	0.023	0.48	0.013	0.24 Nb	-	Jessup 777
254 SMO	20.0	17.9	6.1	0.49	0.013	0.41	0.008	-	-	-
6X	20.35	24.64	6.45	1.39	0.018	0.41	0.001	-	-	AL-6X
20 Mod	21.58	25.52	4.95	0.90	<0.01	0.49	-	-	N08320	Haynes 20 Mod
20 CB-3	19.36	33.22	2.15	0.44	0.020	0.36	0.002	0.51 Nb	-	-
20 Mo 6	23.91	33.44	5.65	0.44	0.031	0.35	0.007	-	-	-
254 SFER	29.4	22.2	2.13	1.72	0.016	0.30	0.001	-	-	-

Table 3.3 - AUSTENITIC >40% NICKEL ALLOYS

Alloy	Composition (wt %)							Other	UNS No.	Other Common Designations
	Cr	Ni	Mo	Nb	C	Si	S			
825	22.02	44.03	2.74	0.35	0.01	0.07	0.004	0.70 Ti	N08825	Incoloy 825
G	22.22	46.84	5.78	1.52	0.007	0.43	-	1.66 Cu	N06007	Hastelloy G
G-3	22.76	43.69	7.01	0.82	0.006	0.37	-	1.85 Cu	-	Hastelloy G-3
625	22.29	61.02	8.48	0.10	0.03	0.24	0.001	2.07 Nb	N06625	Inconel 625
C-276	15.51	54.72	15.49	0.46	0.003	0.04	-	0.19 Nb	N10276	Hastelloy C-276
								3.57 Nb+Ta		
								0.11 Cu		
								1.89 Co		
								1.27 Co		
								3.49 Co		
								Bal Fe		
								1.85 Cu		
								0.28 W		
								0.95 W		
								0.24 Ti		
								3.82 W		
								-		
								1.85 Cu		
								1.85 Cu		
								1.66 Cu		
								Bal Fe		

Table 3.4 - DUPLEX AUSTENITIC-FERRITIC ALLOYS

Alloy	Composition (wt %)						Other	UNS No.	Other Common Designations
	Cr	Ni	Mo	Mn	C	Si	S		
T329	26.98	4.22	1.39	0.28	0.052	0.39	0.014	-	0.09 Cu
441N	25.0	5.9	1.46	1.75	0.028	0.53	0.003	-	0.19 N
Ferrallium	26.15	5.64	3.20	0.77	0.02	0.37	-	0.16 Co	0.19 N
									1.75 Cu

- FERRITIC ALLOYS

Table 3.5

Alloy	Composition (wt %)							Other			UNS No.	Other Common Designations
	Cr	Ni	Mo	Mn	C	Si	S					
T439	17.66	0.31	0.03	0.26	0.047	0.70	0.010	1.68 Al	-	0.40 Ti	S43035	18-SR
T444	18.92	0.07	1.99	0.43	0.020	0.56	0.004	0.020 P	0.012 N	0.13 Ti	S44400	17-2
26-1	25.9	0.13	1.00	0.10	0.002	0.29	0.015	0.010 P	0.006 N	-	S44627	XM-27, E-Brite 26-1
26-1S	25.05	0.15	0.96	0.17	0.054	0.16	0.011	0.015 P	0.009 N	1.06 Ti	S44626	XM-33
29-4	29.6	0.07	4.00	0.10	0.003	0.04	0.011	0.013 P	0.012 N	-	S44700	-
29-4C	28.85	0.79	3.81	0.22	0.012	0.19	0.002	-	0.026 N	0.59 Ti	-	-
29-4-2	29.5	2.20	3.95	0.10	0.002	0.10	0.010	0.010 P	0.013 N	-	S44800	-
SC-1	25.56	2.14	2.94	0.20	0.01	0.25	0.004	0.04 Al	0.016 N	0.51 Ti	S44660	SeaCure
Nonit	25.3	4.1	3.8	0.43	0.012	0.31	0.006	0.37 Cu	-	-	S44635	-

Table 3.6 - CAST ALLOYS

Alloy	Composition (wt %)							Other	UNS No.	Other Common Designations
	Cr	Ni	Mo	Mn	C	Si	S			
CA6N	12.44	8.0	-	0.18	0.02	0.64	0.013	0.010 P	-	-
CF8M	19.30	10.05	2.36	0.95	0.04	0.79	0.019	-	J92900	Cast T316, ESCO 33 G
IN 862	20.92	24.46	5.00	0.47	0.03	0.52	0.009	0.007 P	-	-
CN7MS	19.37	22.10	2.93	1.00	0.05	3.00	0.010	0.006 P	J94650	Worthite
CN7H	20.01	28.18	2.51	0.18	0.04	0.76	0.025	0.007 P	J95150	Alloy 20, ISA 20
625	20.58	63.7	8.53	0.02	0.02	0.01	0.011	0.006 P	-	-
CW 12M-2	18.10	62.8	17.58	0.54	0.01	0.56	0.007	0.010 P	-	Illium W-2, Chlorimet 3
Illium PD	24.55	5.39	1.97	0.86	0.04	0.80	0.016	0.004 P	-	-
Ferrallum ^{Al}	25.2	5.2	2.5	1.	-	1.10	-	-	-	-
* Nominal										

4.1 SAMPLE PREPARATION AND MOUNTING

4.1.1 CYCLIC POLARIZATION

The stock material was first degreased in acetone, scrubbed with a bristle brush, rinsed with water, and dried. Coupons of approximately 1cm by 1cm were cut from sample plates varying in thickness from 1/8 to 1/2 inches using a carbide-bladed saw (Discotem with type 03-TRE blades). These coupons were then polished on all sides and measured with a micrometer for an accurate determination of surface area. A stainless steel wire (Wire 20425 alloy metal) was then spot welded onto the coupon. A Raytheon Weldpower Model 60c spotwelding machine was used. The parameters for the spotwelding process were:

- 1.Parallel-full transformer connection
- 2.Heat setting = 6 to 9
- 3.Capacitance = 56 microfarads
- 4.Input = 42 watts-sec., short pulsed from 1-s powerhead.

Initially there was concern regarding possible thermal effects from the welding operation. With the welding machine configured as above, the minimum time for the current pulse was achieved and no noticeable burning was evident. Great care was taken to minimize heat input to the sample. Initial soldering and spotwelding gave both inconsistent attachments and excessive heat (too hot for touch). Only this spotwelder seemed to provide minimum heat, the sample never being too hot to touch. The weld time appeared to be the key factor to attain to minimal heat.

To isolate the wire, a 1/32 inch ID Tygon tubing sheath was drawn over the wire and firmly positioned close to the coupon. Half-inch length sections of schedule 40 PVC pipe were prepared and a 3/32 inch hole drilled to accommodate the wire. In other environments PVC piping would be unacceptable due to chloride content, but the medium used contained a high chloride concentration, negating the influence of the PVC pipe.

The sample, with wire attached, and the pipe section were placed on double sided adhesive tape over a plate glass and a dam of plasticine was built up around the pipe as shown in Figure 4.1.1. Miller-Stephenson Epon epoxy 825 resin and teta (Triethyenetetramine) curing agent were heated to 80 degrees Centigrade in a Precision Scientific Oven,

Model 104 with digital controller and were mixed in 11:1 proportions (epoxy:teta) while still hot and poured into the molded assembly soon after mixing. Care was taken during the pouring operation and before the epoxy had set (10 - 15 minutes) to minimize the development of bubbles adjacent to the sample. During the initial pourings of the epoxy, bubble formation was a major problem since these locations tended to become crevice corrosion sites. A 70% failure rate was common initially. Later batches done under improved conditions had less than a 20% failure rate. Initial runs were examined with a microscope to check for inclusions and voids. After refining the sample mounting procedure and obtaining consistent polarization data, the confidence level was increased to a point where the microscopic inspections were phased out.

When the epoxy had cured to a tacky consistency the samples were placed in a preheated oven (approximately 70 degrees Centigrade) and allowed to cool in the oven for 2 hours.

When the epoxy had cured completely, the mold was removed from the adhesive tape and the entire assembly thoroughly cleaned with distilled water and ground with 240/320 grit and rinsed again with distilled water and reinspected for inclusions. The acceptable samples were then stored in

air-tight bags. Immediately prior to the polarization experiment, the specimen was ground using Sic grinding wheels up to 600 grit (Carbimet grinding paper -Buehler Ltd:120/240/320/600 grit), followed by a rinsing in distilled water and then transferred to the electrochemical cell. Figure 4.1.2 shows the details of the mounted specimen. To insure maximum stability of the sample during polarization, the Tygon tubing of sample mount was drawn through a pyrex glass tube of proper size. This Pyrex tube was in turn placed in a rubber stopper and secured in the center of the flask.

The above described sample mounting procedure was used for several reasons. First, the relatively large PVC pipe/epoxy mount made grinding and inspection easier. Second, although a major effort was made to develop a system to minimize microcrevices, previous studies (93-94) indicated the complete elimination of microcrevices was not practical, and perhaps not warranted. Finally, this system of mounting prevented accidental exposure of the specimen during handling.

In a comparison of cyclic polarization data generated by Asphahani using ASTM procedures, the data obtained correlated well as seen in Figures 4.1.3 and 4.1.4.

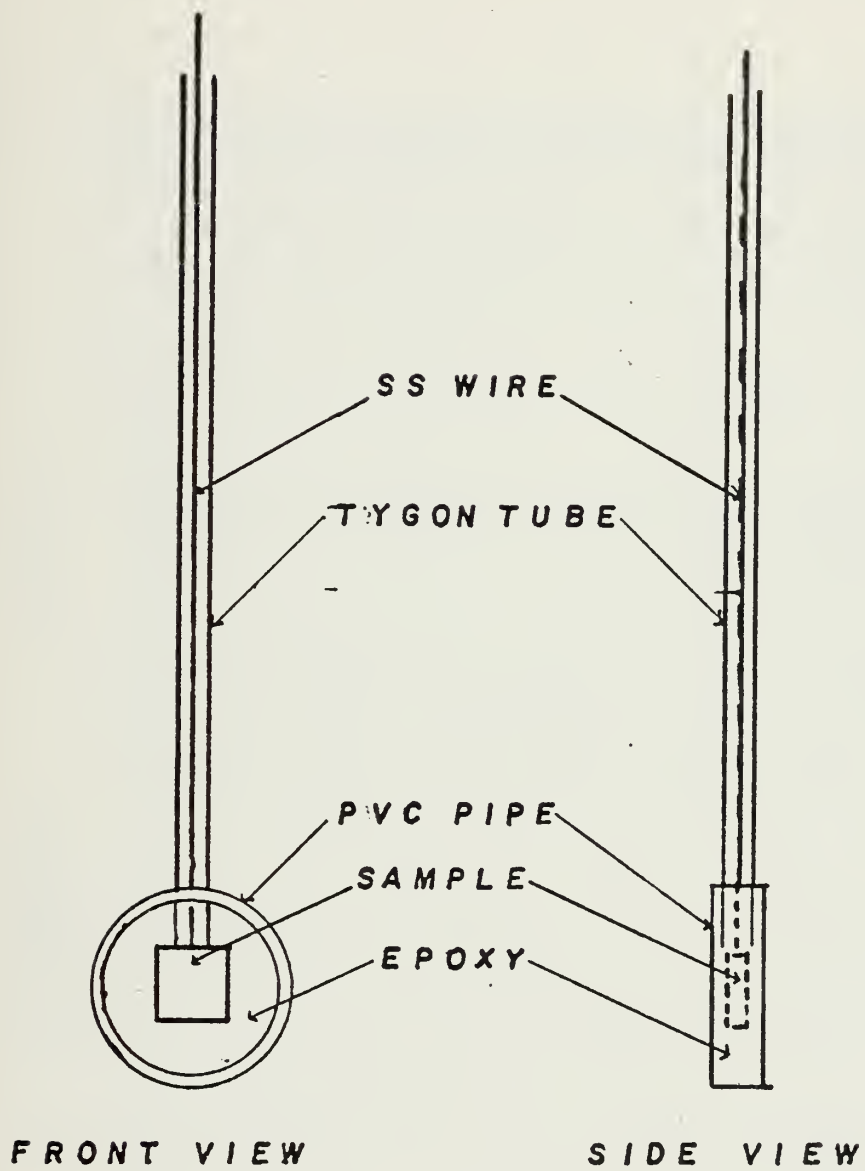
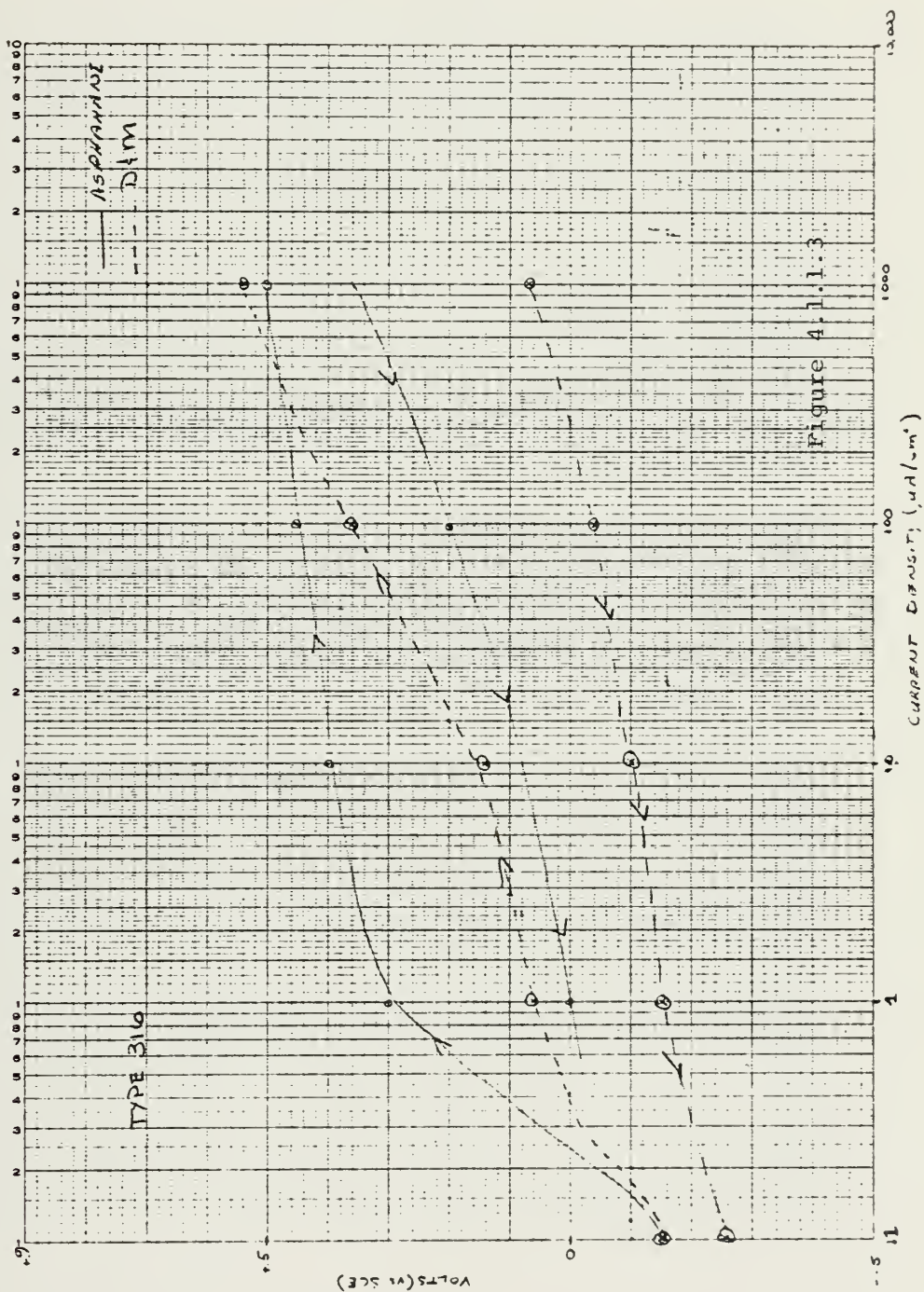


Figure 4.1.1.2 View of Mounted Sample

NO. 340-LS10 DIETZEN GRAPH PAPER
SEMI-LOGARITHMIC
5 CYCLES X 10 DIVISIONS PER INCH

DIETZEN CORPORATION
MADE IN U.S.A.



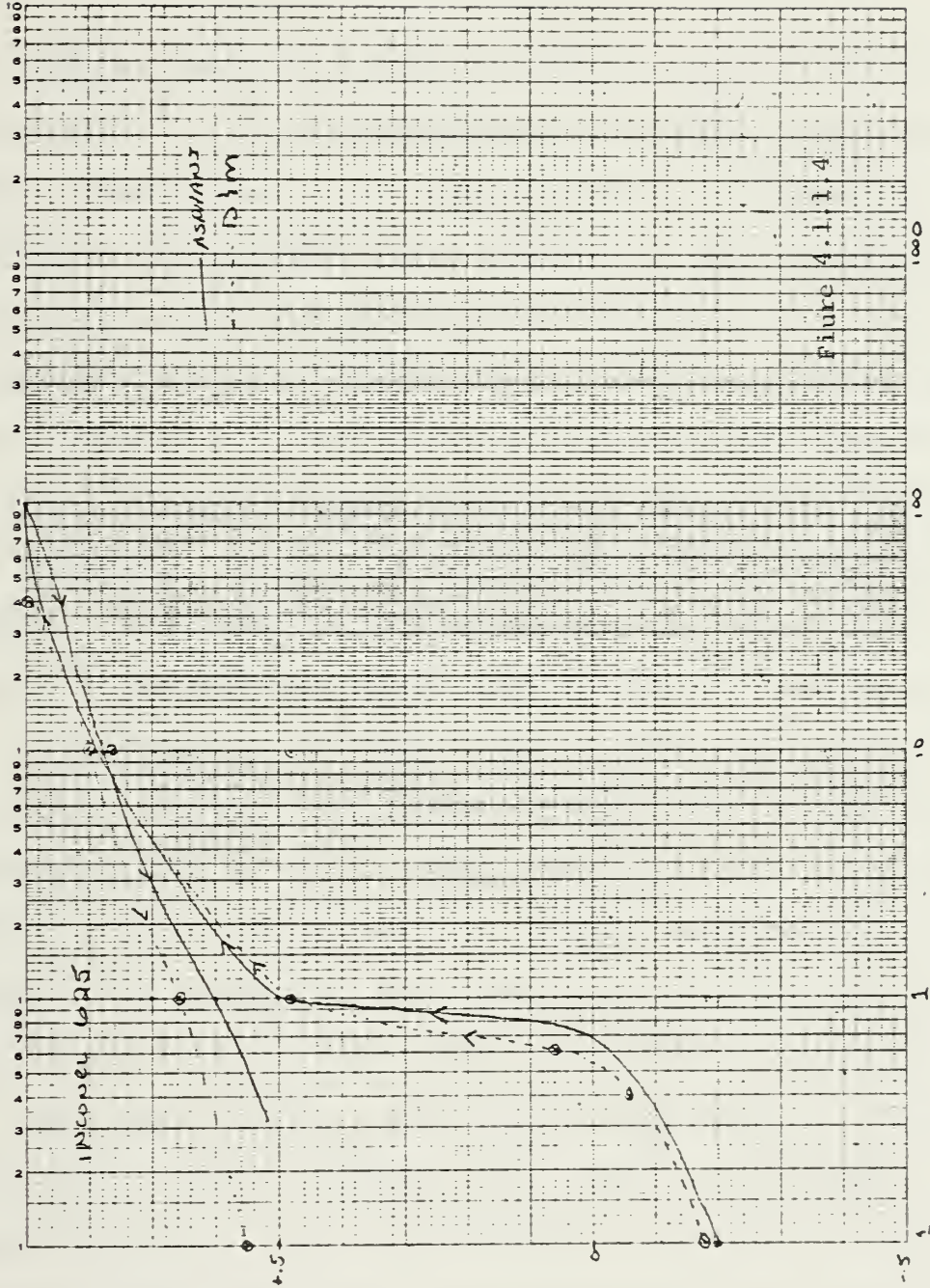


Figure 4.1.1.4

4.2 ELECTROCHEMICAL POLARIZATION TECHNIQUES

4.2.1 ELECTROCHEMICAL CYCLIC POLARIZATION

Samples were prepared according to procedures described in Section 4.1. Each mechanically polished sample was placed into a corrosion cell illustrated in Figure 4.2.1. The corrosion cell vessel was a standard 3-necked 1000 ml boiling flask. The test solution was 4% by weight of NaCl using laboratory distilled water that had been aerated by bubbling pure Oxygen for one hour prior to use. This solution was chosen after a literature search and is similar to that used by Asphahani (95). The electrolytic cell consisted of the sample, a calomel electrode, and a platinum counter electrode. A Luggin-Haber probe with bridge was used to minimize IR drop between the sample and the reference electrode. The distance between the sample and the platinum electrode was approximately 5 cm , which would lead to an estimated IR drop of less than 5mV. The counter electrode was mounted behind the sample so that there was no direct path between the two. This situation was demonstrated to have no effect on the polarization data generated by placing the counter electrode facing directly in front of the sample in test experiments. It was concluded that the conductivity of the solution made the counter electrode positioning an insignificant factor. The pH of the test solution varied between 6.5

to 6.8. The temperature of solution was 21-23 degrees Centigrade.

After immersion of the sample, a working-sense lead was connected to the sample to eliminate errors in controlled potential caused by IR drops in the working electrode. The leads from the potentiostat were connected and the open circuit potential of the samples was determined and recorded. The sample was then polarized to -0.5V, then scanned anodically from -0.5V to -0.9V (SCE), whereupon the scan direction was reversed and run back to -0.5v (SCE). The potentiostat used was an AIS (Floyd Bell Associates, Inc) Model V-2LR, using the potentiostatic mode. A logarithmic converter was used for the plotting of the output current. Plots were recorded on a MFE Model 815m Plotmatic X-Y Recorder on semilogarithmic plotting paper. The potential scan was controlled by an AIS (Floyd Bell Associates) Model Scan-3 Electronic Potential Scanning Unit. Scan rate was 0.6V/Hr with settings as follows: scan range 1.40, scan rate 1.29, scan rate multiplier 0.1. A slow scan rate was selected based on evaluations of various techniques reported in references (96-99).

Approximately 700ml of fresh solution was used in each experiment. The solution was not stirred, and this may have had an effect on the occasional current excursions detected

in the same experiments, which will be discussed in more detail in Section 6.6.

A typical scan experiment lasted 4.25 hours, during which any noticeable events (pits etc.) were recorded. Upon completion, the sample was disconnected from the potentiostat, thoroughly rinsed in distilled water, dried in air, and stored in a polystyrene container for future reference.

4.2.2 ELECTROCHEMICAL POLARIZATION AT CONSTANT POTENTIAL

The sample was mounted and prepared as previous samples tested using the cyclic method. The Luggin-Haber probe was not used in this case. The calomel electrode was placed directly into the corrosion cell. A test sample was run both with and without the probe, and the same results were obtained in each instance. After rinsing with distilled water followed by acetone, the sample was allowed to dry in a desiccator for 15-20 minutes. Plastic paint from a Paper-mate permanent pen (red) was applied to a 3-4mm width of the sample in 3 coats(100). The sample was then allowed to dry in a desiccator for a minimum of ten minutes. Upon being placed in the corrosion cell containing aerated 4% wt NaCl adjusted to a pH of 8.0 using 1% NaOH (pH measurements were made using a Markson Model 2503 digital pH meter), the sample was allowed to sit for one minute. The potentiostat

leads were then connected and the sample was polarized to the desired potential. Readings of current were taken at various time increments until the conclusion of the experiment. The sample was removed and the plastic paint removed with acetone. The coupon was then carefully removed from its epoxy mount to avoid additional contamination. The coupon was then rinsed again with acetone and placed in a desiccator until ready to insert into the AES sample introduction system.

The method of inducing crevice corrosion with the plastic paint was found by experimentation to be more reproducible in results than the more conventional methods such as the use of rubber bands, o-rings, etc. Studies by Degerbeck (100) show that with this method:

1. No halogen ions, heavy metal ions, or oxidizing components have been observed in the paint layers.
2. SEM studies of the layer show that cracks form, approximately perpendicular to the specimen surface, many crevices with a mean estimated gap of 1 micrometer. The crack density is highest at the edge of the film.

4.3 SURFACE ANALYSIS -- AUGER ELECTRON SPECTROSCOPY

Samples which were polarized with an intentionally induced crevice and removed from their epoxy mounting were mounted in 45 degree sample holder and introduced into the AES vacuum chamber which maintained a pressure of approximately 1×10^{-9} Torr during the analysis. The Auger Electron Spectrometer used was a Physical Electronics Industries (PEI) Model 590a. The AES system utilized a PEI Model 25110 cylindrical mirror analyzer.

Spectra were obtained by scanning from 0 to 2000eV. The standard settings used were:

Ep = 5 KeV

ip = .7 Amps

Vmod = 3

Vmult = 1100

RC = 0

Sensitivity = 40x

The first scan was made prior to any sputtering. Thereafter, before a scan, the sample was sputtered for periods of 5-300 seconds with Argon ions. The parameters of the sputtering gun were:

Bv = 500

Cmd = 1000

Obj = 832

Raster = 1 x 1 (20-20)

The analysis was done at the site of active dissolution, and at sites which were under crevice conditions but where no corrosion had apparently taken place. The quality of the scan was a function of the care taken in the process of the polarization and transfer to the AES system. The presence of any value of the sodium peak pointed to insufficient acetone flush of the sample and cast doubt upon the accuracy of the data, especially with regard to chloride content. It was realized that the exposure of the samples to air after polarization would make it impossible to derive information from the Oxygen peaks.

Total sputtering time varied from 70 to 420 seconds. Most spectra showed a bulk composition within 120 seconds, depending on the variability in film thickness or in the amount of contamination.

The Auger spectra were analyzed qualitatively and quantitatively. Quantitative results were taken from the main peak-to-peak Auger transitions of each investigated element. These transitions were: S(L23 M23 M23), Cl(L23 M23 M45),

Cr(L23 M23 M45), Fe(L23 M23 M45), Fe(L23 M45 M45), Ni(L23 M45 M45), Mo(M45 N45 N45). Quantitative data were determined using relative elemental sensitivity factors. This quantitative procedure is simple and straightforward, but does not take into account either the variation in Auger electron yield with changes in chemical state or in variation in the mean escape depth of the Auger electrons from the investigated elements.

The weight percent of the element was calculated by the formula:

$$C_x = \frac{P_x/S_x}{\sum P_x/S_x}$$

Where P_x is the observed peak-to-peak height of the element x on the dN/dE spectrum. S_x is the relative elemental sensitivity factor. The weight percentage is only with respect to the elements investigated, which were normally those of the bulk metal.

5.0 RESULTS OF EXPERIMENTAL RESEARCH

OVERVIEW

In this section the results will be presented in a general context of performance. First, however, a framework for the entire evaluation process will be outlined. Starting with a generalized performance criteria, a logic diagram used in the classification of the results will be described in Section 5.1. Using this framework, the electrochemical results including representative polarization diagrams and a listing of key parameters which can be read from the diagrams will be given in Section 5.2. These key parameters are defined in Appendix A. Finally the results of the surface analysis will be described in Section 5.3.

5.1 FRAMEWORK FOR EVALUATION OF MATERIAL TO LOCALIZED CORROSION

In order to produce a ranking of alloys in their resistance to localized corrosion, the various parameters defined in Appendix A were used. Upon examination of all polarization scans it was evident that four overall groupings could be readily distinguished:

1. No localized corrosion-no visual evidence of pitting was observed.
2. Minimal localized corrosion-minor, random pitting on the surface of the sample.
3. Moderate localized corrosion-definite pit formation, but not developing into large areas of active dissolution as in Group 4.
4. Heavy localized corrosion-initial pitting which eventually coalesced into large areas of active dissolution.

In Section 2.4 the salient points of a polarization diagram were discussed. Determining the qualitative performance can be done if correlation of these variables can be made. As an outgrowth of this attempt to measure performance, a simple logic diagram was constructed and has been used in evaluating these alloys and is shown in Figure 5.1.1. Table 5.1.1 shows which alloys fall into each category. The logic circuit diagram was developed along the lines proposed by Mr. P. Morris of INCO Research and Development Center, Inc (101).

The first step was to determine the existence of a hysteresis loop and a definite pitting potential. If no hysteresis and no pitting potential was distinguishable, then a cutoff value of ($E_{\text{prot}} - E_{\text{corr}}$) was used to distinguish between no localized corrosion and minimal localized corrosion.

If both a hysteresis loop and/or a definite pitting potential was found, then the values of ($E_{\text{x}} - E_{\text{p}}$), I_{max} , ($E_{\text{prot}} - E_{\text{corr}}$), and the loopwidth parameter were used to separate the alloys into the three levels of localized corrosion. While the values of these parameters were somewhat arbitrary, there were very noticeable cutoff values in the alloys evaluated. The loopwidth parameter was used when only a very small hysteresis loop was observed, and the cutoff between no localized corrosion and minimum localized corrosion was made.

An important input for the construction of these rankings was visual examination of the sample for any possible change in the surface appearance. It must also be kept in mind that this ranking was made when the alloy had been polarized beyond its pitting potential i.e., forced to more noble potentials. A relative order of resistance within each ranking could also be attempted, but due to the concen-

tration on the qualitative analysis of these curves any more detailed breakdown would be inappropriate.

As a first blush these rankings are not a definitive evaluation of the alloy's performance, but can be considered a valid starting point in an integrated analysis. For example, factoring in the "in ocean" results can add a significant degree of confidence in the evaluation procedure. "In ocean" results will be compared in Section 6.3. Processing in additional factors would seem appropriate in order to cultivate a more complete analysis, particularly in understanding what events in the alloy led to the end product. For example, were there any trends in the effects of alloying elements? These factors will be discussed in Section 6.4.

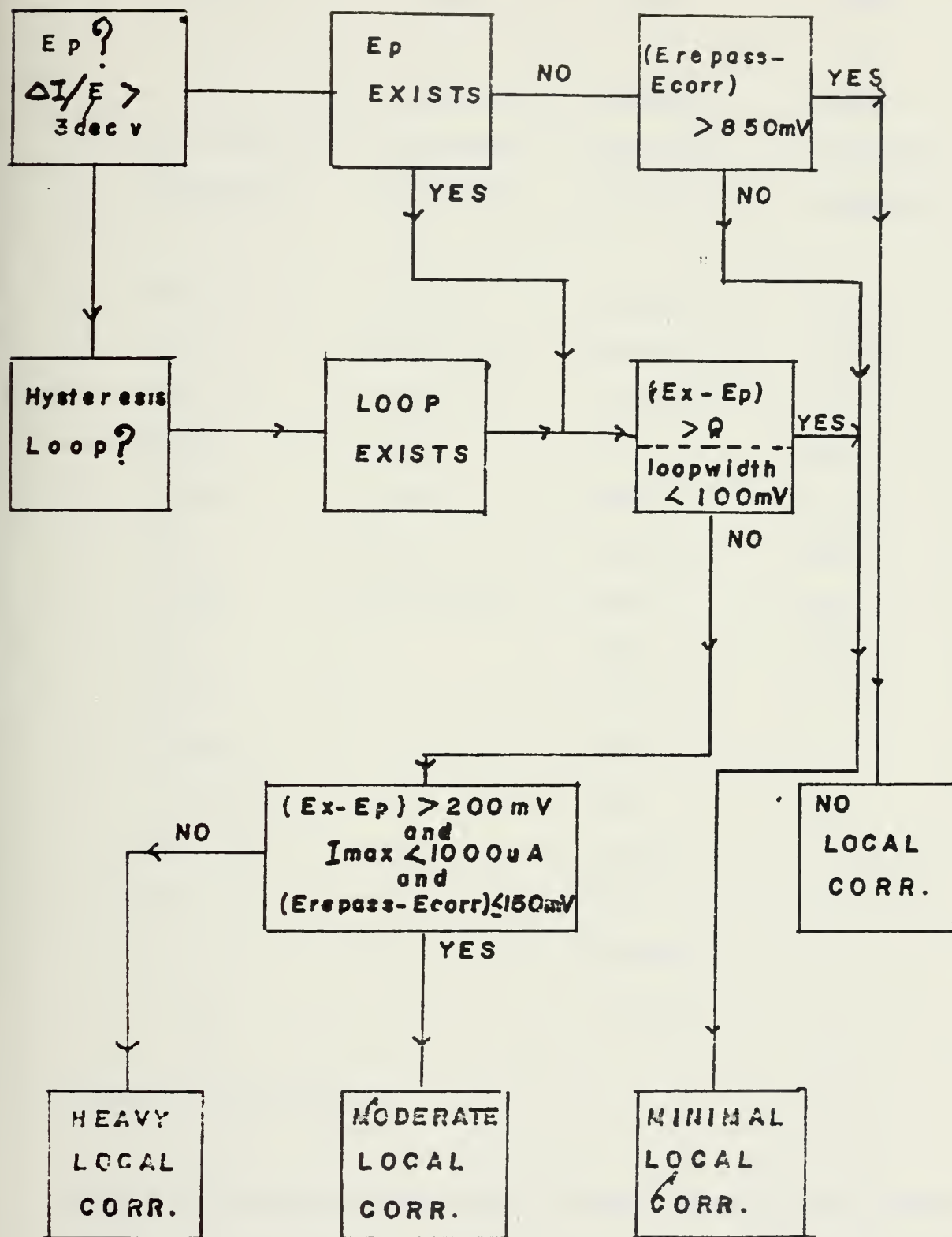


Figure 5.1.1 Logic Circuit Diagram for the Ranking of Stainless Steels

GROUP	GROUP	GROUP	GROUP
1	2	3	4
NO	MINIMAL	MODERATE	HEAVY
LOCALIZED	LOCALIZED	LOCALIZED	LOCALIZED
CORROSION	CORROSION	CORROSION	CORROSION
29-4	Alloy G	Jessop 777	CF 8M *
29-4C	Alloy G3	Jessop 700	20-Cb3
29-4-2	20 Mo 6	254 SFER	CA6N *
MONIT	625	AL-4X	18-2
AL-6X	C-276	904L	18-SR
SC-1	625 *	254 SLX	T316
20 Mod	Illium W2 *	44LN	825
26-1		34LN	CN7M *
26-1S		22-13-5	
254 SMO		T216	
Illium PD *		T329	
Ferralium		T317L+	
Rex 734		T317L	
		T317LM	
		IN 862 *	

* Denotes cast alloys

TABLE OF GROUPINGS VIA THE CYCLIC ANODIC POLARIZATION METHOD

TABLE 5.1.1

5.2 ELECTROCHEMICAL RESULTS

The results of the cyclic anodic polarization experiments are presented in Figures 5.2.1 - 5.2.43 and Tables 5.2.1 - 5.2.6. These results are grouped as they have been in Section 3 and in keeping with Section 5.1. While only one figure is presented here, all samples were run at least twice to ensure that reproducible results were obtained. Values of E_{corr} , E_{prot} , E_p , E_x , $E_{prot}-E_{corr}$, and E_x-E_p are presented in Tables 5.2.1 to 5.2.6, again as grouped by type as in section 3. Appendix A defines these parameters and they will be used in the generalized ranking of the alloys with respect to their resistance to localized corrosion in a later section.

5.2.1 Austenitic Stainless Steels 6% to 16% Nickel

The results are shown in Figures 5.2.1 to 5.2.8 and in Table 5.2.1. In general all these alloys tend to have a moderate to heavy tendency to corrode locally when the analysis in Section 5.1 is applied. A glaring deviation is Rex 734, which indicated no tendency to corrode locally, even though the alloy has less than 3% Mo and less than 10% Ni. This behavior might be explained by the high nitrogen content, which has been shown by Swedish researchers to substantially increase the resistance to localized corrosion

(102). These new Swedish steels performed fairly well in these polarization tests. Rex 734 has an unusually high manganese content, which generally leads to a greater tendency to locally corrode. Alloy T216 also has a high nitrogen content, and shows a greater resistance to corrosion than one might assume from its composition, especially in regard to its unusually high Mn content (8%).

5.2.2 Austenitic Stainless Steels 17% to 40% Nickel

The results are shown in Figures 5.2.9 to 5.2.19. This group generally exhibits a moderate tendency to corrode locally. Exceptions include alloys 254 SMO, 6X, and 20 Mo 6 which show no tendency (254 SMO, 6X) or a minimum tendency (20 Mo 6) to locally corrode. These alloys have a greater amount of Mo (approximately 6%), and alloys 254 SMO and 20 Mo 6 also have a lesser amount of Mn. Alloy 254 SMO also has a moderate amount of nitrogen. Alloy 20 Cb3 exhibited the greatest tendency to corrode, and it has one of the lowest amounts of Mo (2%). In general it can be postulated from the plots that increasing Ni content does not significantly lower localized corrosion susceptibility.

5.2.3 Austenitic Alloys >40% Nickel

The results are shown in Figures 5.2.20 to 5.2.24 and in Table 5.2.3. All alloys exhibit a minimum tendency to locally corrode with the exception of Alloy 825 (Incoloy). Alloy 825 has significantly less Mo and moderately corrodes. All other alloys in this group have at least 5.8% Mo.

5.2.4 Duplex Austenitic-Ferritic Alloys

The results are shown in Figures 5.2.25 to 5.2.27 and in Table 5.2.4. These three alloys have essentially identical compositions with the exception of Ferralium, with 3.2% Mo and 0.19% nitrogen. Ferralium exhibited no tendency to locally corrode, where the others show a moderate tendency to corrode.

5.2.5 Ferritic Alloys

The results are shown in Figures 5.2.28 to 5.2.36 and in Table 5.2.5. In this grouping all alloys with greater than 25% Cr showed no tendency to locally corrode. The two alloys with less than 25% Cr (T439 and T444) both exhibited a heavy tendency, even with a substantial amount of Mo in the case of Alloy T444. It is interesting to note that none of these alloys has greater than 0.43% Mn. Swedish researchers have

had great success in improving corrosion resistance by minimizing Mn content in their alloys (103). The hypothesis used is that the lower manganese content reduces the amount of sulfide inclusions which might otherwise lead to micropits.

5.2.6 Cast Alloys

The results are shown in Figures 5.2.37 to 5.2.43 and Table 5.2.6. There are examples of all four degrees of corrosion in this group. Of particular interest is Illium W-2 which contains 17.58% Mo and 62.8% nickel, but still exhibits some tendency to corrode. The best performer regarding resistance to corrosion was Illium PD, which contains 25% Cr and 2% Mo as well as 5.7% Co. CF8M (the cast equivalent to 316), performed about as well as its wrought counterpart, and 625-cast ranked along with its wrought counterpart.

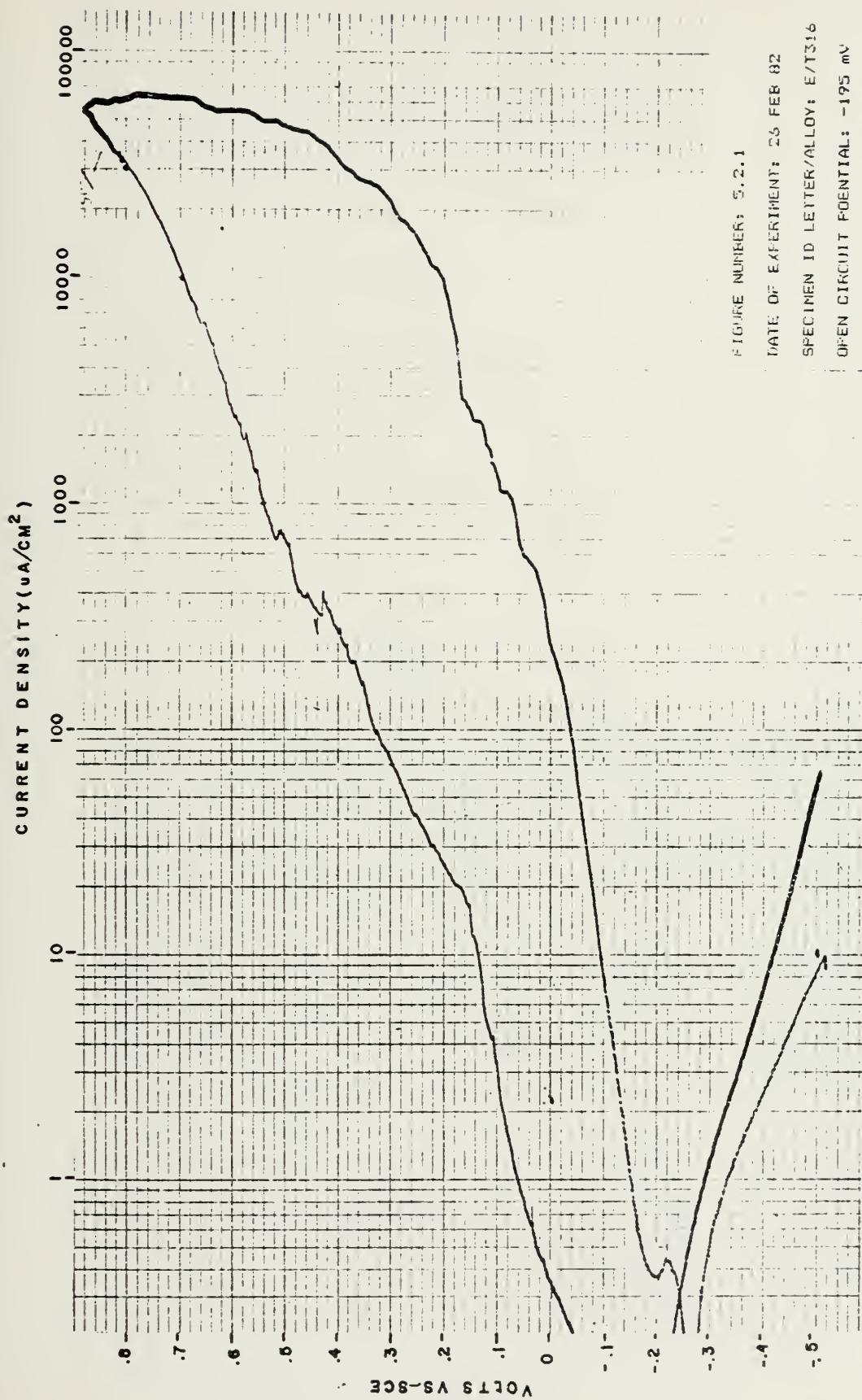


FIGURE NUMBER: 5.2.1

DATE OF EXPERIMENT: 23 FEB 82

SPECIMEN ID LETTER/ALLOY: E/T316

OPEN CIRCUIT POTENTIAL: -195 mV

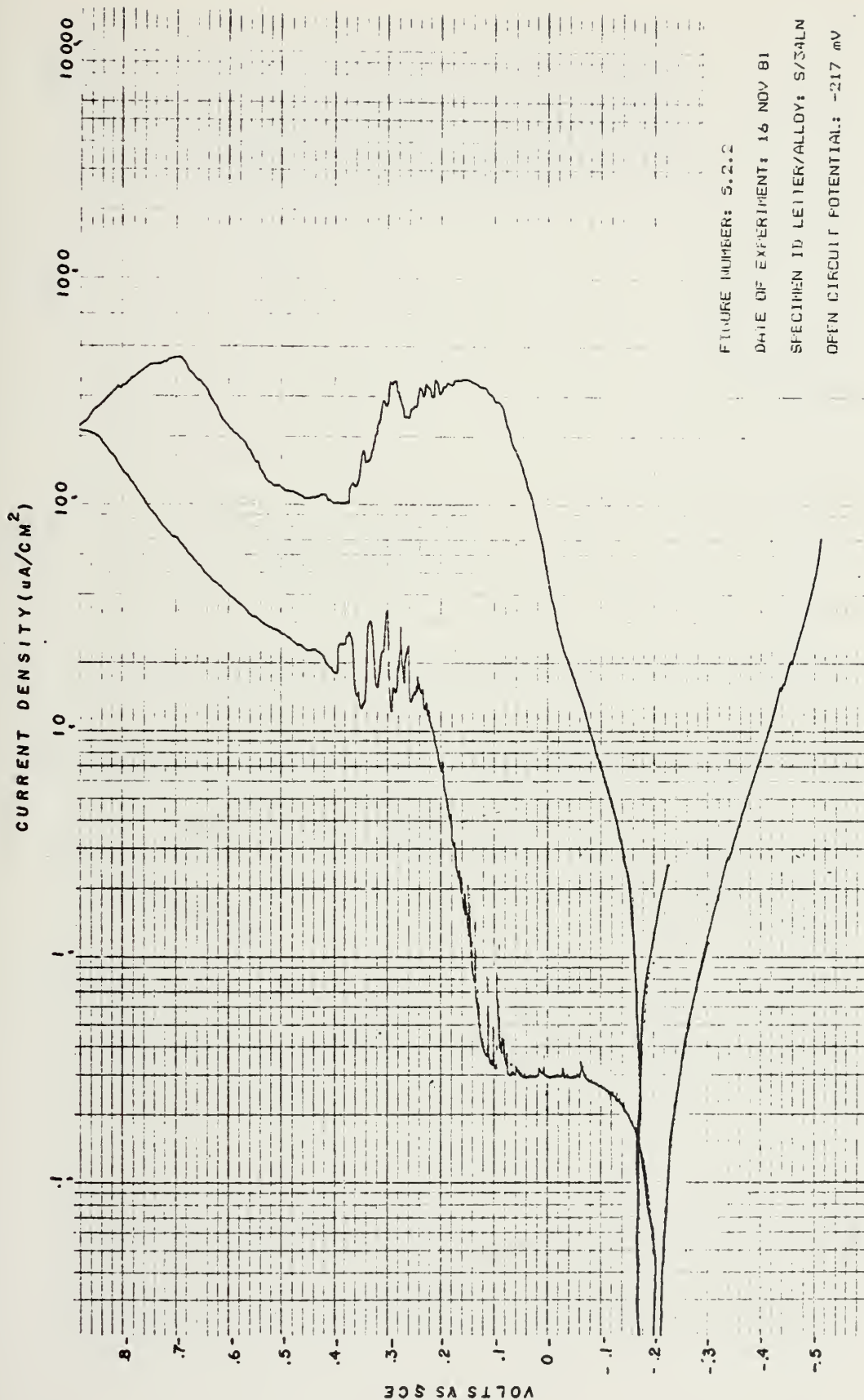
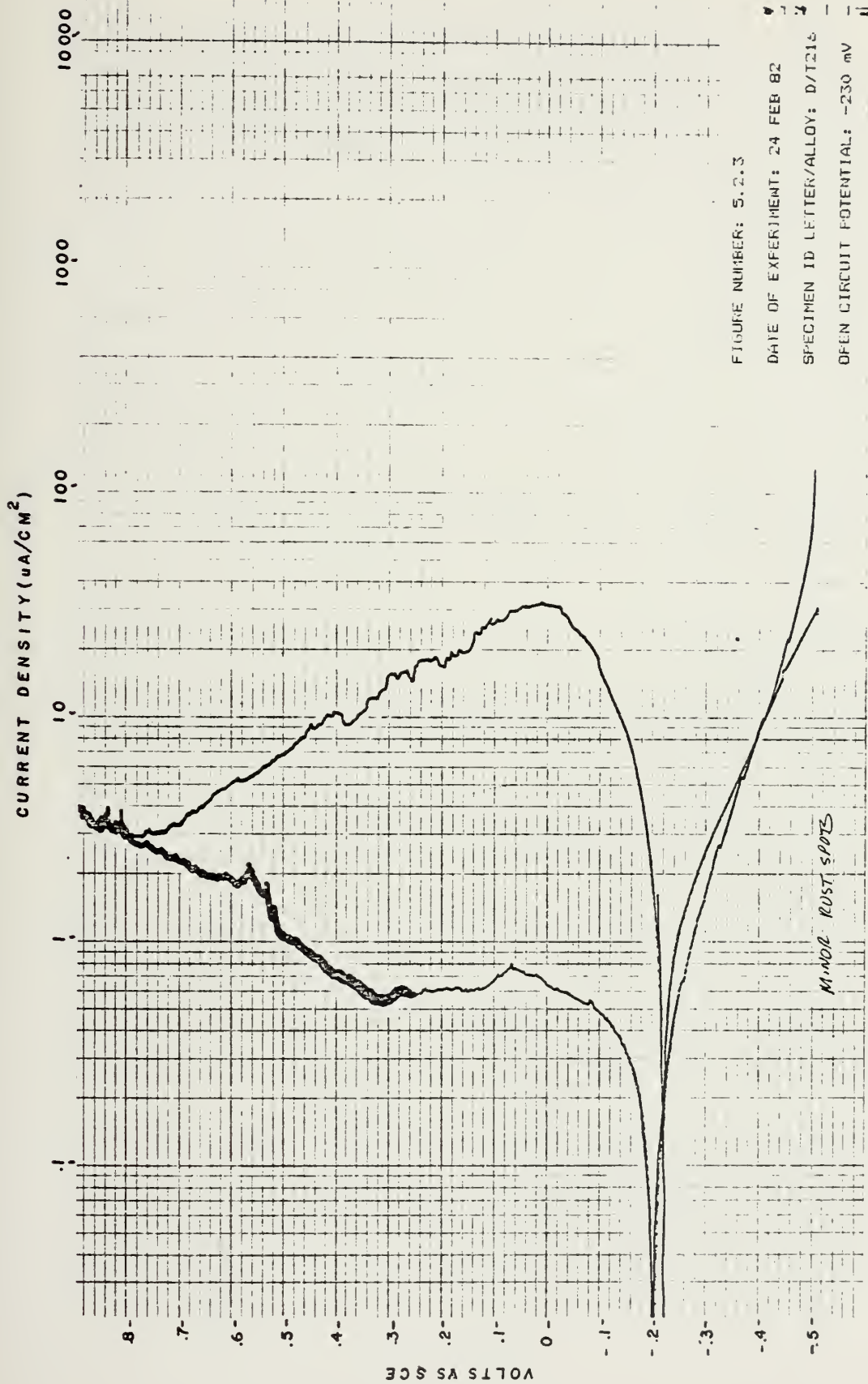


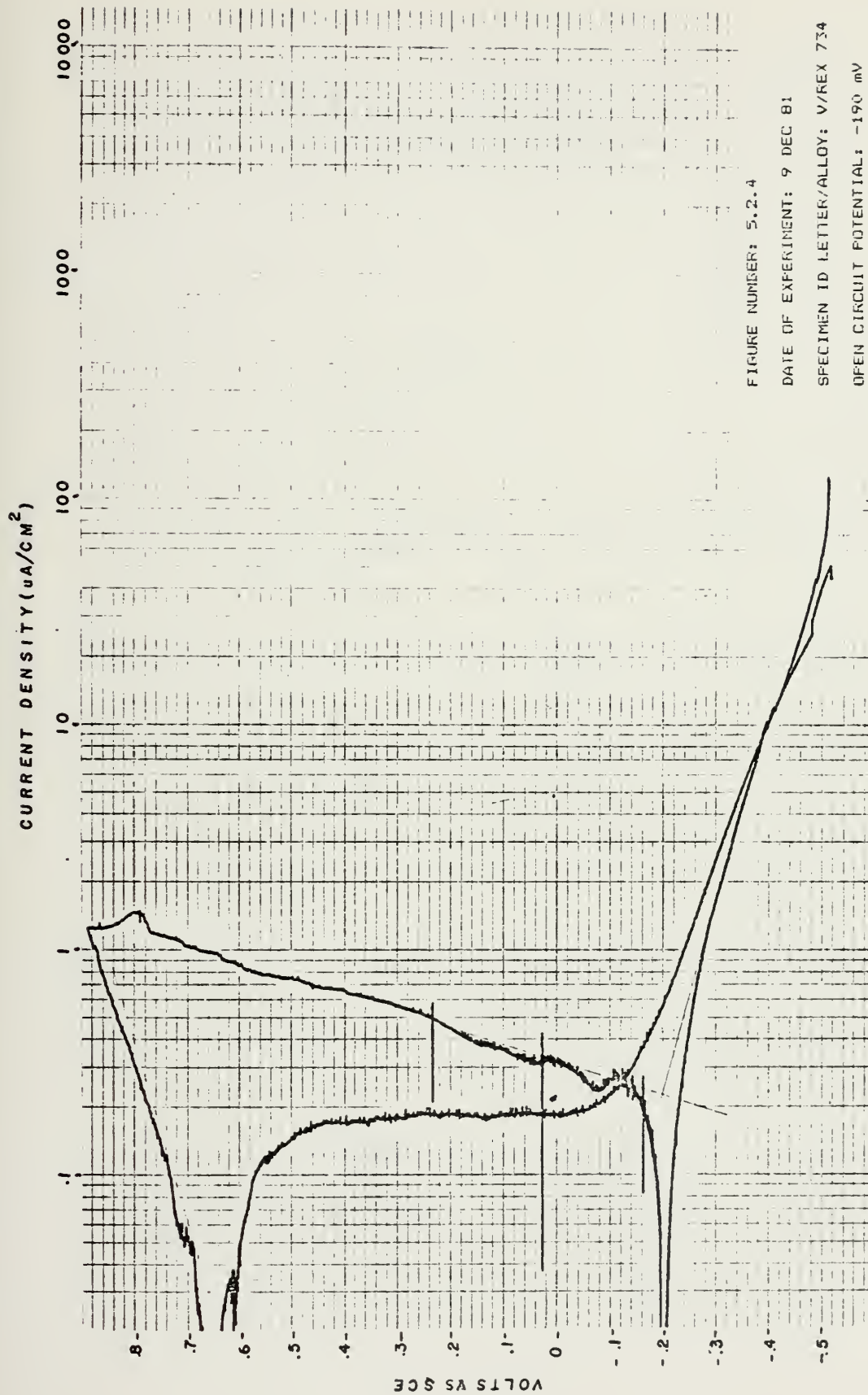
FIGURE NUMBER: 5.2.2

DATE OF EXPERIMENT: 16 NOV 81

SPECIMEN ID LETTER/ALLOY: S/3ALN

OPEN CIRCUIT POTENTIAL: -217 mV





CURRENT DENSITY ($\mu\text{A}/\text{CM}^2$)

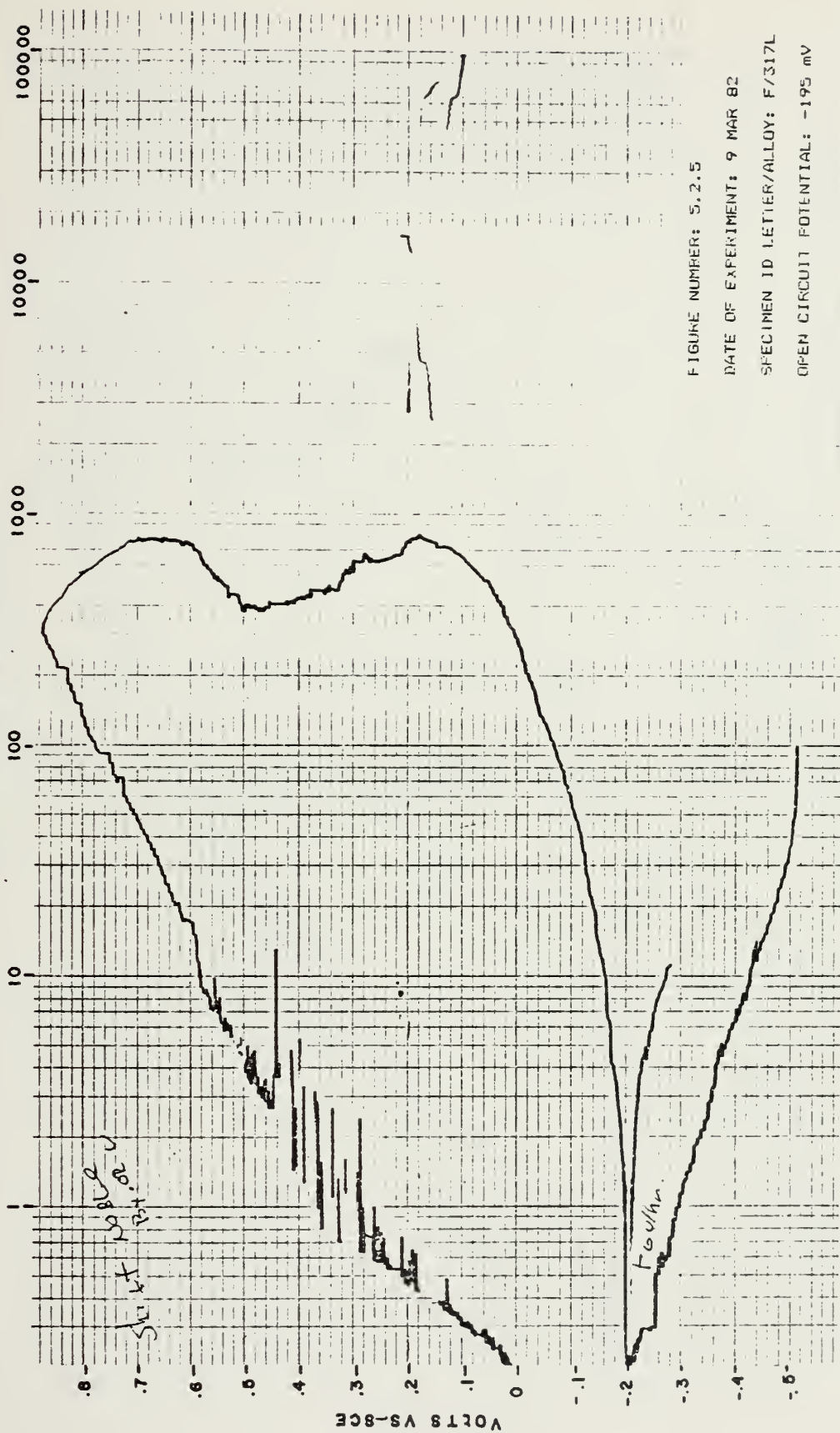


FIGURE NUMBER: S.2.5

DATE OF EXPERIMENT: 9 MAR 82

SPECIMEN ID LETTER/ALLOY: F/317L

OPEN CIRCUIT POTENTIAL: -195 mV

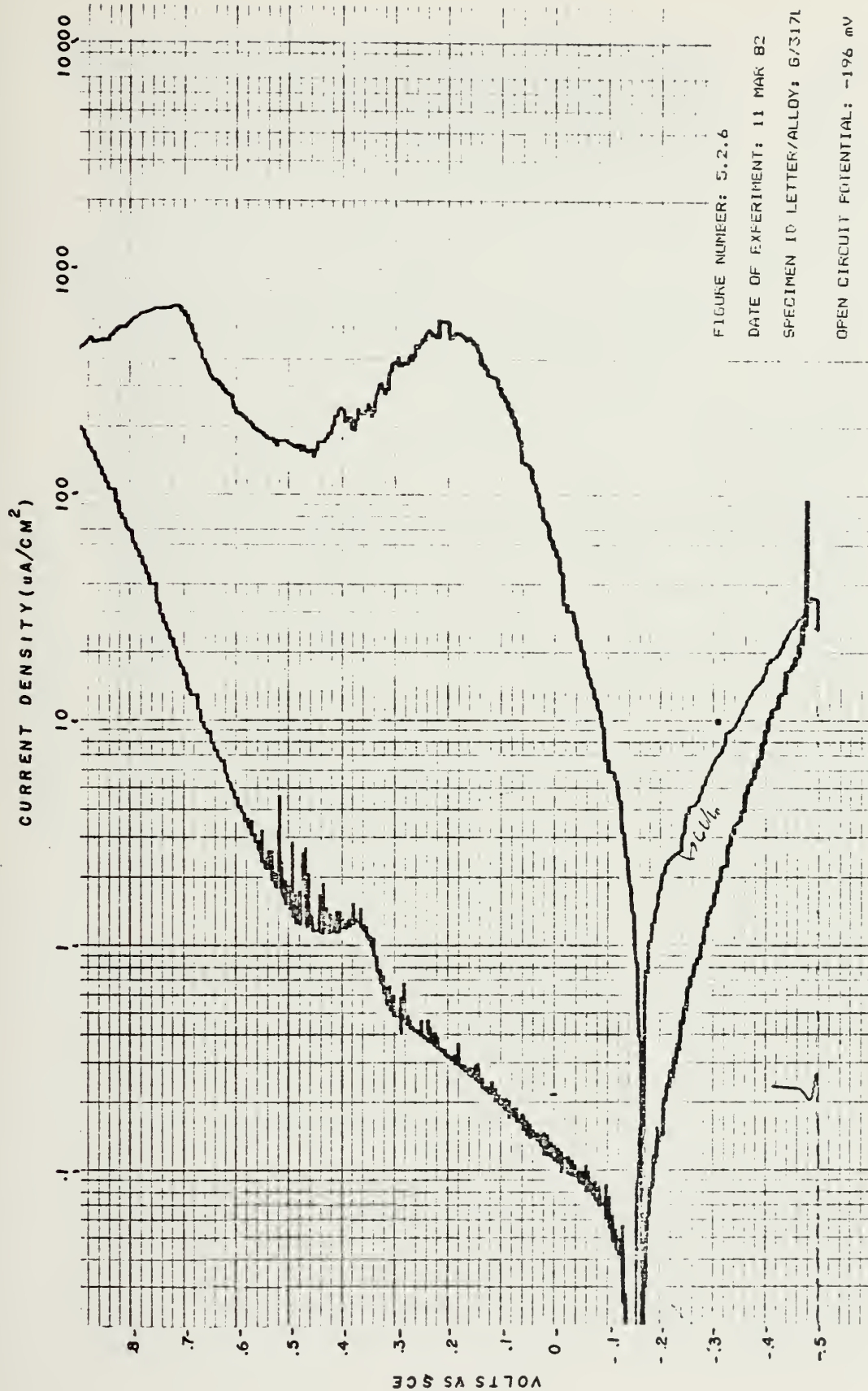


FIGURE NUMBER: 5.2.6

DATE OF EXPERIMENT: 11 MAR 82

SPECIMEN ID LETTER/ALLOY: G/3171

OPEN CIRCUIT POTENTIAL: -196 mV

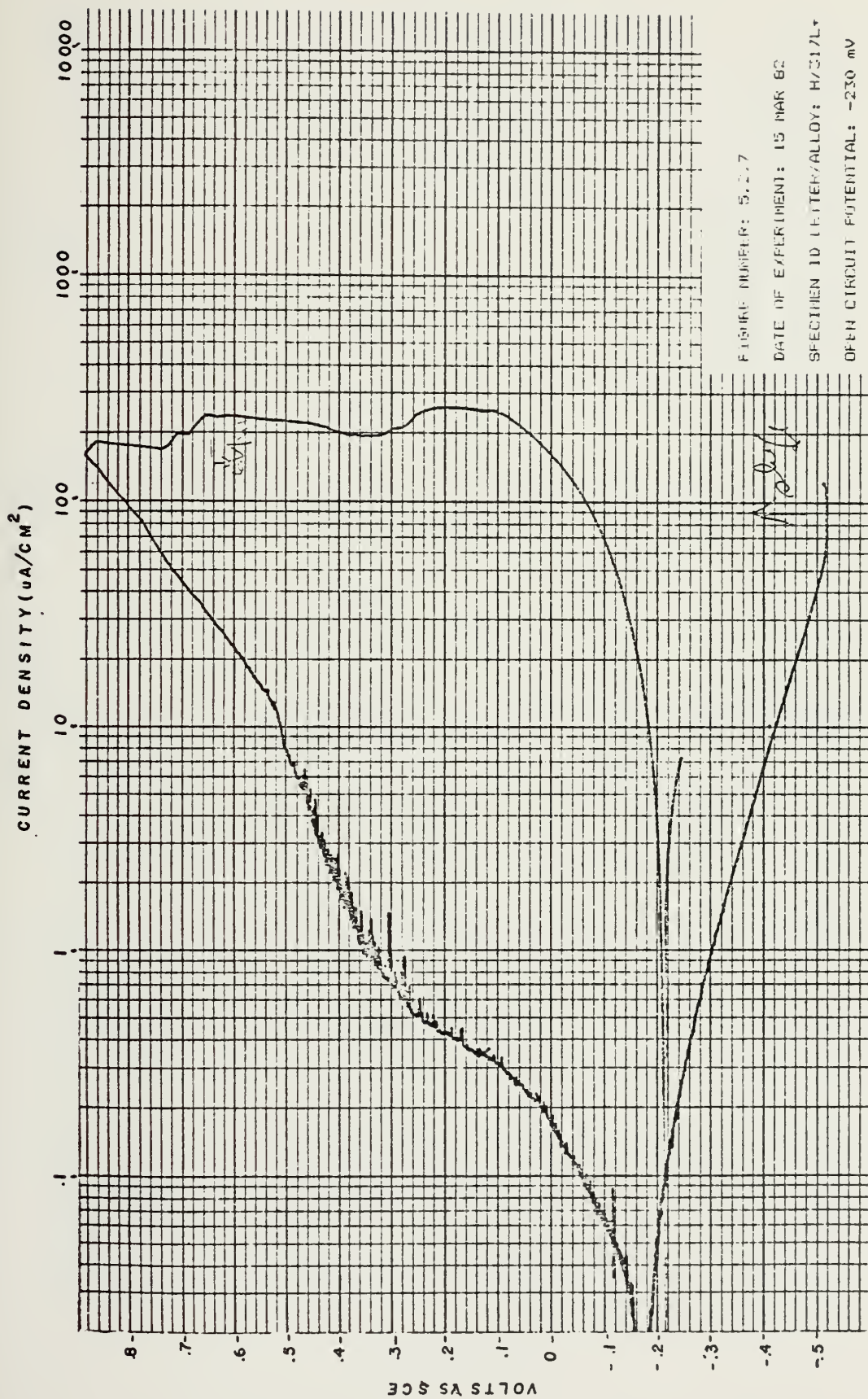


FIGURE NUMBER: 5.2.7

DATE OF EXPERIMENT: 15 MAR 62

SPECIMEN ID LETTER/ALLOY: H/31/L

OPEN CIRCUIT POTENTIAL: -230 mV

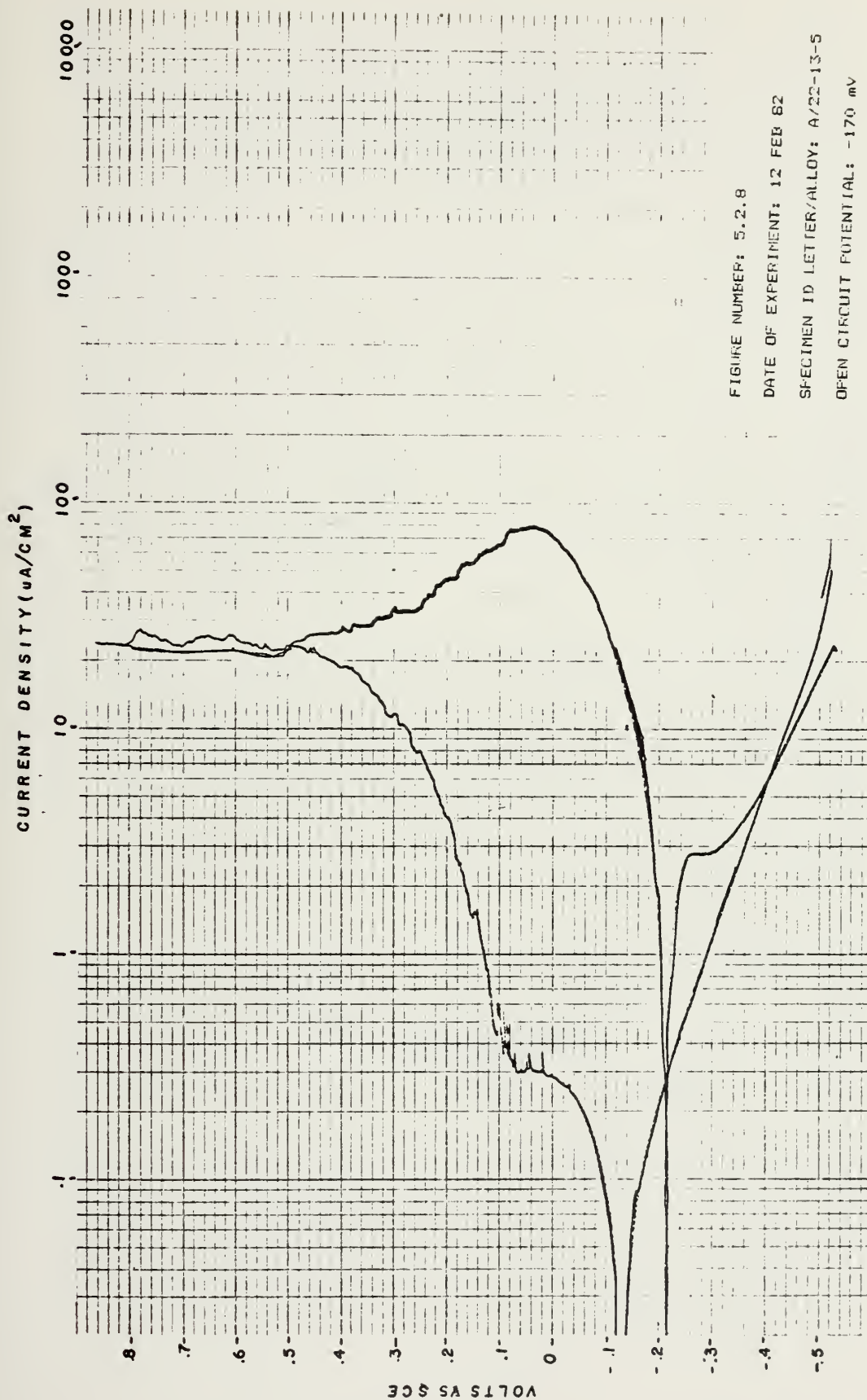


FIGURE NUMBER: 5.2.8

DATE OF EXPERIMENT: 12 FEB 62

SPECIMEN ID LETTER/ALLOY: A/22-13-5

OPEN CIRCUIT POTENTIAL: -170 mV

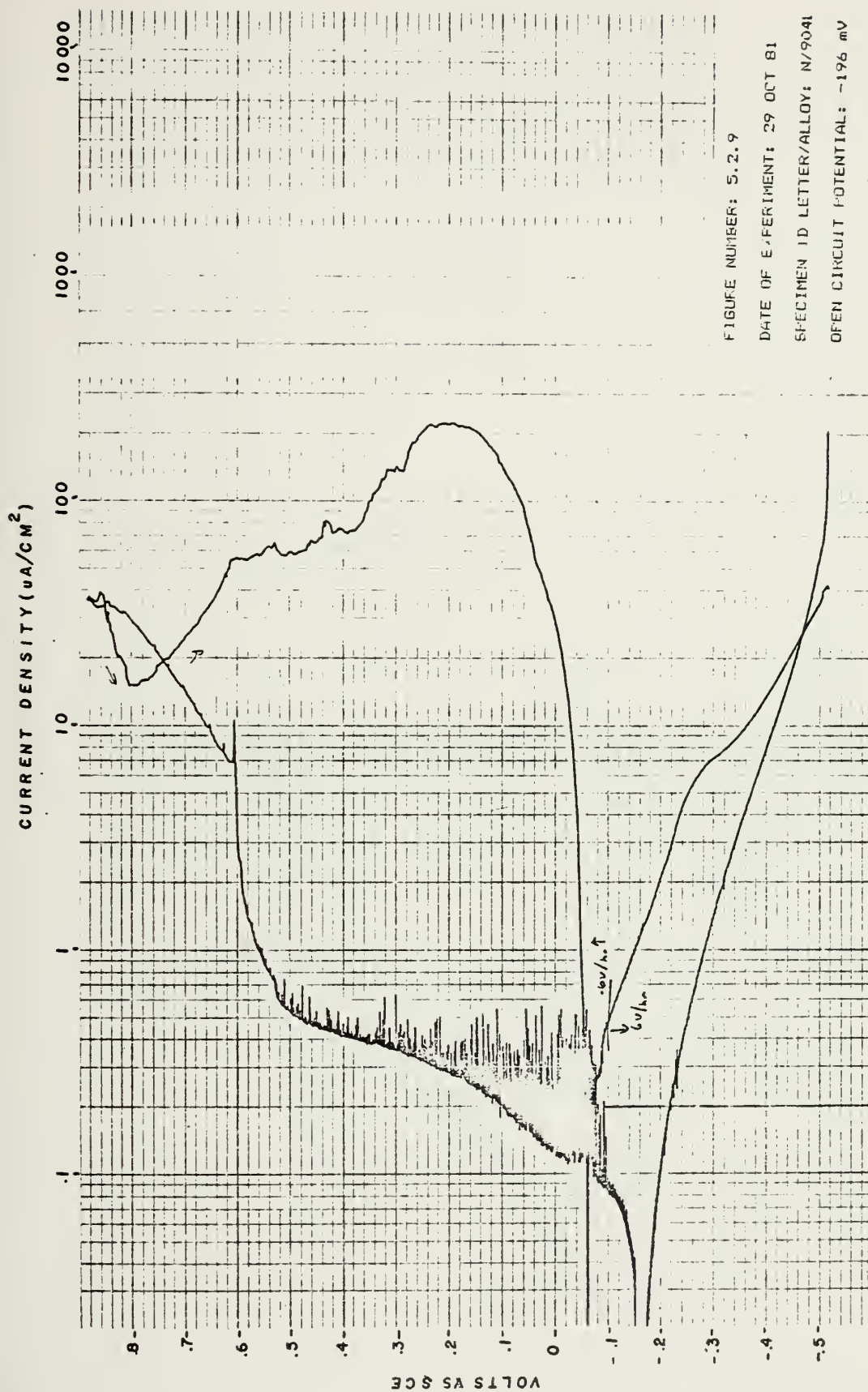
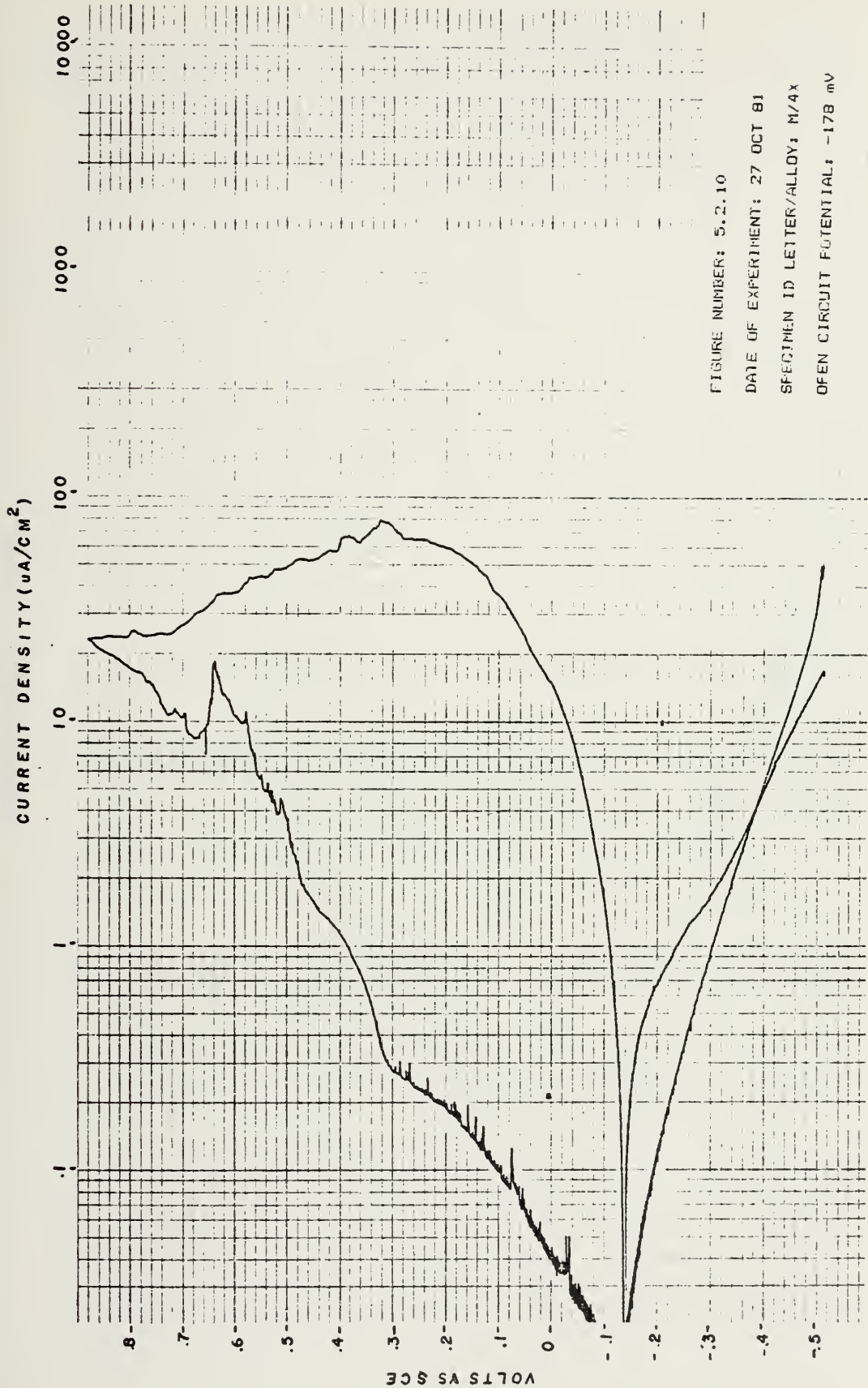


FIGURE NUMBER: 5.2.9

DATE OF EXPERIMENT: 29 OCT 81

SPECIMEN ID LETTER/ALLOY: N/9041

OPEN CIRCUIT POTENTIAL: -196 mV



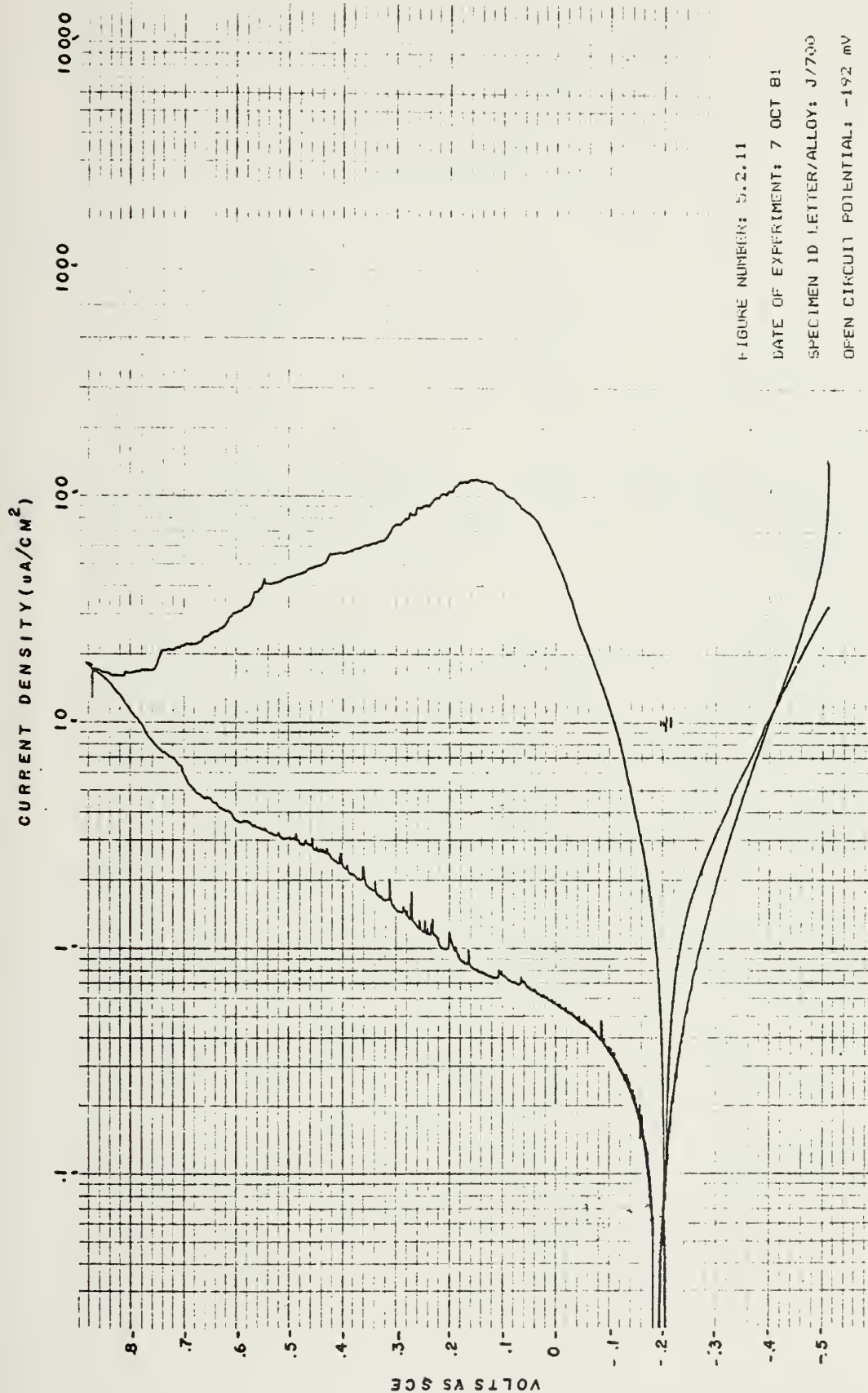
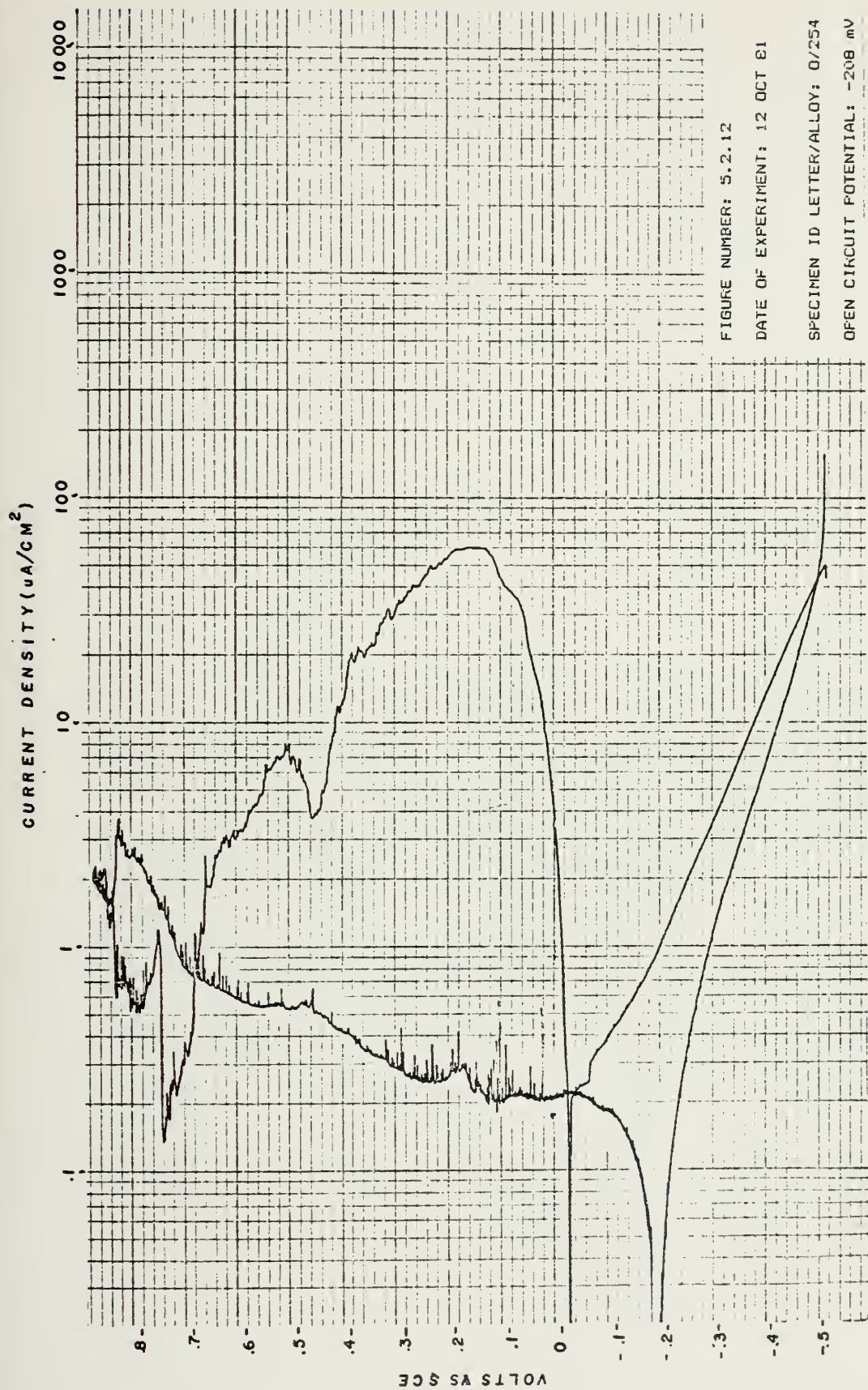


FIGURE NUMBER: 5.2.11

DATE OF EXPERIMENT: 7 OCT 81

SPECIMEN ID LETTER/ALLOY: J/700

OPEN CIRCUIT POTENTIAL: -192 mV



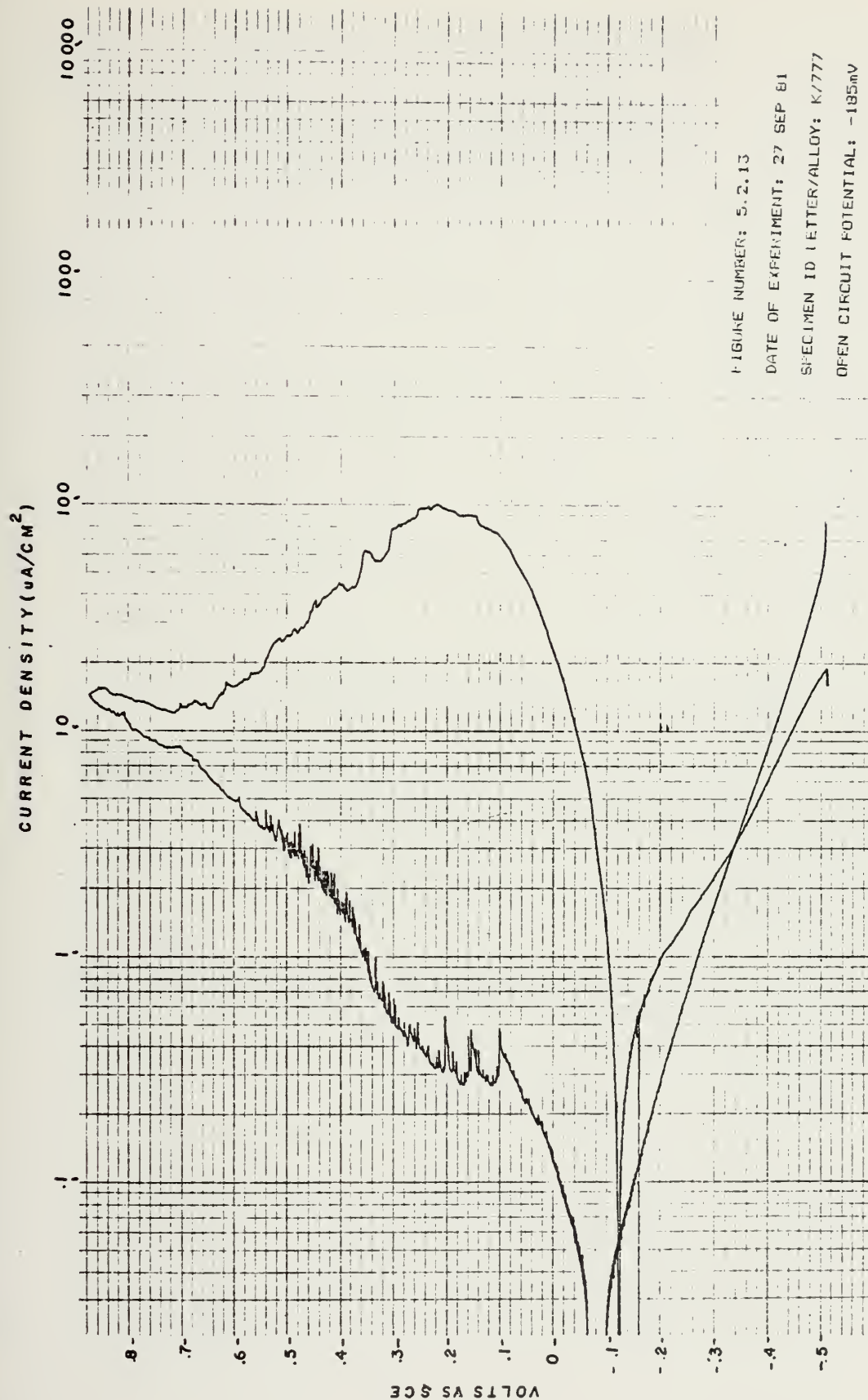


FIGURE NUMBER: 5.2.13

DATE OF EXPERIMENT: 27 SEP 81

SPECIMEN ID (LETTER/ALLOY): K/777

OPEN CIRCUIT POTENTIAL: -185mV

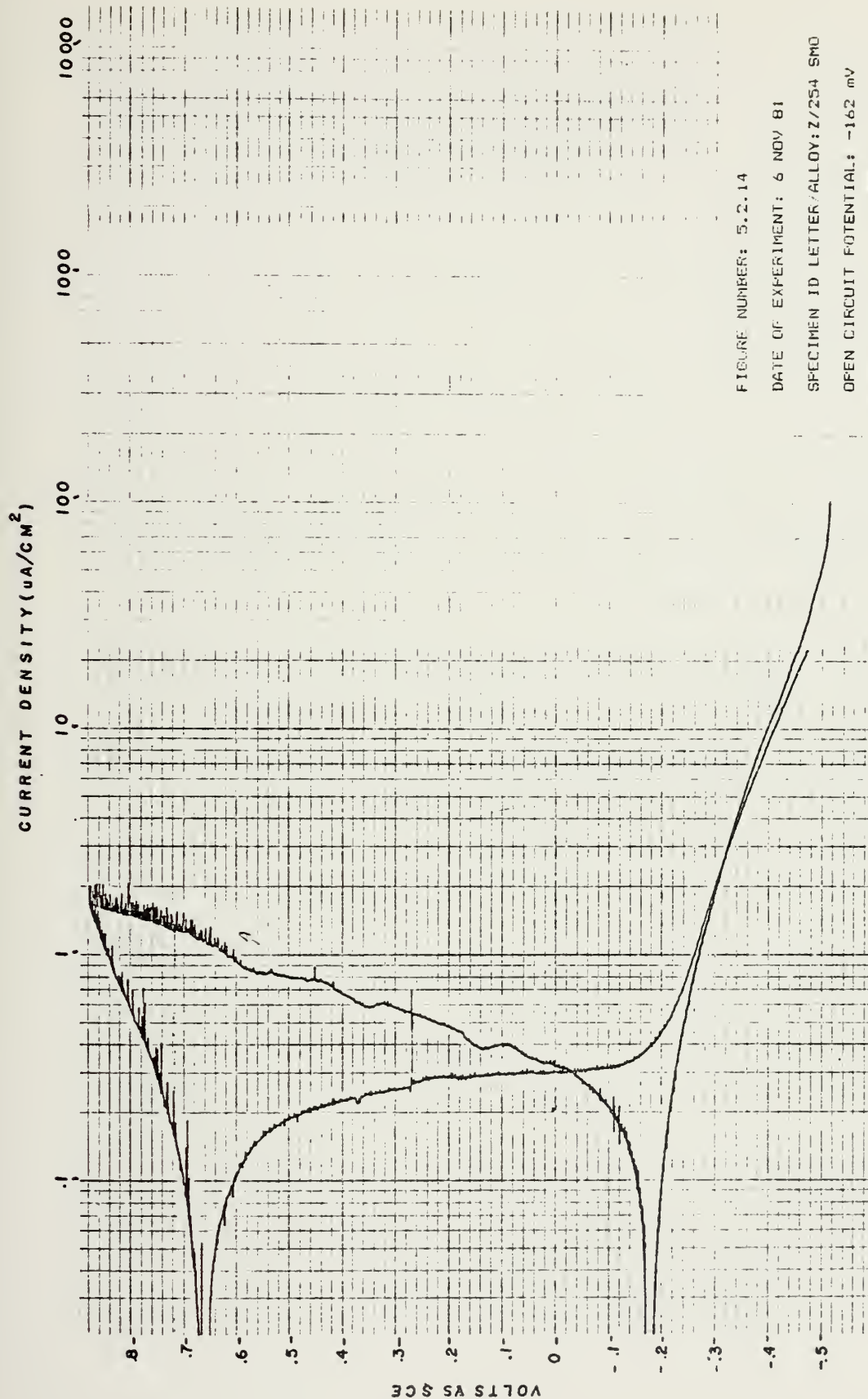


FIGURE NUMBER: 5.2.14

DATE OF EXPERIMENT: 6 NOV 81

SPECIMEN ID LETTER/ALLOY: Z/254 SMO

OPEN CIRCUIT POTENTIAL: -162 mV

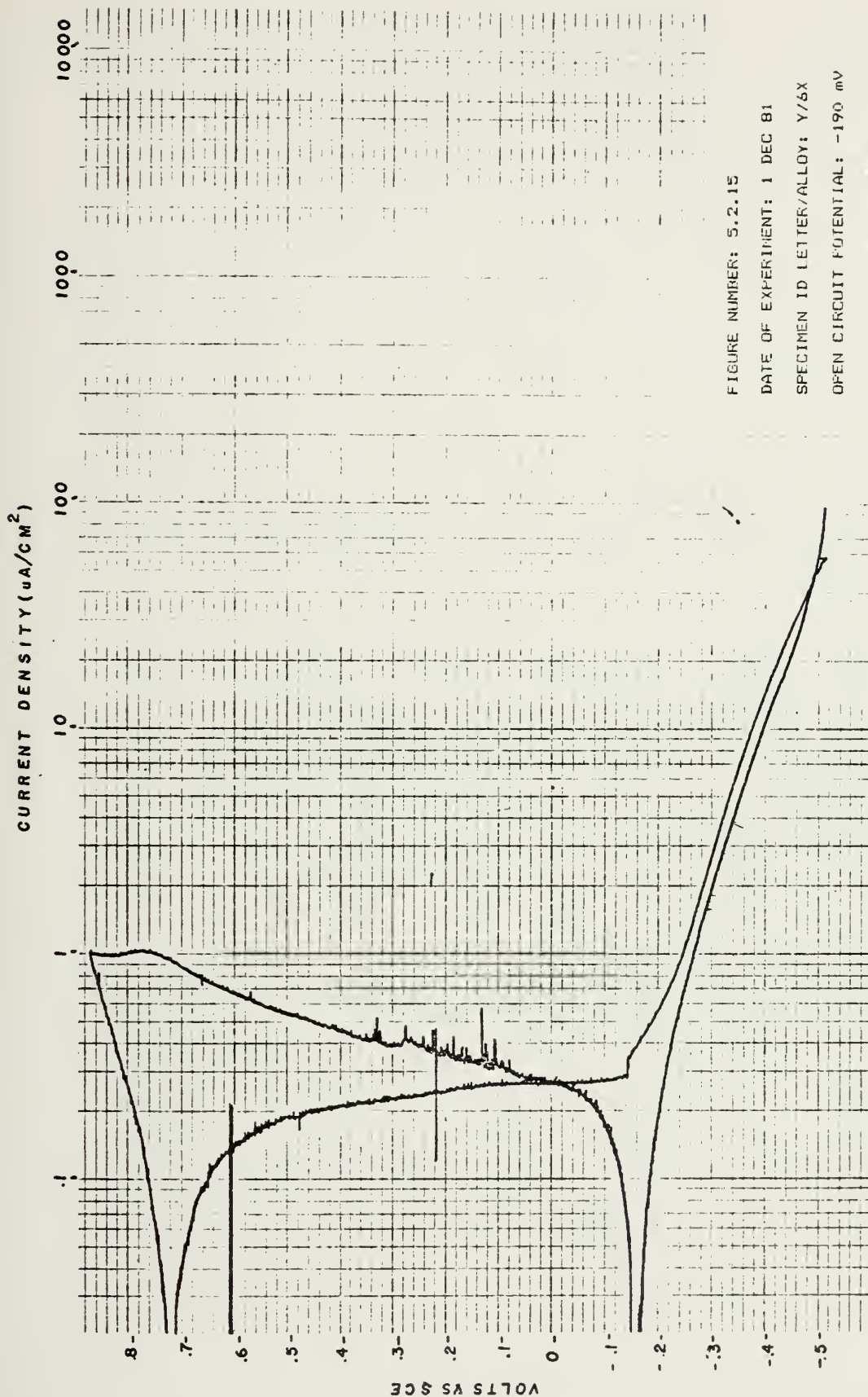


FIGURE NUMBER: 5.2.15
DATE OF EXPERIMENT: 1 DEC 81
SPECIMEN ID LETTER/ALLOY: Y/6X
OPEN CIRCUIT POTENTIAL: -190 mV

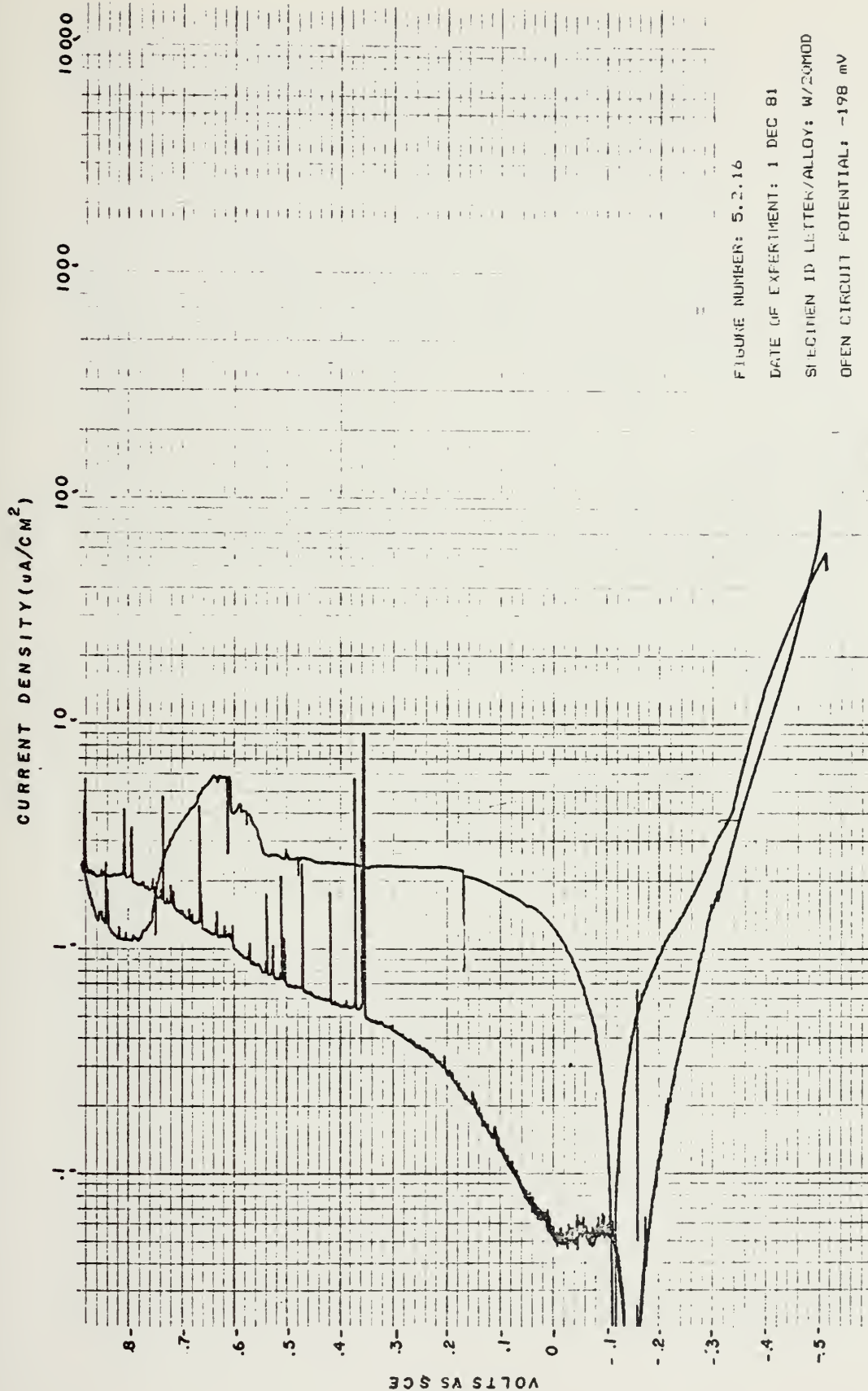


FIGURE NUMBER: 5.2.16

DATE OF EXPERIMENT: 1 DEC 81

SPECIMEN ID LETTER/ALLOY: W/20MOD

OPEN CIRCUIT POTENTIAL: -198 mV

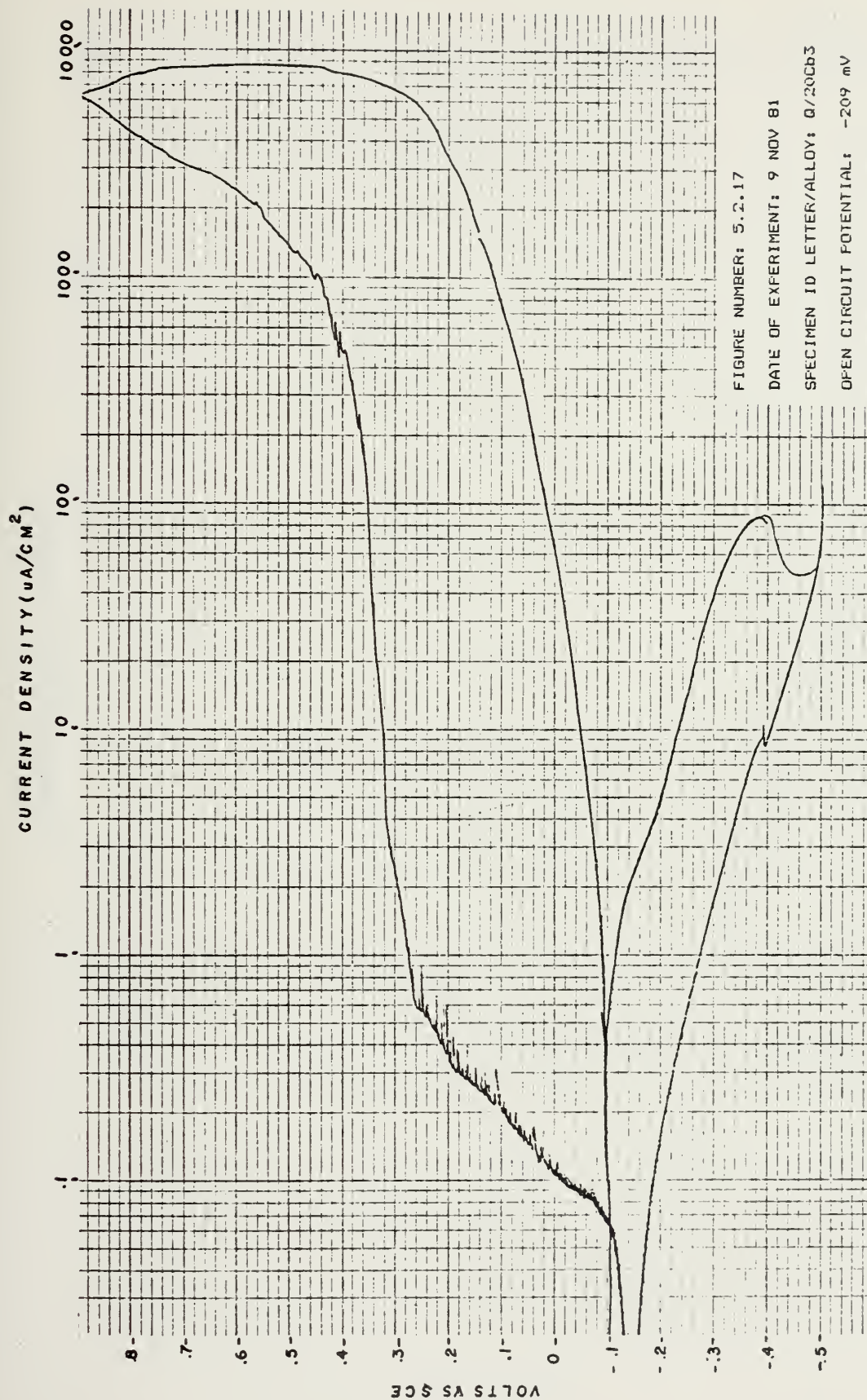
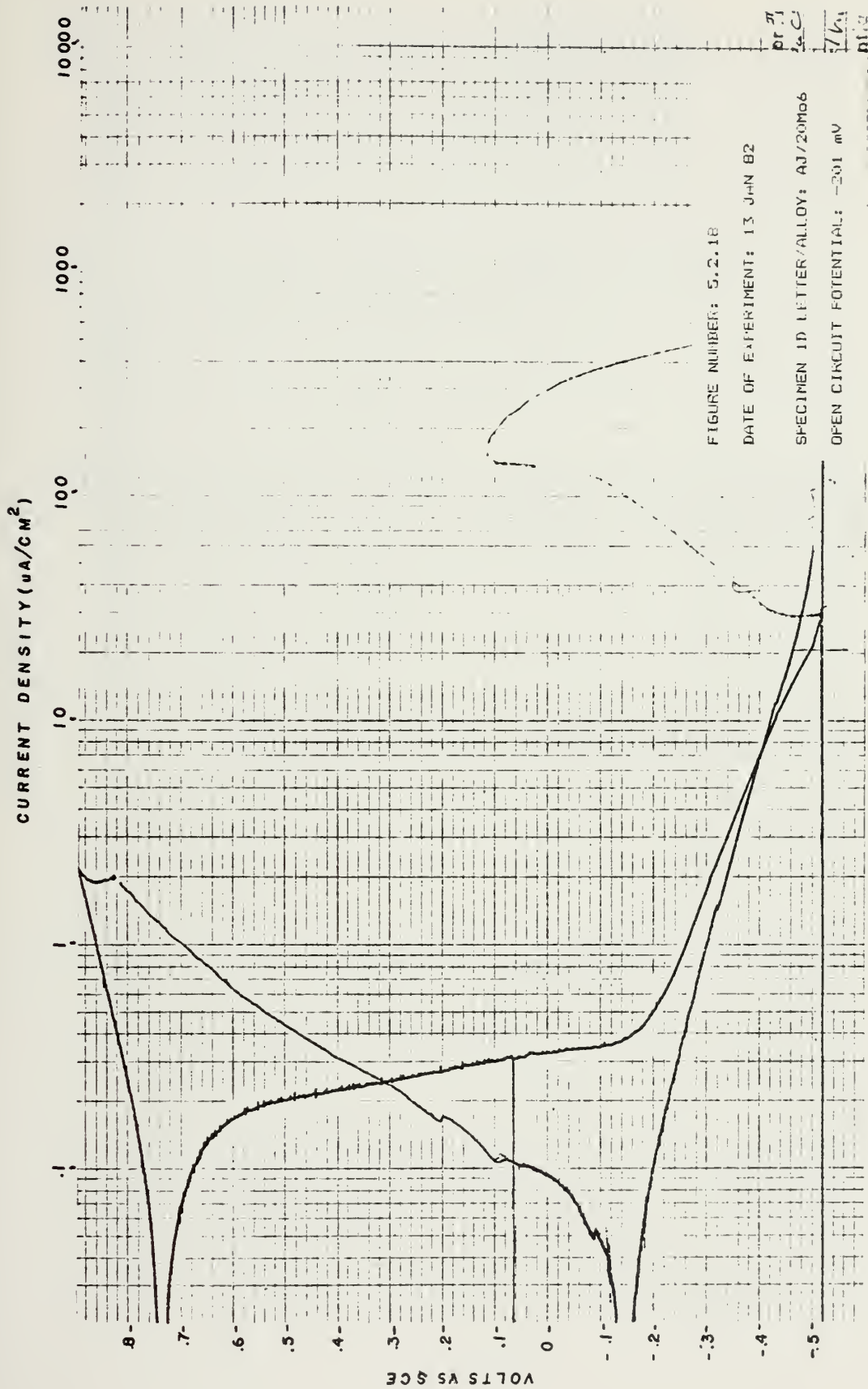


FIGURE NUMBER: 5.2.17

DATE OF EXPERIMENT: 9 NOV 81

SPECIMEN ID LETTER/ALLOY: Q/20Cb3

OPEN CIRCUIT POTENTIAL: -209 mV



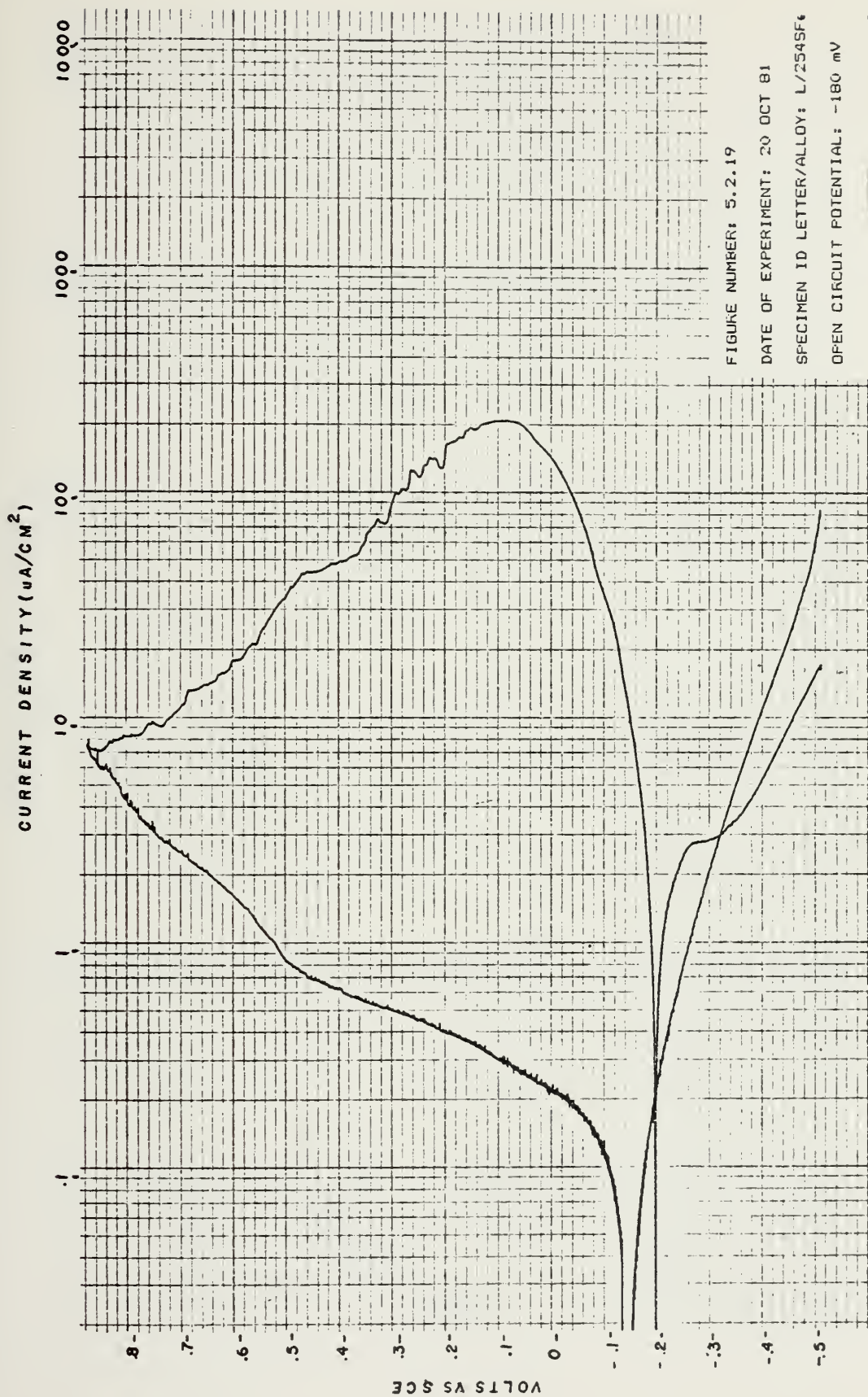


FIGURE NUMBER: 5.2.19

DATE OF EXPERIMENT: 20 OCT 81

SPECIMEN ID LETTER/ALLOY: L/254SF6

OPEN CIRCUIT POTENTIAL: -180 mV

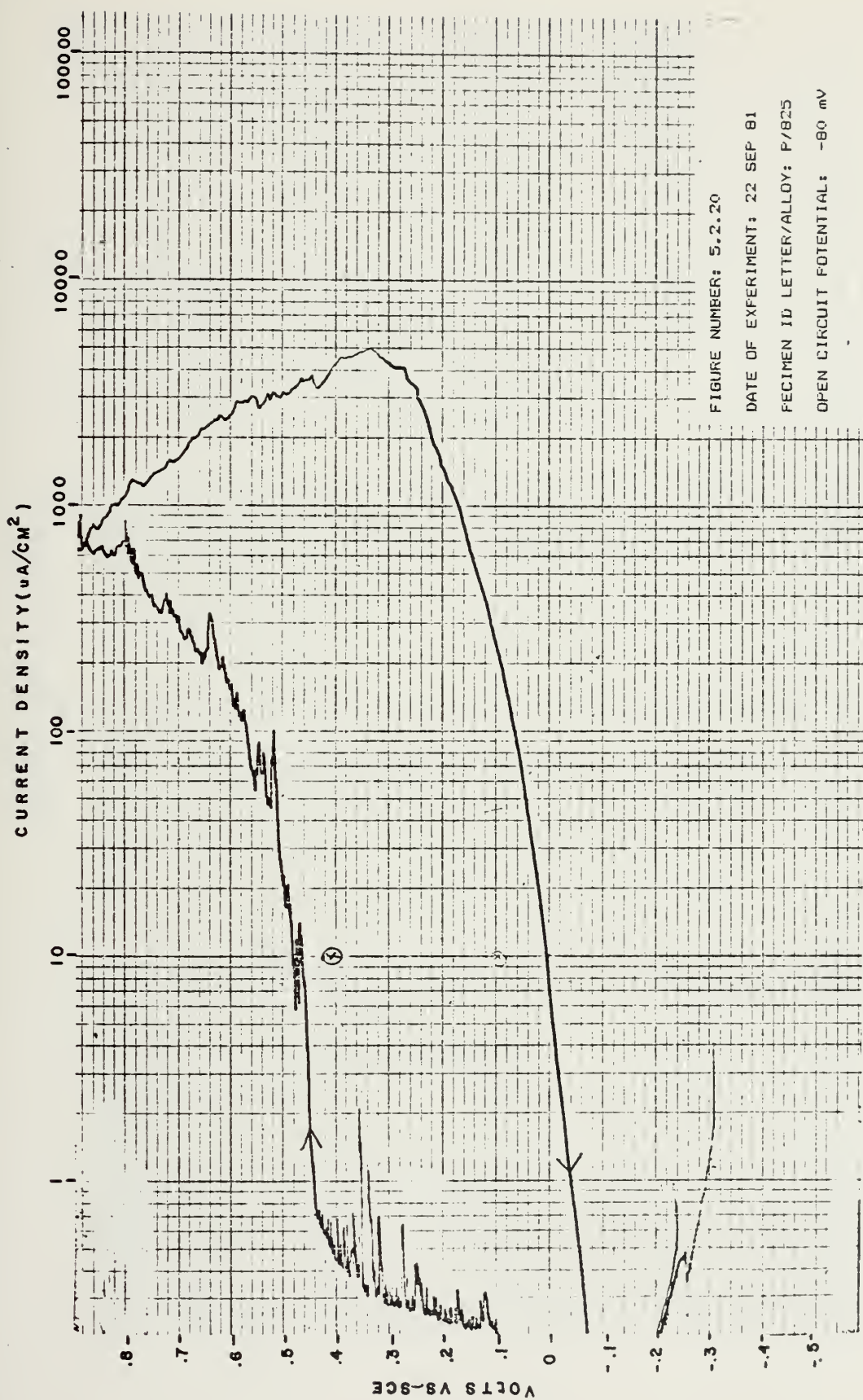


FIGURE NUMBER: 5.2.20

DATE OF EXPERIMENT: 22 SEP 81

SPECIMEN ID LETTER/ALLOY: P/B25

OPEN CIRCUIT POTENTIAL: -80 mV

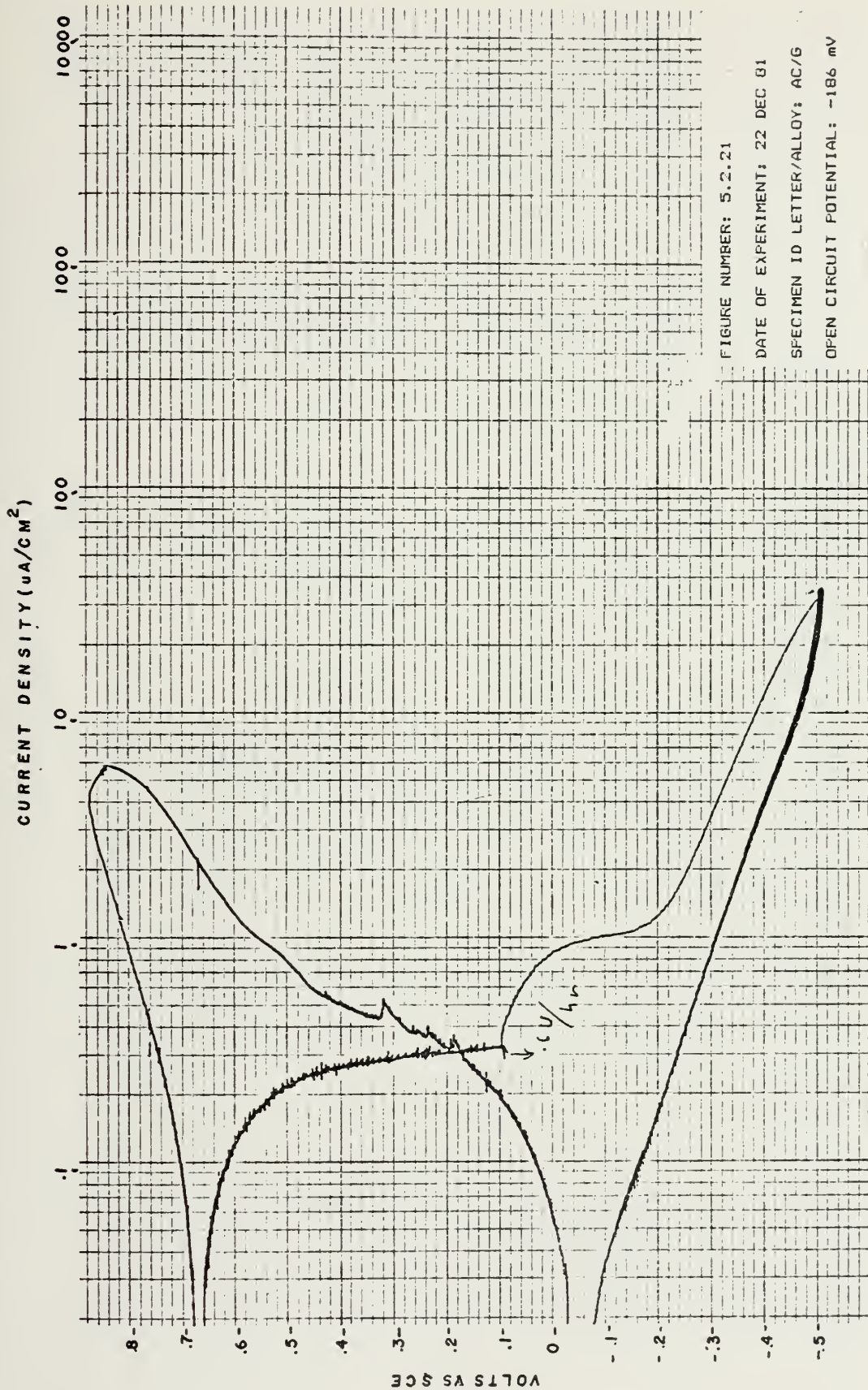


FIGURE NUMBER: 5.2.21

DATE OF EXPERIMENT: 22 DEC 81

SPECIMEN ID LETTER/ALLOY: AC/G

OPEN CIRCUIT POTENTIAL: -186 mV

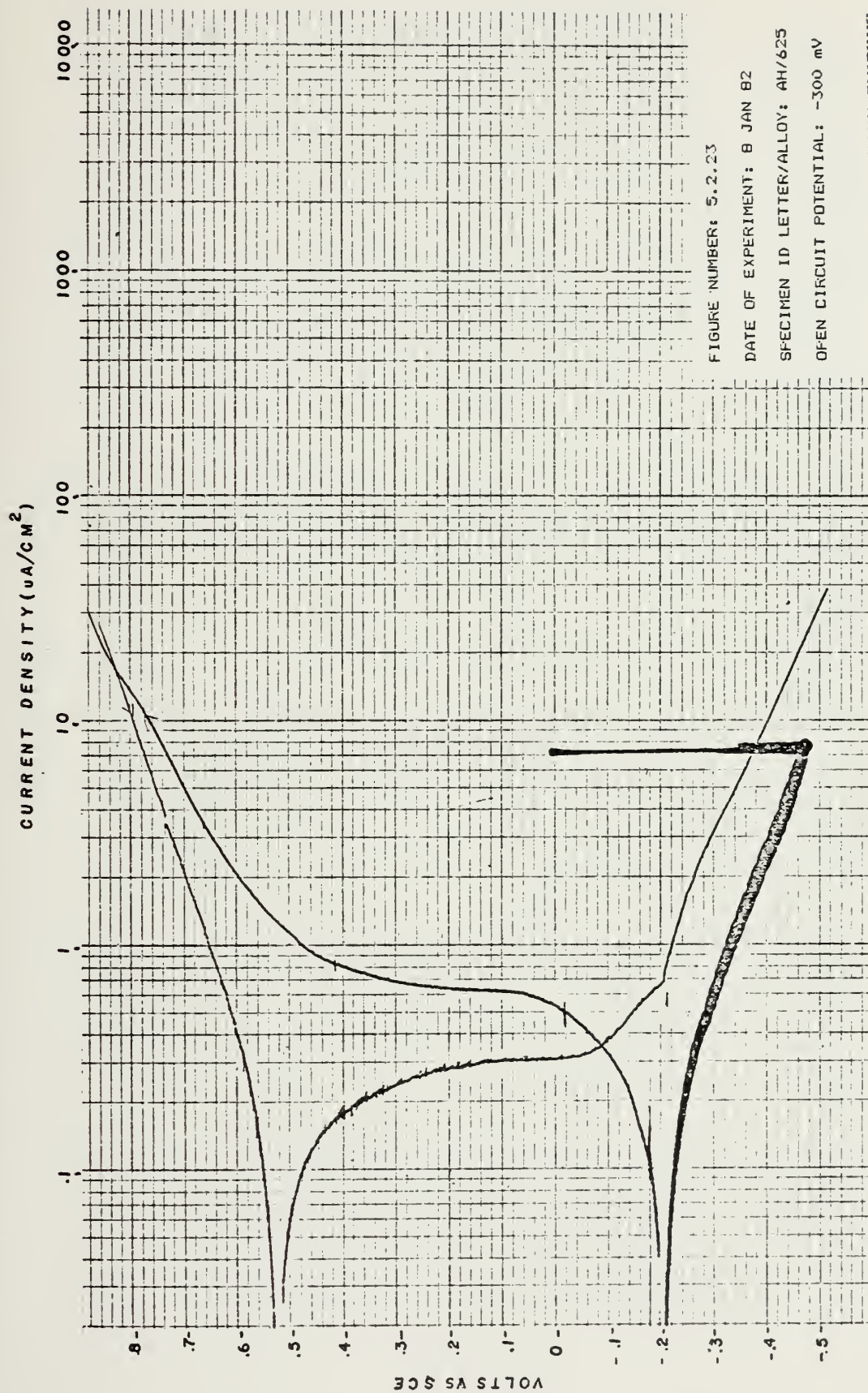


FIGURE NUMBER: 5.2.23

DATE OF EXPERIMENT: 8 JAN 82

SPECIMEN ID LETTER/ALLOY: AH/625

OPEN CIRCUIT POTENTIAL: -300 mV

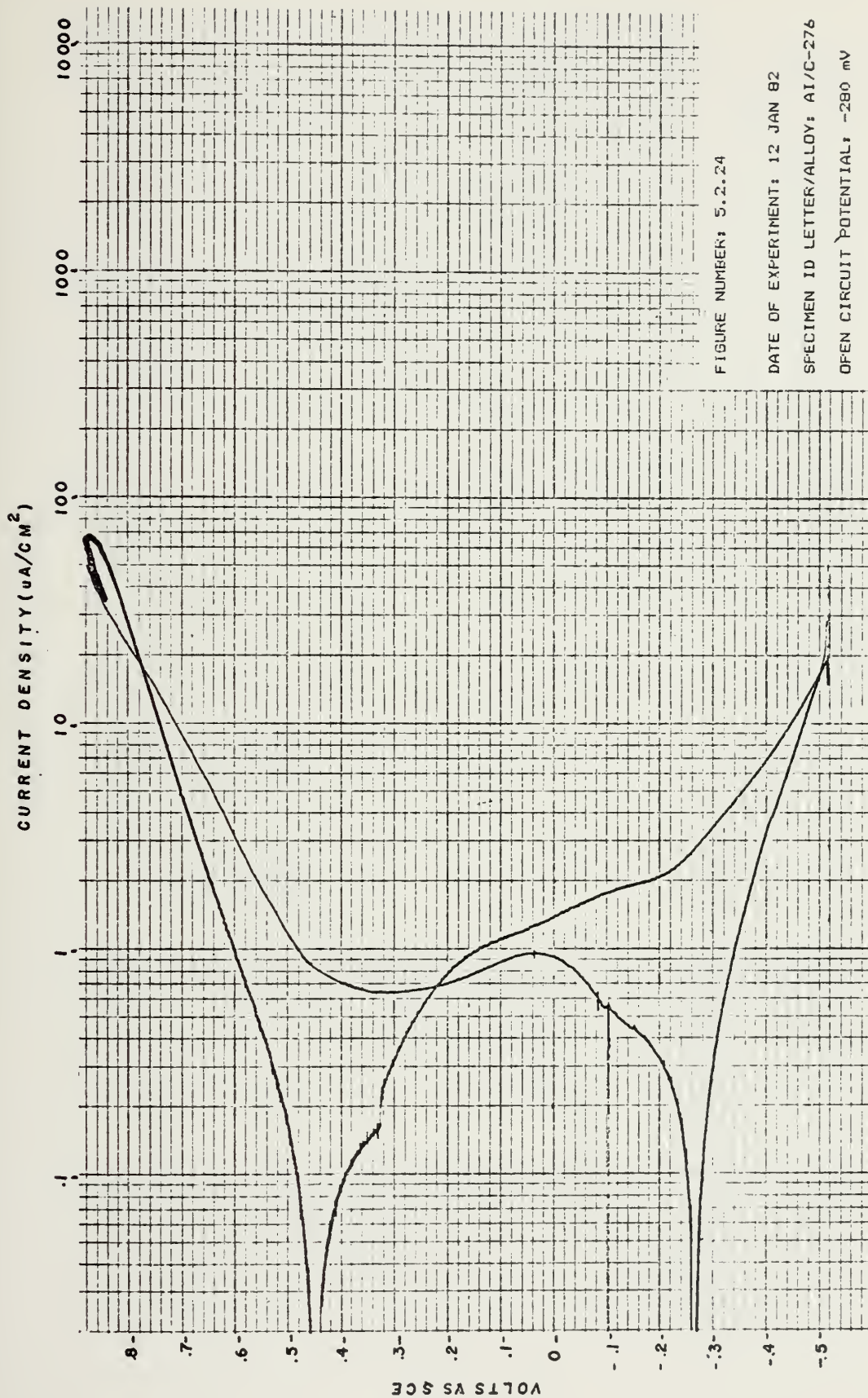


FIGURE NUMBER: 5.2.24

DATE OF EXPERIMENT: 12 JAN 82

SPECIMEN ID LETTER/ALLOY: AI/C-276

OPEN CIRCUIT POTENTIAL: -280 mV

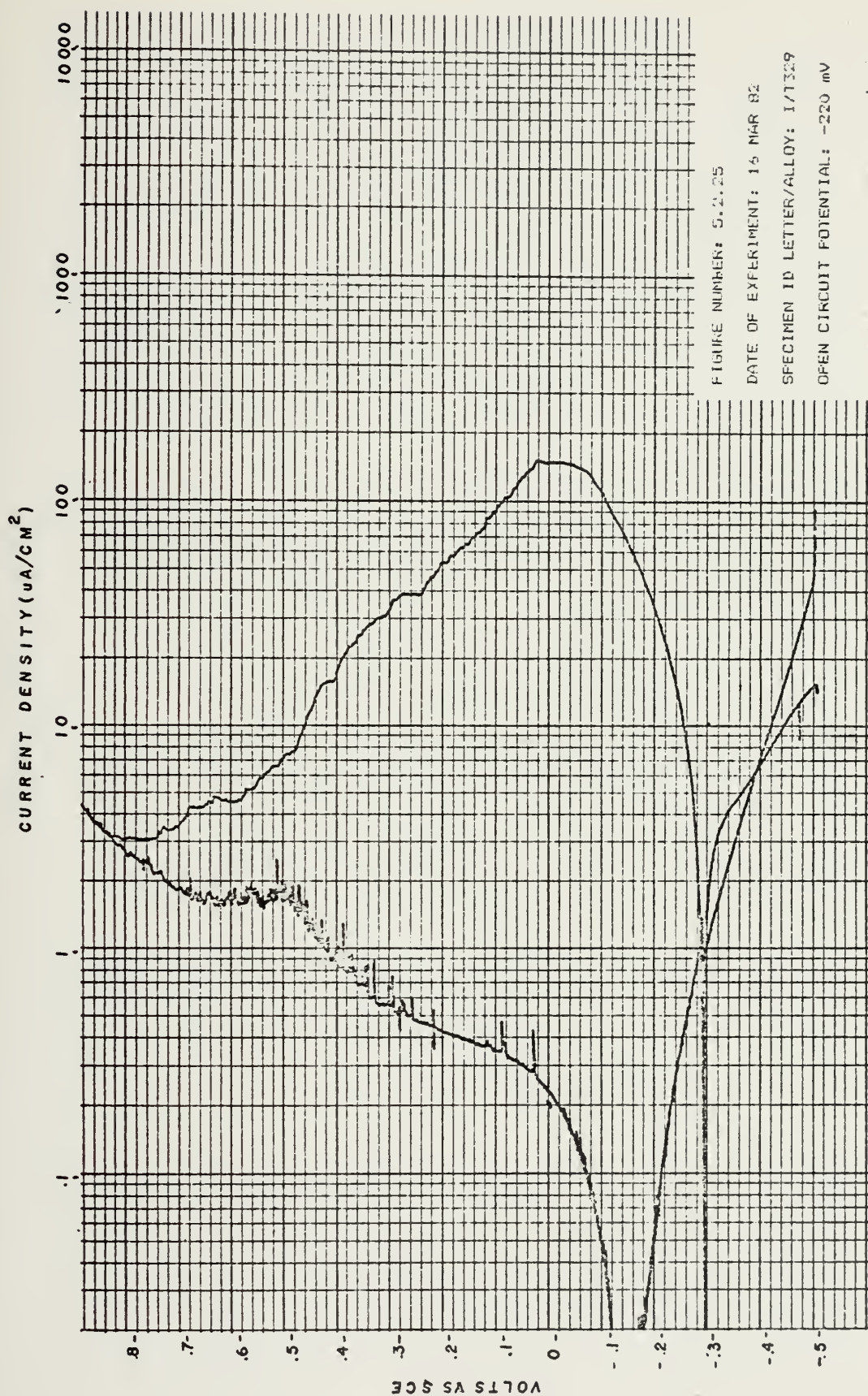
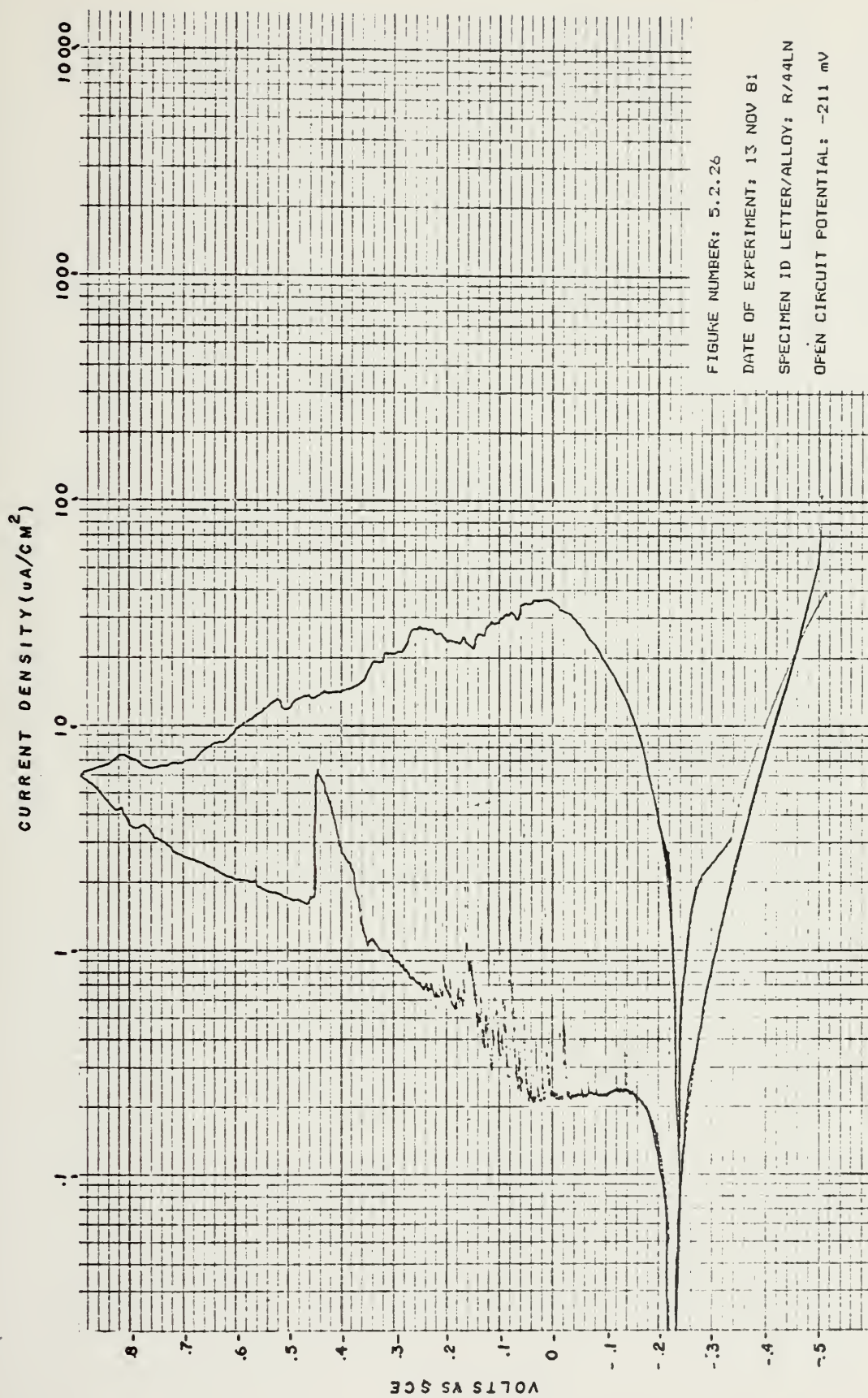


FIGURE NUMBER: 5.2.25

DATE OF EXPERIMENT: 16 MAR 82

SPECIMEN ID LETTER/ALLOY: 171329

OPEN CIRCUIT POTENTIAL: -220 mV



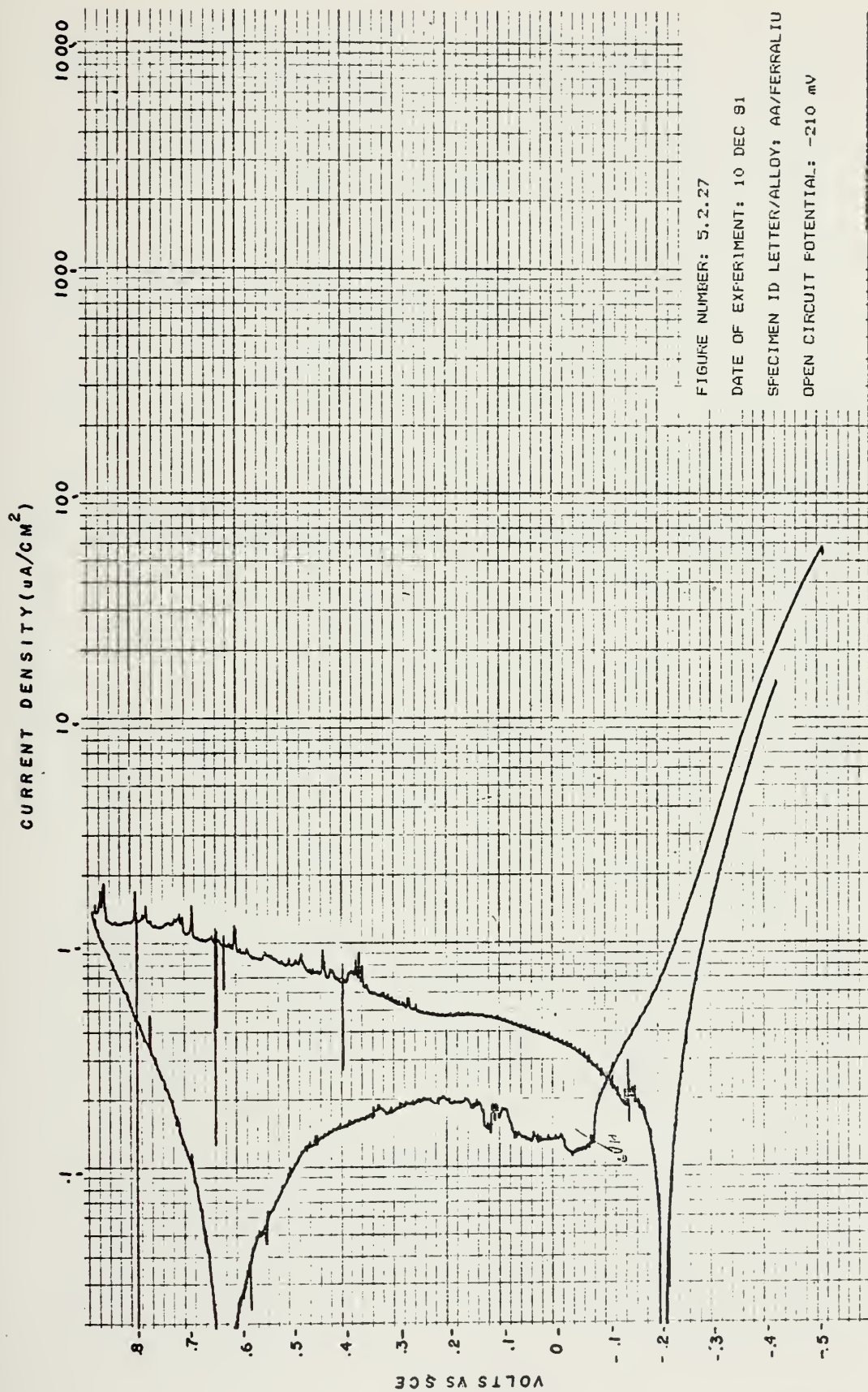


FIGURE NUMBER: 5.2.27

DATE OF EXPERIMENT: 10 DEC 91

SPECIMEN ID LETTER/ALLOY: AA/FERRALIU

OPEN CIRCUIT POTENTIAL: -210 mV

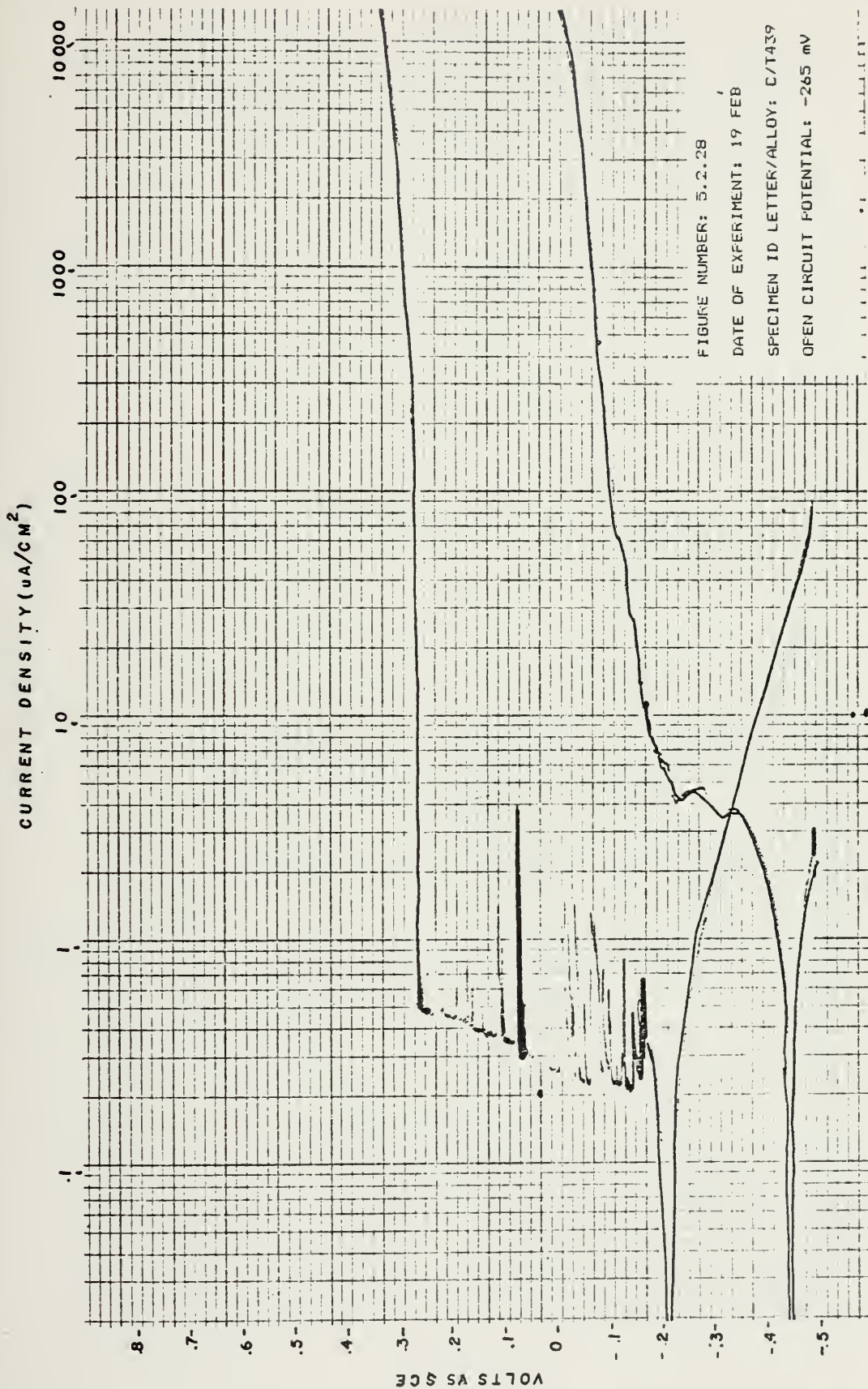


FIGURE NUMBER: 5.2.28

DATE OF EXPERIMENT: 19 FEB

SPECIMEN ID LETTER/ALLOY: C/T439

OPEN CIRCUIT POTENTIAL: -265 mV

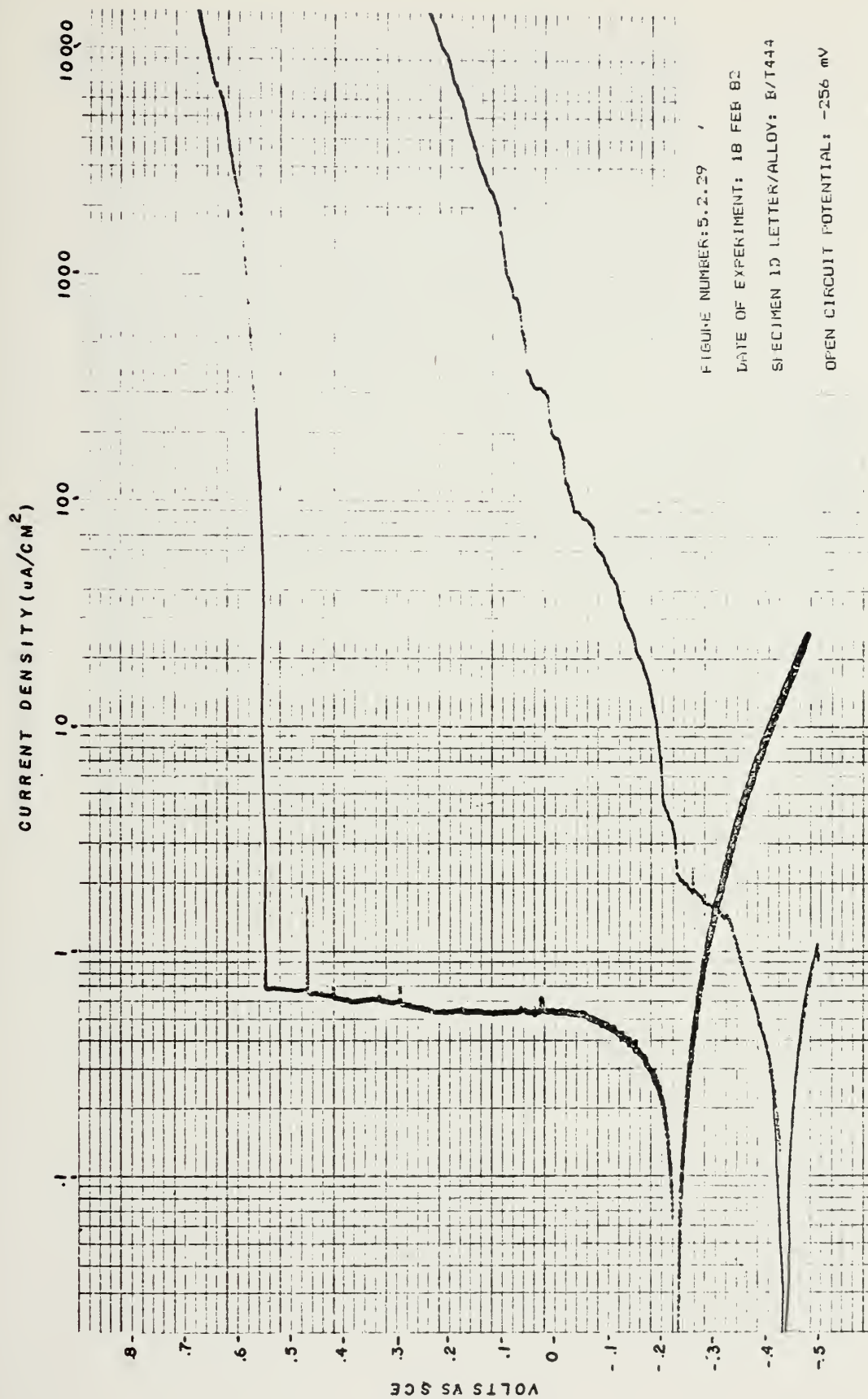
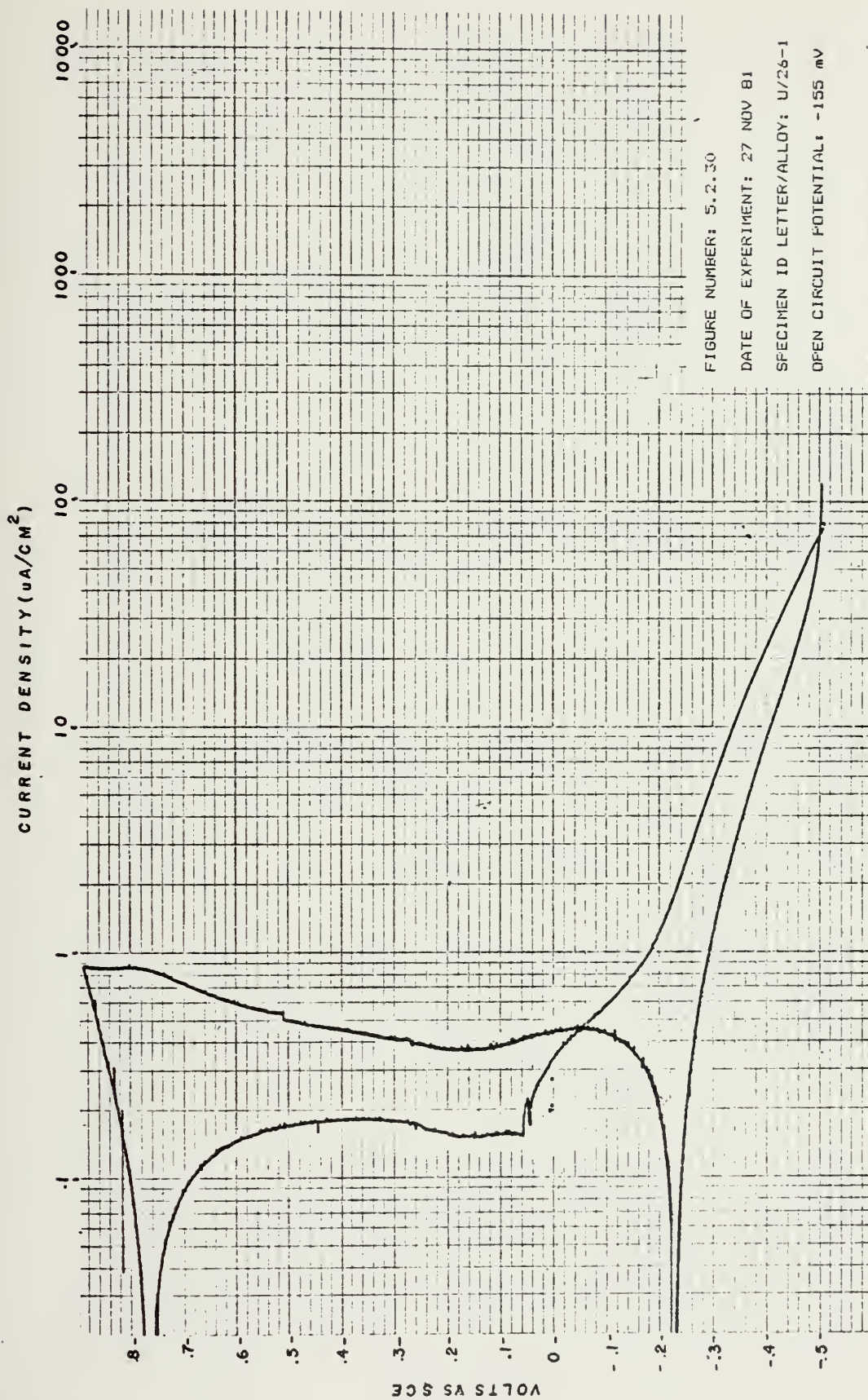


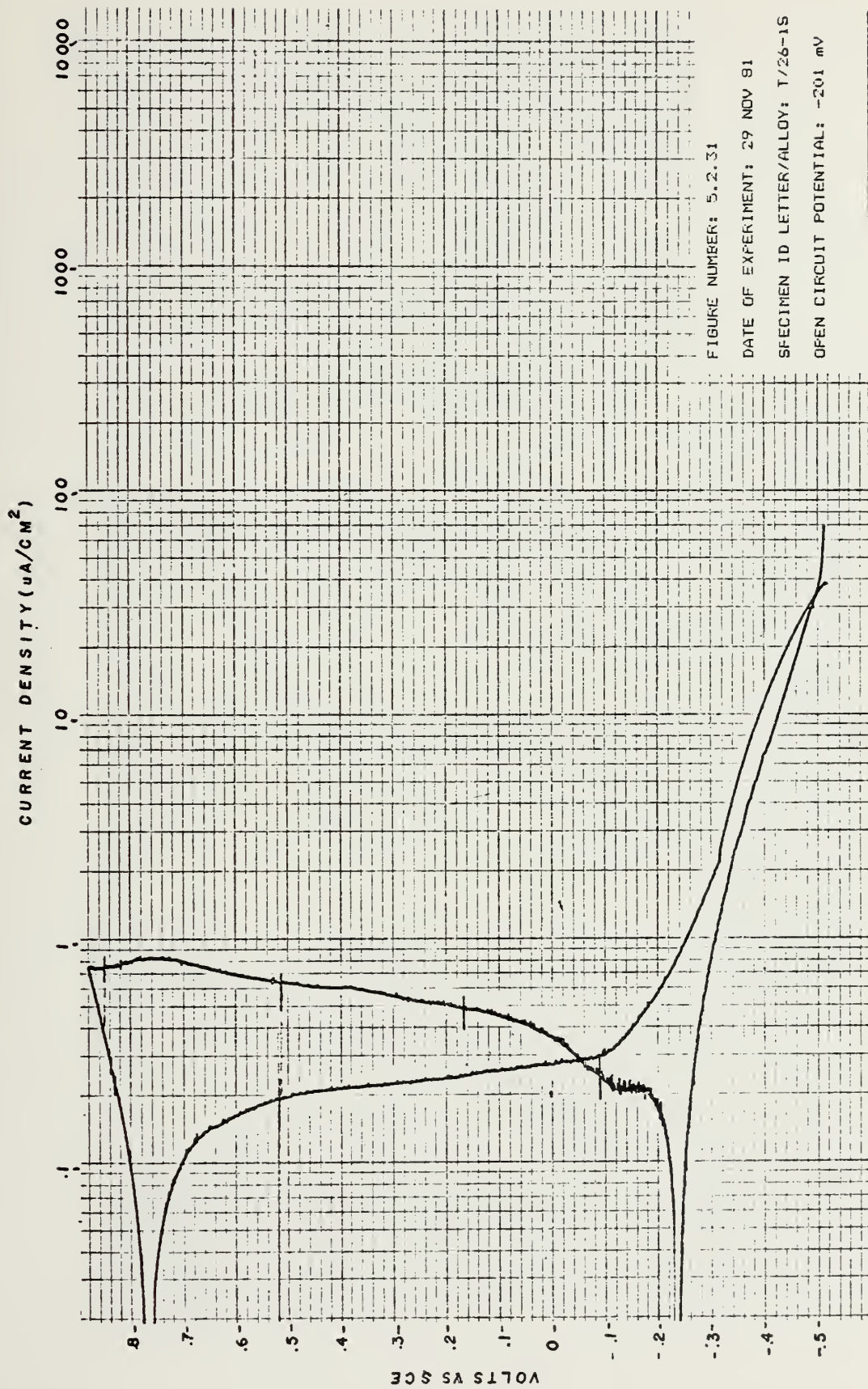
FIGURE NUMBER: 5.2.29

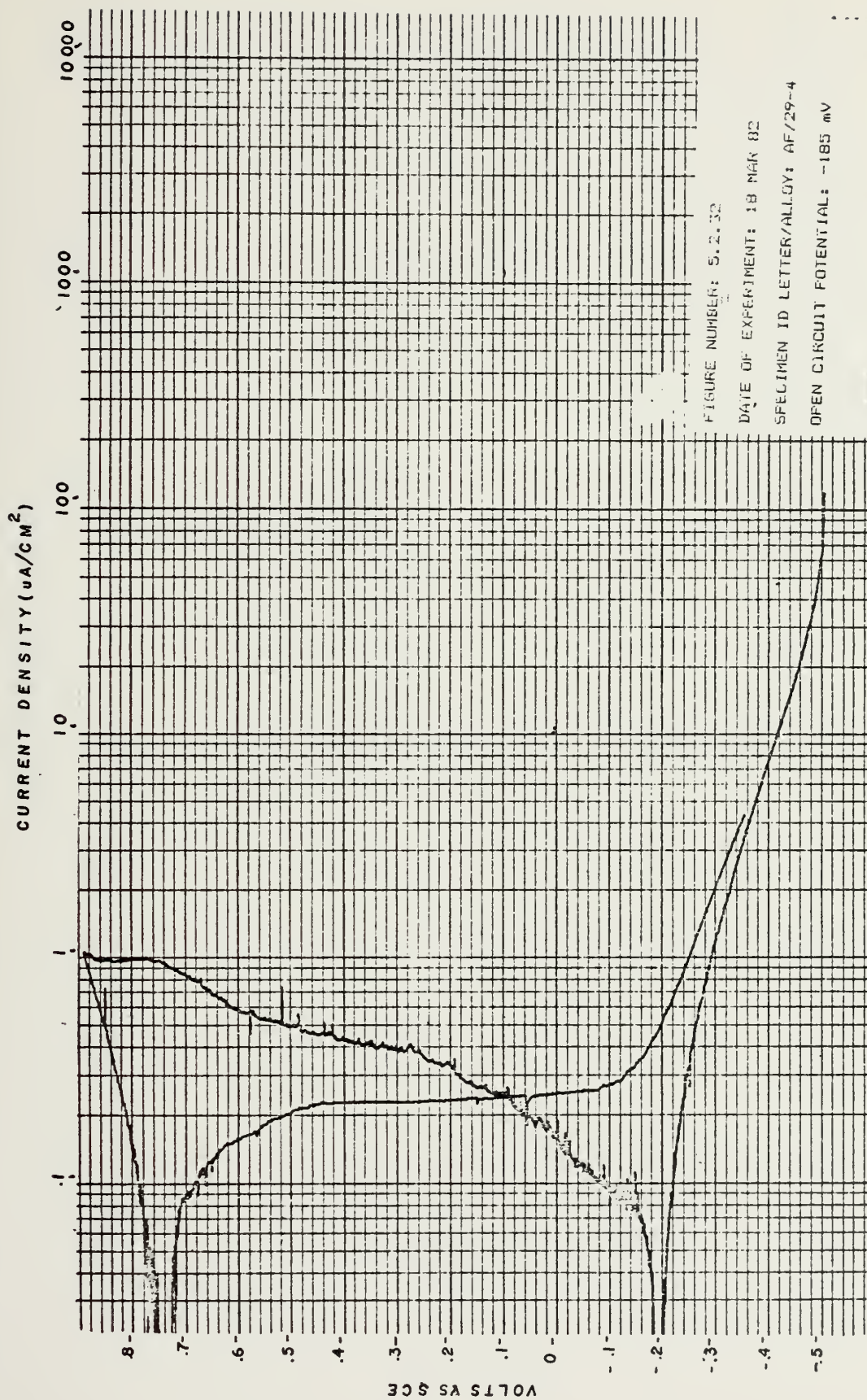
DATE OF EXPERIMENT: 18 FEB 82

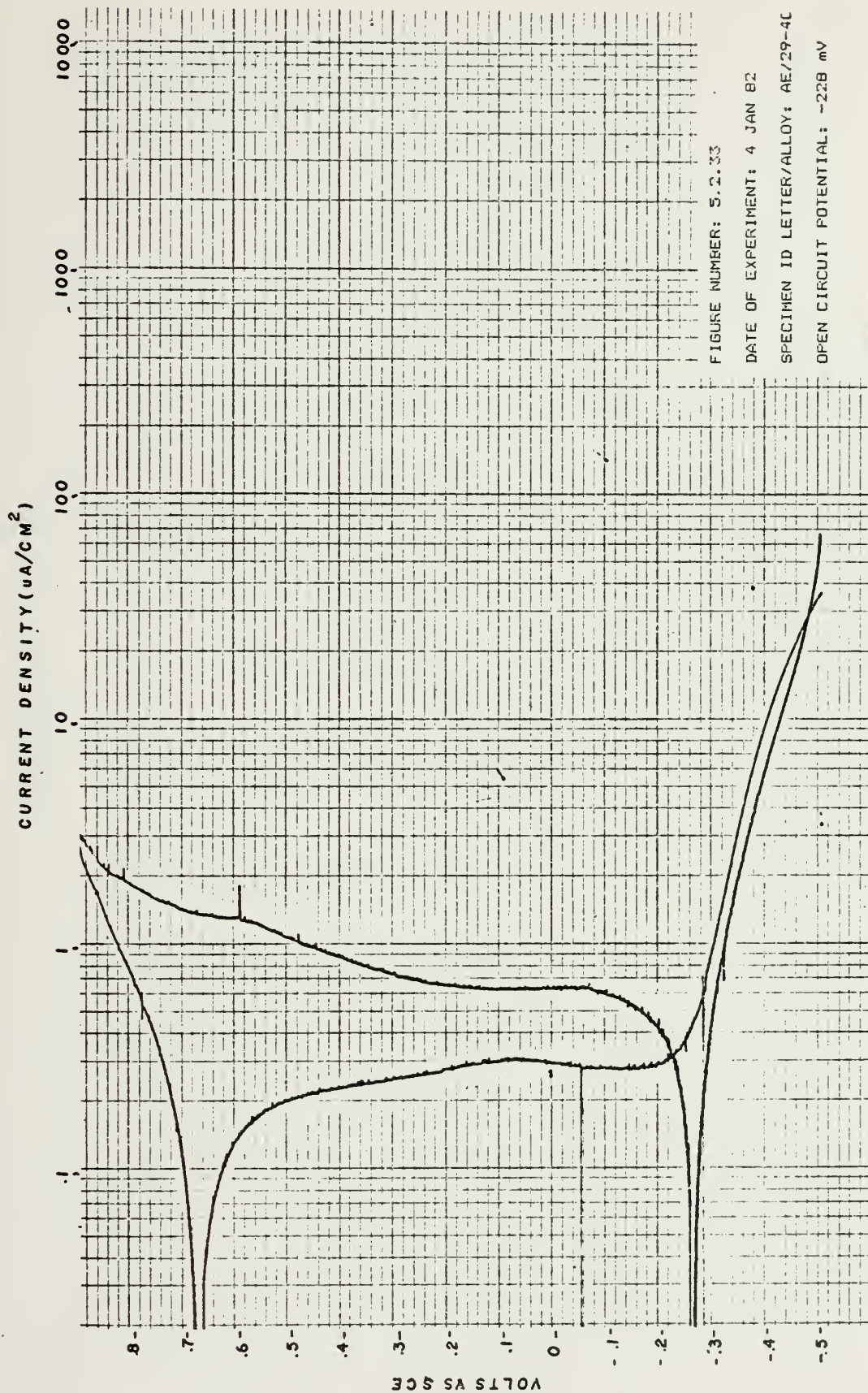
SPECIMEN 1D LETTER/ALLOY: B/T444

OPEN CIRCUIT POTENTIAL: -256 mV









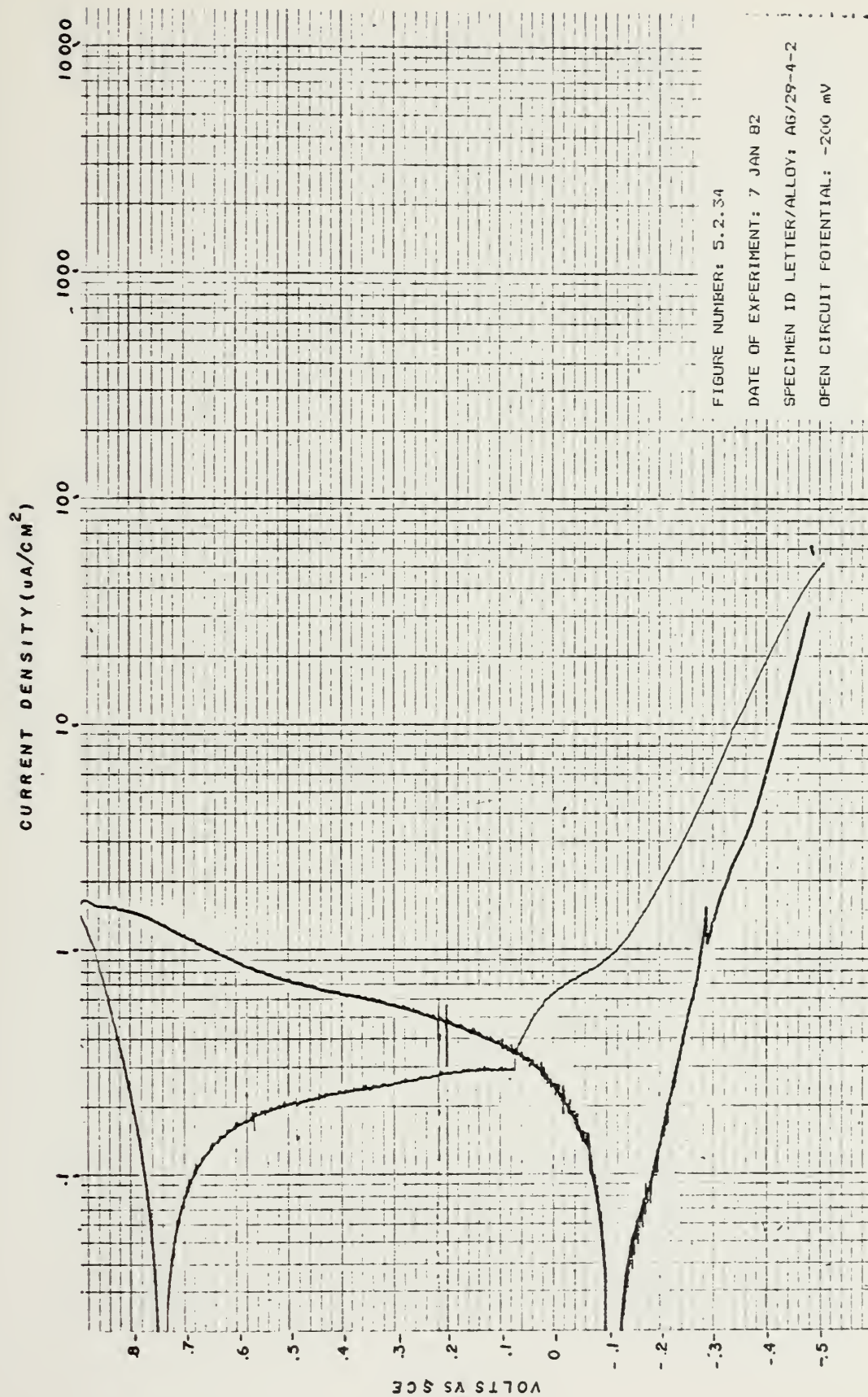


FIGURE NUMBER: 5.2.34

DATE OF EXPERIMENT: 7 JAN 82

SPECIMEN ID LETTER/ALLOY: AG/29-4-2

OPEN CIRCUIT POTENTIAL: -200 mV

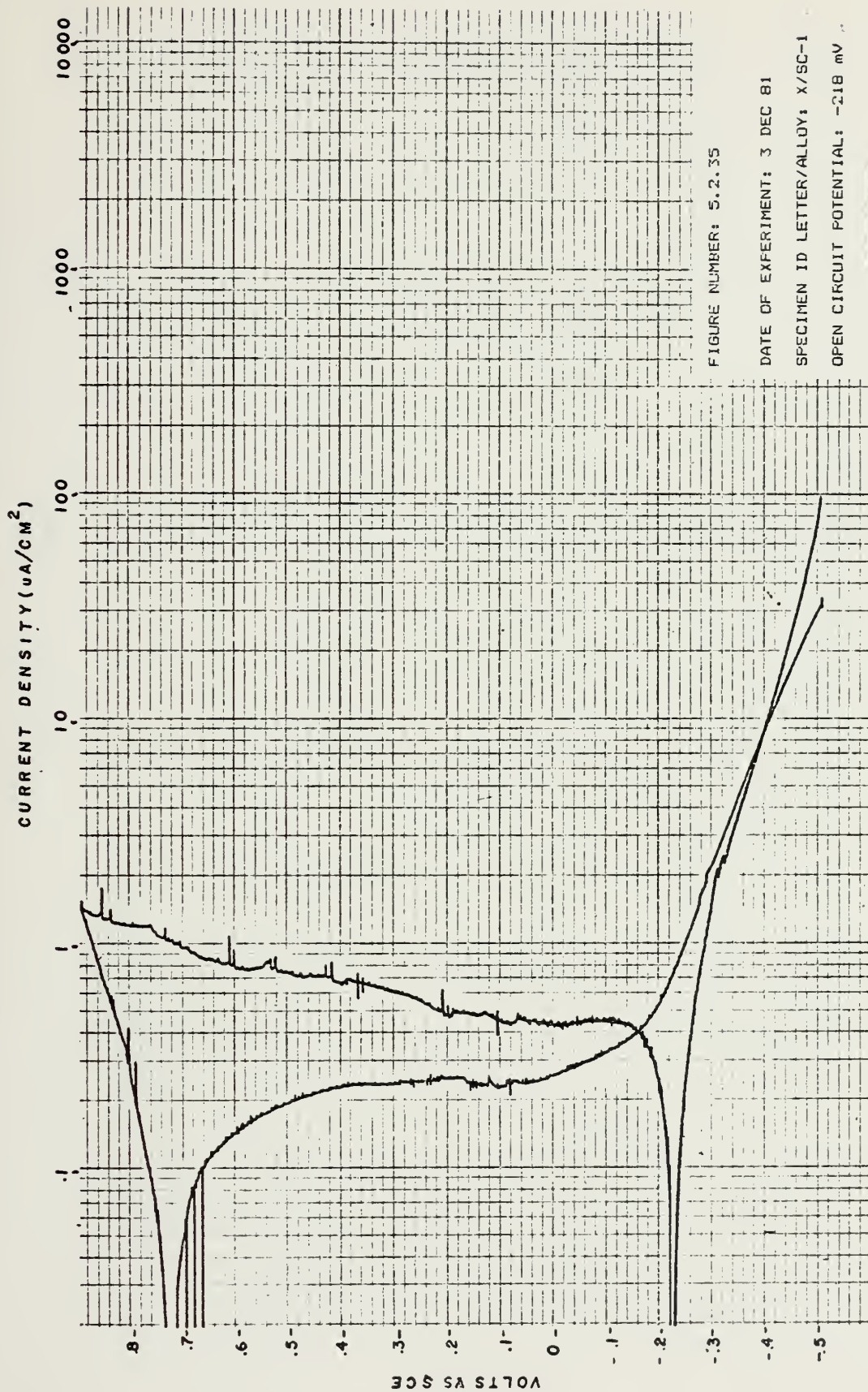
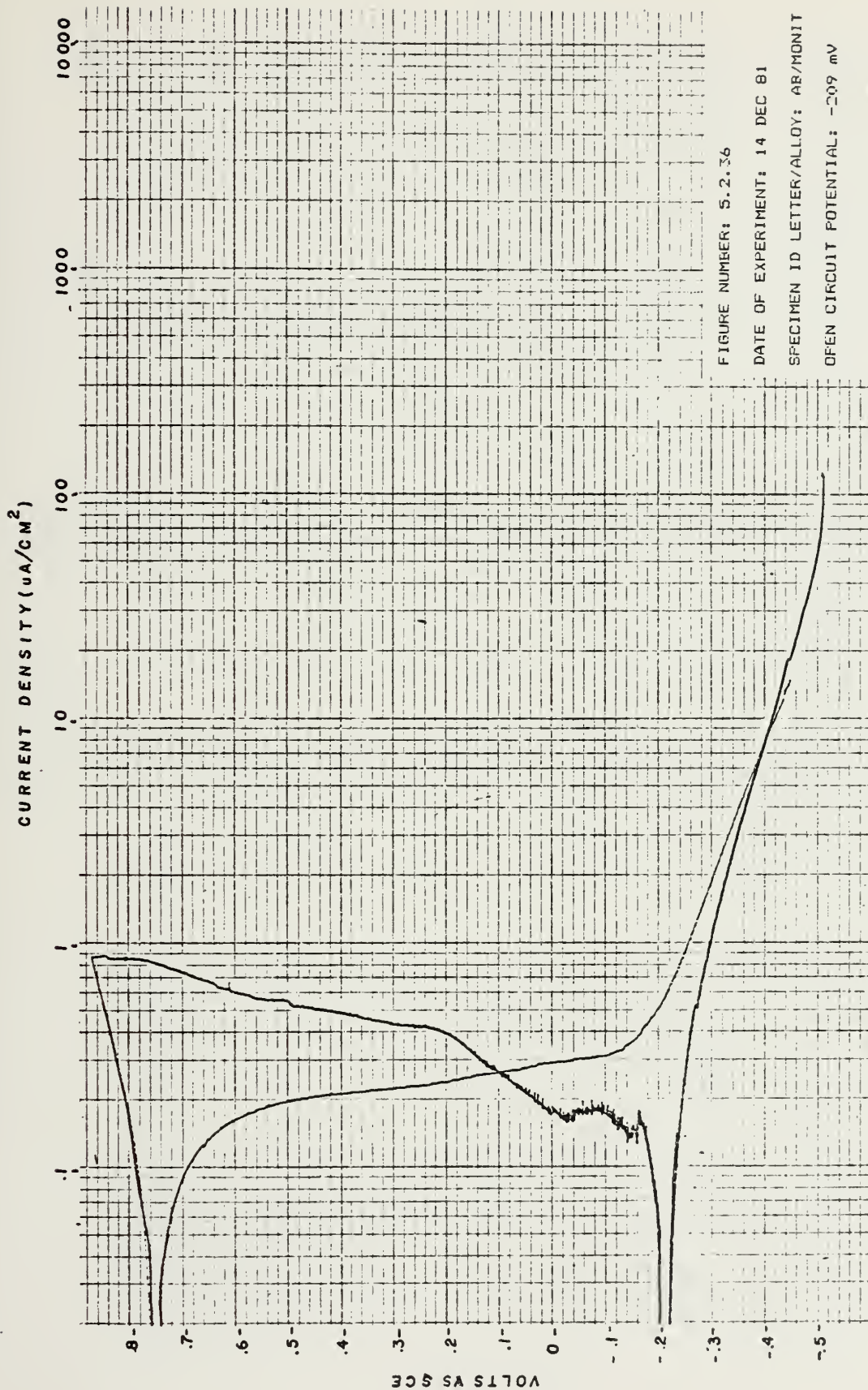


FIGURE NUMBER: 5.2.35

DATE OF EXPERIMENT: 3 DEC 81

SPECIMEN ID LETTER/ALLOY: X/SC-1

OPEN CIRCUIT POTENTIAL: -218 mV



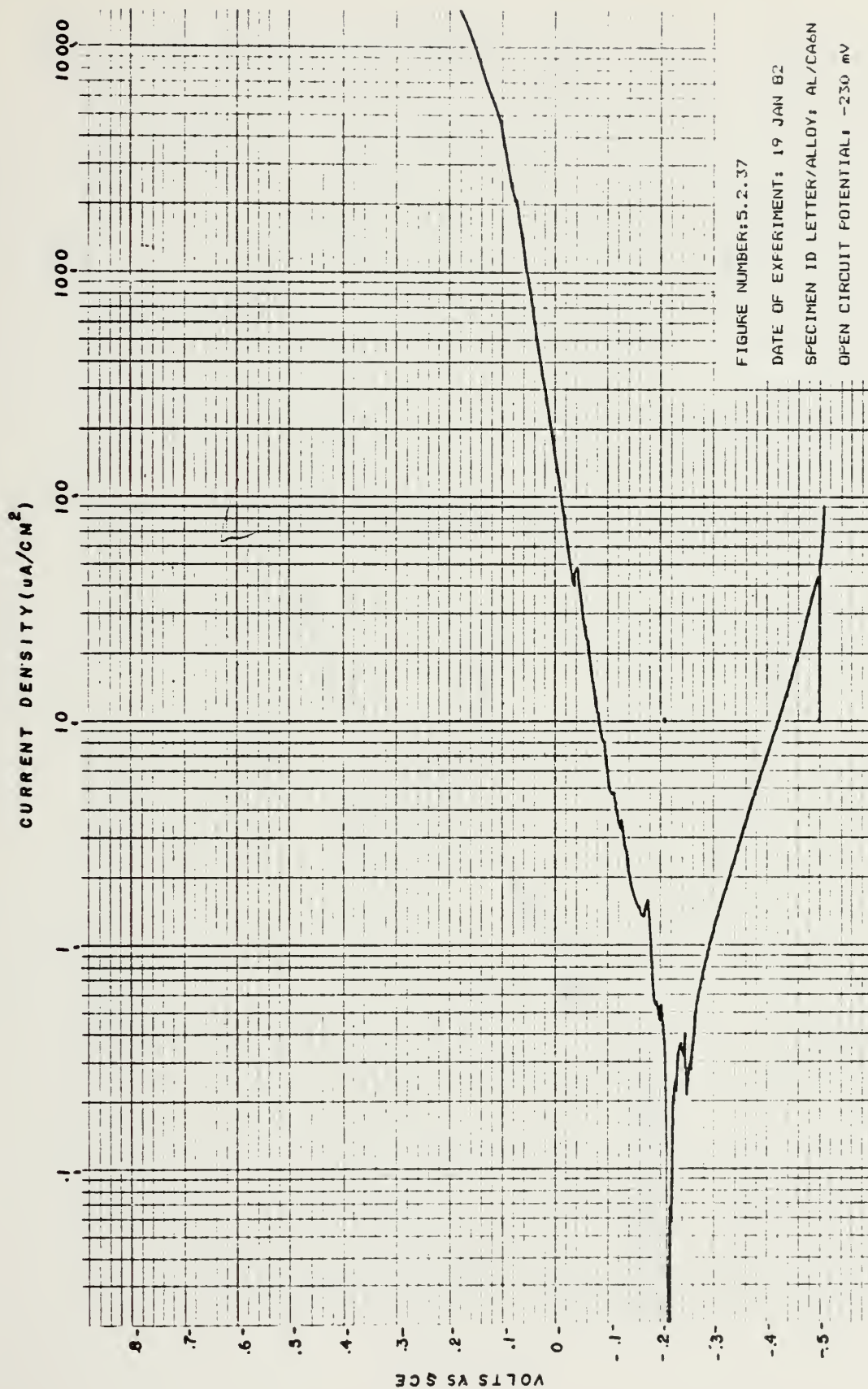
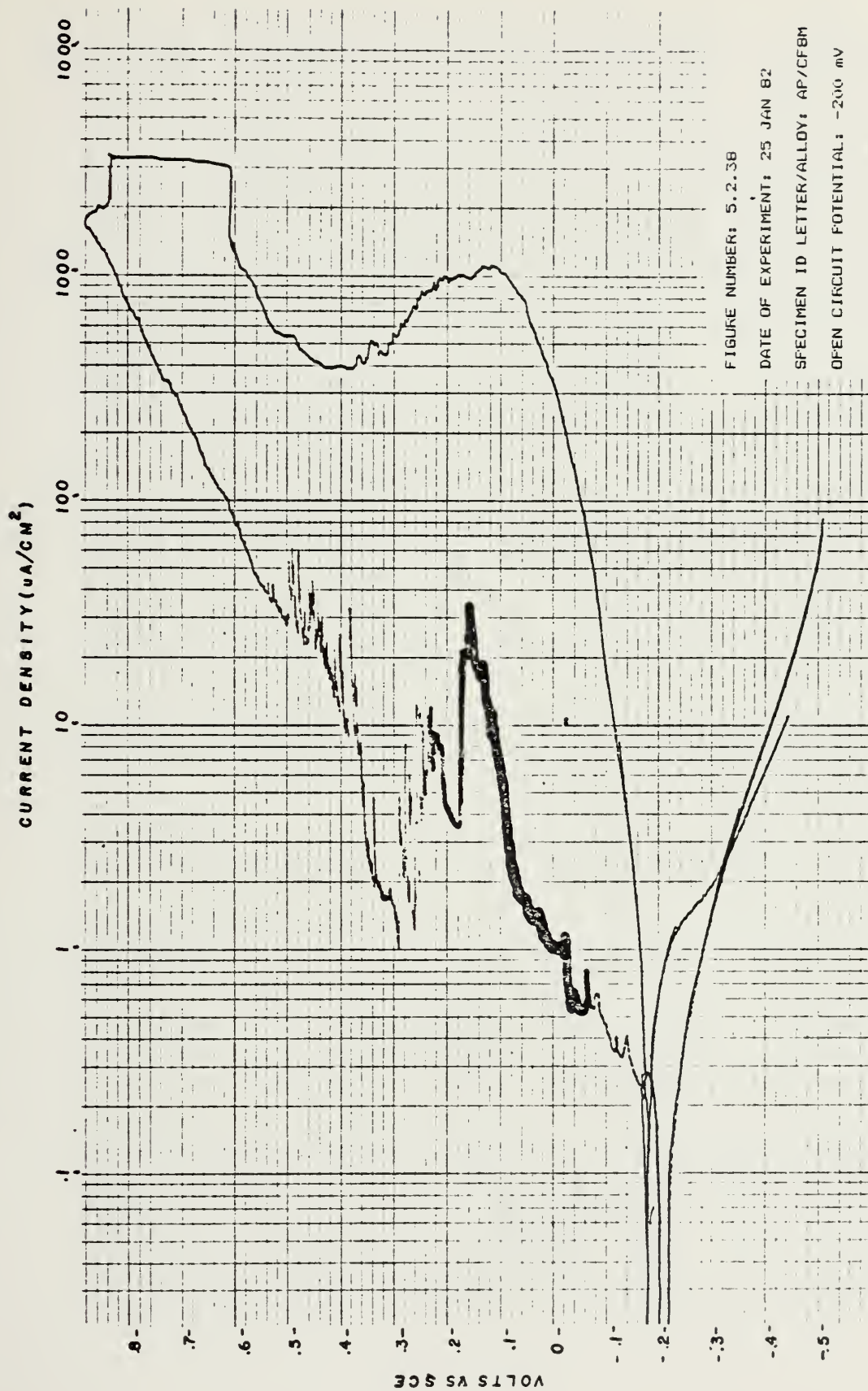


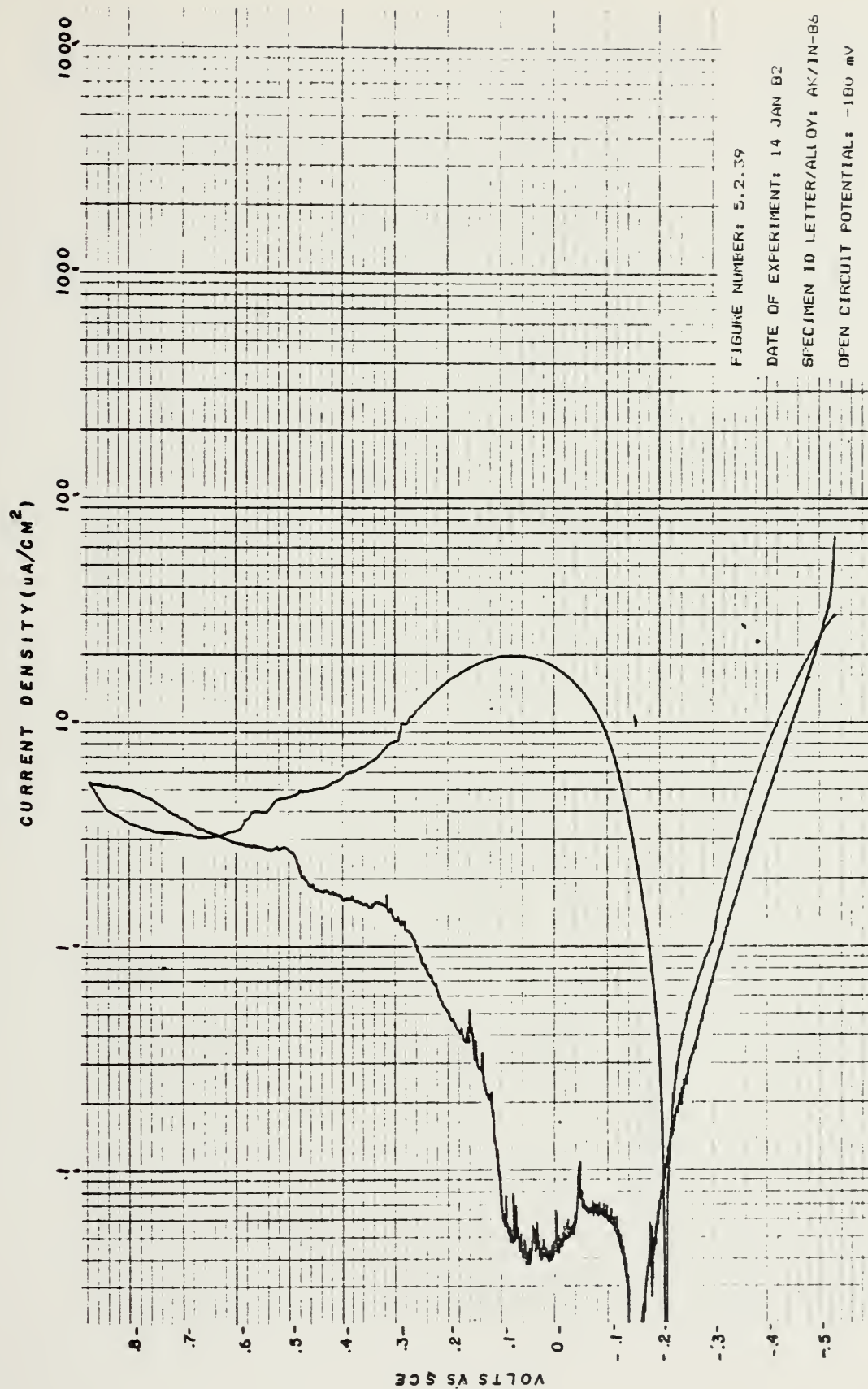
FIGURE NUMBER: S.2.37

DATE OF EXPERIMENT: 19 JAN 82

SPECIMEN ID LETTER/ALLOY: AL/CA6N

OPEN CIRCUIT POTENTIAL: -230 mV





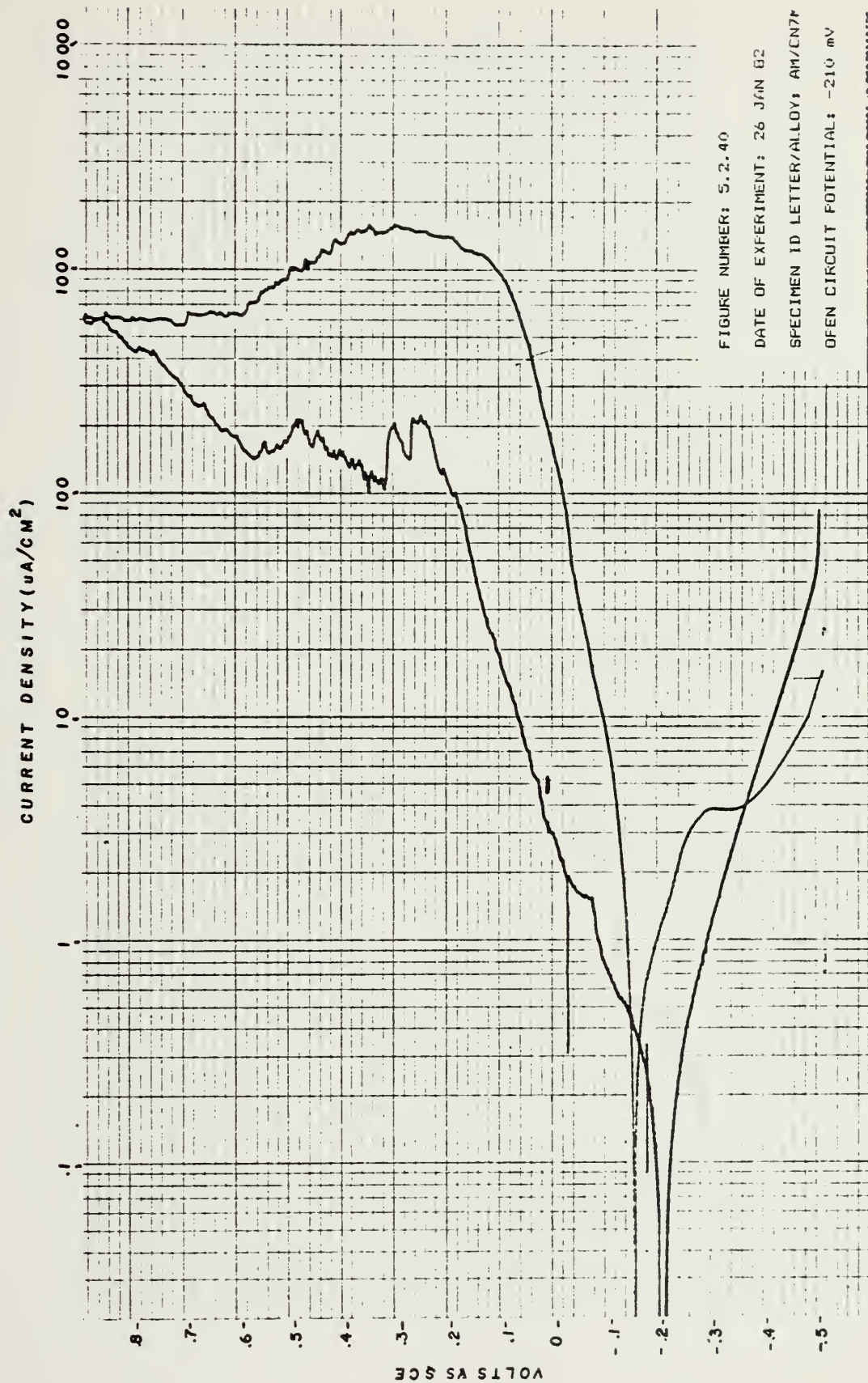


FIGURE NUMBER: 5.2.40

DATE OF EXPERIMENT: 26 JUN 82

SPECIMEN ID LETTER/ALLOY: AM/CN7

OPEN CIRCUIT POTENTIAL: -210 mV

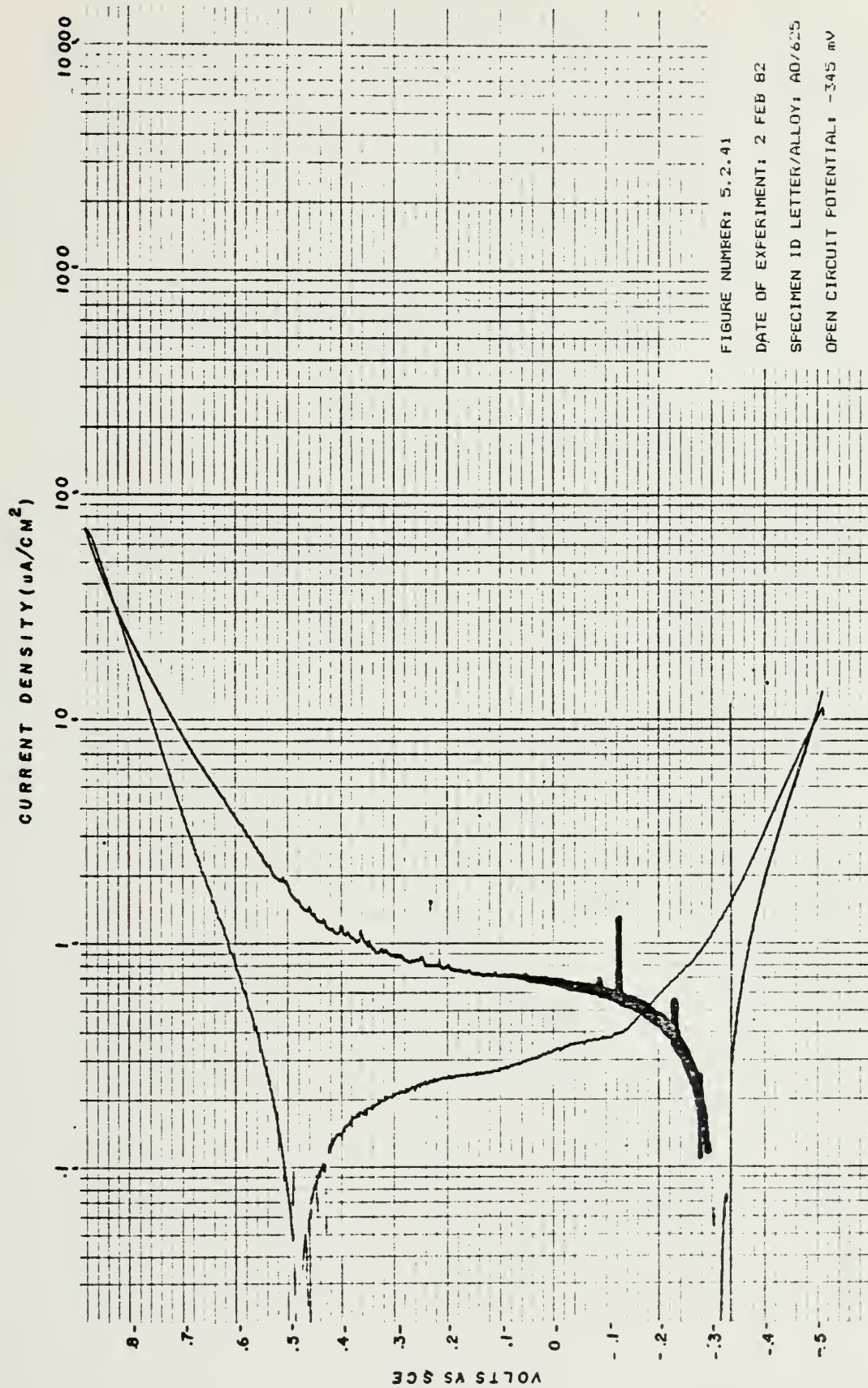
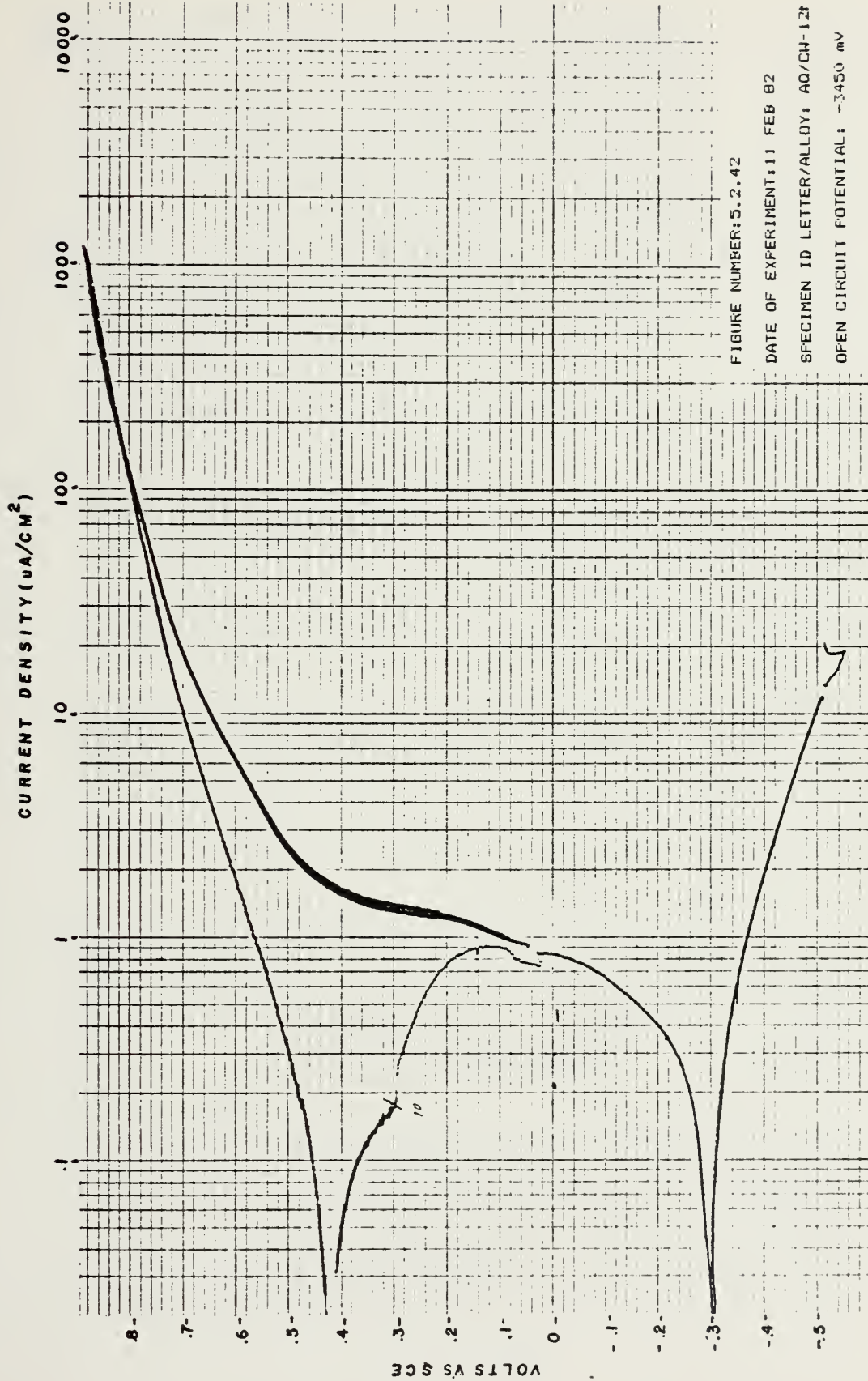


FIGURE NUMBER: 5.2.41

DATE OF EXPERIMENT: 2 FEB 82

SPECIMEN ID LETTER/ALLOY: AD/625

OPEN CIRCUIT POTENTIAL: -345 mV



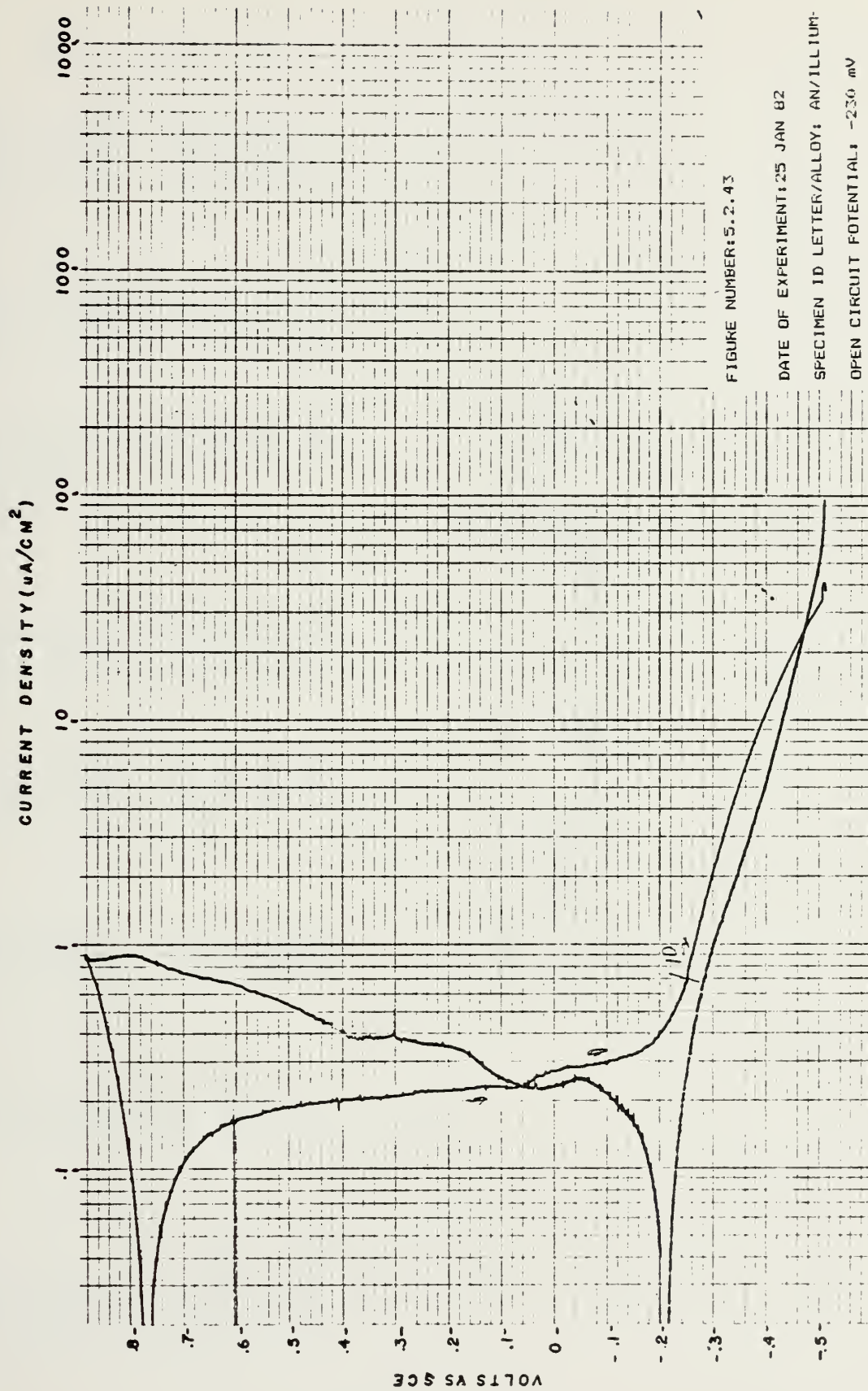


FIGURE NUMBER: 5.2.43

DATE OF EXPERIMENT: 25 JAN 82

SPECIMEN ID LETTER/ALLOY: AN/ILLIUM-

OPEN CIRCUIT POTENTIAL: -230 mV

<u>ALLOY</u>	<u>Ecorr</u>	<u>Ep</u>	<u>Ex</u>	<u>Eprot</u>	<u>Imax</u>	<u>Eprot- Ecorr</u>	<u>Ex-Ep</u>
T316	-110	-40	-170	-180	70,000	-70	-130
34LN	-185	140	-195	-200	330	-15	-335
T216	-200	500	-220	-220	30	-20	-720
Rex734	-190	-	-	700	800	890	-
T317L	-180	300	-220	-230	800	-50	-520
317 LM	-200	250	-220	-220	700	-20	-470
317 L+	-170	300	-220	-220	230	-50	-520
22-13-5	-170	100	-210	-215	80	-45	-310

TABLE 5.2.1 Tabulation of Parameters
For Austenitic 6% to 16% Nickel Alloys
(E in mV vs SCE, I in $\mu\text{A}/\text{cm}^2$)

ALLOY	<u>Ecorr</u>	<u>Ep</u>	<u>Ex</u>	<u>Eprot</u>	<u>Imax</u>	<u>Eprot-Ecorr</u>	<u>Ex-Ep</u>
904L	-190	520	- 65	- 80	210	110	-585
4X	-85	130	-145	-145	80	60	-275
700	-140	150	-205	-205	120	-65	-355
254 SLX	-190	-	- 30	- 30	60	160	-
777	-110	250	-125	-120	100	-20	-375
254 SMO	-175	-	-	+670	2	845	-
6X	-170	-	-	+730	1.3	900	-
20 Mod	-155	-	-	+730	6	885	-
20 Cb-3	-120	285	- 80	- 80	9000	40	-365
20 Mo6	-140	-	-	+730	2	870	-
254 SFeR	-140	120	-190	-190	200	-50	310

TABLE 5.2.2 Tabulation of Parameters
For Austenitic 17% to 40% Nickel Alloys
(E in mV vs SCE, I in $\mu\text{A}/\text{cm}^2$)

<u>ALLOY</u>	<u>Ecorr</u>	<u>Ep</u>	<u>Ex</u>	<u>Eprot</u>	<u>I_{max}</u>	<u>E_{prot}- E_{corr}</u>	<u>Ex-E_p</u>
825	-145	470	-90	-90	5000	55	-560
G	-130	-	-	650	4	780	-
G-3	-150	-	-	580	5	730	-
625	-210	300	830	520	30	730	530
C-276	-230	300	750	530	50	760	450

TABLE 5.2.3 Tabulation of Parameters
For Austenitic >40% Nickel Alloys
(E in mV vs SCE, I in $\mu\text{A}/\text{cm}^2$)

<u>ALLOY</u>	<u>E_{corr}</u>	<u>E_p</u>	<u>E_x</u>	<u>E_{prot}</u>	<u>I_{max}</u>	<u>E_{prot}- E_{corr}</u>	<u>E_x-E_p</u>
T329	-150	350	-300	-300	130	-150	-650
44LN	-230	160	-260	-265	40	-35	-420
Ferralium	-215	-	-	645	2	860	-

TABLE 5.2.4 Tabulation of Parameters
For Duplex Austenitic-Ferritic Alloys
(E in mV vs SCE, I in $\mu\text{A}/\text{cm}^2$)

<u>ALLOY</u>	<u>Ecorr</u>	<u>Ep</u>	<u>Ex</u>	<u>Eprot</u>	<u>Imax</u>	<u>Eprot-Ecorr</u>	<u>Ex-Ep</u>
T439	-230	180	-370	-460	100,000	-230	-550
T444	-250	525	-320	-420	100,000	-170	-845
26-1	-230	-	-	770	1	1000	-
26-1S	-230	-	-	740	1	970	-
29-4	-215	-	-	725	1	940	-
29-4C	-245	-	-	750	2	995	-
29-4-2	-150	-	-	715	2	865	-
SC-1	-230	-	-	720	1	950	-
MONIT	-230	-	-	740	1	970	-

TABLE 5.2.5 Tabulation of Parameters
For Ferritic Alloys
(E in mV vs SCE, I in $\mu\text{A}/\text{cm}^2$)

<u>ALLOY</u>	<u>Ecorr</u>	<u>Ep</u>	<u>Ex</u>	<u>Eprot</u>	<u>Imax</u>	<u>Eprot- Ecorr</u>	<u>Ex-Ep</u>
CA6N	-270	-	-	-	>100,000	-	-
CF8M	-210	-100	-170	-180	3,500	+30	-70
IN862	-150	100	-200	-210	20	-60	-300
CN7M	-200	- 85	-150	-150	1,500	50	65
625	-280	250	830	465	75	745	580
ILLIUM W-2	-310	400	790	475	900	785	390
ILLIUM PD	-225	-	-	705	2	930	-

TABLE 5.2.6 Tabulation of Parameters

For Cast Alloy

(E in mV vs SCE, I in $\mu\text{A}/\text{cm}^2$)

5.3 SURFACE ANALYSIS RESULTS

In this study surface analysis has been used to complement the results of the cyclic polarization measurements and to promote an understanding of the breakdown of passivity. In order to investigate the mechanism of the breakdown of passivity, several alloys were polarized using the methodology described in Section 4.2.2. The results of this investigation must be viewed in the light of the advantages and drawbacks of Auger Electron Spectroscopy discussed in Sections 2.5 and 4.3. All Auger spectra used in this analysis are contained in Appendix B.

Type 316 stainless steel was selected for AES analysis since it was the benchmark for this study. Using the constant potential method with an induced crevice former, Type 316 was polarized at 100 mV above and below its pitting potential as determined in the cyclic polarization experiments. Figure 5.3.1 shows the results of a composition/depth profile analysis of Type 316 stainless steel as described in Section 4.3. This sample was polarized to +300 mV (SCE) for 45 minutes in the presence of an intentionally induced crevice former. The anodic current density at the end of polarization was $1900 \mu\text{A}/\text{cm}^2$. The sample exhibited substantial corrosion under the crevice former.

AES analysis was performed within a site that underwent active dissolution.

Figure 5.3.2 shows the results of a composition/depth profile of Type 316 stainless steel, but it was performed on an area of the sample which was covered by the crevice former but did not undergo visible active dissolution. This site exhibited some discoloration, but no apparent metal loss.

Figure 5.3.3 shows the results of a composition/depth profile of Type 316 stainless steel polarized to +50 mV(SCE) for 45 minutes. Anodic current density was $160 \mu\text{A}/\text{cm}^2$. The sample exhibited only minor corrosion under the crevice former. The analysis was performed within a site that underwent visible localized corrosion.

Another reason for the initial selection of Type 316 stainless steel was to allow correlation of present findings with similar Auger studies and compare them to other theories by Zakipour and Leygraf (104) and Ogawa et al.(105). A widely held theory of resistance to passivity breakdown being the effect of MoO_4 on the inhibition of active dissolution (106).

Figure 5.3.4 shows the results of a composition/depth profile analysis of alloy T439 (UNS No. S43035: 17.6 Cr, 0.3 Ni, 0.26 Mn, more commonly called 18.SR). The sample was polarized to +300 mV(SCE) for 15 minutes. The anodic current at the end of the polarization was 62,000 $\mu\text{A}/\text{cm}^2$. The analysis was performed at a site that had undergone visible localized corrosion.

Figure 5.3.5 shows the results of a composition/depth profile analysis of alloy T444(UNS No. S44400: 18.9 Cr, 1.99 Mo, 0.43 Mn, more commonly called 18-2). The sample was polarized to +600 mV(SCE) for 15 minutes with the anodic current at the end of the polarization was 39,000 $\mu\text{A}/\text{cm}^2$. The analysis was performed at a site that had visible localized corrosion.

Alloys T439 and T444 were polarized to different potentials in order to have each above their specific pitting potential. The pitting potential was determined by the cyclic anodic polarization experiments. If polarization was attempted below the pitting potential, no visible active sites were produced within eight hours. Because of the substantial fall in bulk solution pH and the radically different experimental time, it was decided to polarize above the pitting potential in these two investigations.

Raw data from the Auger spectra were entered into a HP-67 calculator which had a program to determine the values of elemental weight percent. This data was then input into a simple FORTRAN program to utilize the ZETA plotter at the Information Processing Center at MIT, which produced Figures 5.3.1 to 5.3.5.

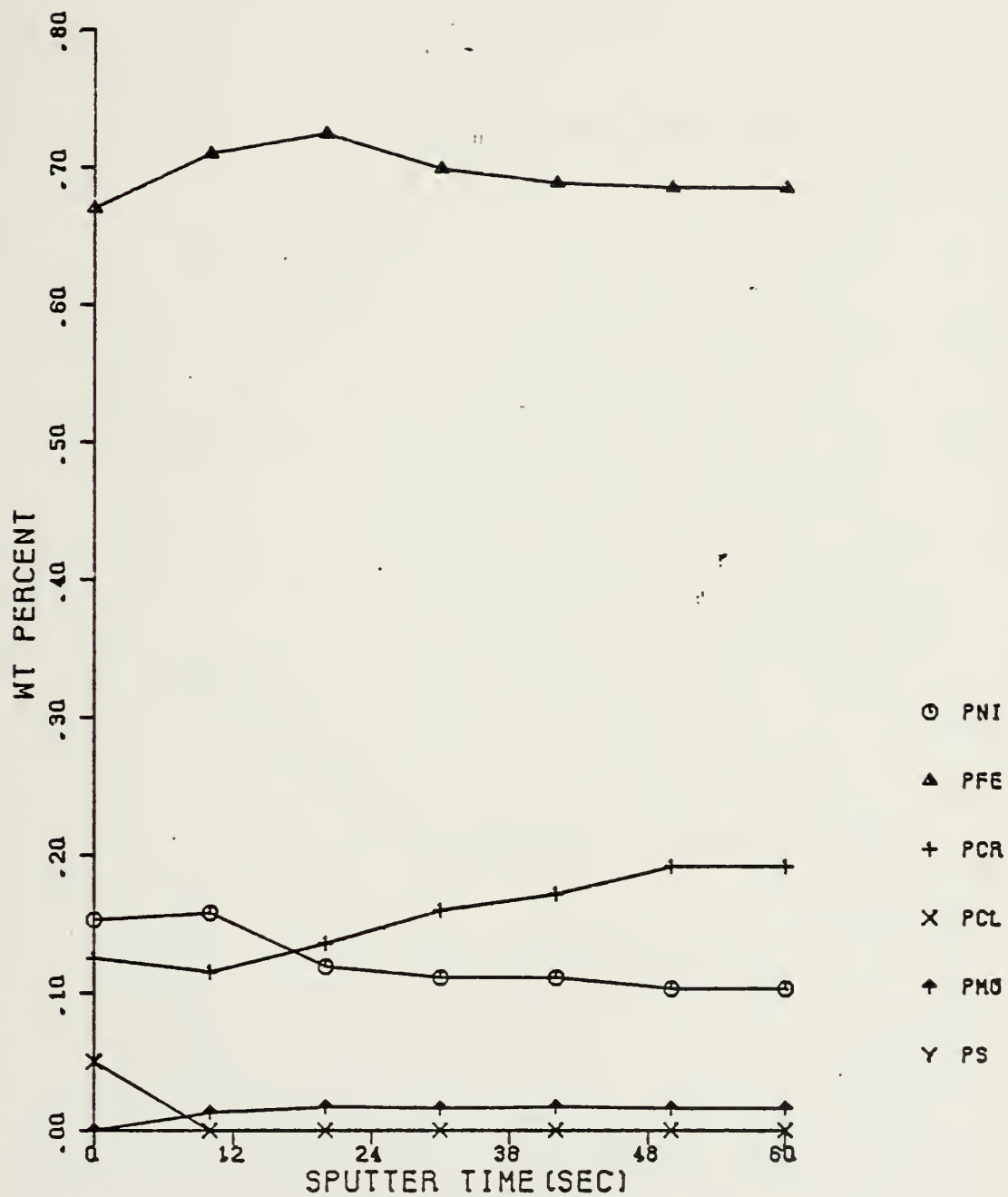


Figure 5.3.1 Composition/Depth Profile of T316
(300 mV-Active Site)

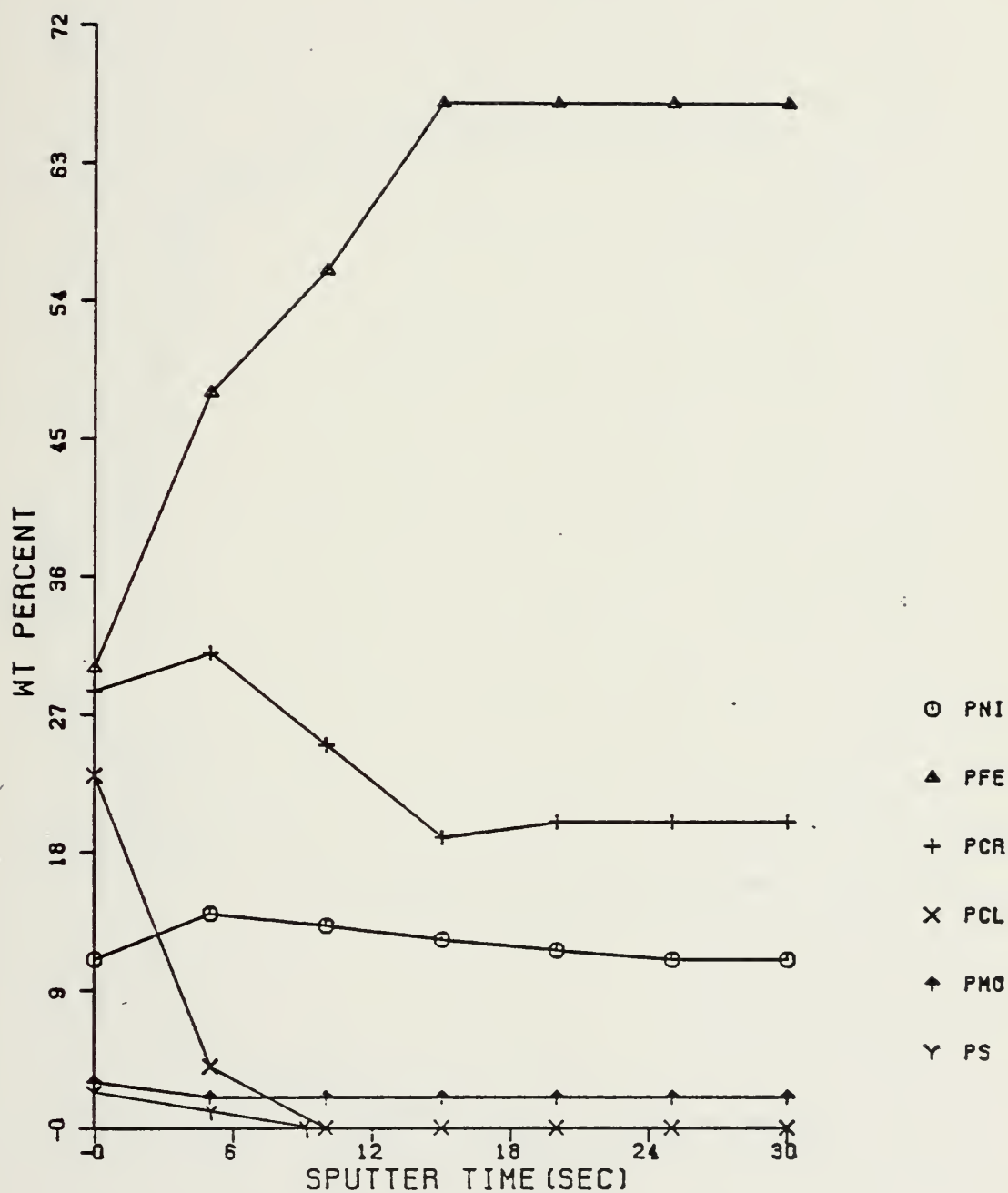


Figure 5.3.2 Composition/Depth Profile of T3]6 (300 mV-Unaffected Site)

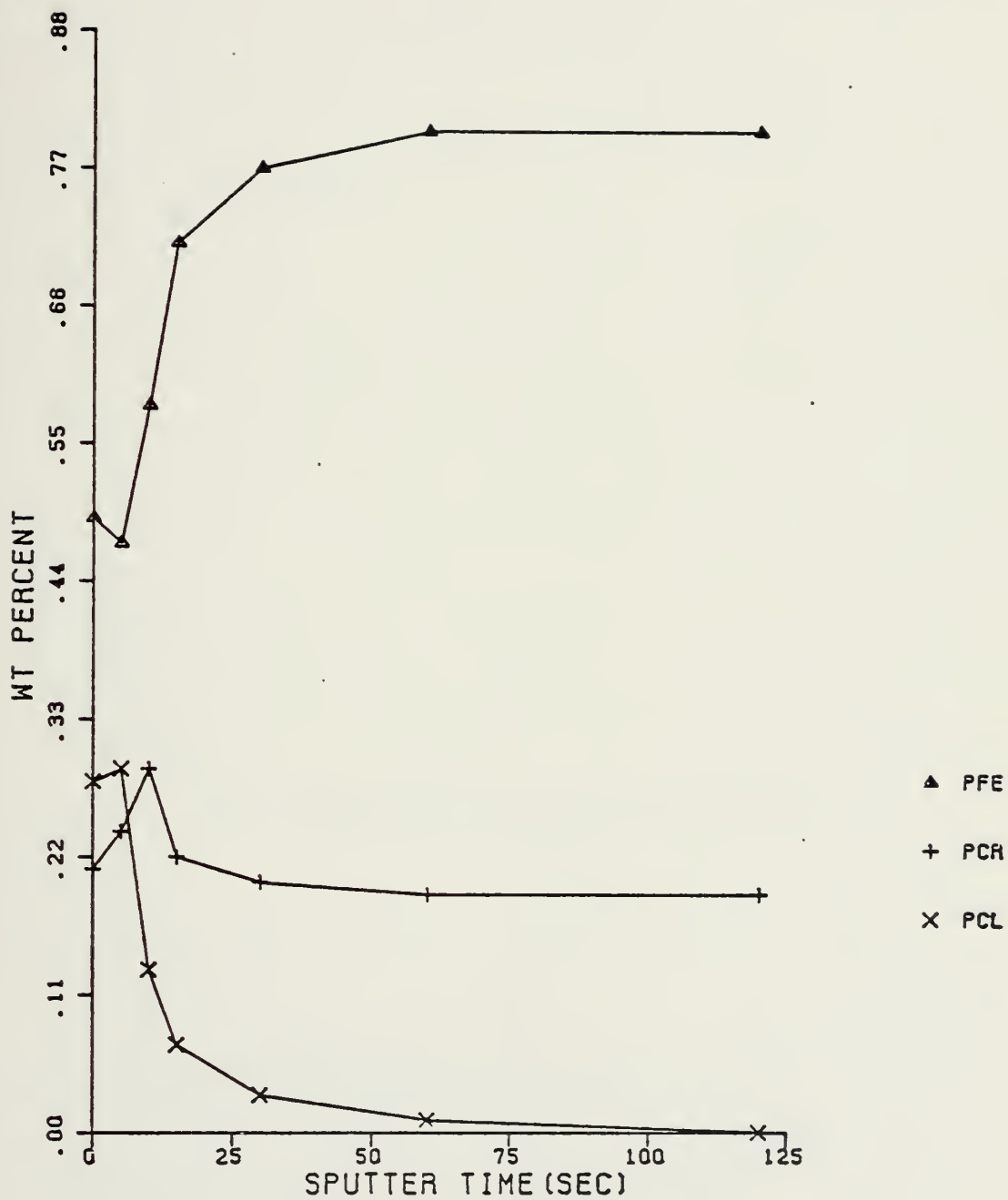


Figure 5.3.3 Compositin/Depth Profile of T3]6
(50mV-Active Site)

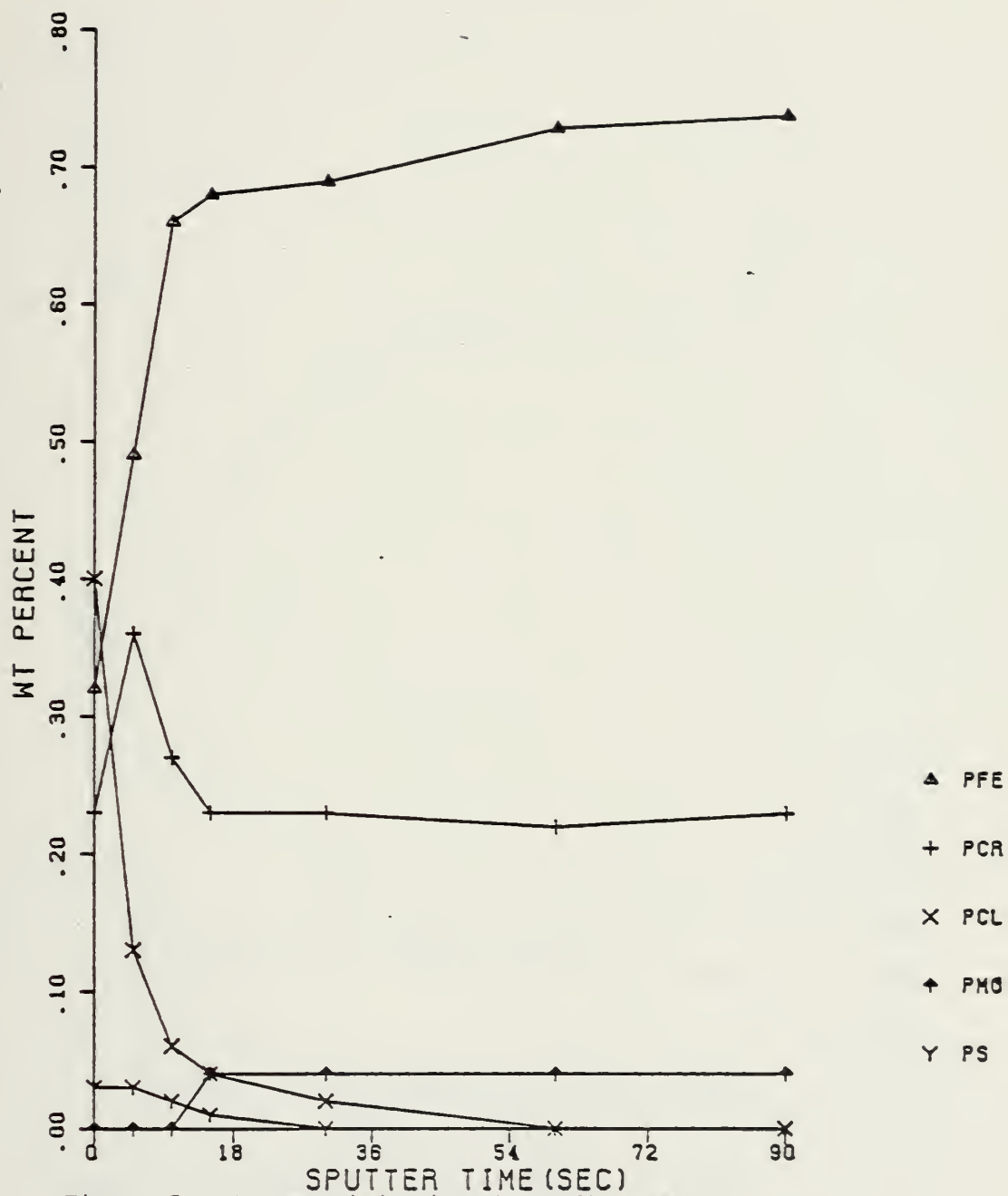


Figure 5.3.4 Composition/Depth Profile of T439
(300mV-Active Site)

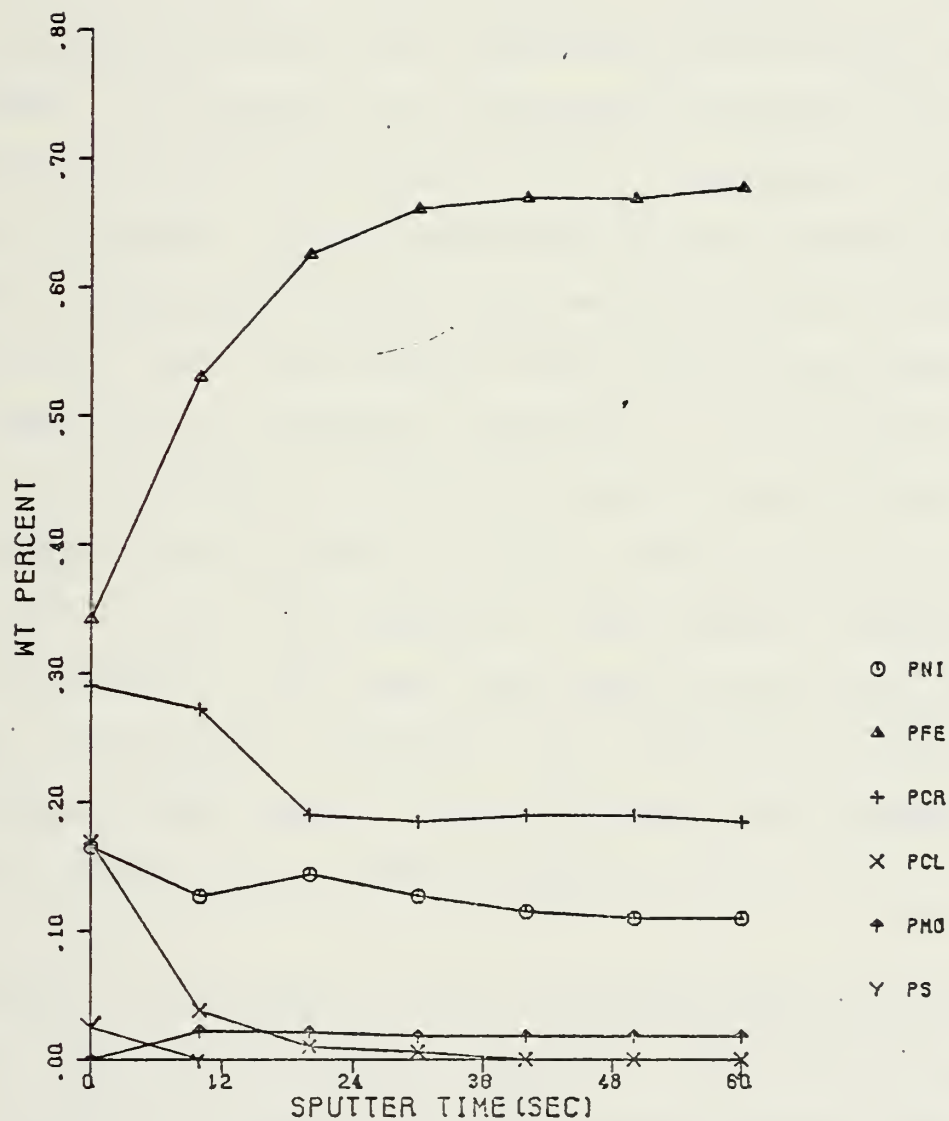


Figure 5.3.5 Composition/Depth Profile of T444
(600 mV-Active Site)

6.0 DISCUSSION OF RESULTS

6.1 GENERAL TREND IN CYCLIC POLARIZATION TESTS

Polarization diagrams have been grouped many ways, in each case the author had to decide how specific or general each group should be. In the imprecise world of polarization diagrams, it is easy to be infatuated with detail. Multiple testing of over forty alloys leads to a plethora of polarization diagrams. Each diagram has its own idiosyncrasies. Taking a step back though, key characteristics, as defined previously, were recorded for each diagram and indexed. At the same time a graphical comparison of the diagrams were made and compared to published results. When the polarization diagrams were studied in detail and key parameters were integrated into the analysis, four general shapes were distinguishable, and these were used to group the various alloys in relative rankings for resistance to localized corrosion. Each shape was associated with a tendency to locally corrode as described in Section 5.1.

Shape 1 (eg. Figure 6.1.a) is distinguished by an anodic current density less than $5 \mu\text{A}/\text{cm}^2$ for the range from E_{corr} to the end of the anodic scan. No pitting potential (E_p) was evident and the protection potential (E_{prot}) was greater than +550 mV (SCE). This shape was associated with no

localized corrosion. (Note: As described in Appendix A, the term E_{prot} , when used in this group, does not refer to a protection potential per se, since no pitting occurred. The term E_{prot} is used, in this grouping, only to maintain consistency of parameters among the four groupings.

Shape 2 was similar to Shape 1 (eg. Figure 6.1.b), but exhibited a distinct rise in anodic current density in the range of +300 to +400 mV (SCE) and exhibited a small hysteresis loop with a crossover potential (E_x) between +750 and +850 mV (SCE). The protection potential was in the range of +300 to +500 mV (SCE). This shape was associated with minimal localized corrosion.

Shape 3 (eg. Figure 6.1.c) also showed a distinct rise in anodic current between +300 to +900 mV (SCE) and exhibited a large hysteresis loop, with a protection potential approximately equal to the corrosion potential. The maximum anodic current density was always noted to be less than 1000 $\mu\text{A}/\text{cm}^2$. This slope was associated with moderate localized corrosion.

Shape 4 (eg. Figure 6.1.d) exhibited large hysteresis loops with maximum anodic current densities in excess of 1000 $\mu\text{A}/\text{cm}^2$. Protection potentials were generally more

cathodic than the corrosion potential. This shape was associated with heavy localized corrosion.

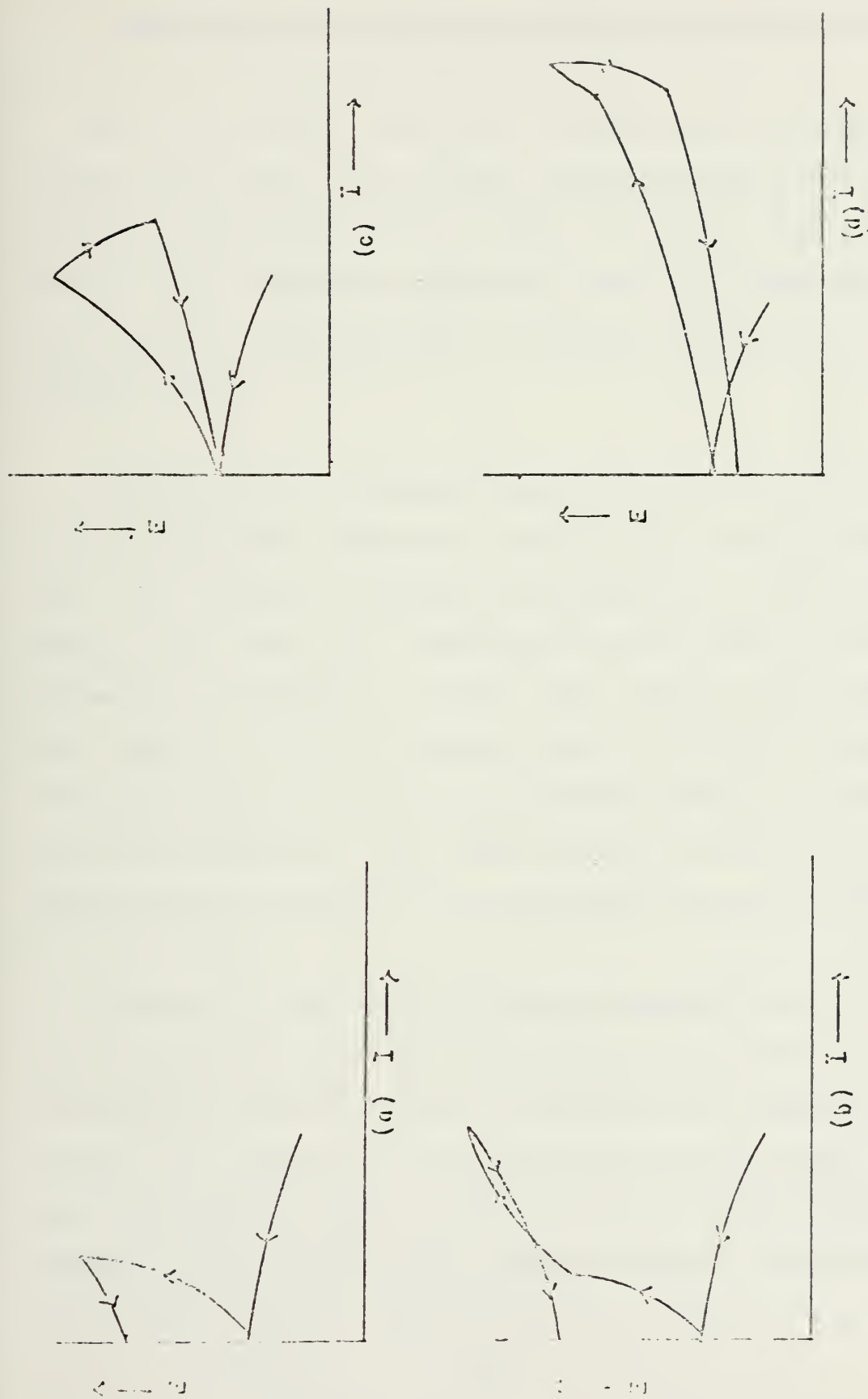


Figure 6.] Schematic Polarization Diagrams for Groupings of Localized Corrosion Tendency

6.2 COMPARISON WITH PUBLISHED ELECTROCHEMICAL RESULTS

Over the years numerous investigations of stainless steels have been made using electrochemical techniques. Section 2.4 enumerated on some of these studies. This section will briefly summarize results of other investigators using the same alloys or similar alloys tested in the present study.

Asphahani (107) conducted tests on Alloy 316, 825, Alloy G, 625, and C-276, using slow and fast scan cyclic polarization and constant potential techniques in 4 wt% NaCl. His ranking in terms of localized corrosion was (in order of decreasing resistance): C-276, 625, Alloy G, 825, and 316. The results of the present study would give the order as C-276/625/Alloy G (Group 2) and 825/316 (Group 4), where the alloy separated by the slash falls into the same general grouping set in Section 5.1 referenced parenthetically.

Trabanelli and Zucchi (108) performed anodic polarization studies in 3 wt% NaCl with alloys T316, C-276, and INCO Alloy IN-X (14.2% Cr, 27.5% Ni, 9.65% Mo) and ranked them as follows (in order of decreasing resistance): IN-X, C-276, and 316. The present study would have predicted the same order, except of IN-X which was not tested. Given the high

austenitic character and its high Mo content, it can be presumed that IN-X would probably fall into Group 1.

Morris and Scarberry (109) used the anodic polarization techniques at various temperatures in 10% H_2SO_4 to study alloys 825 and 625 among others. Their study predicted a much better performance of 625 compared to 825. This study concurs with that finding.

Manning (110) studied alloys 20 Cb3, Ferralium, 20 Mod, 825, and Alloy G in 4 wt% NaCl +.01m HCl at 70 degrees C and found Alloy G to show no propensity toward pitting corrosion and ranked the others (in order of decreasing resistance to pitting): Ferralium, 825, 20 Mod, and 20-Cb3. the present study would rank these alloys: 20 Mod/Ferralium (Group 1), Alloy G (Group 2), and 20-Cb3/825 (Group 4). Manning also concluded that the fast scan polarization tests were not adequate, and the best candidates for test methods for localized corrosion resistance are the slow scan rate potentiodynamic and constant potential tests.

Kain (111) evaluated alloys 20-Cb3, 825, 625, and Alloy G using both "in ocean" testing and fast scan cyclic anodic polarization techniques. Kain concluded that prediction based on electrochemical techniques alone can be misleading, especially in the alloys susceptible to moderate localized

corrosion. The present study makes no claims that one can exclusively depend upon one technique: but in comparing the slow scan-rate data generated in this study to the fast scan data, the slow scan rate technique gives much better resolution between the various alloys. This is supported by the Asphahani and Manning research discussed above (110).

Garner (112) used a chemical potentiostat, (ie. FeCl_3) to rank alloys (among others): T316L, 904L, Jessop 700, AL-6X, 34LN, T317L, T317L+, 254 SMO and 20-Cb3. A conservative estimate of resistance to localized attack was made and his ranking is (in order of decreasing resistance to localized corrosion): 254 SMO, AL-6X, 34LN, Jessop 700, 904L, T317L+, and 20 Cb 3/T316L/T317L. The present study would rank these alloy as follows: 254 SMO/AL-6X (Group 1) and the other alloys in Group 3. Again the relative lack of sensitivity of the present study is seen. However, other logic circuit diagrams as in Figure 5.1.1 could be made to delineate relative rankings within each of the four groupings.

While the above references to other research shows a general agreement in results, it shows that, in general, no one method can be assumed correct for all situations, and that if several methods are combined, a more precise prediction results.

6.3 COMPARISON WITH IN OCEAN TEST RESULTS

The alloys considered in the cyclic polarization experiments were divided into four groups, depending upon their tendency to locally corrode. The experimental procedure was based upon the absence of intentionally applied crevices, and therefore, the data generated would not be expected to predict an alloys' tendency to crevice corrode. However, this Section will describe the crevice corrosion testing done with the same alloys tested in the present study. The correlation of results between the two studies was surprisingly good, and deemed worthy of elaboration.

As mentioned in Section 3, "in ocean" testing was conducted at Laque Center for Corrosion Technology under the direction of Robert M. Kain (113). Materials tested were commercial grade alloys supplied by Allegheny Ludlum, Armco, Avesta Jernverks, Cabot, Carpenter Technology, Crucible, Eastern, Firth-Brown, Huntington, Jessup, Langley Alloys, and Uddeholm. Harvey P. Hack used the data generate from the Laque tests to evaluate the performance of these alloys (114).

Samples provided were cut to 100 by 150 mm rectangles. Sample thickness ranged from 0.5 to 5mm. In each case a 13 mm diameter hole was drilled in the center of the sample to

allow for the attachment of the crevice formers. Samples were then ground using wet 120-grit silicon carbide abrasive paper.

The experimental procedure is described in detail in reference (115). Some highlights of the procedure include installation of a Devrin washer torqued to the sample leaving an exposed-surface/shielded surface area ratio of 150/1. All samples were tested in triplicate for a duration of 30 days. To minimize run to run variations, samples were tested using the same racks within four months of each other. Visual inspections were made regularly, but these observations were made without disturbing or removing the samples from their seawater environment. At the completion of the 30 day exposure test, samples were removed and immersed in cold 30% HNO_3 for 15 minutes, rinsed and brushed with a pumice-detergent to remove corrosion products and staining. The key parameters are as follows:

pH	7.7 to 8.2
Salinity	34.4 to 39.1 mg/l
Chloride	19.2 to 21.7 mg/l
Dissolved Oxygen	5.3 to 6.7 mg/l

Percent Saturation 84.7 to 100.0

Mean Temperature 27.7 Degrees C
standard deviation
of 1.4 degrees Centigrade

Nominal Velocity 0.02 m/sec

Fresh, filtered seawater was introduced at a rate of 6 to 7 times daily.

Results measured the depth of attack to the nearest 0.01 mm, the number of sites attacked, and time to initiation. Sample corrosion varied from no attack to over twenty sites of localized corrosion. Attack was also as deep as 3 to 4 mm, and as early as thirty-six hours after test initiation. Using the grouping defined in Section 3.0, the materials performed in the following manner.

6.3.1 ALLOY PERFORMANCE "IN OCEAN"

AUSTENITIC STAINLESS STEELS WITH LESS THAN 17% NICKEL

As shown in Table 6.3.1 , all these alloys had at least one crevice site. The majority had site development in the first four days. The presence of molybdenum did not seem to affect the number of sites of attack or the time to initiation. There was also no statistical correlation between the amount of nickel, manganese, and chromium content.

AUSTENITIC STAINLESS STEELS WITH 17 TO 40% NICKEL

These alloys experienced the largest variation and most inconsistent results. That is, several samples of the same alloy did not experience any corrosion while others suffered some attack. Alloys 254 SLX and 777 suffered multiple attacks on all samples. No statistical conclusions could be drawn from these results, but several trends were noted. The alloys with the highest molybdenum content had the shallowest depth of attack, while the alloys with low molybdenum had the greatest depth of attack. Harvey Hack conjectured that the longer initiation time of higher molybdenum alloys resulted in a shorter time for propagation. Once again other alloying elements seemed to have no significant impact on performance.

AUSTENITIC ALLOYS WITH OVER 40% NICKEL

Performance of these alloys appeared to be dependent on the amount of molybdenum in the alloy. For example, the superalloy Incoloy 825 suffered corrosion on all six of its samples. The other superalloys seemed to experience corrosion relative to molybdenum content. That is, alloys with 7% or more experienced hardly any corrosion. The molybdenum factor covered any other significant correlation.

DUPLEX AUSTENITIC-FERRITIC

The correlation of molybdenum content and amount of attack once again seemed strong. Those with lower molybdenum and only traces of copper experienced attack on all samples. Ferralium with 3.2% Mo and 1.8% copper experienced attack on only one panel. The correlation of copper with corrosion could not be predicted from the other groups shown above, but will at least be noted here for comparison with laboratory results.

FERRITIC STAINLESS STEELS

The effect of molybdenum again seemed to correlate with the corrosion noted, but content level required to cut

corrosion dropped to 3.5% compared to the 8% level needed for the austenitics.

CAST ALLOYS

Results for these cast alloys seemed to follow their wrought counterparts. Molybdenum had a beneficial effect on both the total number of sites and depth of attack. The one exception was the cast Ferralium with 1% less molybdenum performed significantly worse than its wrought counterpart. Alloys with more than 8% molybdenum did not suffer any significant attack.

GENERAL REVIEW

Corrosion of these alloys seemed to be in general agreement with published results although the levels were usually greater than previous tests. Experimental detail could vary in all these ocean tests-- different washers, torque values, and sample preparation. Harvey Hack noted that these results confirm the requirement for more consistent conditions. Molybdenum effects followed literature predictions in that corrosion resistance improved with corresponding increases of molybdenum. All other alloying elements had statistically insignificant effects on crevice corrosion behavior. Several

alloys proved to be more corrosion resistant in seawater than Type 316 stainless steel.

The NSRDC Report then grouped results into four groups similar to the method used in Section 5.1. Groupings were based on the amount of attack (the number sites) on the sample. Table 6.3.2 shows these rankings. These four groupings were made of all alloys based on amounts of relative corrosion. A qualified confidence in these groupings was reported in the NSRDC Report.

Comparison of "In Ocean" and Polarization Groupings

The groupings of the polarization results and the "In ocean" results compared favorably for all alloys except two. The "In ocean" results and the polarization results were within one category for all alloys except Rex 734 and Illium PD. Table 6.3.3 shows all metals and their corresponding ranking of corrosion resistance.

Looking at the results in a macro-sense, there is a fairly high correlation if the groupings are combined that is, little to no corrosion versus moderate to heavy corrosion. Using this method, all but four alloys fall into these two groups or a 90% agreement between the two methods. Alloys 254 SFER, AL-4X, Rex 734, and Illium PD are the only

alloys which did not have their grouping corresponding similarly for both tests. In the polarization tests for Rex 734 and Illium PD virtually no corrosion occurred while the ocean tests exhibited fairly high corrosion. Illium PD and Rex 734 were the only alloys which did not come close to matching.

Rather than propose a specific category with a fairly high level of uncertainty, the global ranking of two categories is the most specific correlation proposed and is shown in Table 6.3.4.

There are several explanations for the excellent correlation of the "in ocean" crevice tests and the cyclic anodic polarization experiments in the absence of an intentionally applied crevice. One explanation may be that the polarization experiments without crevices can, in fact, predict the tendency to crevice corrode in the alloys considered, as addressed by Asphahani (107). A second possible explanation could be that the sample preparation methods used in the present study leads to some form of microcrevices which were not screened out in the quality control process. Finally, the correlations observed were artifacts, and an insufficient number of experiments to confirm the correlation were performed.

Summarizing the discussion of this section, a coordinated method of ranking of stainless steels in a marine environment has been proposed. Validity of the methodology can be easily questioned, but the evaluation process must begin somewhere and two independent methods using the same material seems like a reasonable origin. Obviously a more comprehensive system is ideal and proposals for such will be given in the conclusion (Section 7) and in the remainder of this Section. Suffice it to say, the input of more data would give rise to a higher confidence in determining the ability of a stainless steel to perform in seawater in terms of corrosion.

CREVICE CORROSION RESULTS FOR AUSTENITIC ALLOYS

Material	Approximate Composition (wt %)					No. of Sites Attacked		No. of Sites Attacked	Depth of Attack (mm)	Initiation Time (hr)
	Cr	Ni	Mo	Mn	Cu	Per Side	Total			
T316	17.5	10.7	2.4	1.6	0.3	1-13	33	6	0.24-1.93	24-102
34 LN	16.8	13.8	4.2	1.6	-	12-20	102	6	0.10-1.04*	36-102
T216	20.	6.	2.5	8.	-	7-10	50	6	0.10-0.64	51-77
Rex 734	21.3	9.4	2.7	3.8	-	2-9	39	6	0.01-1.00	51
T317L	18.9	12.2	3.6	1.7	-	7-20	91	6**	0.18-1.92	51-77
317LM	19.5	14.5	4.1	1.3	0.2	19-20	116	6	0.01-1.07	51-77
317L+	18.7	15.8	4.2	1.5	0.2	1-12	44	6***	0.18-1.09	51-479
22-13-5	21.1	13.7	2.3	4.8	-	16-20	112	6	0.10-1.10	36-77
904L	20.5	24.7	4.7	1.5	1.6	0-13	36	5	0.14-0.74	51-365
4X	20.2	24.4	4.4	1.4	-	0-4	8	4	0.14-0.50	77-245
700	20.7	25.2	4.1	1.6	0.2	0-20	17	5	0.08-2.00	51-171
254 SLX	19.9	25.0	4.7	1.6	1.7	7-15	70	6	0.08-0.92	51-77
777	20.8	25.6	4.5	1.4	2.2	8-12	60	6	0.03-2.90	36-77
254 SMO	20.0	17.9	6.1	0.5	0.8	0-7	18	5	0.02-0.51	51-479
6X	20.4	24.6	6.4	1.4	-	0-3	11	4	0.01-0.62	51-365
20 Mod	21.6	25.5	5.0	0.9	-	0-5	6	2	0.12-0.36	51-365
20 Cb-3	19.4	33.2	2.2	0.4	3.2	0-15	49	5	0.14-3.10	51-171
20 Mo-6	23.9	33.4	5.6	0.4	3.3	0-6	13	3	<0.01-0.53	365-507
254 SFER	29.4	22.2	2.1	1.7	0.1	0-3	11	5	0.34-0.90	102-221
825	22.0	44.0	2.7	0.4	1.7	4-13	37	6**	0.25-2.42	51-221
G	22.2	46.8	5.8	1.5	1.8	0-2	6	4	0.02-0.87	365-673*
G-3	22.8	43.7	7.0	0.8	1.8	0-2	2	1	0.06-0.21	102
625	22.3	61.0	8.5	0.1	-	0	0	0	-	-
C-276	15.5	54.7	15.5	0.5	0.1	0	0	0	-	-

CREVICE CORROSION RESULTS FOR DUPLEX AND FERRITIC ALLOYS

Material	Approximate Composition (wt %)					No. of Sites Attacked		No. of Sites Attacked	Depth of Attack (mm)	Initiation Time (hr)
	Cr	Ni	Mo	Mn	Cu	Per Side	Total			
T329	27.0	4.2	1.4	0.3	0.1	9-15	73	6	0.02-1.29*	51-102
44LN	25.0	5.9	1.5	1.8	0.1	14-20	104	6	0.04-3.35	36-51
Ferrallium	26.2	3.6	3.2	0.8	1.8	0-1	2	2	0.03-0.08	365*
T439	17.7	0.3	-	0.3	-	1-17	58	6**	0.42-0.72*	24-77
T444	18.9	0.1	2.0	0.4	-	6-12	54	6	0.33-1.21*	51-245
26-1	25.9	0.1	1.0	-	-	0-5	10	4	0.15-0.46	51-107
26-1S	25.0	0.2	1.0	0.2	-	0-2	6	4	0.06-0.30	171-553
29-4	29.6	0.1	4.0	-	-	0	0	0	-	-
29-4C	23.8	0.8	3.8	0.2	-	0	0	0	-	-
29-4-2	29.5	2.2	4.0	-	-	0	0	0	-	-
SC-1	25.6	2.1	2.9	0.2	-	0-1	1	1	0.05	+
Monit	25.3	4.1	3.8	0.4	0.4	0	0	0	-	-

CREVICE CORROSION RESULTS FOR CAST ALLOYS

Material	Approximate Composition (wt %)					No. of Sites Attacked		No. of Sites Attacked	Depth of Attack (mm)	Initiation Time (hr)
	Cr	Ni	Mo	Mn	Cu	Per Side	Total			
CA6N	12.4	8.0	-	0.2	-	15-20	111	6***	0.01-2.00	126-169*
CF8M	19.3	10.0	2.4	1.0	-	4-17	74	6	0.16-3.77	126*
IN-862	20.9	24.5	5.0	0.5	-	1-16	52	6	0.12-1.22	126-217*
CN7MS	19.4	22.1	2.9	1.0	1.6	14-20	102	6***	0.08-3.82	126
CN7M	20.0	28.2	2.5	0.2	3.1	13-18	49	6***	0.15-2.33	126*
625	20.6	63.7	8.5	-	-	0	0	0	-	-
CW 12N-2	18.1	62.8	17.6	0.5	0.1	0	0	0	-	-
Illium PD	24.6	5.4	2.0	0.9	-	3-20	73	6	0.08-4.53	48-126*
Ferrallium	25.2	5.2	2.5	1.0	3.2	0-14	37	4***	0.03-2.21	126-169

** Gravity-assisted tunneling.
 *** Some attack initiating outside of crevice area.
 + Initiation not observed on some panels where attack occurred.

Table 6.3.] Results from Crevice Testing at LaQue Center for Corrosion Technology

GROUP	GROUP	GROUP	GROUP
1	2	3	4
NO	MINIMAL	VARIABLE	HEAVY
LOCALIZED	LOCALIZED	LOCALIZED	LOCALIZED
CORROSION	CORROSION	CORROSION	CORROSION
UNDERLINE			
29-4	Alloy G	Jessop 777	CA6N *
29-4C	Alloy G3	Jessop 700	317LM
29-4-2	20 Mo 6	904L	22-13-5
MONIT	20 Mod	254 SLX	44LN
625	4X	T216	34LN
C-276	6X	IN 862 *	CN7M *
Illium W2 *	26-1S	T317L+	
	SC-1	T317L	
	Ferralium	20-Cb3	
		T316	
		Rex 734	
		825	
		T439(18-SR)	
		T444(18-2)	
		CF 8M *	
		Illium PD *	

* Denotes cast alloys

TABLE OF GROUPINGS VIA "IN OCEAN" TESTS

Table 6.3.2

GROUP 1	GROUP 2	GROUP 3	GROUP 4
NO	MINIMAL	MODERATE	HEAVY
LOCALIZED CORROSION	LOCALIZED CORROSION	LOCALIZED CORROSION	LOCALIZED CORROSION
(1)29-4	(2)Alloy G	(3)Jessop 777	(3)CF 8M *
(1)29-4C	(2)Alloy G3	(3)Jessop 700	(3)20-Cb3
(1)29-4-2	(2)20 Mo 6	(3)Jessop 770	(4)CA6N *
(1)MONIT	(1)625	(2)254 SFER	(3)18-2
(2)AL-6X	(1)C-276	(3)904L	(3)18-SR
(2)SC-1	(1)625 *	(3)254 SLX	(3)T316
(2)20 Mod	(1)ILLIUM W2 *	(4)44LN	(3)825
(2)26-1		(4)34LN	(4)CN7M *
(2)26-1S		(4)22-13-5	
(2)254 SMO		(3)T216	
(3)Illium PD *		(3)T329	
(2)Ferralium		(3)T317L+	
		(3)T317L	
		(4)T317LM	
		(3)IN 862 *	

* Denotes cast alloys

(X) Denotes ranking from in ocean tests

TABLE OF COMBINED GROUPINGS-- POLARIZATION AND "IN OCEAN"

Table 6.3.3

GROUPING		GROUPING	
1&2		3&4	
MINIMAL		HEAVY TO	
TO NO		MODERATE	
LOCALIZED		LOCALIZED	
CORROSION		CORROSION	
29-4	Ferralium	Jessop 777	CF 8M *
29-4C	Rex 734	Jessop 700	20-Cb-3
29-4-2	Alloy G	254 SFER	CA6N *
MONIT	Alloy G3	AL-6X	18-2
AL-6X	20 Mo 6	904L	18-SR
SC-1	625	254 SLX	T316
20 Mod	C-276	44LN	825
26-1	625 *	34LN	CN7M *
26-1S	Illium W2 *	22-13-5	T216
254 SMO	Illium PD *	T329	T317L
		IN 862 *	T317L+
			T317LM

* Denotes cast alloys

TABLE OF NEW GROUPINGS-- POLARIZATION AND "IN OCEAN"

Table 6.3.4

6.4 ALLOYING EFFECTS

In an overview of all the alloys investigated, a few generalizations can be made regarding the effects of alloying upon the resistance to localized corrosion.

For the austenitic alloys the best results are obtained in alloys with greater than 20% Cr, 17% Ni, and 5% Mo. As stated in Section 5.2, minimization of Mn and having greater than 0.4% nitrogen gives dramatically increased resistance to localized corrosion (116). Increasing the nickel content from 17% to 61% did not significantly reduce the susceptibility to localized corrosion unless the molybdenum content was above 5%.

With the duplex austenitic-ferritic alloys, the amount of Mo seemed to be the deciding factor in minimizing the chances of localized attack, although here again, reduction of Mn appears to be a factor. The duplex alloys are such a small group, three, that generalizations are difficult to make. It might be noted, however, that since two of the three alloys did undergo extensive localized corrosion such alloys may not be suitable replacements for T316. Ferralium's good performance was somewhat unique in that its polarization diagram had attributes of both Group 1 and Group 2, Figure 5.2.25.

The ferritic alloys investigated in this study had excellent resistance to localized corrosion, in general. Greater than 25% Cr and greater than approximately 3% Mo ensures no localized corrosion tendencies. Surprisingly, alloys 26-1 and 26-1S, each with about 1% Mo and 25% Cr, also showed excellent resistance to localized corrosion. No other alloying differences are immediately evident and one difference distinguishing these ferritics from the poorly performing austenitic alloys is the fact that they have greater than 25% Cr. This points to the difference of Mo alloying effects between austenitic and ferritic alloys. A smaller amount of Mo is needed in ferritic alloys than austenitic alloys to have reasonable corrosion resistance.

The best performing cast alloy (Illium PD) is similar in content to the duplex alloy, Ferralium with 24.5% Cr, 5.4% Ni, 2% Mo. As in the case of the high nickel austenitic alloys, increasing the nickel content in these cast alloys to large values (60-65%) did little to improve corrosion resistance without a substantial amount of Mo.

Reviewing all the alloys, it can be definitively stated that the presence of molybdenum has a beneficial effect on an alloys' corrosion resistance. This is not a profound statement since a multitude of articles have previously confirmed this statement before. For example, Yoshii working

with Ambrose at the University of Florida indicates that the advantage of molybdenum in the alloy may be in improving the bonding at the metal oxide interface and in decreasing the activity at the active surface sites (117). Section 6.5 will consider the subject more deeply and investigate the role of the molybdate ion in corrosion resistance. Nickel appears to have only a role in the stabilization of the austenitic phase, and other investigators have found no measurable effect of nickel on the resistance to localized corrosion in alloys already completely austenitic (118).

6.5 COMPOSITION PROFILE OF THE STAINLESS STEEL SURFACE

As stated in Section 5.2 several alloys were analyzed using Auger Electron Spectroscopy. The approach used in this surface analysis was to start with the alloy which led to this testing program, Type 316 stainless steels. Further investigation has been tied to trying to understand the various variables which could possibly have an effect on the corrosion process. Alloying effects and the impact of trace elements on similar alloys were given specific consideration in order to examine possible theories of passivity, its breakdown, and repassivation. For example, surface analysis concentrated on alloys of similar content except for one or two elements.

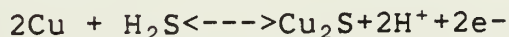
TYPE 316 STAINLESS STEEL

Analysis of Type 316 stainless steel seems appropriate. From the results of the analysis of this alloy, Figures 5.3.1 to 5.3.3, several generalizations may be made. The active sites showed a chromium enrichment with concomitant depletion of iron. All results indicated essentially bulk composition after 60 seconds of sputtering. The evidence of chromium enrichment is supported by several other investigators from previous research (119-123). All profiles showed the presence of molybdenum within ten seconds of sputtering.

The presence of sulfur was detected in the active areas, but never in the unaffected area within a crevice site where there was no active corrosion. The sulfur concentration in the initiation areas was substantially above that found in bulk metal. The presence of sulfur under these circumstances points to the possible mechanism for the initiation of localized corrosion. Localized corrosion is initiated at the site of a MnS inclusion, which upon dissolution leads to enrichment of the local environment in H₂S as described in reaction 6.5(1). These inclusions along with grain boundaries are sites of high activity in the alloy.



Further, the sulfur in the form of H₂S is readily able to react with elements in the base metal, such as copper, since H₂S is a known catalyst in dissolution in active state of the alloy. For instance in the case of copper a typical reaction is:



Cu₂S, being very insoluble in water, would then be deposited. Zakiipour reported there was approximately twice the amount of copper (by atomic weight percent) compared to the amount of sulfur in his investigations (124). Strong SEM

evidence showed the existence of copper nodules at the bottom of the crevice (126). No evidence of copper was found in the AES spectra, even though the bulk composition contains a trace of the element. This could be due to the insensitivity in this analysis.

The sulfur in the form of H_2S may also react with the Mo of the bulk metal to aid in the formation of the molybdate ion. This reaction in turn could aid in the inhibition of alloy dissolution by the mechanism described by Ogawa et al. (126). According to Ogawa, the molybdate ion is adsorbed on the metal surface at the point of passive film breakdown effectively covering the surface and allowing the passive film to regenerate. Using two similar alloys which differed only in the presence of molybdenum, an initial evaluation of the Ogawa theory was made. The results from Type 439 (18SR) and Type 444 (18-2) tended to support the Ogawa theory (Figures 5.2.4 and 5.2.5). In this series, sulfur was never found at the active site on alloy T439, which has only a trace of molybdenum. This dependence on the presence of molybdenum in the detection of sulfur suggests a dual role of sulfur, first as an initiator in the form of MnS , then the sulfur in the form of H_2S acts as a catalyst to produce the protective molybdate ion.

Chloride is also a major variable, and its presence in the profile is linked to molybdenum. When no molybdenum is present, chloride is detected all the way down to the base metal, whereas in alloys containing Mo, chloride disappears after much less sputtering (Figure 5.2.5).

To summarize, all of the evidence, Figure 6.5.1 shows a possible mechanism of the role of molybdenum in the improved resistance to localized corrosion.

Figure 6.5.1a shows the metal with a protective layer in the presence of either the crevice solution or, in the case of pits with the bulk solution. The passive layer is broken by a certain mechanism (various mechanisms have been discussed in Section 2.3). The MnS inclusion serves as an initiating point for alloy dissolution and a small local volume is formed which, depending upon the presence of Mo, contains the molybdate ion in conjunction with other species(Figure 6.5.1b) or simply the products shown in Figure 6.5.1d. If molybdate ion is present, Figure 6.5.1c the penetration of the chloride rich solution is blocked, thus limiting the dissolution process because of the blockage of a mobile charge carrier (Cl^-) and/or the molybdate ion serves as an adsorbed protected species as suggested by Ogawa. This assumes that the molybdate is at least partially bonded to the passive film.

When molybdenum is not present as in the case of Type 439 (18SR), and the passive film is broken down, then there is a free passage of the chloride solution allowing the alloy dissolution process to proceed at a greater rate. The AES data showed high chloride content throughout the film area.

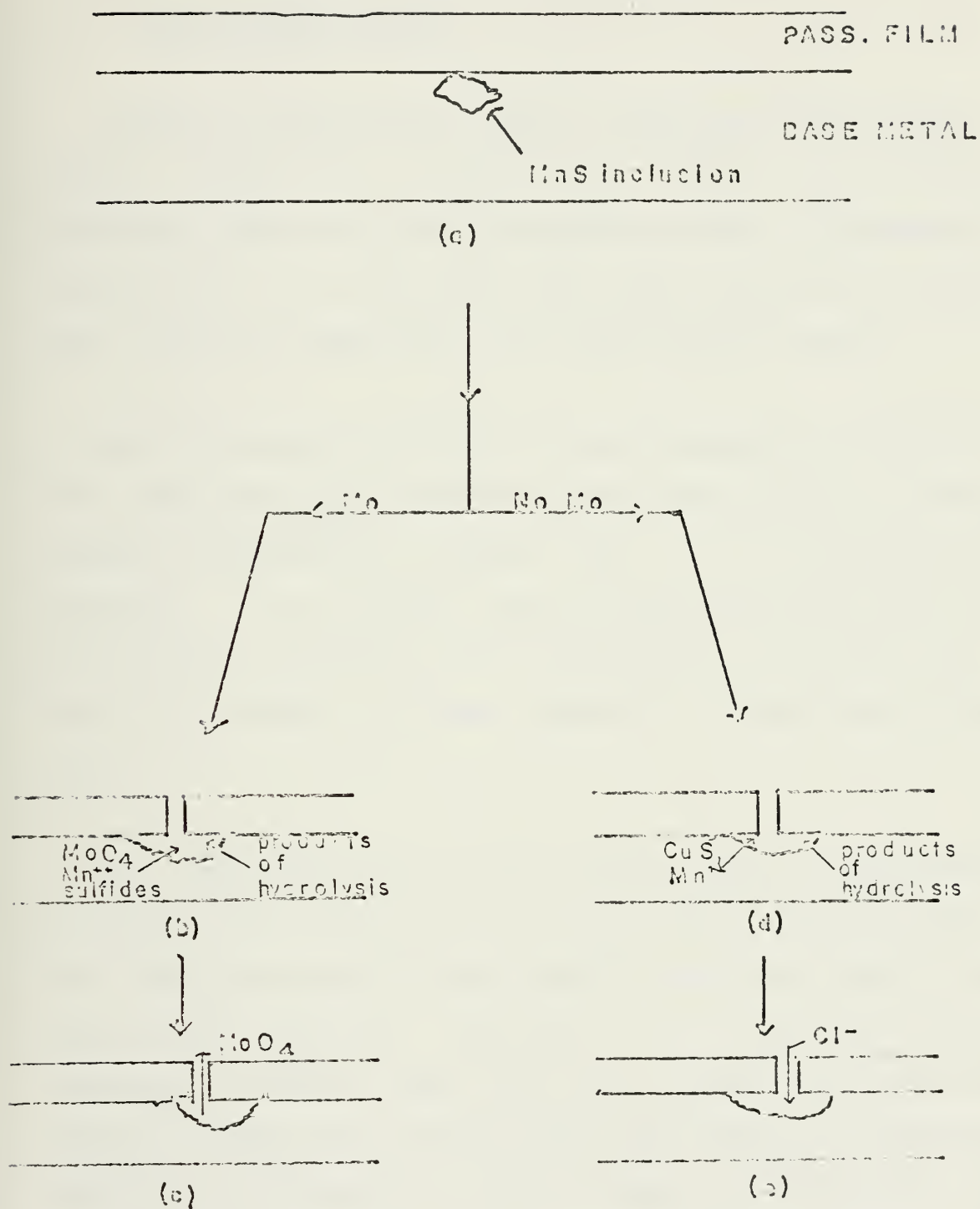


Figure 6.5.1 Mechanism for Mo Involvement in Resistance toward Localized Corrosion

6.6 COMMENTS ON PERTURBATIONS IN CYCLIC POLARIZATION CURVES

Several polarization curves exhibited current fluctuations during the anodic scan, above the corrosion potential. There are several explanations for this behavior. Williams et al. (127) argue that these fluctuations represent transient passivation and repassivation events.

These fluctuations did not occur consistently in different experiments for the same alloys, which point to a more probable explanation, namely, that of the experimental procedure. The solution was not being stirred during the polarization experiments and this resulted in current fluctuations similar to those observed in previous studies (128).

As mentioned before, great care was taken in developing an experimental procedure that was as reproducible as possible. Microcrevices could be linked to the bulk alloy or the epoxy/alloy interface. Crevice in the bulk alloy seems improbable because each alloy was ground in the same sequence ending with the final 600 grit abrasive in the same horizontal direction. A more likely candidate is the epoxy/alloy interface as a crevice initiator. While every sample had its vertical faces ground with 240 grit, this

area seems more susceptible to problems as witnessed in sample preparation discussed in Section 4.1.

In the final analysis, these local fluctuations do not seem to be important. The polarization curve groupings proposed in Section 5.1 factor these fluctuations out in the first review. It is felt that these fluctuations should be noted, but not tied to the overall ranking of the alloy. It is also believed that any further attempt to improve the epoxy/alloy interface would require significantly more stringent laboratory controls not in keeping with a massive general test and evaluation program.

7.0 CONCLUSION.

At the beginning of this study several researchers recommended a more specific, less comprehensive approach concentrating on a few of the alloys available rather than forty-three diverse alloys. After over 100 slow scan polarization experiments which have correlated fairly well with the 43 alloys tested "in ocean", persistence seems to have succeeded. This research has only begun to establish a specific ranking of alloys, but a starting point has been defined. On the otherhand, the use of the slow scan cyclic anodic polarization method developed in this study appears suitable in rating stainless steels with regard to their resistance to localized corrosion. In particular, using the slow scan method, the localized corrosion resistance of an alloy compared to T316 can be confidently determined. This measurement allows one to determine if the alloy is either more corrosion resistant than T316, or just as good. No refinement beyond this can be accurately made, but for the purpose of this study the former is all that is required.

A more sensitive analysis could be achieved if other testing methods and surface analytic studies are integrated into a given approach. In this study factoring in the "in ocean" results complemented the laboratory research. Ferric chloride testing, constant potential tests, "in situ" AES

evaluation, and other surface techniques could also be factored into the overall testing program. Care would have to be taken that as many variables as possible be removed in order to improve correlation of data. Probably the strongest point of this analysis is the consistency of the sample preparation and test procedure. Any complementary testing must incorporate this consistency.

Of the alloying elements, molybdenum was most effective at increasing resistance to localized corrosion. Austenitic alloys with greater than 5% Mo showed no tendency to corrode locally. Ferritic alloys with greater than 25% Cr and 3% Mo also showed no tendency to corrode.

The role of Molybdenum in improved resistance to localized corrosion is related to the presence of the molybdate ion which serves to protect the exposed metal surface and/or block the entrance of a mobile charge carrier chloride (Cl^-) into the local corrosion cell. Surface analysis supported this theory.

The reduction of manganese and the incorporation of 0.4% nitrogen dramatically improved the corrosion resistance of a given alloy. More research in this inexpensive method of alloy improvement seems very appropriate.

A greater sensitivity to ranking could be achieved with even greater attention to detail, but this must be weighed against the benefits of a more comprehensive general test program. Presently the splitting of alloys into the minimal/no corrosion and moderate/heavy corrosion seems adequate if a go/no go replacement for T316 is used. If a more precise analysis is required, then caution should be used in drawing any more definite conclusions about the corrosion resistance of a given alloy.

Finally, as stated in the introduction, replacement of an alloy must take into account several key factors, not the least of which is cost. Maybe an inexpensive cathodic protection system is more appropriate. In any case, one should not summarily define an alloy as the "nirvana of alloys" because in all probability there is some drawback in that alloy's performance.

8.0 FUTURE WORK

Now that a framework for a consistent large scale testing method has been established, further research in this area should concentrate on surface chemistry utilizing Auger Electron Spectroscopy (AES), X-ray Photoelectron Spectroscopy (XPS), Low Energy Electron Diffraction (LEED), and Scanning Potential Microprobe (SPM). These techniques can further delineate the mechanistics of the localized corrosion process.

Other work that could have a high return would be constant potential test of selective alloys, particularly those four alloys which did not correspond to the overall grouping proposed in Section 6.3. Cast alloy performance also seems to require more study.

The next step in the refinement of the logic circuit diagram would be a development of the capability of predicting absolute corrosion rates. A closer look at temperature, scan rate, and solution content would be valuable. This should be based on the premise that introducing complication to the overall testing program, if it cannot be streamlined, is unacceptable.

In summary, future analysis can take several paths, all of which can lead to an improved evaluation process of these alloys.

REFERENCES

1. Pourboix, M., "The Electrochemical Basis for Localized Corrosion", Localized Corrosion, NACE, Houston, Texas 1974.
2. France, W.D., "Crevice Corrosion of Metals," ASTM-STP 516, American Society for Testing and Materials, 1972, p. 164.
3. Fontana, M.G. and Greene, N.D., Corrosion Engineering, McGraw-Hill Book Company, New York, 1967.
4. Oldfield, J.W. and Sutton, W.H., "Crevice Corrosion of Stainless Steels: I. A Mathematical Model", British Corrosion Journal, Vol. 13, No. 1, pp. 13-22, 1978.
5. Oldfield, J.W. and Sutton, W.H., "Crevice Corrosion of Stainless Steels: II. Experimental Studies", British Corrosion Journal, Vol. 13, No. 3, pp. 104-110, 1978.
6. Sedriks, A.J., Corrosion of Stainless Steels, John Wiley And Sons, New York, pp. 88-109, 1979.
7. Kain, R.M., "Crevice Corrosion of Stainless Steels in Seawater and Related Environments", Corrosion 81, Paper NO. 200, NACE, Houston Texas.
8. Jones, D.A. and Wilde, B.E., "Galvanic Reactions during Localized Corrosion on Stainless Steel," Corrosion Science, Vol. 18, pp. 631-643, 1978.
9. Oldfield, J.W. and Sutton, W.H., in reference 4, p. 14.
10. Frankenthal, R.P., Journal of the Electrochemical Society, Vol. 116, p. 580, 1969.
11. Oldfield, J.W. and Sutton, W.H., in reference 4, p.13.
12. Oldfield, J.W. and Sutton, W.H., in reference 5, p. 105.
13. Turnbull, A., and Gardner, M.K., "Potential and pH Measurements in a Crevice of the Steel BS4360 50D in 3.5% NaCl and Artificial Seawater", British Corrosion Journal, Vol. 16, No. 3, pp. 260-262, 1981.
14. Oldfield, J.W. and Sutton, W.H., in reference 4, pp. 13-22.

15. Rowlands, J.C., "Crevice Corrosion of Stainless Steels and Nickel Alloys under Marine Conditions," British Corrosion Journal, Vol. 11, No. 4, pp. 195-198, 1976.
16. Oldfield, J.W. and Sutton, W.H., in reference 4, pp. 20-22
17. Janik-Czachor, M., Wood G.C. and Thompson, G.E., "Assessment of the Process Leading to Pit Nucleation", British Corrosion Journal, Vol. 15, No. 4, pp. , 1980.
18. Lunarko, E., Szklarska-Smialowska, Z. and Janik-Czachor, M., "Susceptibility of Cr-Ni-Mn Stainless Steels to Pitting in Cl Solutions", Corrosion, Vol. 31, No. 7, pp. 231-234, 1975.
19. Sato, N., "The Stability of Pitting Dissolution of Metals in Aqueous Solutions", Journal of the Electrochemical Society, Vol. 129, No. 2, pp. 261-264, 1982.
20. Uhlig, H.H., "History of Passivity, Experiments and Theories", Passivity of Metals, ed. by R.P. Frankenthal and J. Kruger, the Electrochemical Society, Princeton, New Jersey, pp. 1-28, 1978.
21. Uhlig, H.H., in reference 20, pp. 23-26.
22. Olefjord, I. and Elfstrom, B., "Composition of the Surface during Passivation of Stainless Steels", Corrosion, Vol. 38, No. 1, pp. 46-52, 1982.
23. Hara, N. and Sugimoto, K., "The Study of the Passivation Films on Fe-Cr Alloys by Modulation Spectroscopy", Journal of Electrochemical Science and Technology, Vol. 126, No. 8, 1979.
24. Teramoto, K., Asami, K. and Hashimoto, K., "The Composition of Passive Films on Ferritic 30Cr Stainless Steels in H_2SO_4 ", Boshoku Gijutsu, Vol. 27, pp. 57-61, 1978.
25. Engell, H.J., "Stability and Breakdown Phenomena of Passivating Films", Electrochimica Acta, Vol. 22, pp. 987-993, 1977.
26. Frankenthal, R.P., "On Passivity of Iron at its Alloys", Passivity and its Breakdown on Iron and Iron Based Alloys, NACE, Houston, Texas, pp. 10-17, 1976.

27. Frankenthal, R.P., in reference 26, pp. 15-17.
28. "Discussion: Nature of the Passive Film on Iron and Iron Based Alloys", in reference 26, pp. 85-89.
29. Frankenthal, R.P., in reference 26.
30. Furneaux, R.X., Thompson, G.E., and Wood, G.C., "The Coloured Film Formed on Stainless Steel in Hot Chromic/Sulfuric Acid Solutions", Corrosion Science, Vol. 21, pp. 23-29, 1981.
31. Revesz, A.G. and Kruger, J., "The Role of Non-crystalline Films in Passivation and Breakdown of Passivation", Proceedings of the 7th International Congress on Metallic Corrosion, International Corrosion Council, pp. 330-340, 1978.
32. Sato, N., "The Passivity of Metals and Passivating Films", in reference 20, pp. 29-58.
33. Rosenfeld, I.L., Danilou, I.S. and Oranskaya, R.N., "Breakdown of the Passive State and Repassivation of Stainless Steels", Journal of the Electrochemical Society, Vol. 125, No. 11, pp. 1729-1735, 1978.
34. Galvele, J.R., "Present State of Understanding of the Breakdown of Passivity and Repassivation", in reference 20, pp. 285-327.
35. Sato, N., "A Theory for Breakdown of Anodic Oxide Films on Metals," Electrochimica Acta, Vol. 16, pp. 1683-1692, 1971.
36. Staehle, R.W., "Mechanical Rupture of Protective Films on Iron Based Alloys in Aqueous Environments", in reference 26, pp. 155-160.
37. Fromhold, A.T., "Stress in Passive Films due to Electrochemical Potential Gradients", in reference 26, pp. 161-164.
38. Yahalom, J. and Poznansky, A., "Surface Energy and the Stability of the Passive Layer", in reference 20, pp. 328-336.
39. Sato, N., "Anodic Breakdown of Passive Films on Metals", Journal of the Electrochemical Society, Vol. 129, No. 2, pp. 255-260, 1982.

40. Sato, N., in reference 19, pp. 261-264.
41. Hoare, J.P., "On the Transpassive Dissolution of Oxide Films on Steel Anodes in Neutral Electrolytes", in reference 20, pp. 505-519.
42. Schwabe, K., Herman, S., and Oelssner, W., "Influence of Water on Anodic Dissolution and Passivation Metals", in reference 20, pp. 413-435.
43. Sharp, W.B.A. and Laliberte, L.H., "Chemical Breakdown of Passivity of Stainless Steels in Simulated Crevice Solutions", in reference 20, pp. 407-409.
44. Ambrose, J.R., and Kruger J., "Breakdown of Passive Films on Iron by Chloride Ion", Localized Corrosion, NACE, Houston, Texas, pp. 698-705, 1974.
45. Engell, H.J., in reference 25, pp. 987-993.
46. Kruger, J., "Chemical Breakdown of Passivity", in reference 26, pp. 91-98.
47. Uhlig, H.H., "Competitive Adsorption as a Mechanism for Breakdown", in reference 26, pp. 110-111.
48. Yahalom, J., "On the Initiation and Propagation of Pits", in reference 26, pp. 121-123.
49. Wilde, B.E., "Chloride Ion Adsorption and Pit Initiation on Stainless Steels in Neutral Media", in reference 26, pp. 129-130.
50. Cakir, A. and Scully, J.C., "The Breakdown of Passive Films on Iron by Halide Ions," in reference 20, pp. 385-402.
51. Barbosa, M. and Scully, J.C., "Repassivation Kinetics on a Stainless Steel", in reference 20, pp. 385-402.
52. Sharp, W.B.A. and Laliberte, L.H., in reference 20, pp. 407-409.
53. Okamoto, G. and Shibata, T., "Passivity and the Breakdown of Passivity of Stainless Steel", in reference 20, pp. 646-677.

54. Kolotyikin, Ya.M. and Uhlig, H.H., Journal of the Electrochemical Society, Vol. 108, p. 209, 1961.
55. Richardson, J.A. and Wood, G.C., Journal of the Electrochemical Society, Vol. 120, p. 193, 1973.
56. Hoare, J.P., in reference 41, pp. 509-519.
57. Rosenfeld, I.L., Danilou, I.S., and Oranskays, R.N., in reference 33, pp. 1730-1731.
58. Azzerri, N., Giuliani, L. and Bombara, G., "Influence of Surface Finish on Passivity Retention of Stainless Steels", Corrosion, Vol. 26, No. 9, pp. 381-386, 1970.
59. Smialowska, Z.S., "Passivating Anion", in reference 20, pp. 443-462.
60. Hashimoto, K., and Asami, K., "Factors Determining Corrosion Resistance of Chromium-Bearing Alloys", in reference 20, pp. 749-752.
61. Asphahani, A.I., "Corrosion Resistance of High Performance Alloys", Materials Performance, Vol. 19, No. 12, pp. 33-42, 1980.
62. Walker, M.S. and Rowe, L.C., "The Use of Electrochemical Techniques for Corrosion Research in the Automotive Industry", Electrochemical Techniques for Corrosion, NACE, Houston, Texas, pp. 79-87, 1977.
63. Syrett, B.C., "PPR Curves - A New Method of Assessing Pitting Corrosion Resistance", Corrosion, Vol. 33, No. 6, pp. 221-224, 1977.
64. Chen, W.Y.C. and Stephens, J.R., "Anodic Polarization Behavior of Austenitic Stainless Steel Alloys with Lower Chromium Content", Corrosion, Vol. 35, No. 10, pp. 443-450, 1979.
65. Drugli, J.M. and Bardal, E., "A Short Duration Test Method for Prediction of Crevice Corrosion Rates on Stainless Steels", Corrosion, Vol. 34, No. 12, pp. 419-424, 1978.
66. Dean, S.W., "Electrochemical Methods of Corrosion Testing", in reference 62, pp. 52-63.

67. Hickling, J. and Wieling, N., "Electrochemical Investigations of the Resistance of Inconel 600, Incoloy 800, and Type 347 Stainless Steel to Pitting Corrosion in Faulted PWR Secondary Water at 150 to 250 C", Corrosion, Vol. 37, No. 39, pp. 148-152, 1981.
68. Jackson, R.P. and van Rooyen, D., "Electrochemical Evaluation of Resistance of Stainless Alloys to Chloride Media", Corrosion, Vol. 27, No. 5, pp. 203-210, 1971.
69. Man, H.C. and Gabe, D.R., "A Study of Pitting Potentials for Some Austenitic Stainless Steels Using a Potentiodynamic Technique", Corrosion Science, Vol. 21, No. 9, pp. 713-721, 1981.
70. Hladky, K. and Dawson, J.L., "The Measurement of Localized Corrosion Using Electrochemical Noise", Corrosion Science, Vol. 21, No. 4, pp. 317-322, 1981.
71. Lizlous, E.A. and Bond, A.P., "An Evaluation of Some Electrochemical Techniques for the Determination of Pitting Potentials of Stainless Steel", Corrosion, Vol. 31, No. 6, pp. 219-222, 1975.
72. Man, H.C. and Gabe, D.R., "The Determination of Pitting Potentials", Corrosion Science, Vol. 21, No. 4, pp. 323-326, 1981.
73. Morris, P.E. and Scarberry, R.C., "Anodic Polarization Measurements of Active-Passive Nickel Alloys by Rapid-Scan Potentiostatic Techniques", Corrosion, Vol. 26, No. 7, pp. 109-179, 1970.
74. Prazak, M., Sen, T.X. and Kuchynka, D., "Selective Corrosion Study by Anodic Stripping of CrN: Steel", Electrochimica Acta, Vol. 25, pp. 509-513, 1980.
75. Verink, E.D. and Pourbaix, M., "Use of Electrochemical Hysteresis Techniques in Developing Alloys for Saline Exposures", Corrosion, Vol. 27, No. 12, pp. 495-505, 1971.
76. Greene, N.D., "Predicting Behavior of Corrosion Resistant Alloys By Potentiostatic Polarization Methods", Corrosion, Vol. 18, No. 4, pp. 136-142, 1962.
77. Wilde, B.E., "A Critical Appraisal of Some Popular Laboratory Electrochemical Tests for Predicting Localized Corrosion Resistance of Stainless Alloys in Seawater", Corrosion, Vol. 28, No. 8, pp. 283-291, 1972.

78. Kain, R.M., "Localized Corrosion Behavior in Natural Seawater: A Comparison of Electrochemical and Crevice Testing of Stainless Alloys," Corrosion/80, paper No. 74, NACE, 1980.
79. Geisert, R.E., Greene, N.D. and Agarwala, V.S., "A Versatile Polarization Cell System", Corrosion, Vol. 32, No. 10, pp. 407-410, 1976.
80. Sedriks, A.J., in reference 6.
81. Sedriks, A.J., in reference 6.
82. Sedriks, A.J., in reference 6.
83. Private conversation with Mr. P.E. Morris on 24 March 1982.
84. Szalkowski, F.J., "Electron Spectroscopy: A Source of Chemical Information for Corrosion Research", Corrosion/82, Paper No. 268, NACE, 1982.
85. Lumsden, J.B., Staehle, R.W., "Application of Auger Electron Spectroscopy to the Determination of the Composition of Passive Films on Type 316 Stainless Steel", Scripta Metallurgica, Vol. 6, pp. 1205-1208, 1972.
86. deCunha Belo, M., Randot, B., Pons, F., Le Hericy, J. and Langeron, J.P., "Study by Auger Spectroscopy and Cathodic Reduction of Passive Films Formed on Ferritic Stainless Steels", Journal of the Electrochemical Society, Vol. 124, No. 9, pp. 1317-1324, 1977.
87. Olefjord, I. and Elfstrom, B., in reference 22.
88. Zakipour, S. and Leygraf, C., "Surface Composition of Stainless Steel During Propagation of Crevice Corrosion," Corrosion, Vol. 37, No. 1, pp. 21-28, 1981.
89. Ogawa, H., Omata, H., Itoh, I. and Okada, H., "Auger Electron Spectroscopic and Electrochemical Analysis of The Effect of Alloying Elements on the Passivation Behavior of Stainless Steels", Corrosion, Vol. 34, No. 2,
90. Hultquist, G., Leygraf, C., "Surface Composition of a Type 316 Stainless Steel Related to Initiation of Crevice Corrosion", Corrosion, Vol. 36, No. 3, pp. 126-129, 1980.
91. Olefjord, I. and Elfstrom, B., in reference 22.

92. Frankenthal, R.P. and Thompson, D.E., "Effect of Ion Sputtering on the Quantitative Analysis of Iron-Chromium Alloys and Their Oxides", in reference 20, pp. 262-270.
93. Kain, R.M., in reference 78.
94. Asphahani, A.I., in reference 61.
95. Asphahani, A.I., in reference 61.
96. Asphahani, A.I., in reference 61.
97. Marsh, G.P., Williams, D.E., Wescott, C., "Electrochemical Techniques for Studying Localized Corrosion", Research Symposium, Session 5 - Localized Corrosion, NACE, Corrosion/82, Houston, Texas, 1982.
98. Hardman, K., Kruger, J., Mingdah, W., "Pit Initiation and Propagation Rates of 304 Stainless Steel in Chloride Environments", in reference 97.
99. "Panel Discussion: Methods of Evaluating Localized Corrosion Behavior in Marine Environments", in reference 97.
100. Degerbeck, J. and Gille, I., "Crevice Corrosion - A New Crevice Former", Corrosion Science, Vol. 19, pp. 1113-1115, 1980.
101. Private Communication from Mr. P.E. Morris, 28 March 1982.
102. Bandy, R. and van Roogen, D., "Pitting Resistant Alloys in Highly Concentrated Chloride Media", Corrosion/82, paper No. 71, NACE Conference 22-26 March 1982, Houston, Texas.
103. Blom, K.-J., "Corrosion Resistance and Industrial Experience of Low Manganese Austenitic Stainless Steel Grades", Corrosion/82, paper No. 87, NACE Conference 22-26 March 1982, Houston, TX.
104. Zakipour, S. and Leygraf, C., in reference 88.
105. Ogawa, H., et al, in reference 89.
106. Ogawa, H., et al, in reference 89.
107. Asphahani, A.I., in reference 61.

108. TrabANELLI, G., and Zucchi, F., "Measuring the Corrosion Resistance of Four Alloys in Chloride Solutions", Materials Protection and Performance, July, 1970, pp. 16-20.
109. Morris, P.E., Scarberry, R.C., in reference 73.
110. Manning, P.E., "The Effect of Scan Rate on Pitting Potentials of High Performance Alloys in Acidic Chloride Solutions", Corrosion, Vol. 36, No. 9, pp. 468-474, 1980.
111. Kain, R.M., in reference 78.
112. Garner, A., "Crevice Corrosion of Stainless Steels in Seawater" Correlation of Field Data with Laboratory Ferric Chloride Tests", Corrosion, Vol. 37, No. 3, pp. 178-184, 1981.
113. Kain, R.M., "Crevice Corrosion Evaluations of Passive Alloys," Research Report, February 1981, La Que Center for Corrosion Technology, Inc.
114. Hack, H.P., "Crevice Corrosion Behavior of 45 Molybdenum-Containing Stainless Steels in Seawater", David W. Taylor Naval Ship Research and Development Center Report No. SME-81187, pp. 1-27, 1981.
115. Hack, H.P., in reference 114.
116. Lunarka, E., et al, in reference 18.
117. Yoshii, T., "Study on Anodic Dissolution of Fe-Mo Alloys", Ph.D. Thesis, University of Florida, pp. 28-30, August 1981.
118. Brigham, R.J. and Tozer, E.W., "Effect of Alloying Additions on the Pitting Resistance of 18% Cr Austenitic Stainless Steel", Corrosion, Vol. 30, No. 5, pp. 161-166, 1974.
119. da Cunha Belo, M, et al, in reference 86.
120. Olefjord, I. and Elfstrom, B., in reference 22.
121. Zakipour, S., and Leygraf, C., in reference 88.
122. Ogawa, H., et al, in reference 89.
123. Hultquist, G., and Leygraf, C., in reference 90.

- 124. Zakipour, S., and Leygraf, C., in reference 88.
- 125. Zakipour, S., and Leygraf, C., in reference 88.
- 126. Zakipour, S., and Leygraf, C., in reference 88.
- 127. Williams, D.E., et al, in reference 97.
- 128. Private conversation with Professor H.H. Uhlig on
31 March 1982.

APPENDIX A

CATALOG OF PARAMETERS USED IN ANALYSIS

In the analysis of the polarization curves generated by this study, several important parameters have been selected. With the exception of E_x , all of the below-listed parameters have been previously explained(20). Care must be taken, because a variety of names have been associated with each one. These parameters are shown diagrammatically in Figure 2.4.1.

E_{corr} - corrosion potential is the potential at which the cathodic and anodic curves intersect.

E_p - pitting potential is the potential above which pits may be formed, usually associated with a well-defined change in slope on an E-I plot.

E_x - crossover potential is the potential where, on the reverse scan (anodic--->cathodic) the anodic curves intersect either the anodic or cathodic curve of the forward scan.

E_{prot} - protection potential(against pitting) is the potential at which the anodic and cathodic curves transition occurs on the reverse scan.

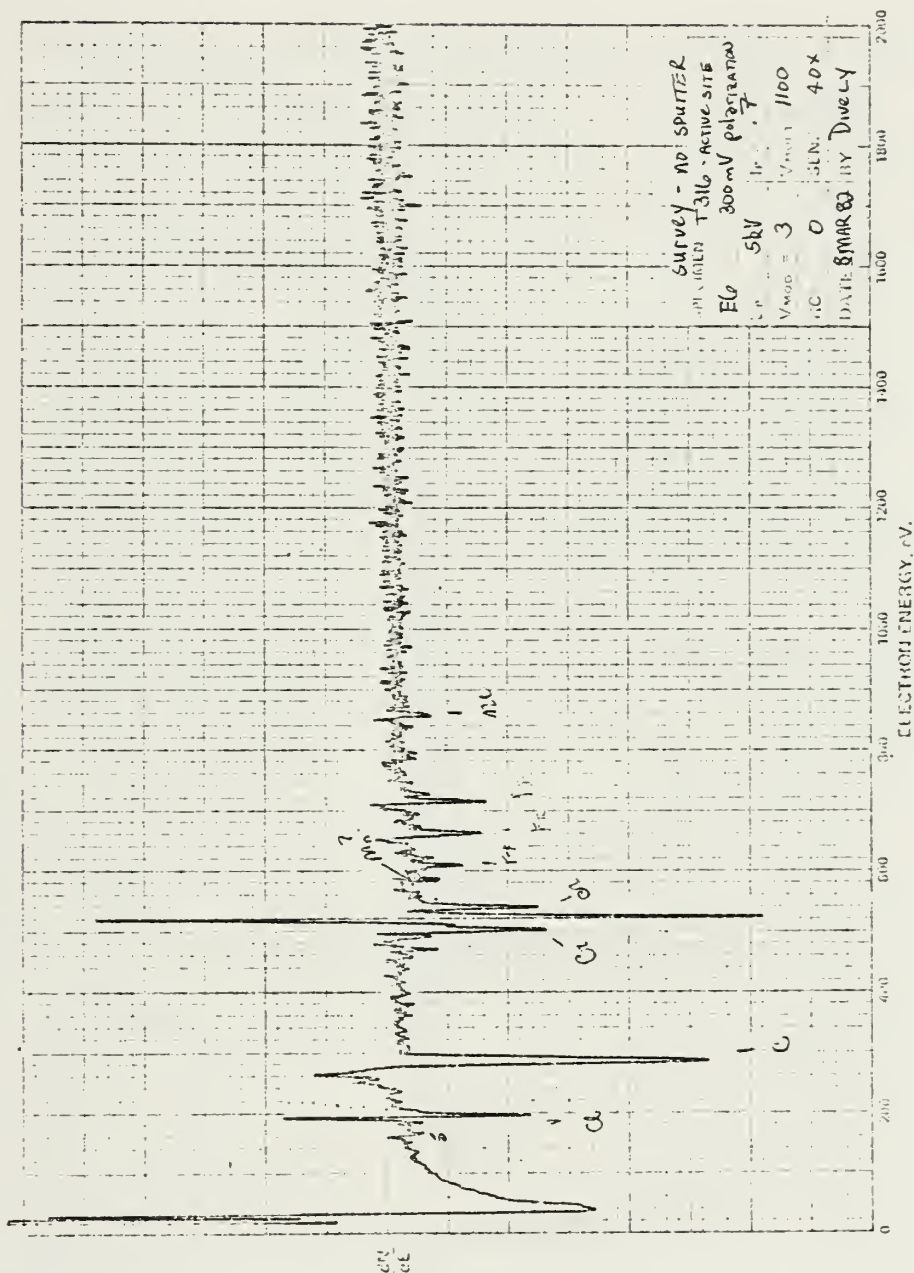
(Note: When used in Group 1(no localized corrosion), the term E_{prot} was used only to maintain continuity of parameters among the four groups. Since no pitting occurred in Group 1, an E_{prot} would not be defined.)

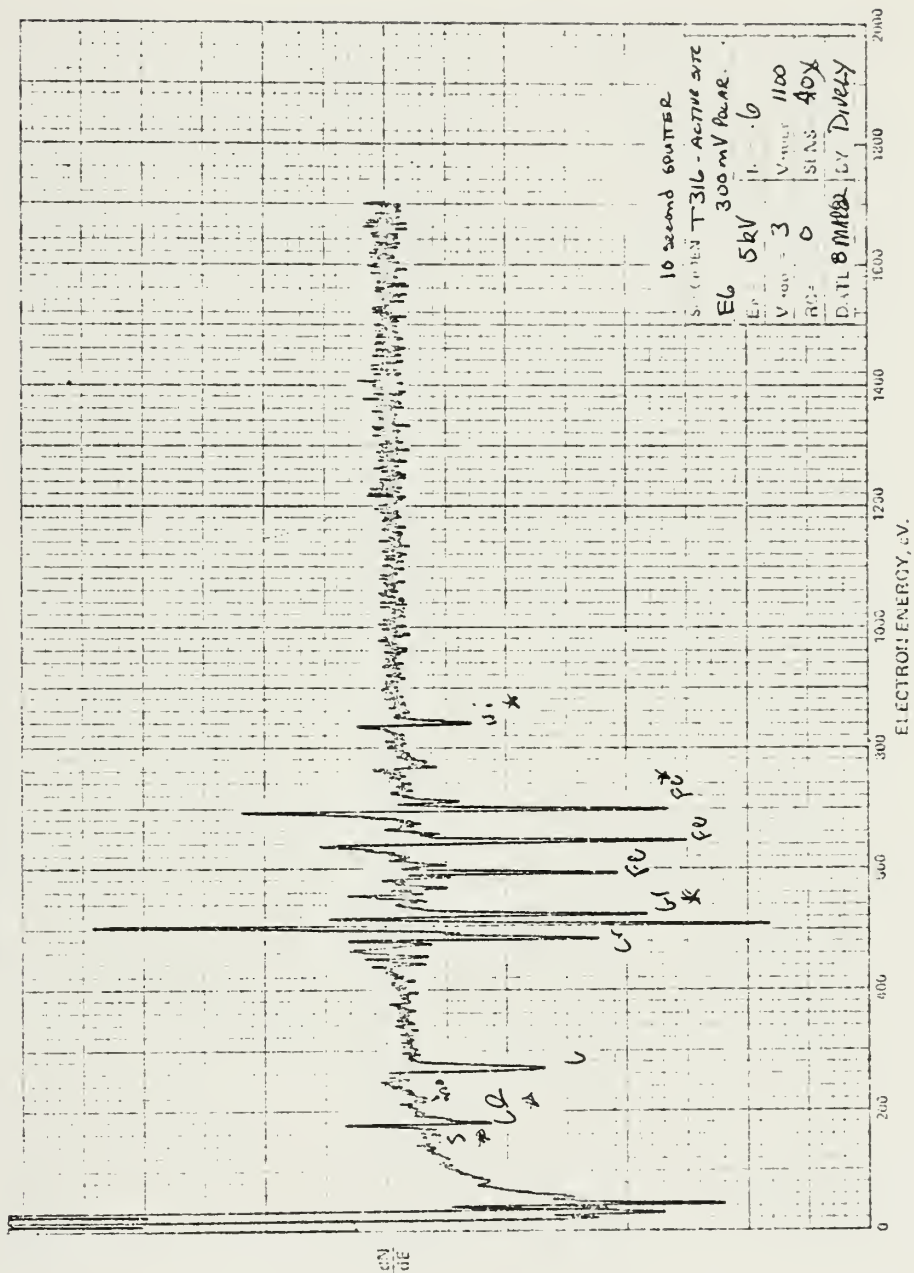
I_{max} - is the maximum current achieved in the anodic curve of the polarization scan.

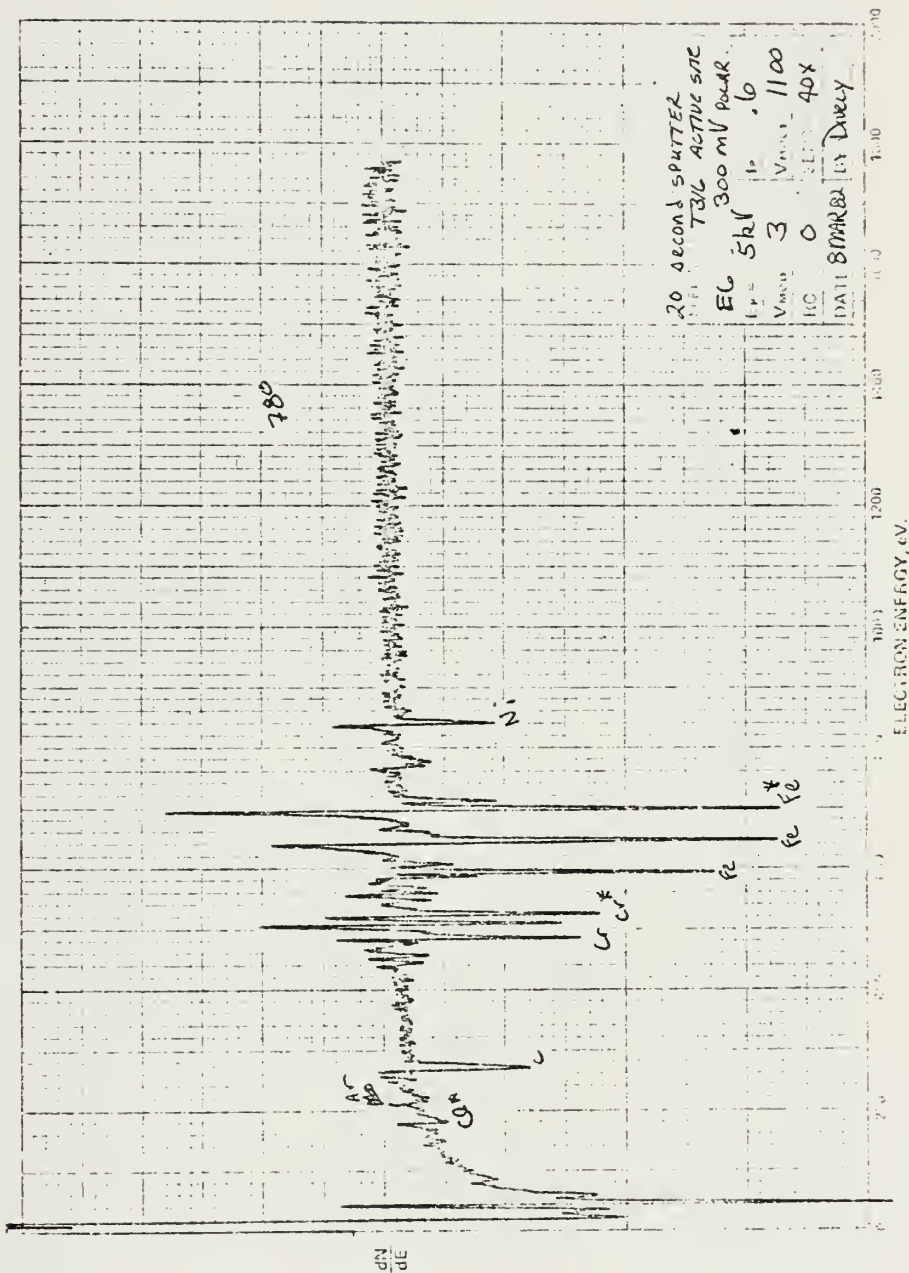
$E_{prot} - E_{corr}$ - is an indication of the size of the anodic hysteresis loop.

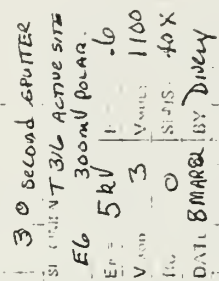
$E_x - E_p$ - is an indication of the size of the anodic hysteresis loop.

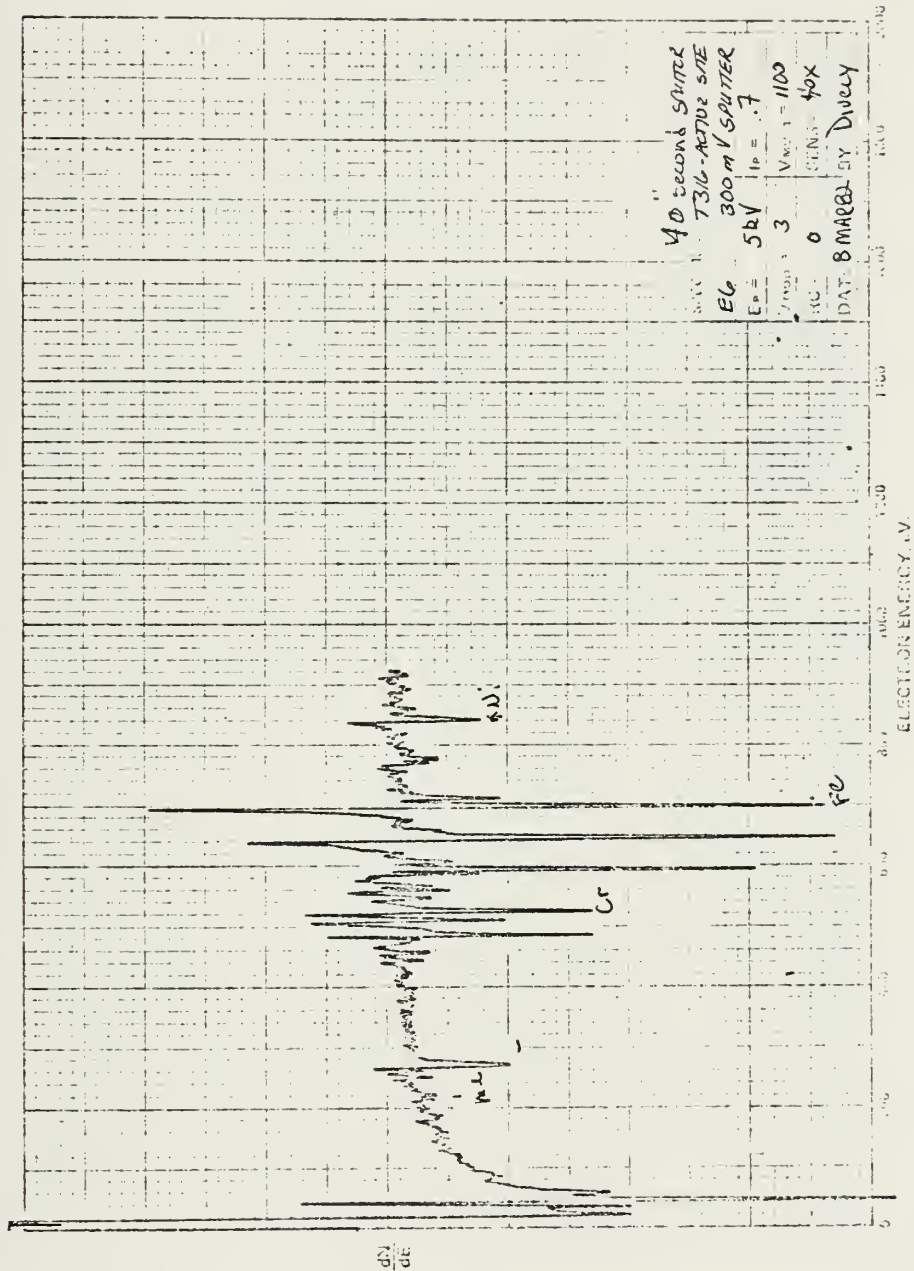
APPENDIX B

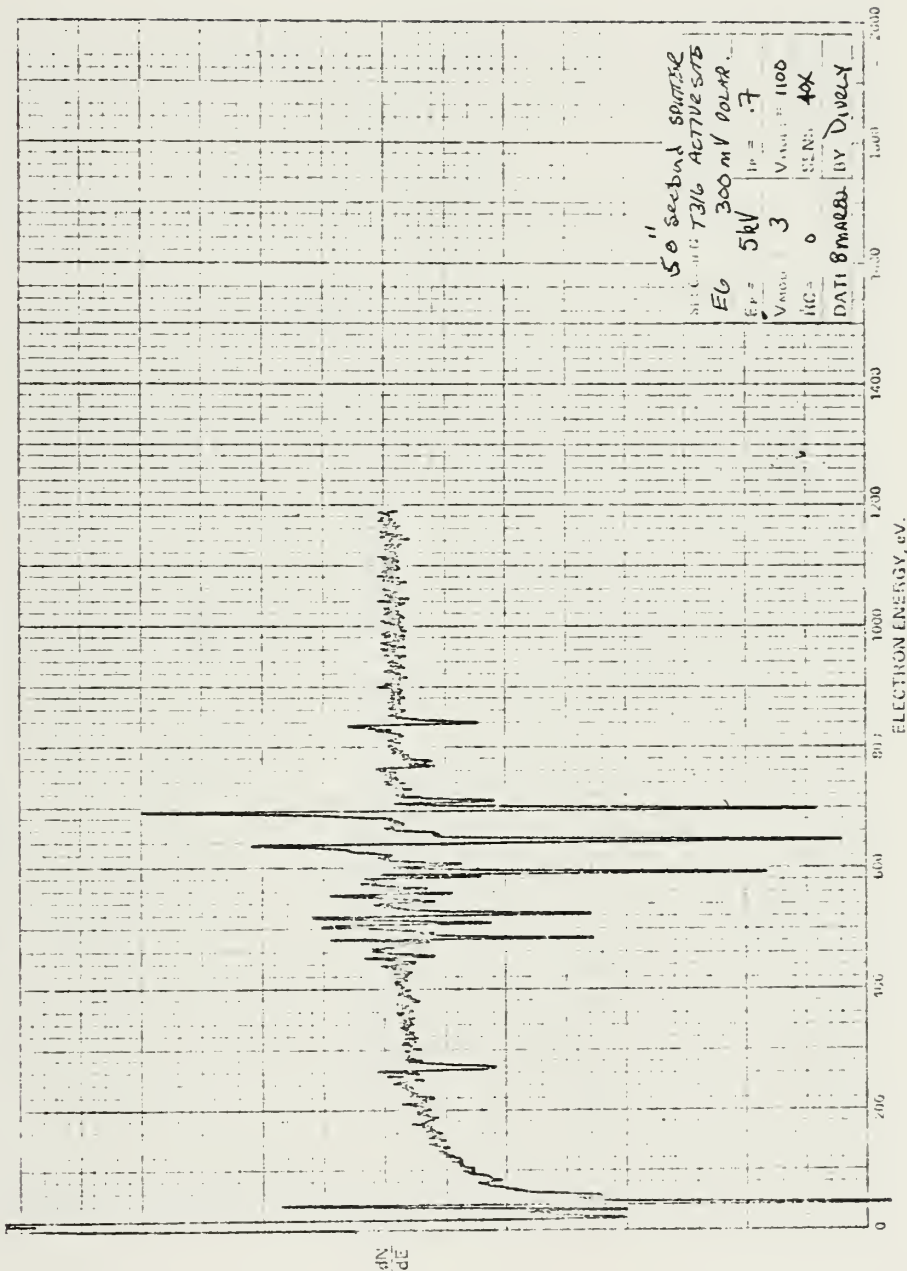


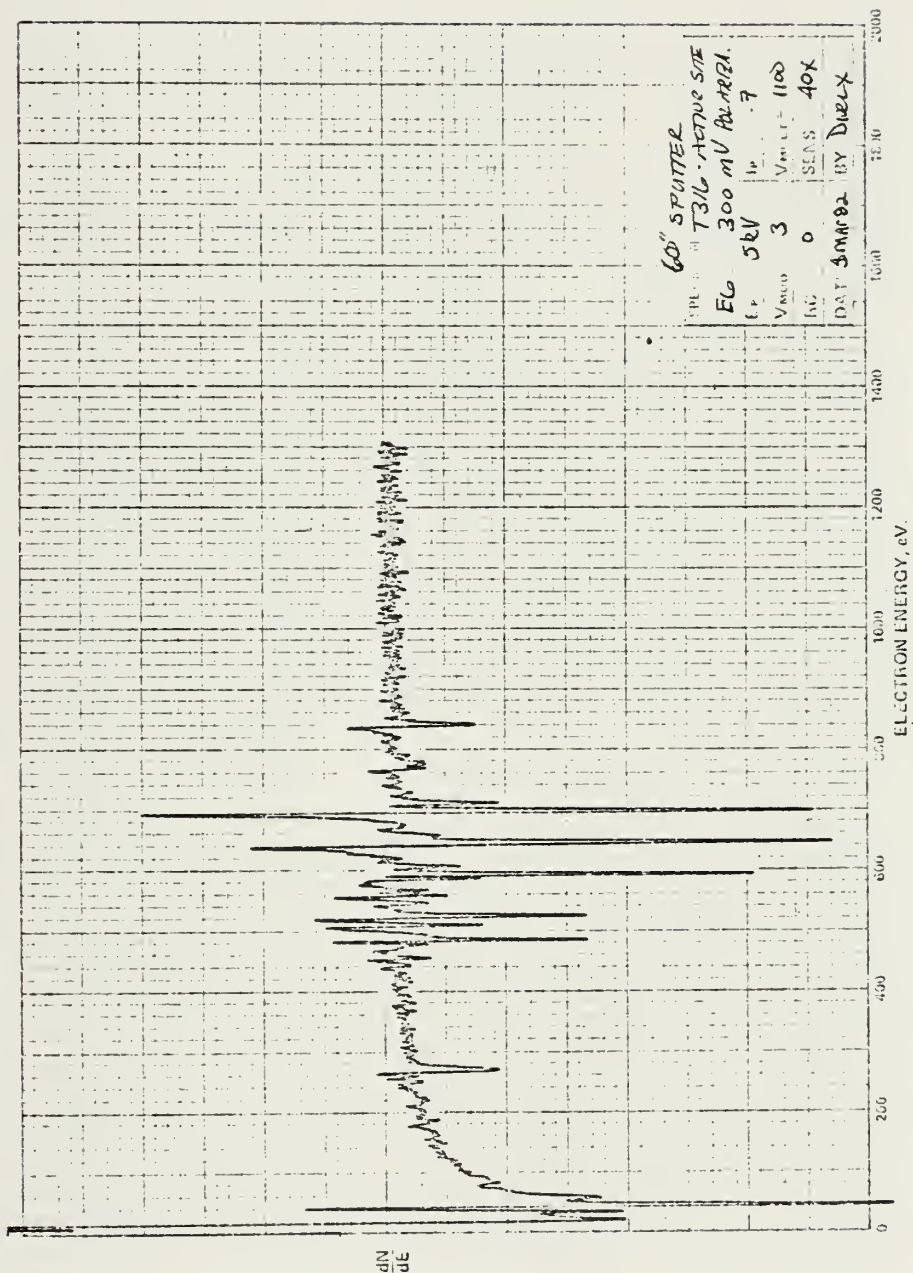




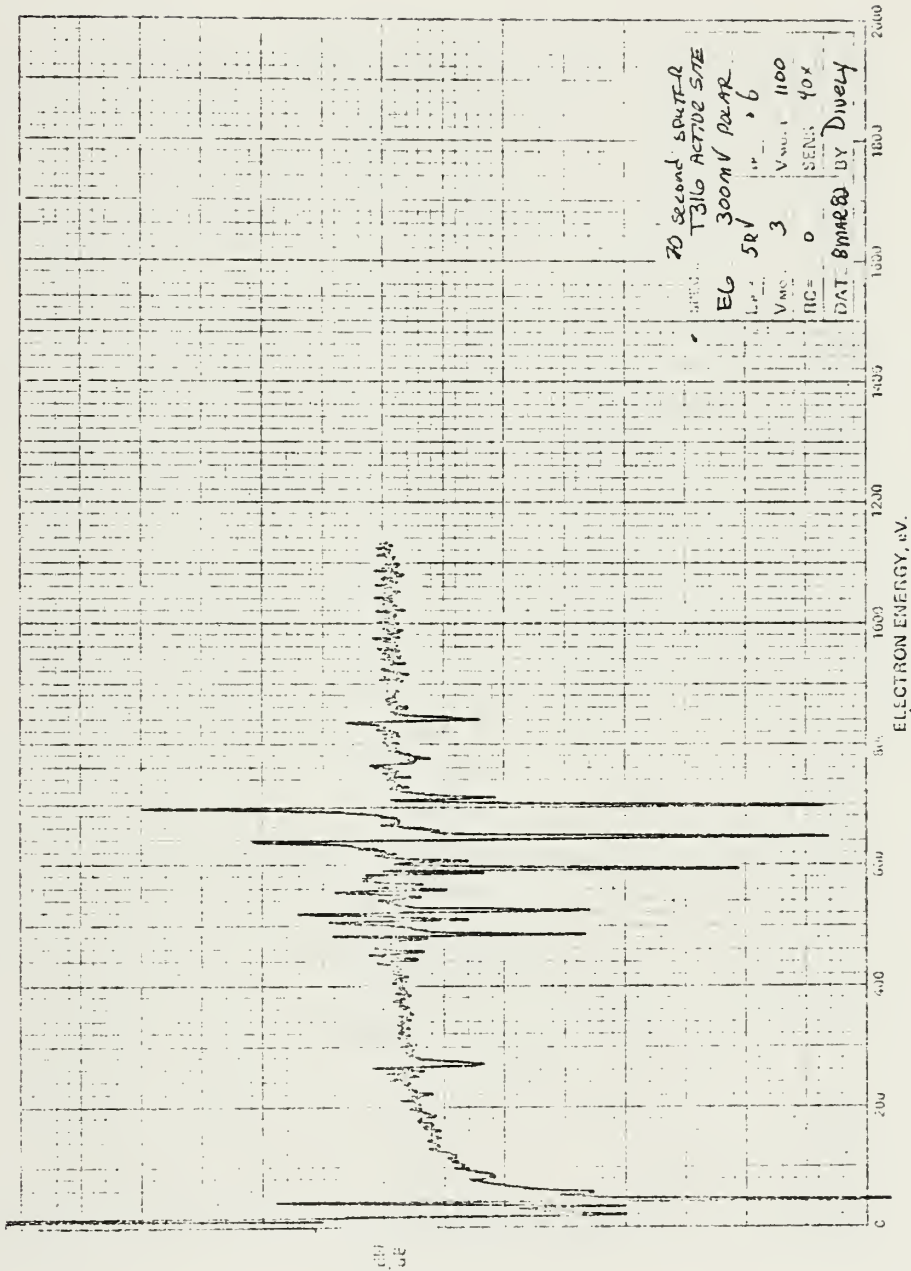


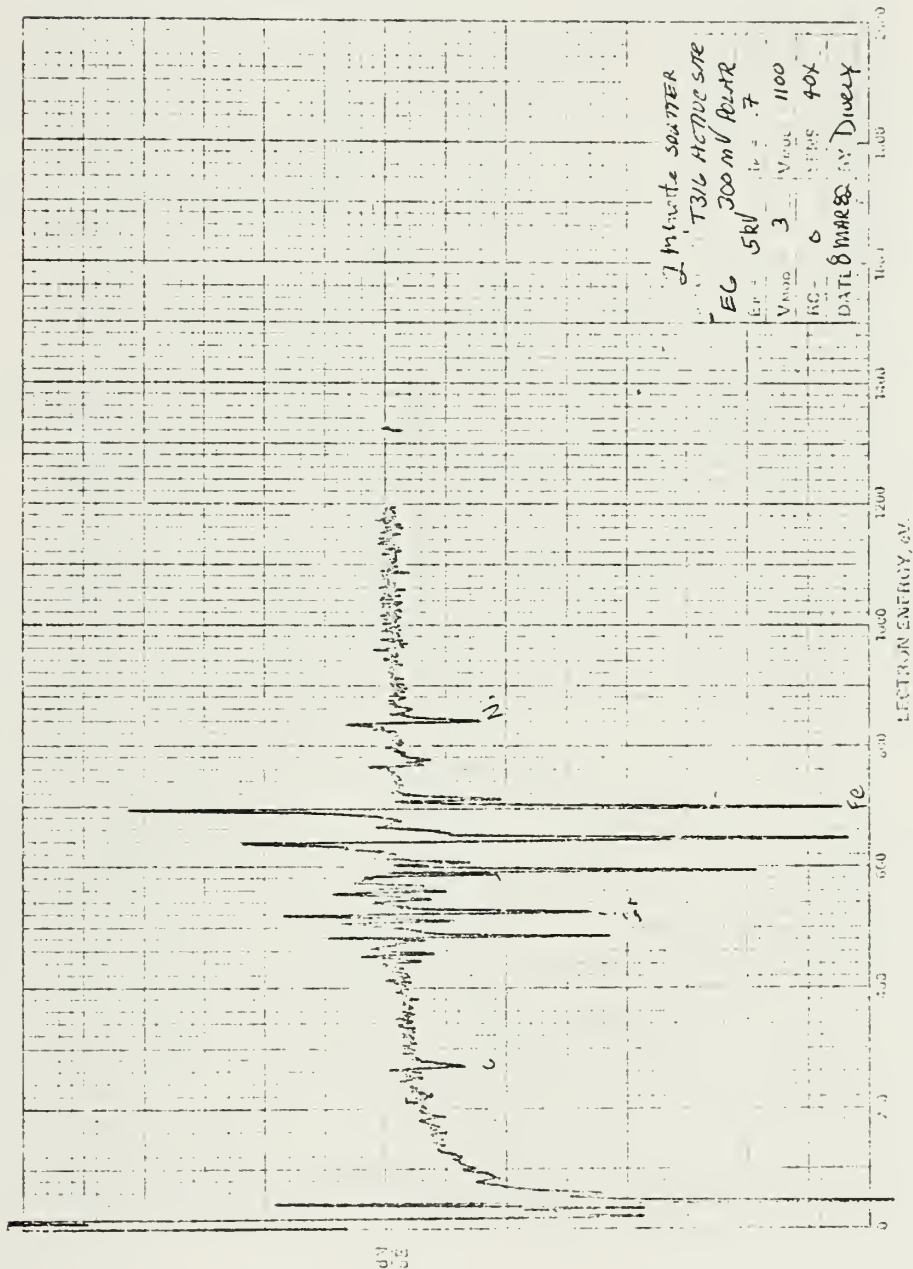


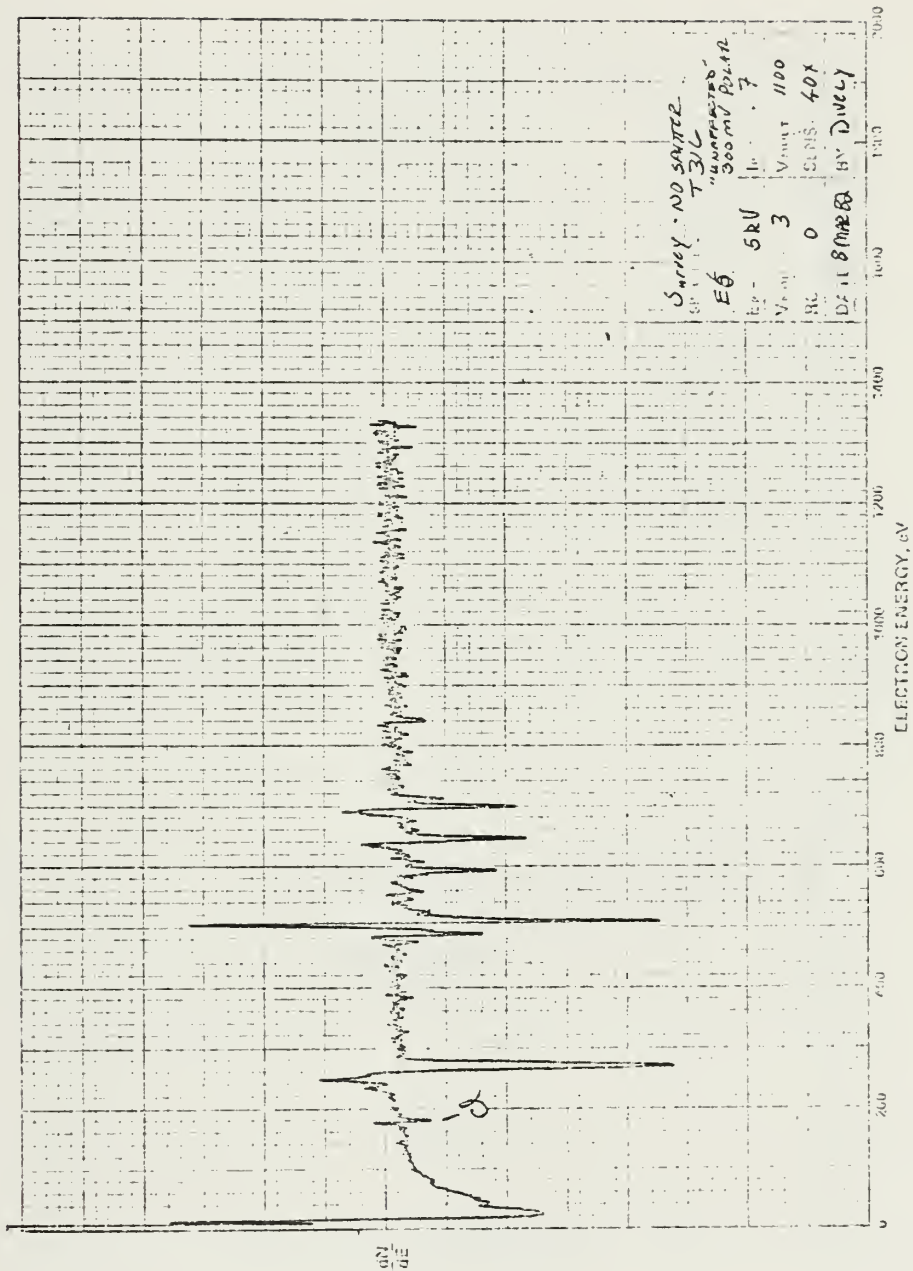


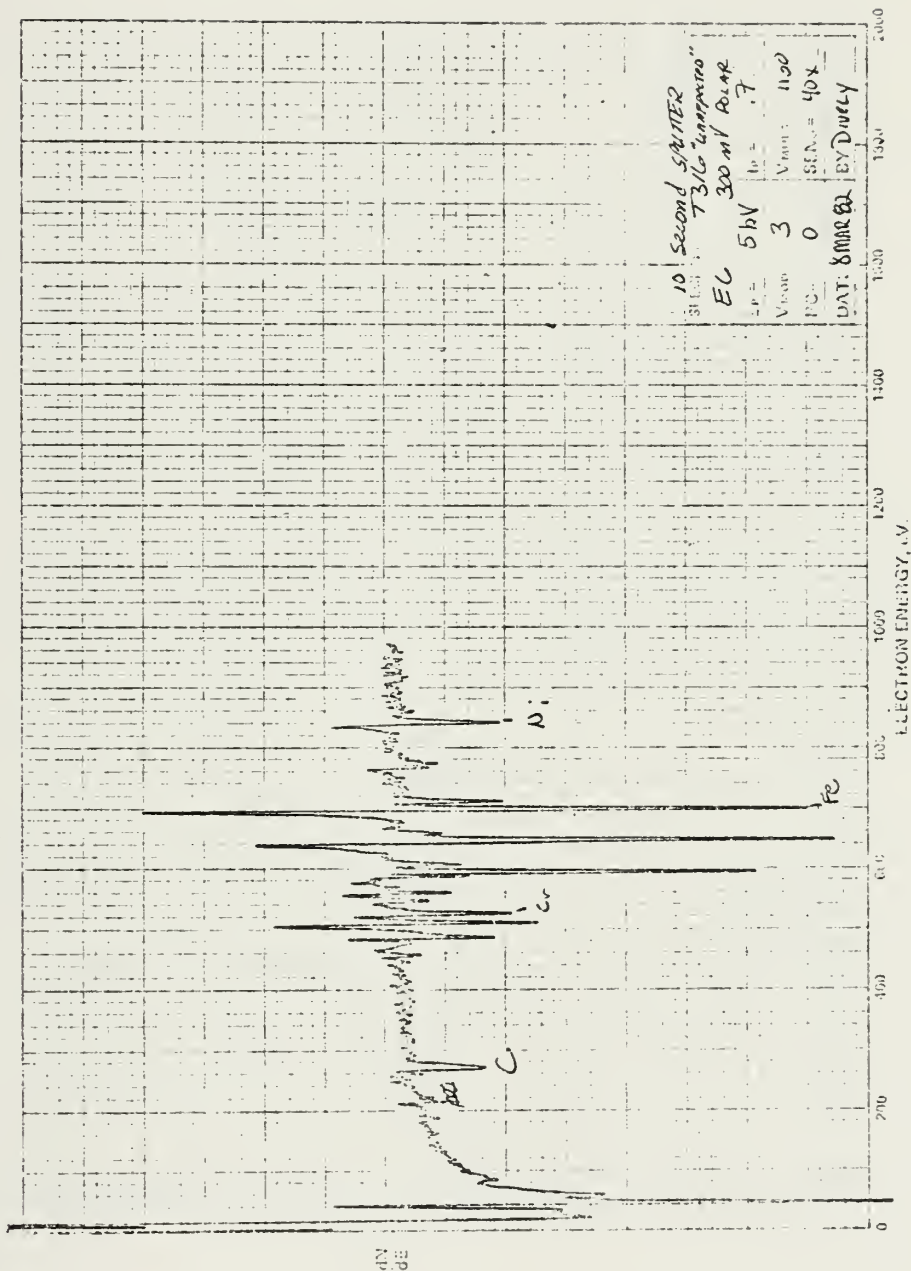


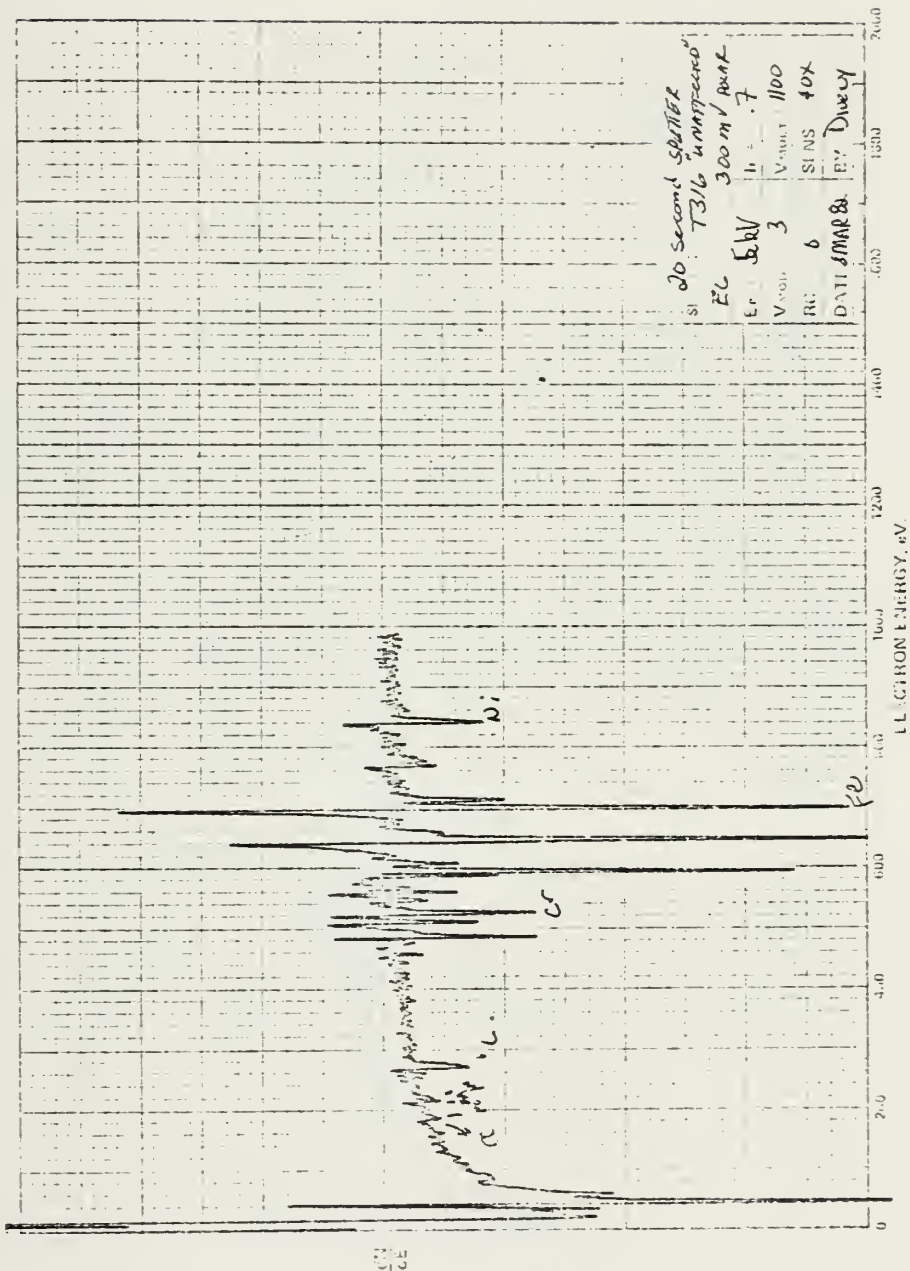
PHYSICAL ELECTRONICS INDUSTRIES
4011 CHASE DRIVE

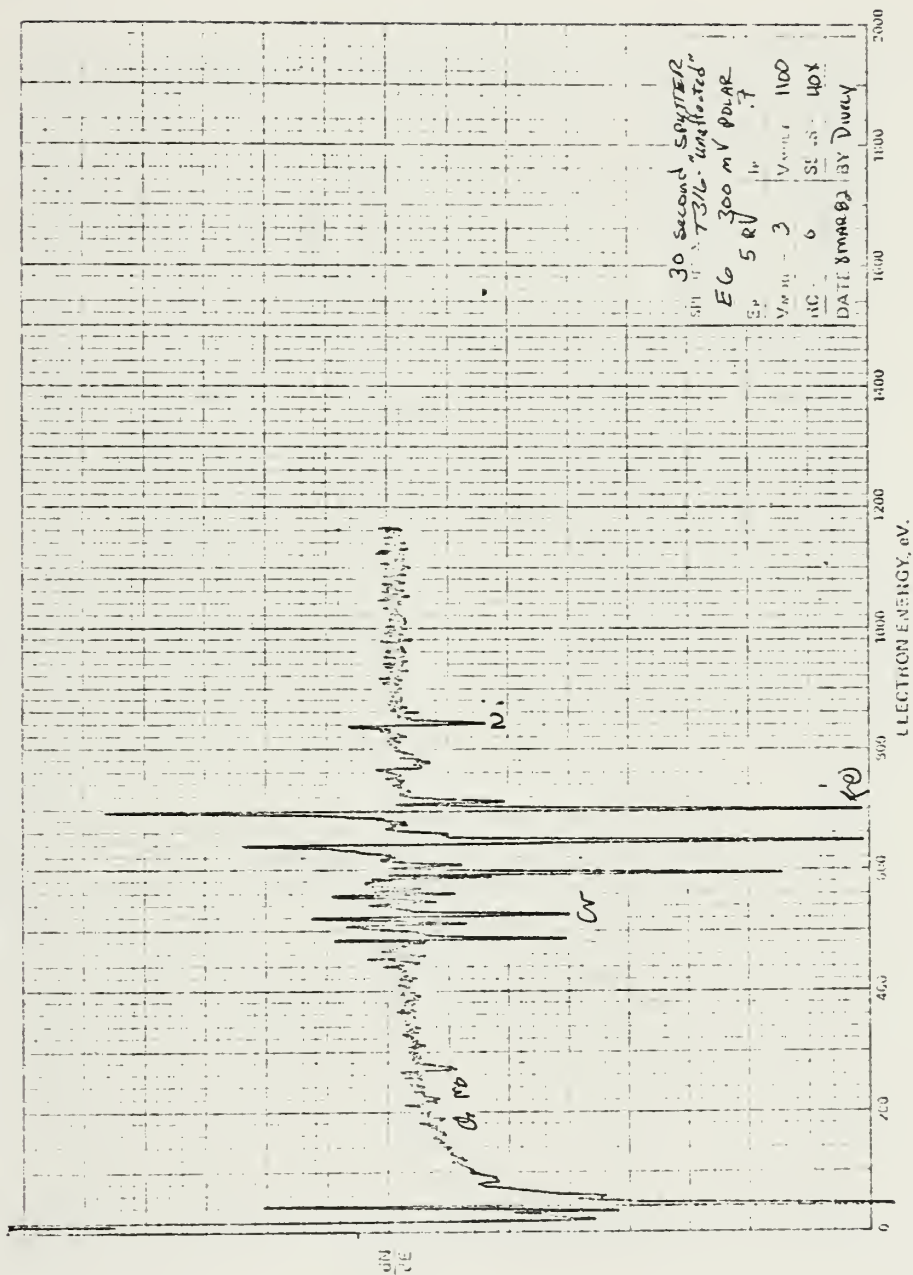


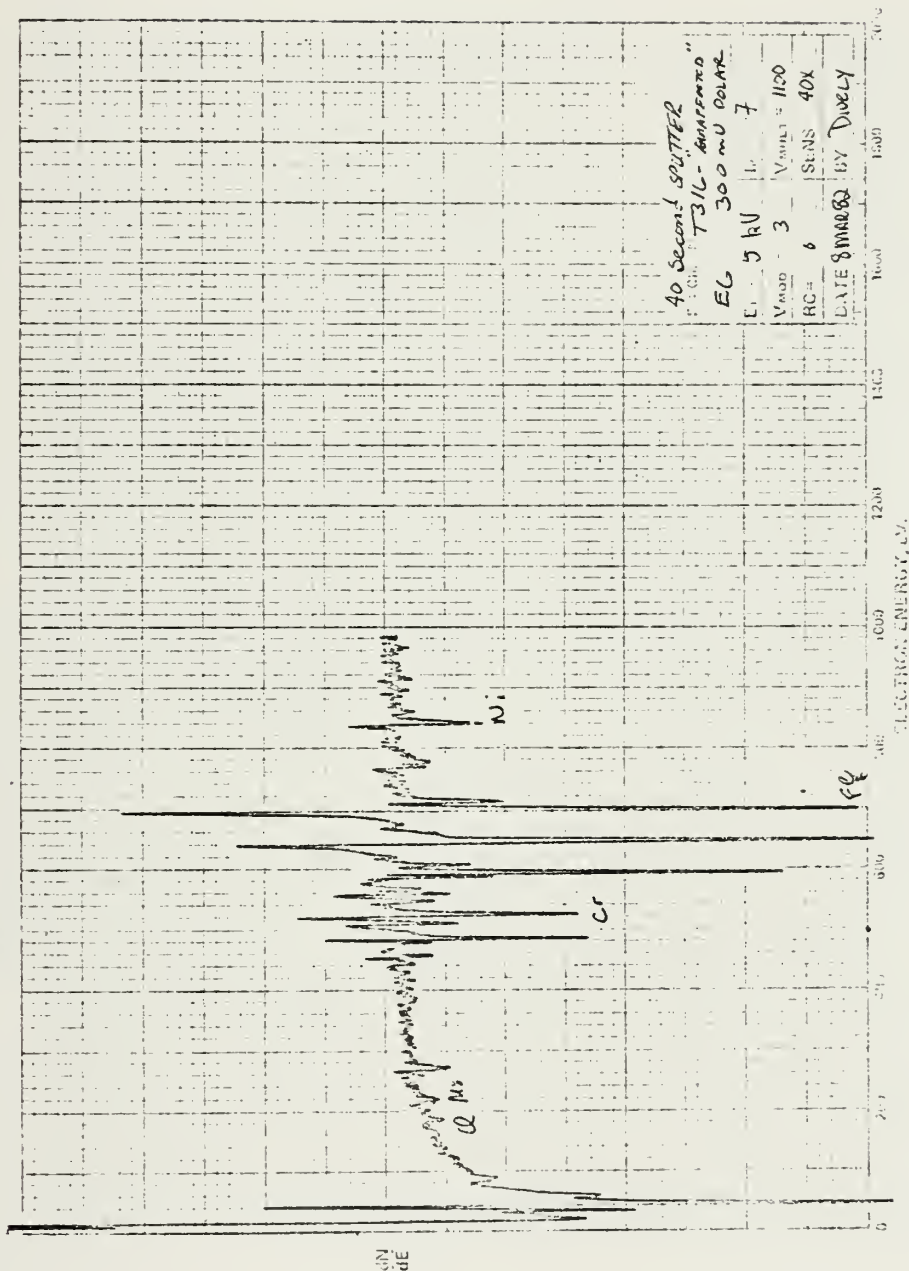


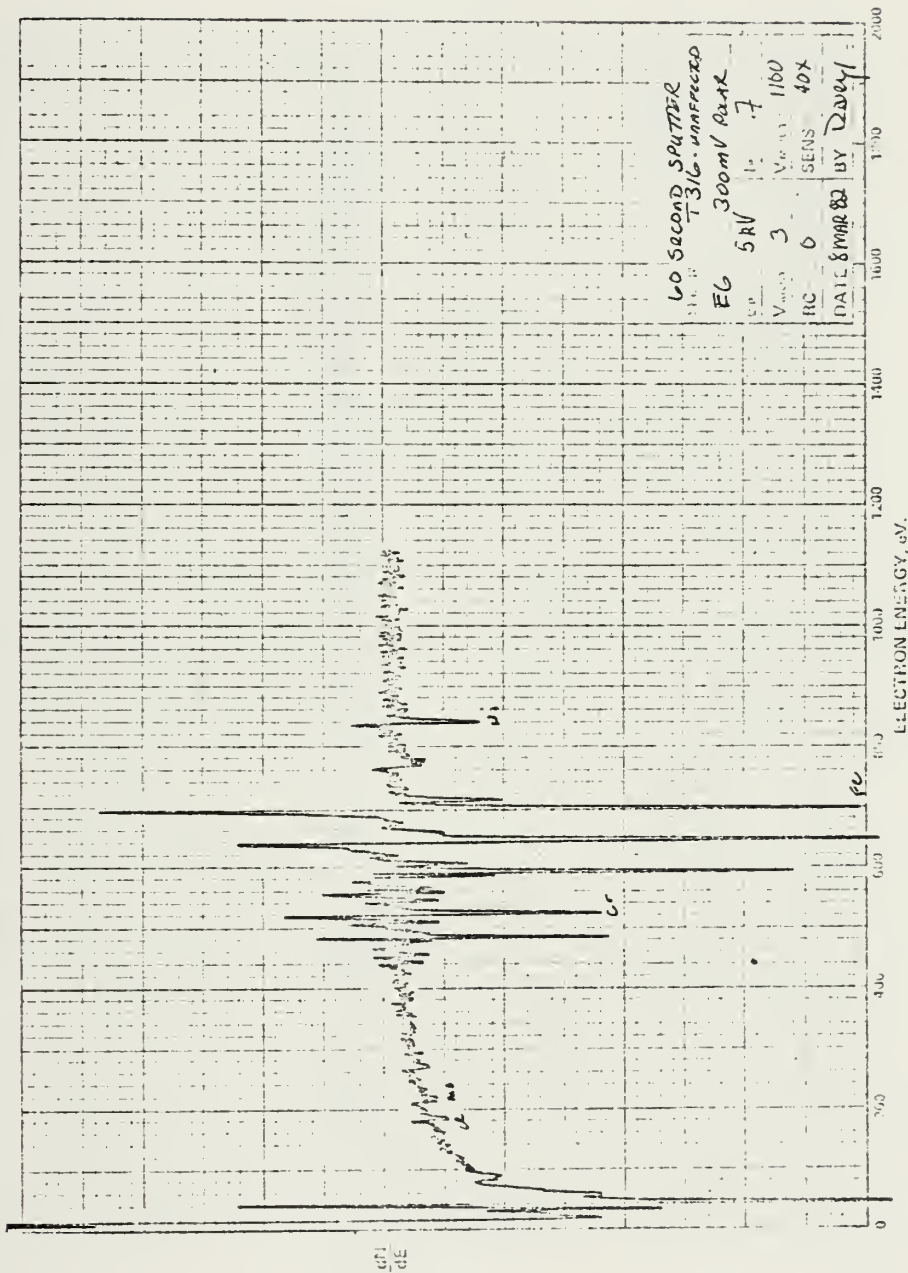


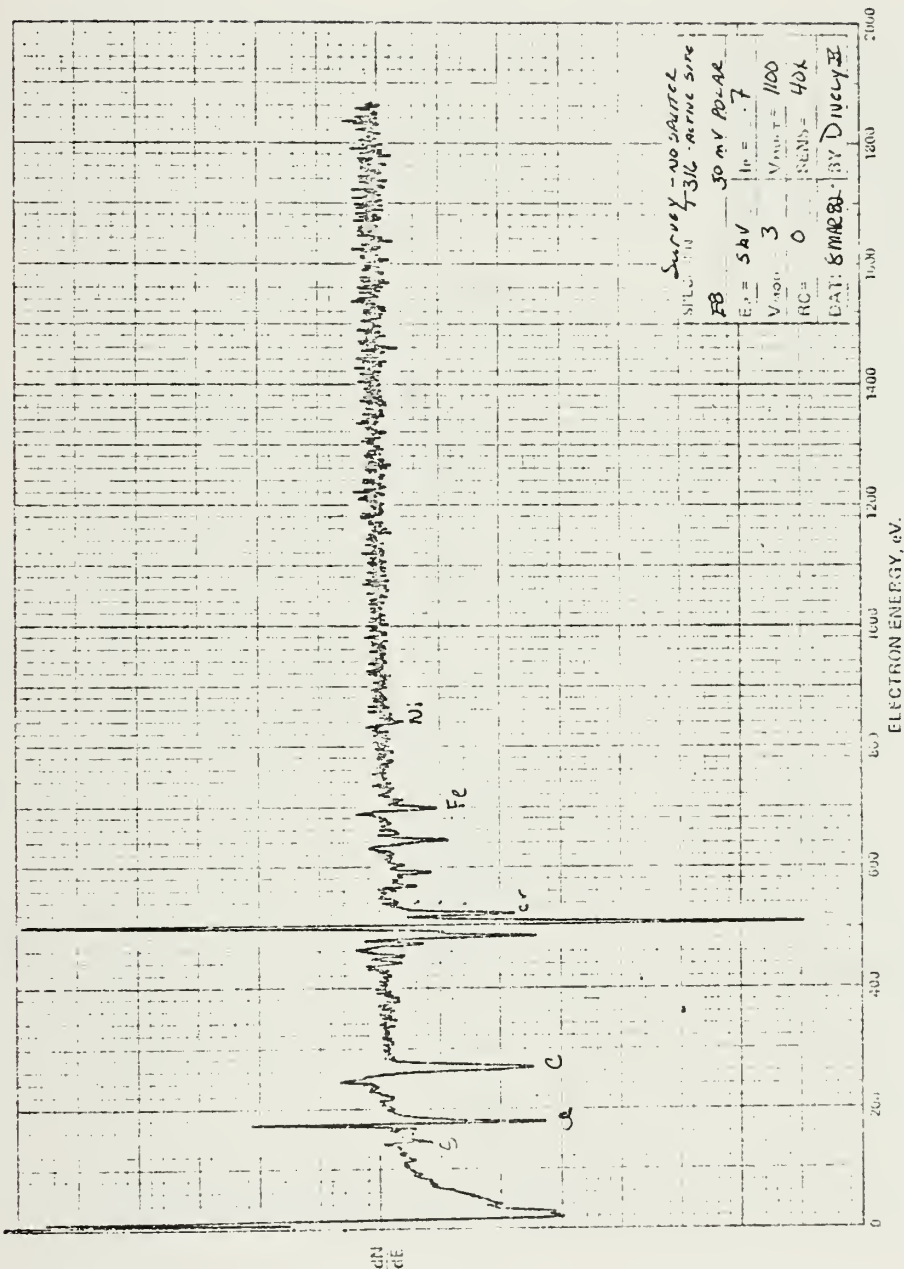


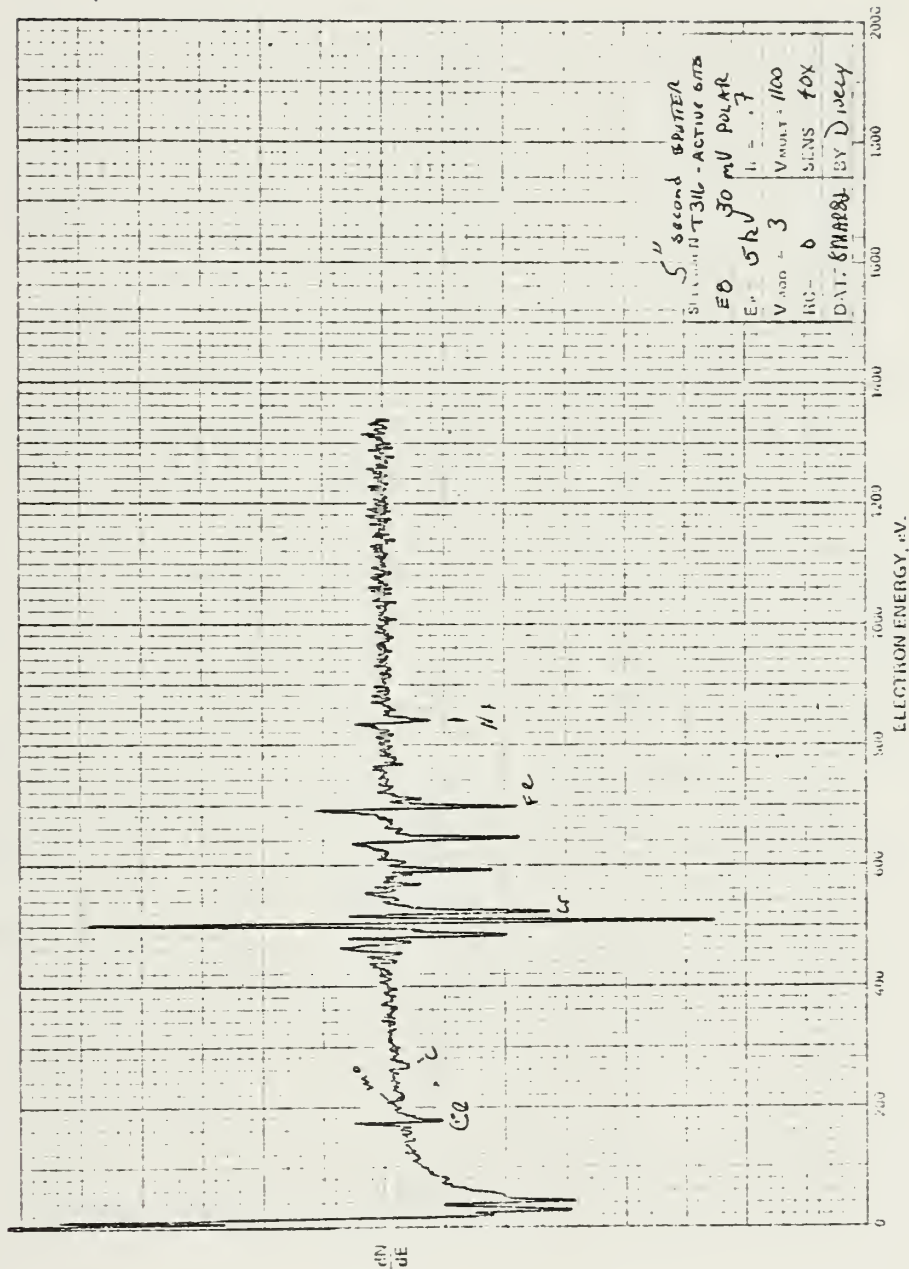


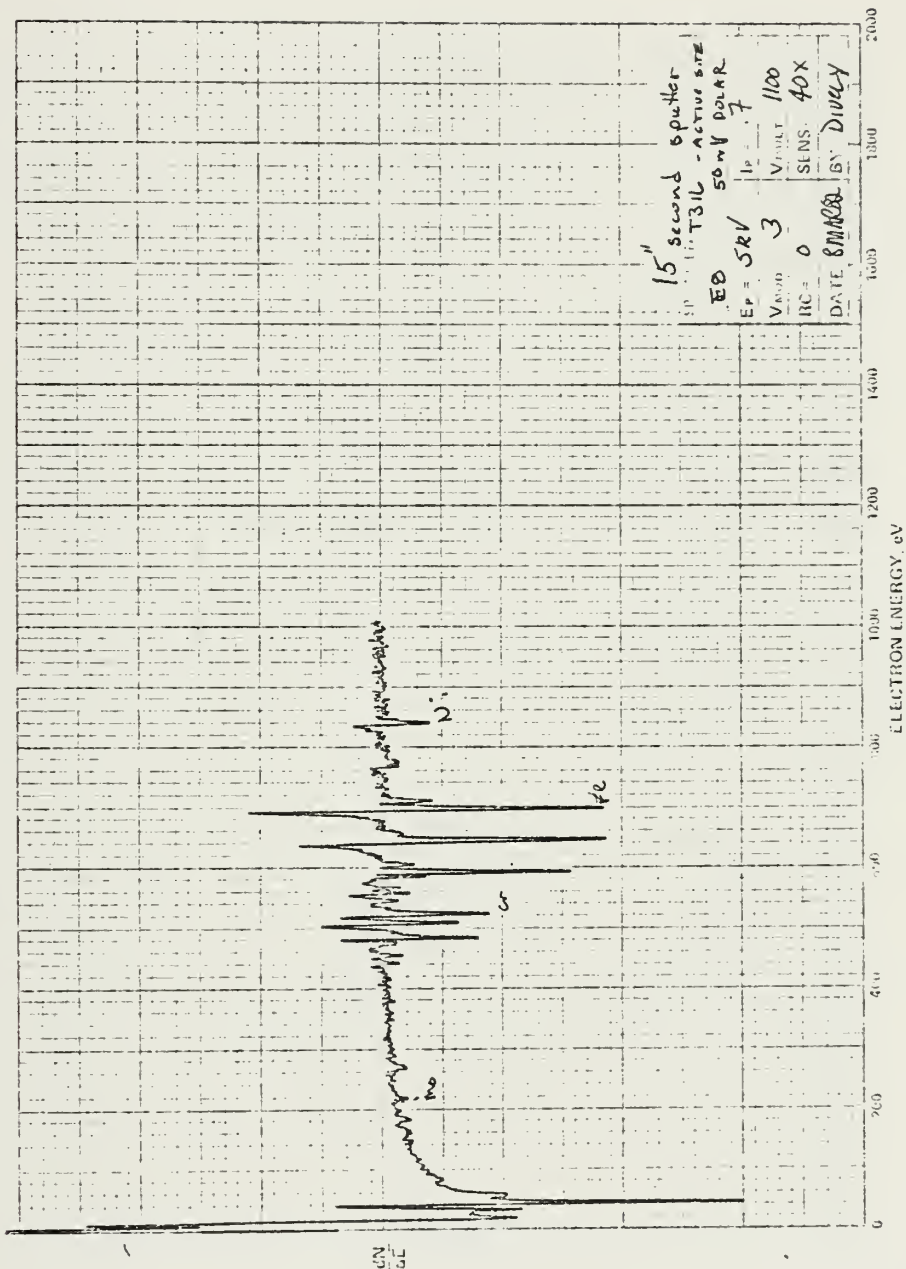


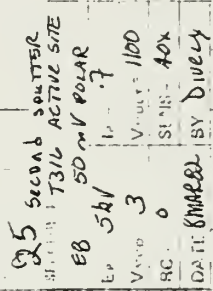


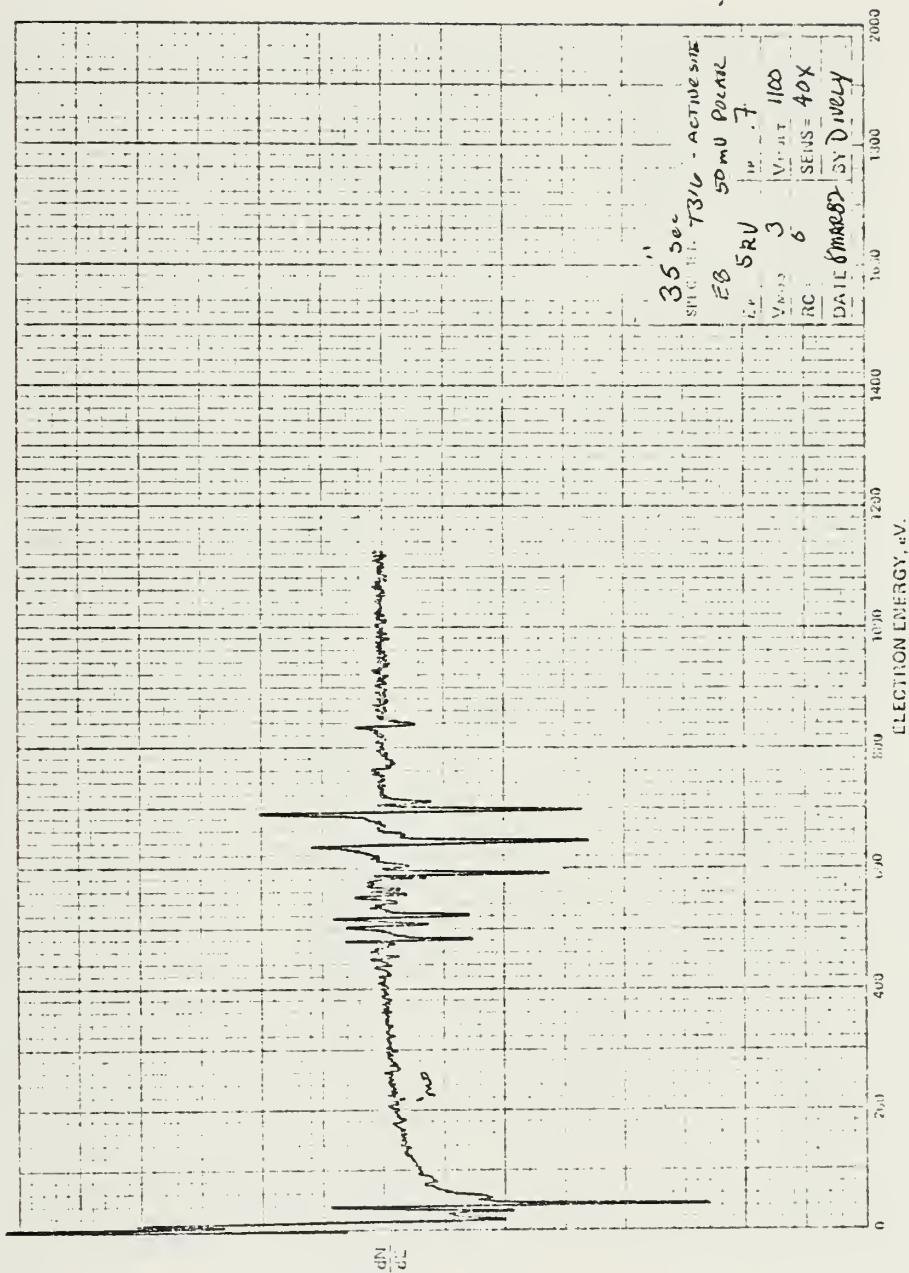


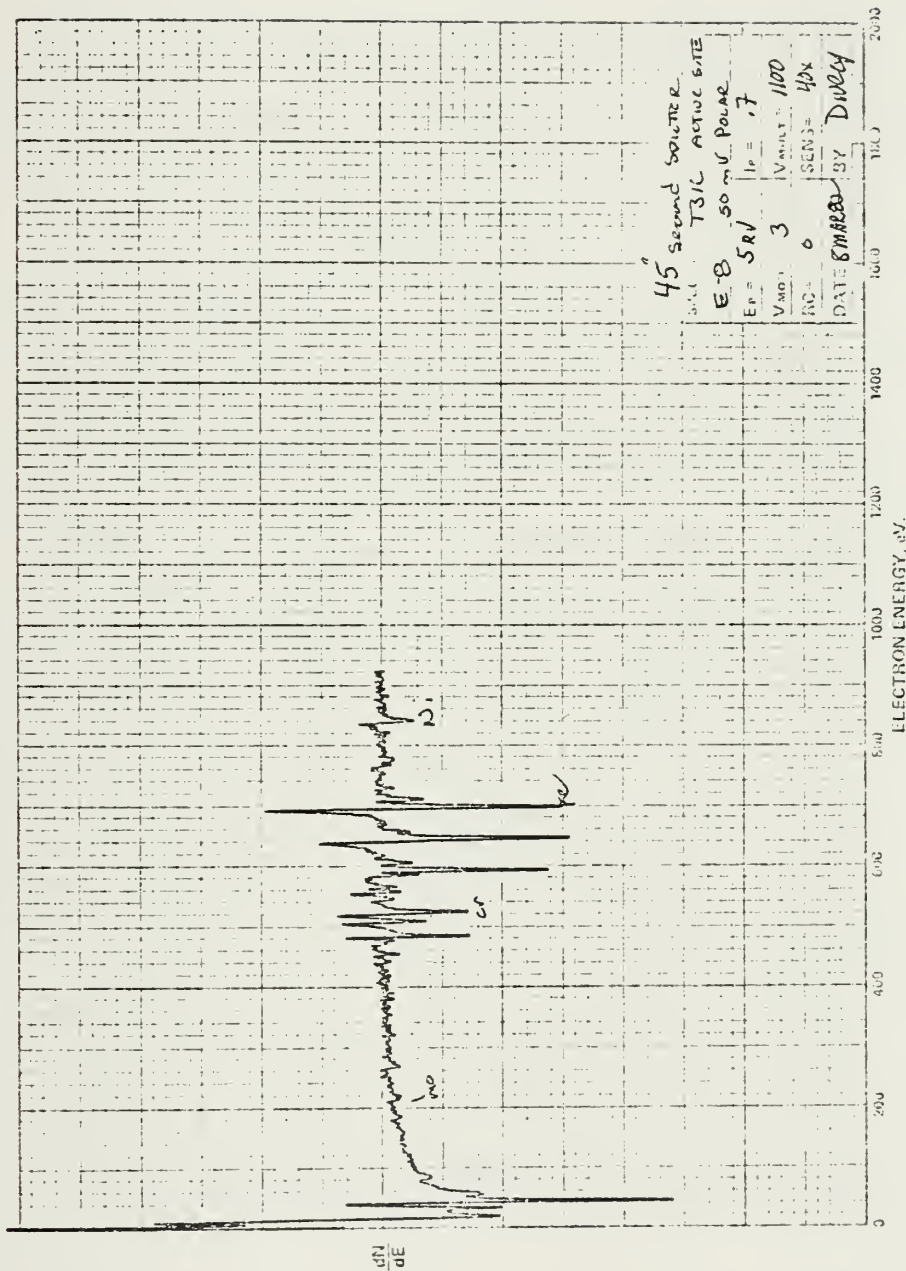


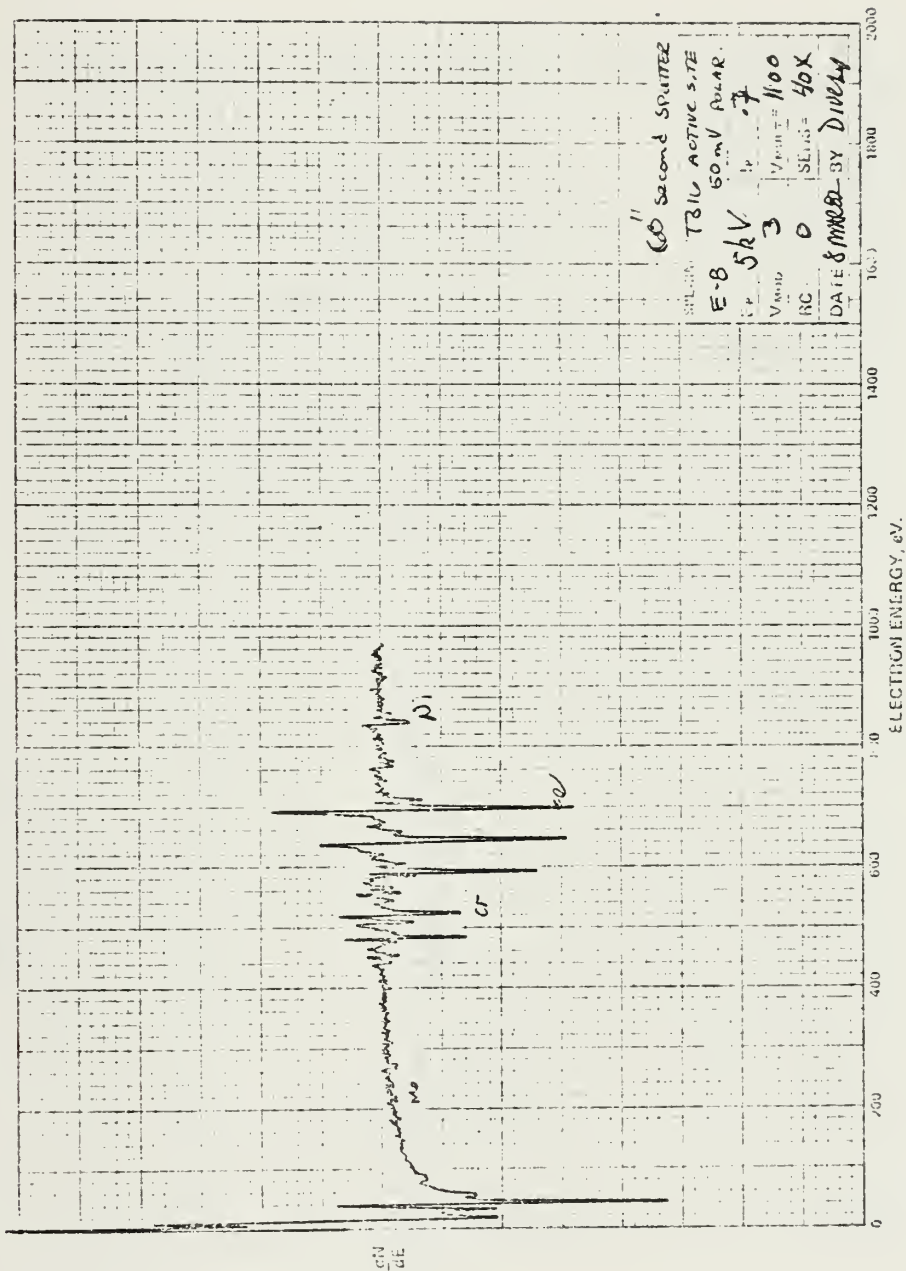


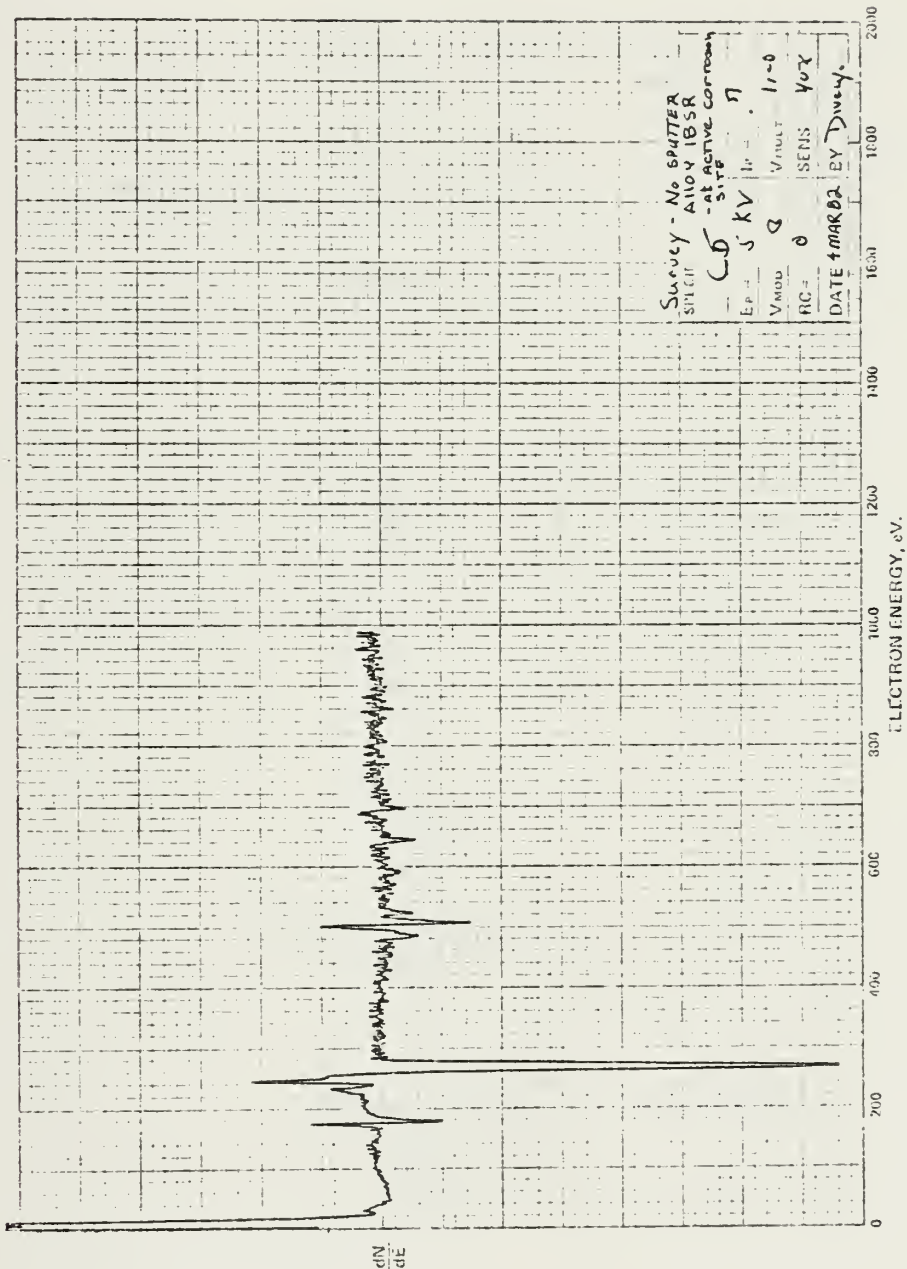






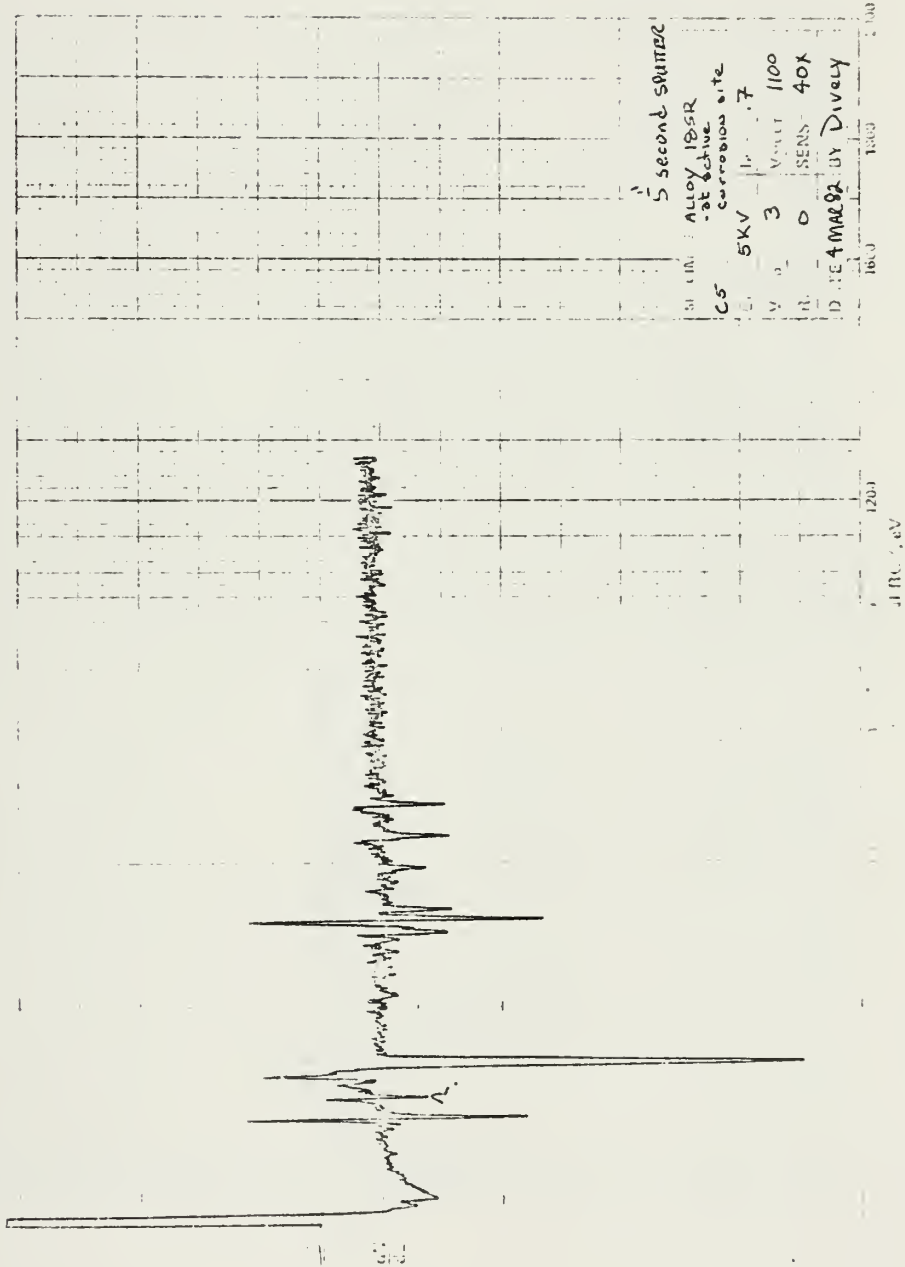


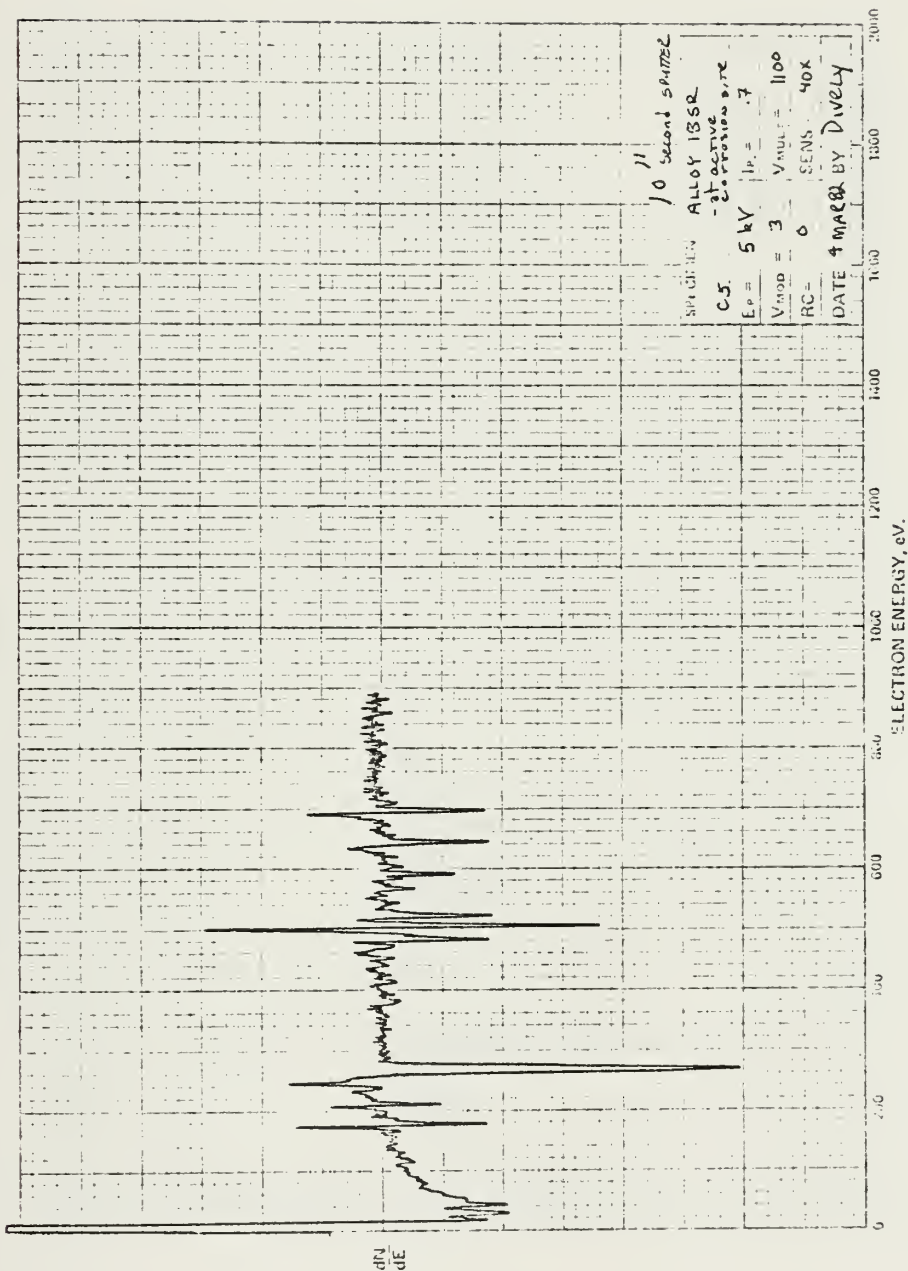


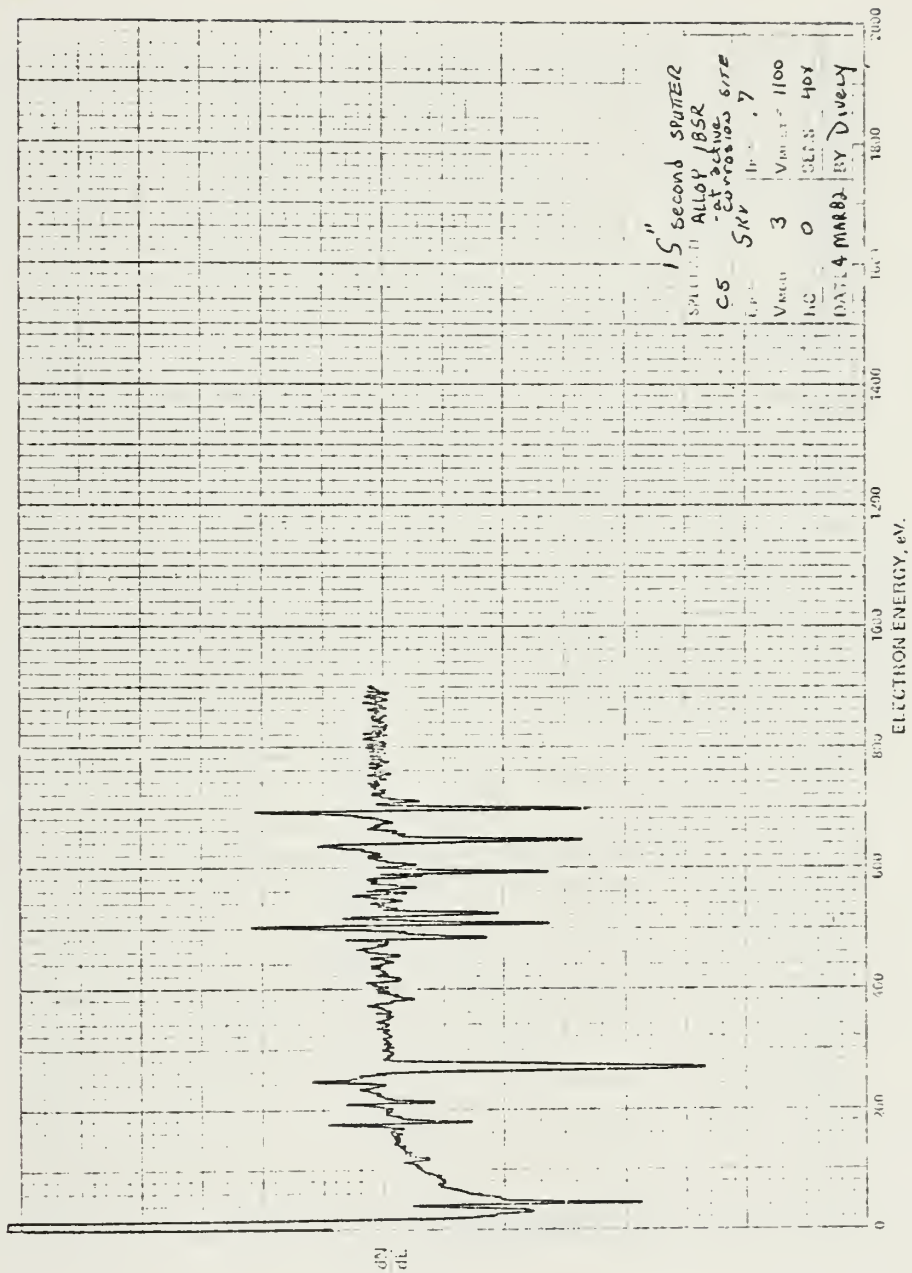


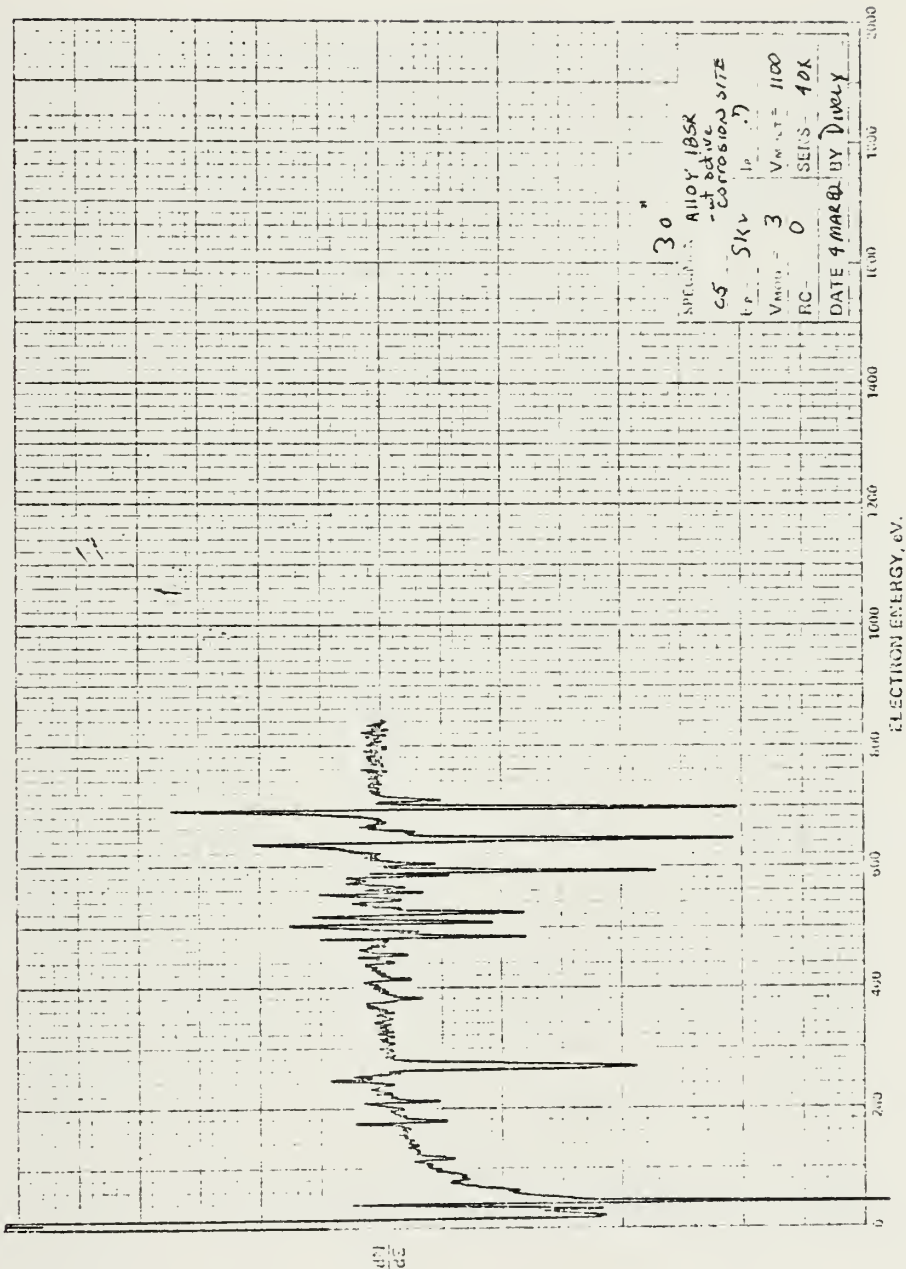
Survey - No SPATTER
SILICON ALLOY IBSR
-at Active Corrosion
Site
Ep = 5 KV Ip = 7
Vmod 0 Vmult 11-0
RC# 0 SENS 40X
DATE 4MAR82 BY Diney.

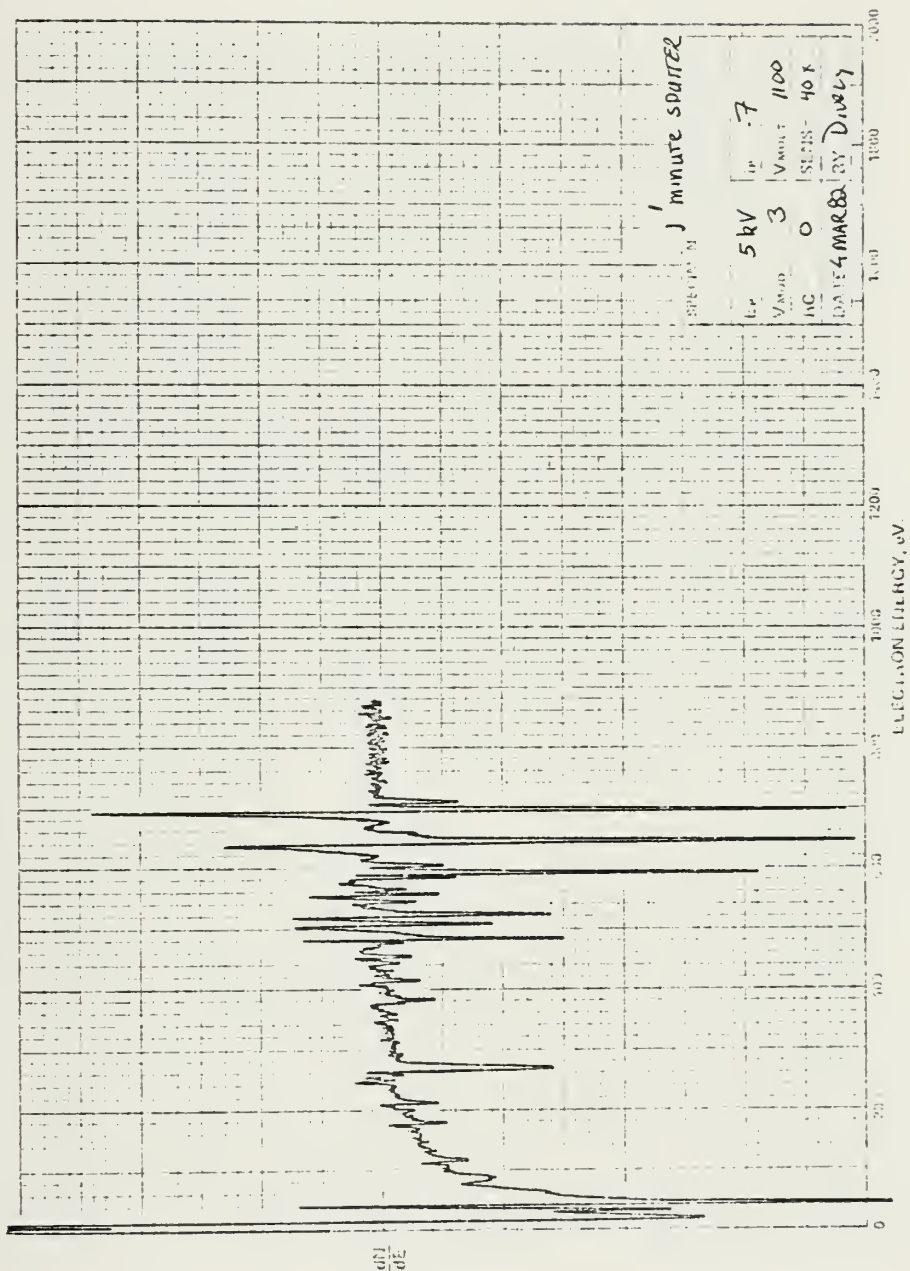
100 500 1000

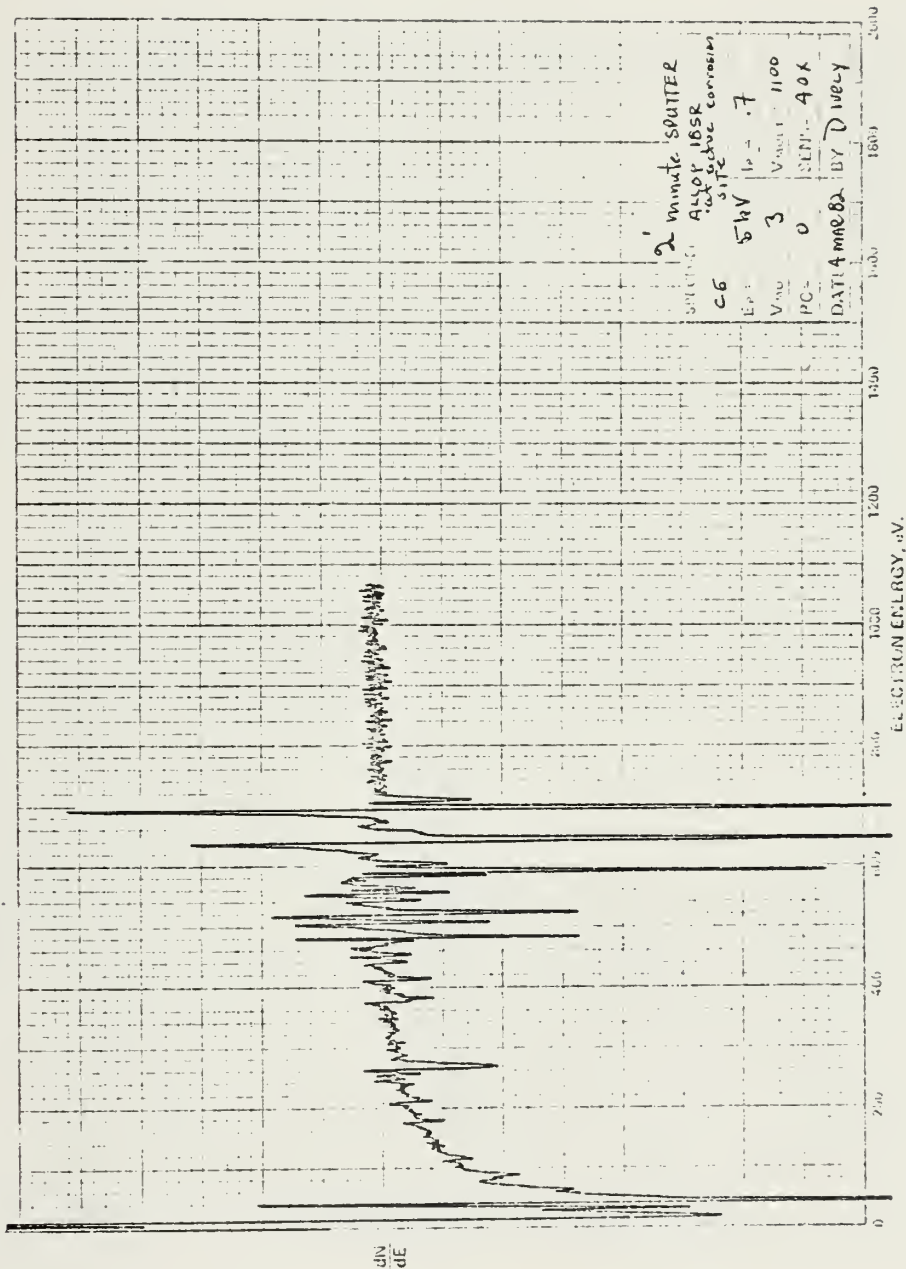


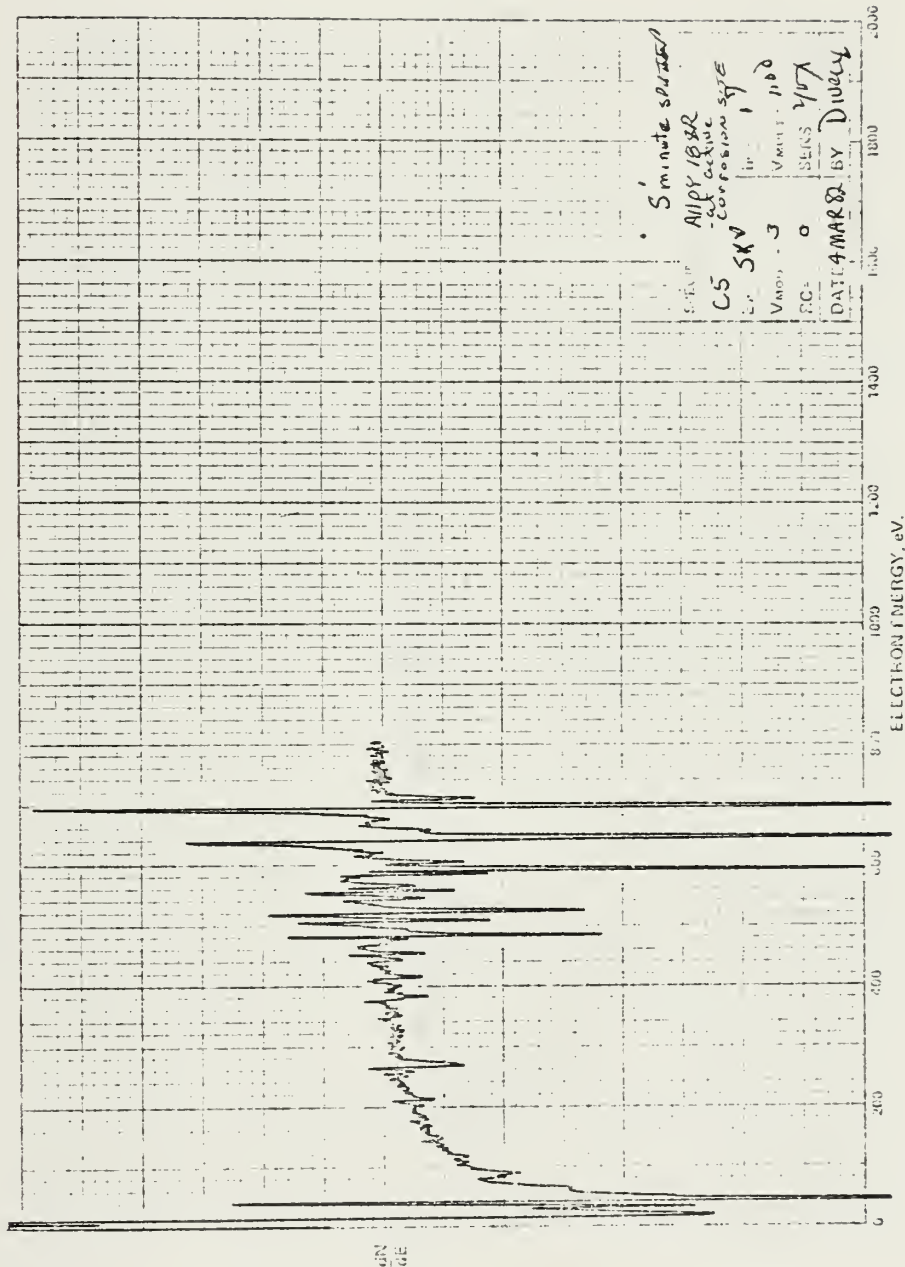


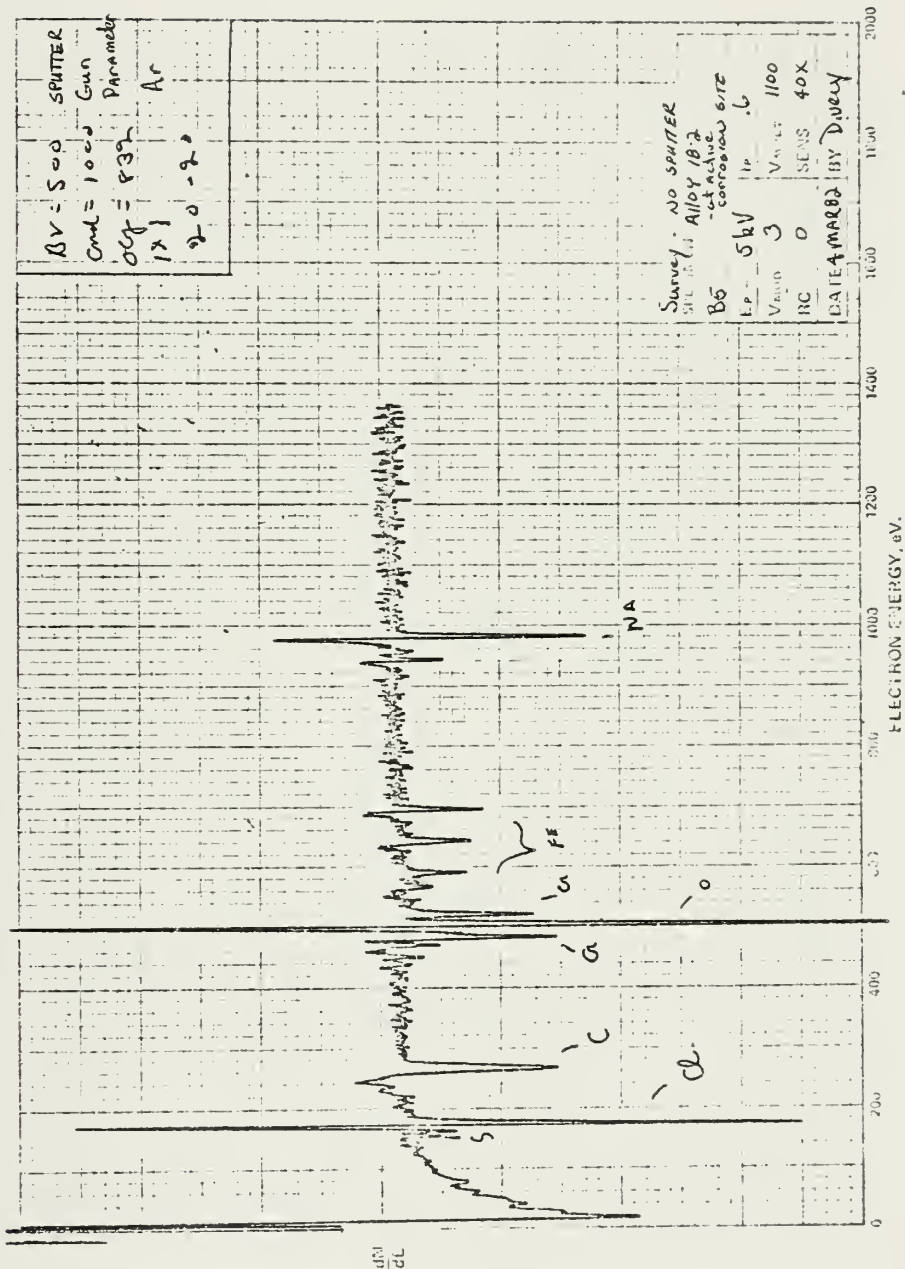


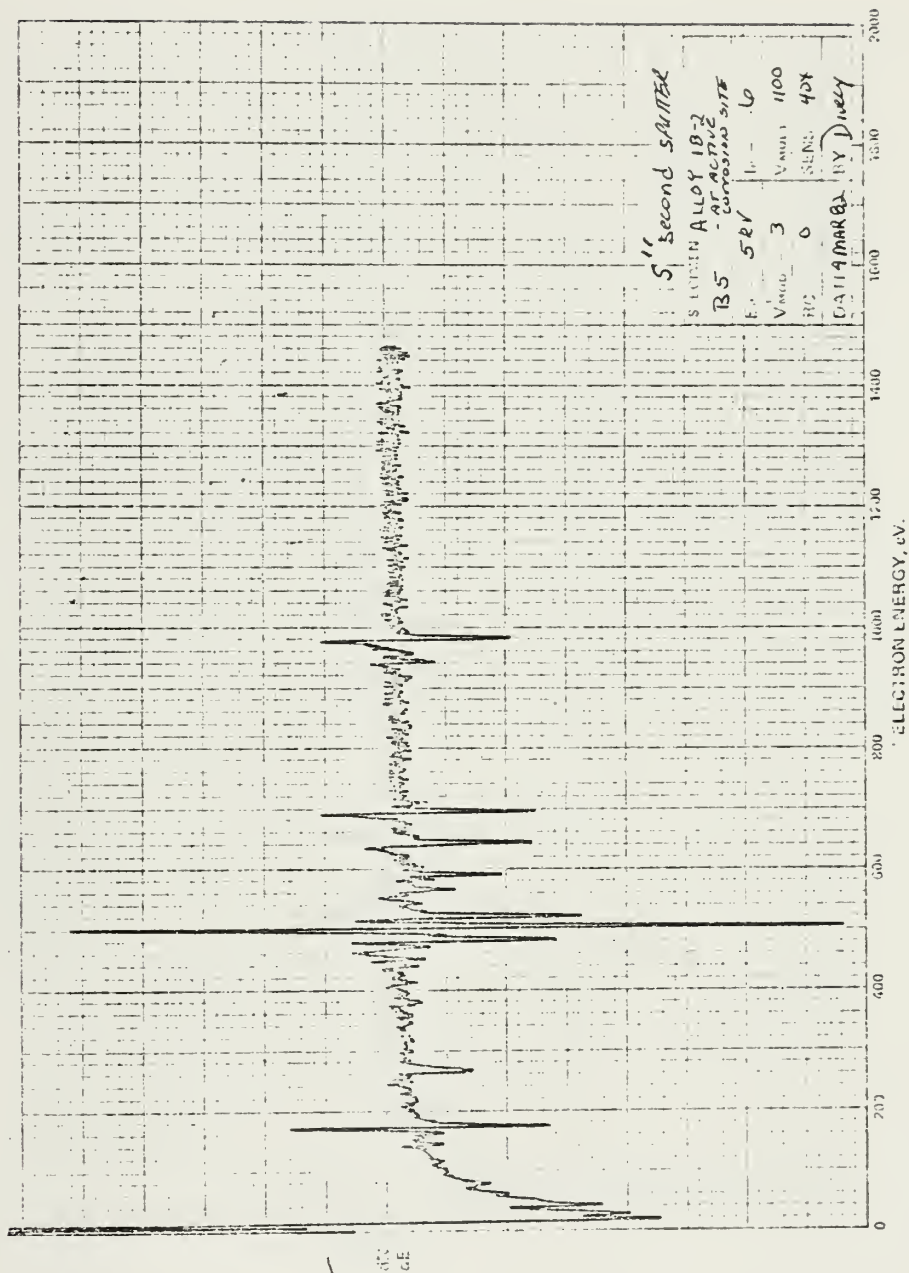


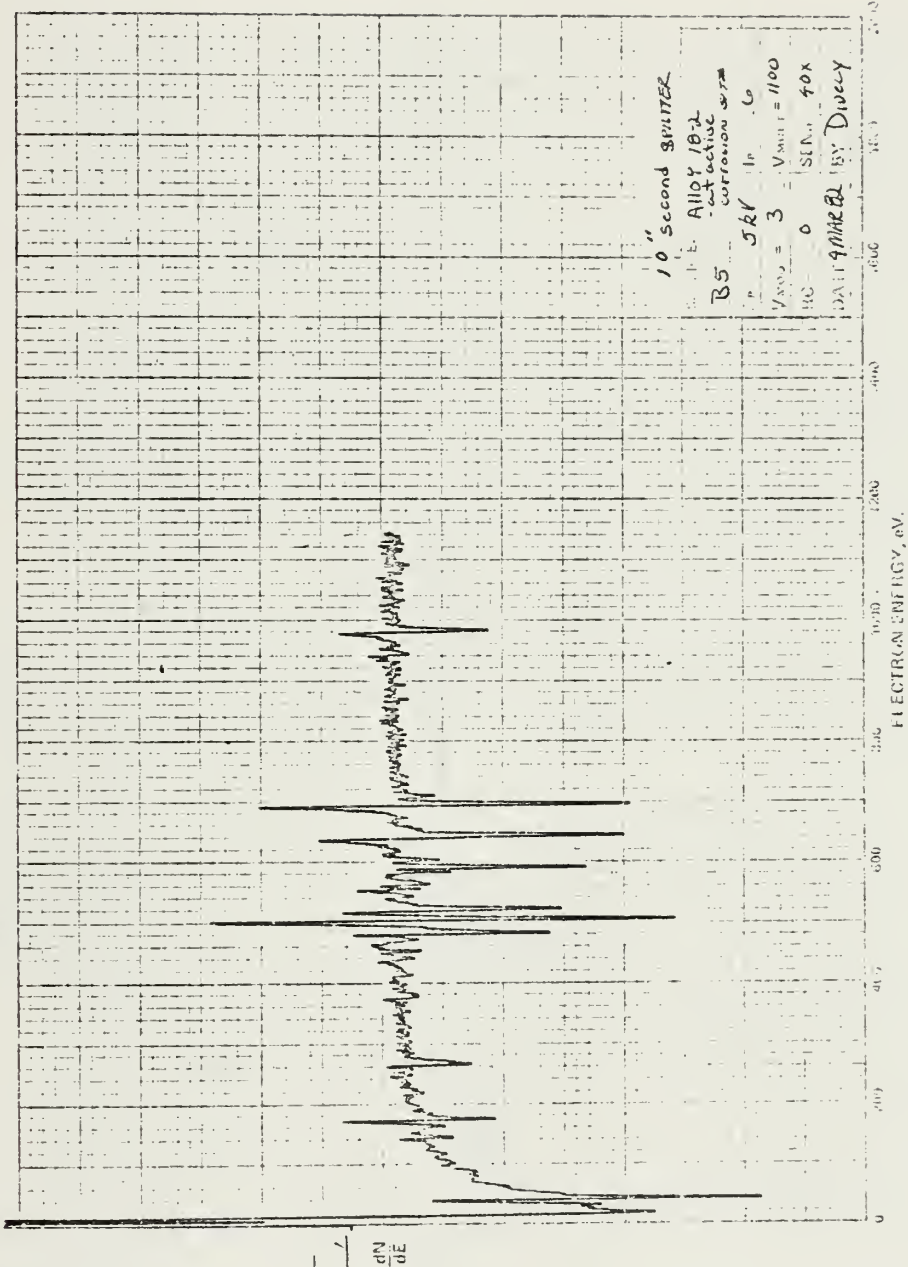


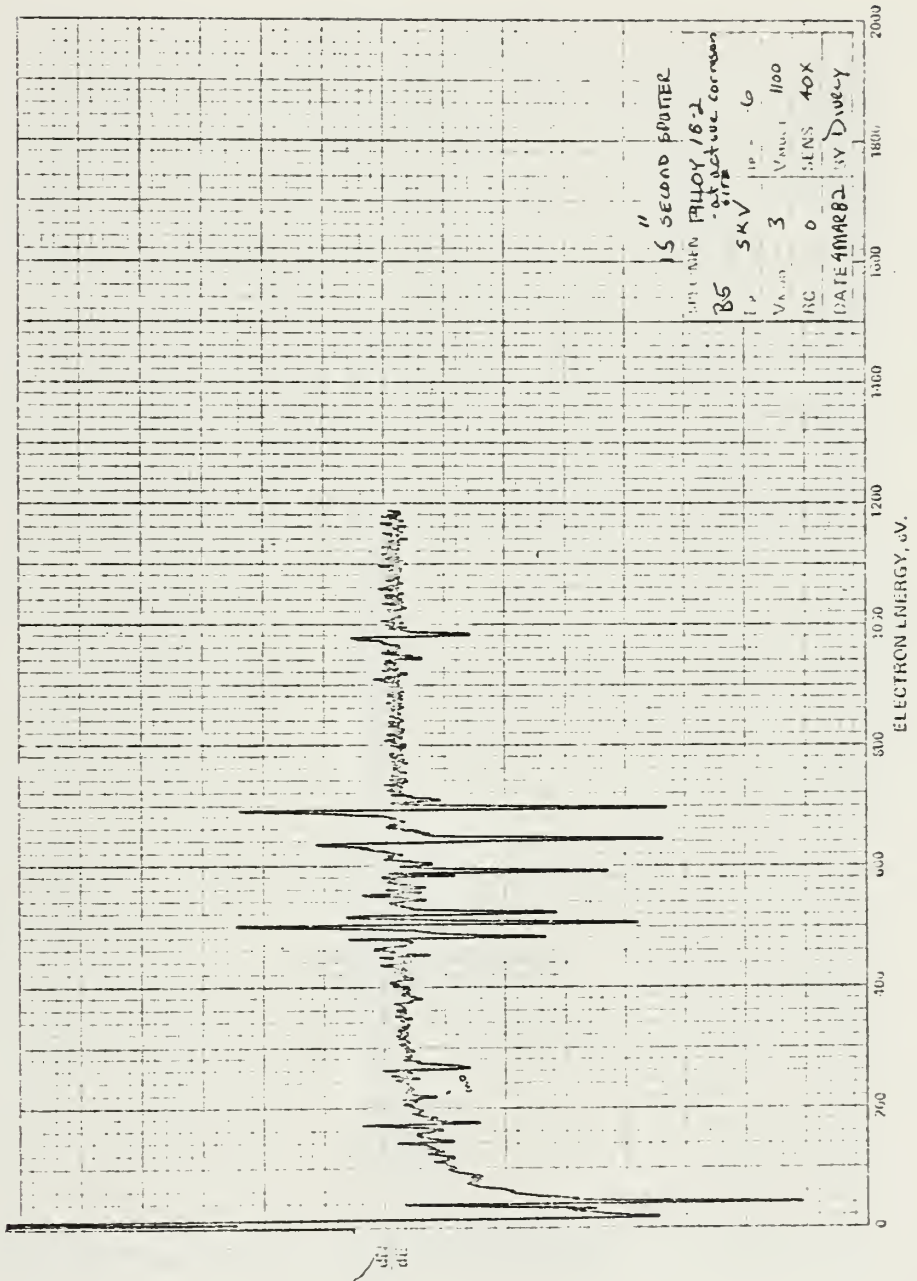


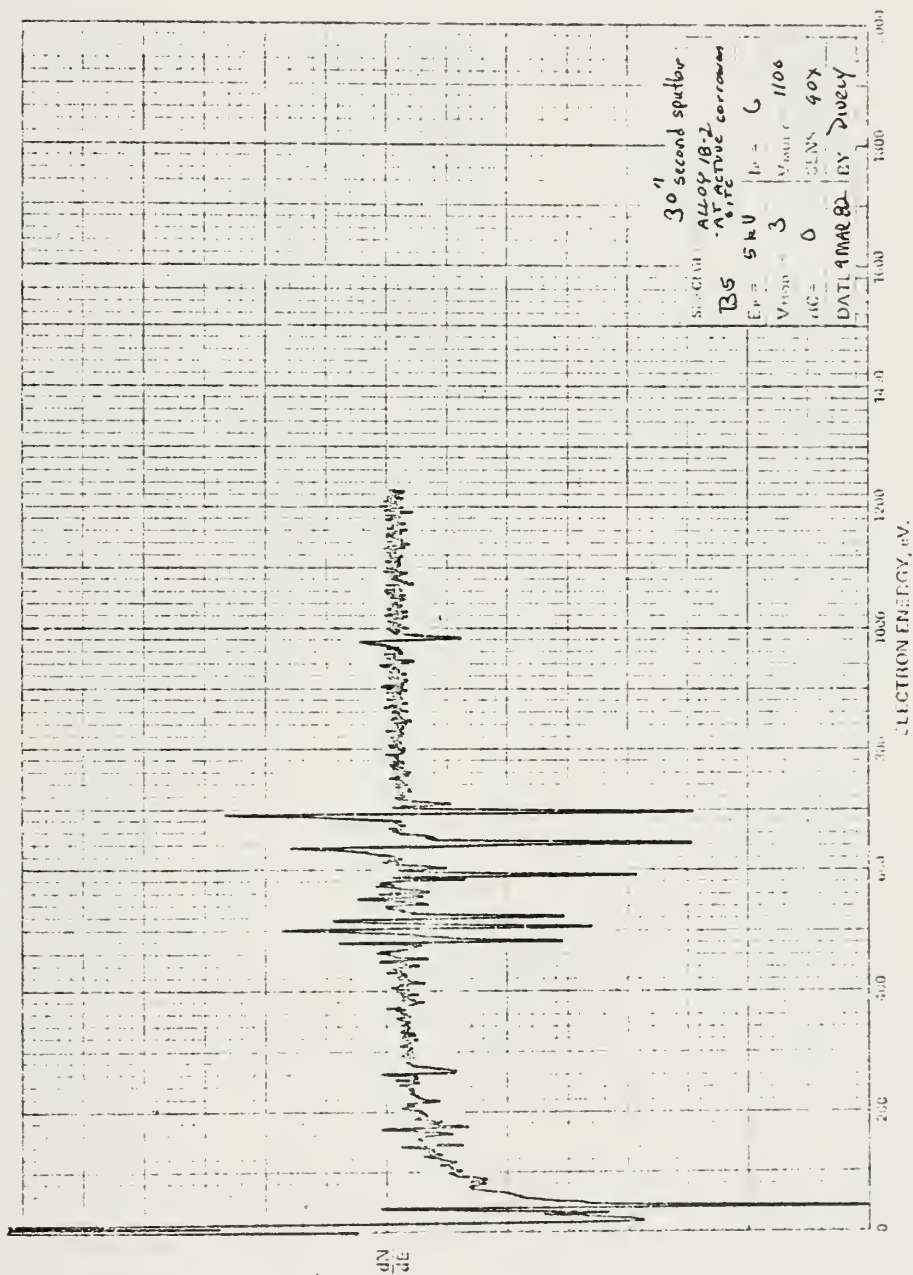


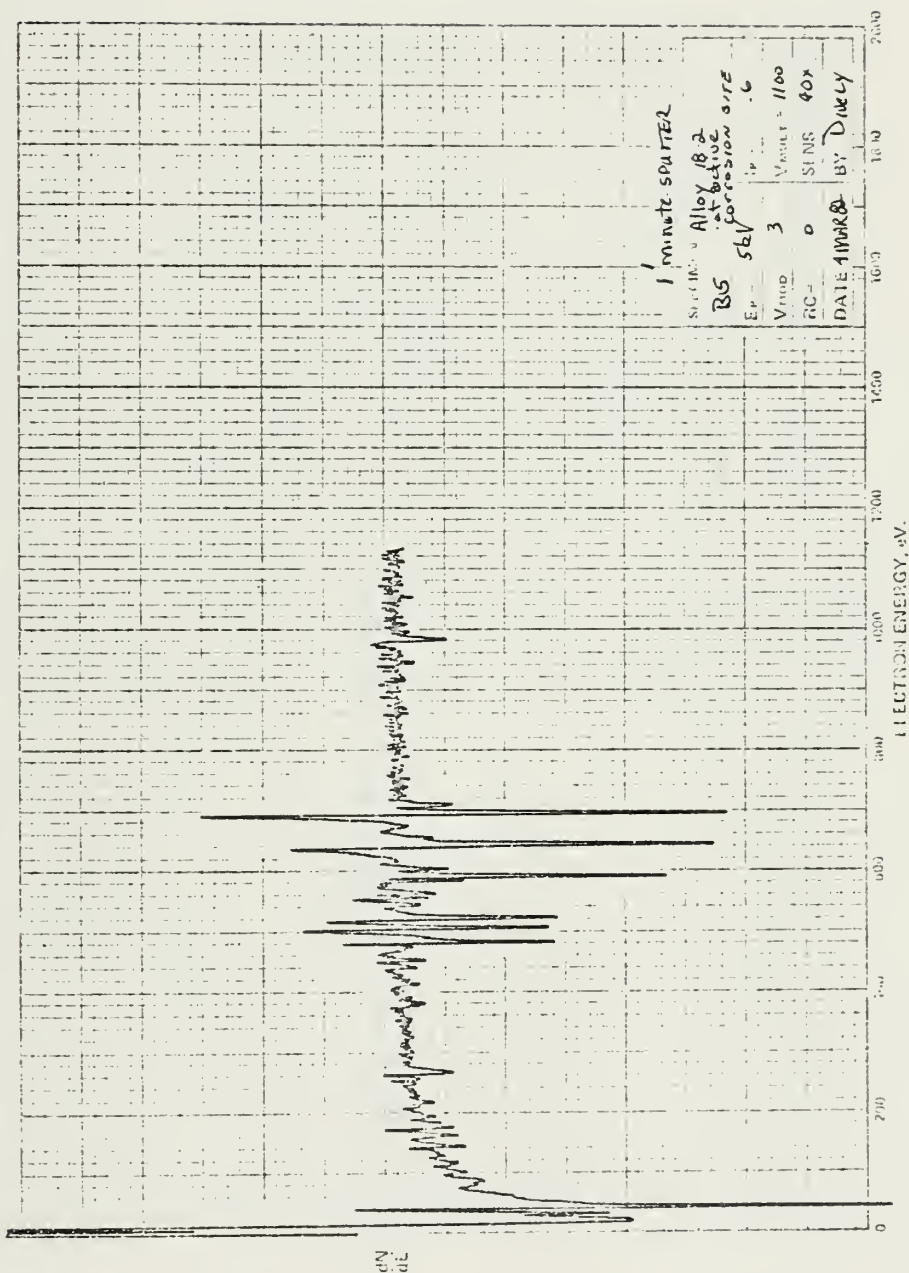


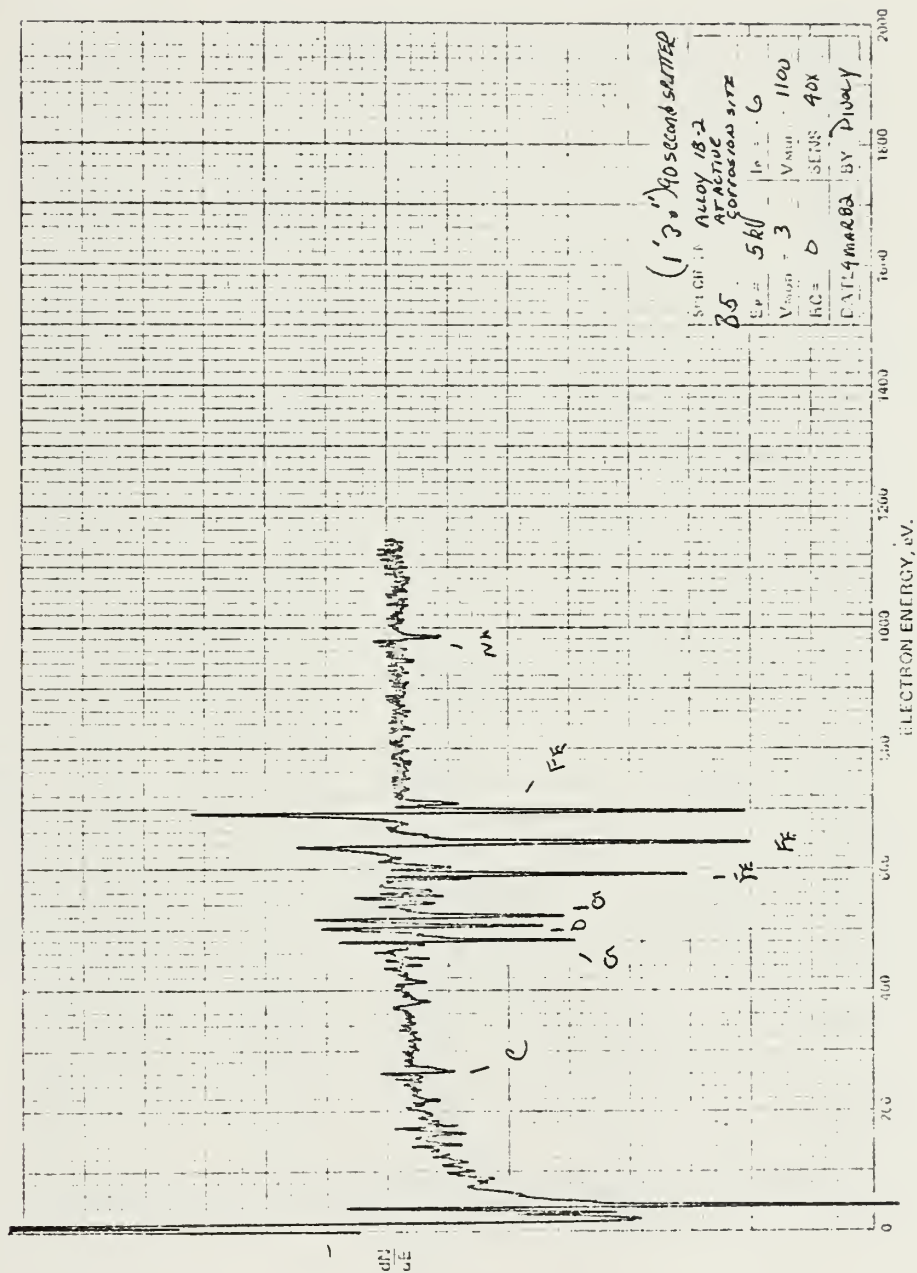






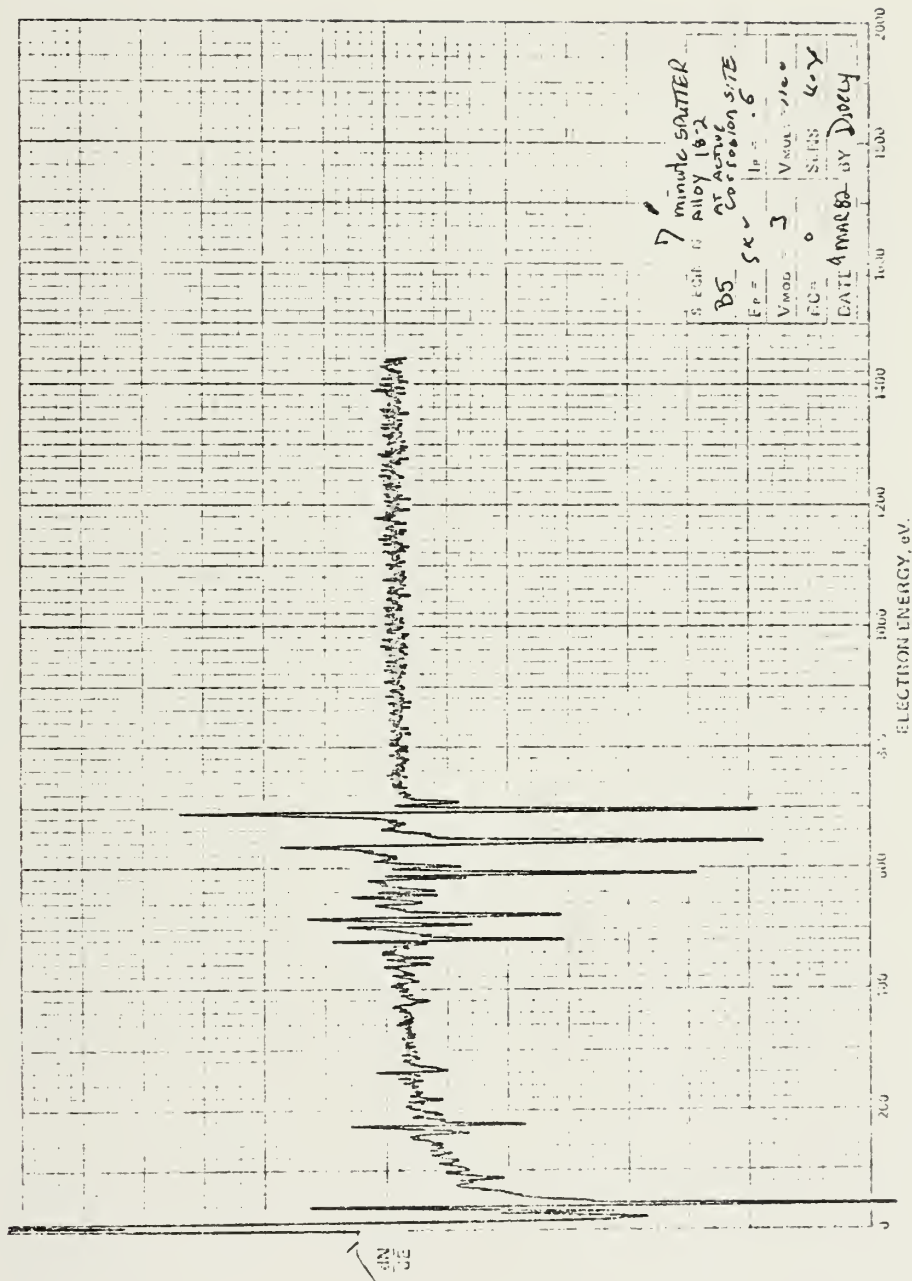








PHYSICAL ELECTROCHEMISTRY



Thesis
D5983
c.1

Dively

199471

An investigation
into the phenomenon of
localized corrosion in
various austenitic,
ferritic, duplex, and
cast stainless steels.

Thesis
D5983
c.1

Dively

199471

An investigation
into the phenomenon of
localized corrosion in
various austenitic,
ferritic, duplex, and
cast stainless steels.



3 2768 001 89427 2
DUDLEY KNOX LIBRARY